UNIVERSITY OF ALBERTA

FUNCTIONAL MATURATION OF PHRENIC MOTONEURON ELECTRICAL PROPERTIES AND DIAPHRAGM CONTRACTILE PROPERTIES DURING PERINATAL DEVELOPMENT IN THE RAT

by

MIGUEL MARTIN-CARABALLO ©

A THESIS SUBMITTED TO THE FACULTY OF GRADUATE STUDIES IN
PARTIAL FULFILMENT OF THE REQUIREMENTS FOR THE DEGREE OF
DOCTOR OF PHILOSOPHY IN PHYSIOLOGY

EDMONTON, ALBERTA
FALL, 2000

National Library
of Canada

Acquisitions and
Bibliographic Services

395 Wellington Street
Ottawa ON K1A 0N4
Canada

Bibliothèque nationale
du Canada

Acquisitions et
services bibliographiques

395, rue Wellington
Ottawa ON K1A 0N4
Canada

Your file Votre référence

Our file Notre référence

The author has granted a non-exclusive licence allowing the National Library of Canada to reproduce, loan, distribute or sell copies of this thesis in microform, paper or electronic formats.

L'auteur a accordé une licence non exclusive permettant à la Bibliothèque nationale du Canada de reproduire, prêter, distribuer ou vendre des copies de cette thèse sous la forme de microfiche/film, de reproduction sur papier ou sur format électronique.

The author retains ownership of the copyright in this thesis. Neither the thesis nor substantial extracts from it may be printed or otherwise reproduced without the author's permission.

L'auteur conserve la propriété du droit d'auteur qui protège cette thèse. Ni la thèse ni des extraits substantiels de celle-ci ne doivent être imprimés ou autrement reproduits sans son autorisation.

0-612-59632-X

Canada

UNIVERSITY OF ALBERTA

LIBRARY RELEASE FORM

Name of the author: MIGUEL MARTIN-CARABALLO

Title of Thesis: FUNCTIONAL MATURATION OF PHRENIC MOTONEURON ELECTRICAL PROPERTIES AND DIAPHRAGM CONTRACTILE PROPERTIES DURING PERINATAL DEVELOPMENT IN THE RAT.

Degree: DOCTOR OF PHILOSOPHY

Year this Degree Granted: 2000

Permission is hereby granted to the University of Alberta Library to reproduce single copies of this thesis and to lend or sell such copies for private, scholarly or scientific research purposes only.

The author reserves all other publication and other rights in association with the copyright in this thesis, and except as herein before provided, neither the thesis nor any substantial portion thereof may be printed or otherwise reproduced in any material form whatever without the author's prior written permission.

Miguel Martin-Caraballo
514 - 10028 106 Ave
Edmonton AB
T5H 4A3

Date Submitted: May 10/2000

ABSTRACT

There is a critical period at approximately embryonic day (E)17 during which phrenic motoneurons (PMNs) undergo a number of pivotal developmental events including the inception of functional recruitment via synaptic drive from medullary respiratory centres, contact with spinal afferent terminals, the completion of diaphragm innervation and a major transformation of PMN morphology. The objective of this thesis was to test the general hypothesis that there would be a marked maturation of PMN electrophysiological and diaphragm contractile properties occurring in conjunction with these developmental processes. PMN properties were measured via whole-cell patch recordings utilizing a cervical slice-phrenic nerve preparation isolated from perinatal rats. Muscle force recordings and intracellular recordings of endplate potentials were measured using phrenic nerve-diaphragm muscle *in vitro* preparations isolated from rats on E18 and postnatal day (P) 0-1.

Development of PMN electrophysiogical properties: From E16 to P1, PMN property changes included the following: i) 10 mV hyperpolarization of the resting membrane potential, ii) three-fold reduction in the input resistance, iii) 12 mV increase in amplitude and 50% decrease duration of action potential, iv) major changes in the shapes of afterpotentials, v) increases in rheobase current and steady state firing rates. Electrical coupling between PMNs was detected in 15-25% of recordings at all ages studied.

Development of K^{+} conductances: PMNs expressed outward rectifier (I_{KV}) and A-type K^{+} currents which regulated action potential and repetitive firing properties throughout the perinatal period. There was an age-dependent leftward shift in the activation voltage and a decrease in the time to peak of I_{KV} during the period from E16

through to birth. The most dramatic change during the perinatal period was the increase in Ca^{++}-activated K^{+} currents which were responsible for the emergence of fAHP (maxi-type-mediated) and mAHP (small conductance-mediated).

Development of Ca^{++} conductances: Changes between E16 and P0-1 included the following; i) an ~ 2-fold decrease in the density of LVA Ca^{++} conductances, and ii) an ~3-fold increase in the density of HVA conductances. The decline in the ratio of LVA Ca^{++} and A-type K^{+} conductances reduced rebound depolarization expression in neonatal PMNs. The increase in L- and N-type Ca^{++} currents were concomitant with the emergence of Ca^{++}-dependent 'hump-like' ADP and mAHP, respectively.

Development of diaphragm contractile properties: The following age-dependent changes occurred between ages E18 and P1: i) twitch contraction and half-relaxation times decreased ~ 2- and 3-fold, respectively, ii) maximal tetanic force levels increased ~5-fold, iii) the range of forces generated by the diaphragm in response to graded nerve stimulation increased ~ 2.3-fold, iv) the force-frequency curve was shifted to the right, and vi) the propensity for neuromuscular transmission failure decreased. In conclusion, the diaphragm contractile and PMN repetitive firing properties develop in concert so that the full-range of potential diaphragm force recruitment can be utilized and problems associated with diaphragm fatigue are minimized.

University of Alberta

Faculty of Graduate Studies and Research

The undersigned certify that they have read, and recommended to the Faculty of Graduate Studies and Research for acceptance, a thesis entitled **Functional Maturation of Phrenic Motoneuron Electrical Properties and Diaphragmatic Contractile Properties During Prenatal Development in the Rat** submitted by **Miguel Martin-Caraballo** in partial fulfilment of the requirements for the degree of **Doctor of Philosophy.**

J. J. Greer, Ph.D., Supervisor

Greg Funk
G.D.Funk, Ph.D. External Examiner

William F. Dryden
W.F. Dryden, Committee Member

P A Smith
P.A. Smith, Committee Member

D J Bennett
D.J. Bennett, Committee Member

C.B. Benishin, Committee Chair

April 20, 2000
Date

Acknowledgments

This thesis would not be possible without the support and encouragement of many people who helped me throughout my work at the University of Alberta. In this short space, I would like to acknowledge their contribution. In particular, I would like to thank:

Dr. J.J. Greer for accepting me as a PhD student in his laboratory and providing all the financial, academic and moral support for my work.

The members of my committee Dr. P.A. Smith, Dr. R.B. Stein and Dr. D.J. Bennett for their advice and helpful discussions during my thesis work.

Dr. W.F. Dryden and Dr. W.F. Colmers for providing answers to some of my questions on a regular basis. Special thanks to Dr. Dryden for letting me use his experimental setup for the study of the diaphragm contractile properties.

Dr. B. Jassar and Dr. C. Wong for teaching me some of the subtleties of electrophysiological recordings and discussing some of the bizarre findings I got along the way.

Dr. D. Allan and Mr. Randy Babiuk for the friendly atmosphere they provided while working together on a daily basis in the laboratory. Special thanks to Douglas for opening the path for my investigation as the result of his pioneering work in uncovering the most important morphological steps in PMN and diaphragm maturation.

Mrs. Wei Zhang for helping me with the Western blots.

All my friends in Edmonton, who made me laugh and helped me overcome my despair and depression during the long winters here.

Dr. D. Bieger and Mrs. Janet Robinson, who provided me with a great deal of encouragement from The Rock (Newfoundland) and who always believed in me and my abilities to finish my thesis.

The Department of Physiology and the Faculty of Medicine at the University of Alberta, the Alberta Heritage Foundation for Medical Research, the Alberta Lung Association and the NeuroScience Canada Foundation who provided me with all the financial support throughout my work.

My wife for her tolerance and support during this work and to my family, especially my mother, for their encouragement.

Table of Contents

CHAPTER 1

INTRODUCTION . . . . -1-
  General Overview . . . . -2-
  I. Anatomical and functional organization of the respiratory system . . . . -2-
  I-A. Embryonic development of the respiratory function . . . . -6-
  I-B. Morphological and functional maturation of PMNs . . . . -8-
  I-C. Maturation of the diaphragm and the neuromuscular junction . . . . -11-
  II. Development of electrical excitability in differentiating neurons . . . . -12-
  II-A. Role of electrical activity and Ca^{++} transients in regulating neuronal excitability during development . . . . -19-
  II-B. Role of gap junctions and electrotonic coupling during development . . -22-
  II-C. Role of target-derived trophic factors in regulating electrical excitability during development . . . . -23-
  III. Rationale for studying the functional maturation of the respiratory neuromuscular system . . . . -24-

  REFERENCES . . . . -28-

CHAPTER 2

METHODS AND MATERIALS . . . . -40-
  Perinatal rat models . . . . -41-
  Cervical slice-phrenic nerve preparation . . . . -41-
  Whole-cell recordings . . . . -42-
  Intracellular and extracellular solutions . . . . -44-
  Drugs . . . . -45-
  Phrenic nerve-diaphragm preparation . . . . -48-
  Measurements of diaphragm contractile properties . . . . -48-
  Determination of muscle weight and protein content . . . . -50-
  Measurements of endplate potentials (epp) . . . . -51-
  Statistics . . . . -52-

  REFERENCES . . . . -53-

CHAPTER 3

ELECTROPHYSIOLOGICAL PROPERTIES OF RAT PHRENIC MOTONEURONS DURING PERINATAL DEVELOPMENT . . . . -54-

INTRODUCTION . . . . -55-

METHODS . . . . -55-
    Whole-cell recording . . . . -55-
    Drugs . . . . -56-

RESULTS . . . . -56-
    Membrane properties . . . . -57-
    Action potential characteristics . . . . -65-
    Ionic conductances underlying the components of the action potential -72-
    Ionic dependence of action potential characteristics . . . . -72-
    Ionic dependence of afterdepolarizing potentials . . . . -72-
    Electrotonic coupling between PMNs . . . . -76-
    Repetitive firing properties . . . . -81-

DISCUSSION . . . . -89-
    Development of membrane properties . . . . -89-
    Presence of electrical coupling amongst perinatal PMNs . . . . -91-
    Development of action potential characteristics and associated ionic conductances . . . . -92-
    Development of repetitive firing properties . . . . -94-

REFERENCES . . . . -96-

CHAPTER 4

DEVELOPMENT OF POTASSIUM CONDUCTANCES IN PERINATAL RAT PHRENIC MOTONEURONS . . . . -100-

INTRODUCTION . . . . -101-

METHODS . . . . -102-
    Whole-cell recordings . . . . -102-
    Intracellular and extracellular solutions . . . . -103-
    Drugs . . . . -103-
    Western Analysis . . . . -104-

RESULTS . . . . -105-
    Effects of blocking multiple K^+ conductances . . . . -105-
    Effects of blocking K^+ currents with TEA . . . . -106-
    Effects of blocking A-type K^+ conductances with 4-AP . . . . -107-
    Role of Ca^{++}-activated K^+ conductances in controlling firing properties and afterpotential formation . . . . -115-
    Electrophysiological and pharmacological properties of the mAHP . -120-

Electrophysiological and pharmacological properties of the fAHP . . -121-
Voltage-clamp analysis of voltage-dependent K$^+$ currents . . . . -132-
Western analysis of Ca^{++}-activated K$^+$ channels . . . . -142-

DISCUSSION . . . . -145-
Ca^{++}-dependent K$^+$ conductances . . . . -145-
Maxi-type Ca^{++}-dependent K$^+$ current . . . . -145-
Small conductance Ca^{++}-dependent K$^+$ current . . . . -146-
Outward rectifier and A-type K$^+$ conductances . . . . -147-

REFERENCES . . . . -151-

CHAPTER 5

VOLTAGE-SENSITIVE CALCIUM CURRENTS AND THEIR ROLE IN REGULATING PHRENIC MOTONEURON ELECTRICAL EXCITABILITY DURING THE PERINATAL PERIOD . . . . -154-

INTRODUCTION . . . . -155-

METHODS . . . . -156-
Whole-cell recordings . . . . -156-
Intracellular and extracellular solutions . . . . -157-
Drugs . . . . -157-

RESULTS . . . . -157-
Whole-cell voltage-clamp recordings . . . . -158-
Pharmacological characterization of Ca^{++} currents . . . . -159-
Developmental changes in LVA and HVA Ca^{++} current densities . . -160-
Whole-cell current-clamp recordings . . . . -172-
LVA Ca^{++} currents . . . . -172-
HVA Ca^{++} currents . . . . -173-

DISCUSSION . . . . -187-
LVA or T-type Ca^{++} conductance . . . . -187-
HVA Ca^{++} currents . . . . -189-

REFERENCES . . . . -192-

CHAPTER 6

CONTRACTILE AND FATIGUE PROPERTIES OF THE RAT DIAPHRAGM MUSCULATURE DURING THE PERINATAL PERIOD 195

INTRODUCTION . . . . -196-

METHODS . . . . -196-
- Drugs . . . . -196-

RESULTS . . . . -197-
- Force measurements . . . . -197-
- Twitch characteristics . . . . -197-
- Relationship between force development and stimulation frequency -198-
- Relationship between declines in diaphragm force levels and nerve stimulation paradigms . . . . -198-
- Measurements of endplate potentials (epps) . . . . -209-

DISCUSSION . . . . -213-
- Consideration of in vitro conditions . . . . -213-
- Twitch contraction and relaxation times . . . . -214-
- Force development . . . . -215-
- Force-frequency relationship . . . . -215-
- Neuromuscular fatigue . . . . -217-

REFERENCES . . . . -220-

CHAPTER 7

GENERAL DISCUSSION . . . . -223-
- Role of calcium influx during PMN development . . . . -224-
- Regulation of PMN firing properties . . . . -227-
- Correlation between inception of inspiratory drive and maturation of PMN-diaphragm properties . . . . -230-
- Correlation between PMN firing properties and diaphragm force generation -232-

REFERENCES . . . . -236-

List of Figures

Figure 1.1. Time-line indicating some of the key events involved in phrenic motoneuron-diaphragm development . . . . -14-

Figure 2.1. Schematic of experimental setup for recording PMN electrical properties, diaphragm contractile properties and end-plate potentials . . . . -47-

Figure 3.1. Membrane responses to the injection of hyperpolarizing current pulse revealed the presence of a rebound excitation (arrow) in E16 PMNs and the lack of sag depolarization at all ages examined . . . . -62-

Figure 3.2. Characterization of the rebound depolarizations observed in E16 PMNs. -64-

Figure 3.3. Typical action potentials recorded from E16, E18 and P0 PMNs. . . . . . . -69-

Figure 3.4. The amplitudes of ADPs and AHPs were dependent on the membrane holding potential (held at -50, -60 and -75 mV). . . . . -71-

Figure 3.5. Role of Na^+ and Ca^{++} conductance in the generation of action potentials. -75-

Figure 3.6. Multiple criteria were used as evidence for electrical coupling between PMNs. . . . . -80-

Figure 3.7. Examples of repetitive firing patterns generated in E16, E18 and P0 PMNs . . . . -86-

Figure 3.8. Plots of the instantaneous firing rates as a function of injected current or interspike interval . . . . -88-

Figure 4. 1. Block of multiple of K^+ conductances revealed plateau potentials in PMNs . . . . -110-

Figure 4.2. Effect of externally applied TEA (10 mM) on the firing pattern of PMNs . . . . -112-

Figure 4.3. Effect of 4-aminopyridine (4-AP, 1 mM) on the action potential duration and firing pattern of one representative E18 PMN. . . . . -114-

Figure 4.4. Effect of Ca^{++}-free medium on the repetitive firing properties of PMNs. -117-

Figure 4.5. Plots of the firing frequency of PMNs as a function of injected current or interspike interval. . . . . -119-

Figure 4.6. Electrophysiological and pharmacological properties of the medium-duration AHP in a P0 PMN . . . . -124-

Figure 4.7. Electrophysiological and pharmacological properties of the fast AHP in a P0 PMN . . . . -126-

Figure 4.8. Effect of Ca^{++}-activated K^{+} conductances in regulating the firing pattern of two representative P0 PMNs. . . . . -128-

Figure 4.9. Plots of the firing frequency of PMNs as a function of injected current or interspike interval following treatment with apamin and iberiotoxin . . . -130-

Figure 4.10. Voltage-clamp recordings of K^{+} currents in a E16 PMN . . . . -136-

Figure 4.11. Effect of 4-AP (3 mM) on the A-type and outward rectifier K^{+} conductances. . . . . -138-

Figure 4.12. Electrophysiological and pharmacological properties of the outward rectifier K^{+} conductance. . . . . -140-

Figure 4.13. Age-specific expression of maxi-type and small-conductance, Ca^{++}-activated K^{+} channel proteins as detected by immunoblot analysis. . . -144-

Figure 5.1. Whole-cell voltage-clamp recordings of LVA and HVA Ca^{++} conductances from an E16 PMN. . . . . -162-

Figure 5.2. Effects of Ca^{++}-free medium on the Ca^{++} currents measured in a P0 PMN. . . . . -164-

Figure 5.3. Effect of blocking T-type Ca^{++} conductances in a E16 PMN . . . . -166-

Figure 5.4. Effects of blocking N- and P-type Ca^{++} currents in P0 PMNs. . . . . -168-

Figure 5.5. Effects of blocking L-type Ca^{++} currents in a P0 PMN. . . . . -170-

Figure 5.6. Effects of blocking T-type Ca^{++} conductances on action potential characteristics of perinatal PMNs. . . . . -176-

Figure 5.7. Electrophysiological and pharmacological properties of the rebound depolarization in an E16 PMN. . . . . -178-

Figure 5.8. Interactions of T-type Ca^{++} and A-type K^{+} currents in determining the response of PMNs to hyperpolarizing pulses. . . . . -180-

Figure 5.9. The contribution of L-type Ca^{++} conductances to the afterpotentials of two representative P0 PMNs. . . . . -182-

Figure 5.10. Effect of L-type Ca^{++} channels blocker, verapamil on the repetitive firing pattern of a P0 PMN . . . . -184-

Figure 5.11. Effect of blocking N- and P-type Ca^{++} currents on action potential characteristics of P0 PMNs . . . . -186-

Figure 6.1. Age-dependent changes in twitch and tetanus characteristics. . . . . -202-

Figure 6.2. Plot of the normalized peak force at the onset of muscle (open squares) and nerve stimulation (solid squares) vs. stimulus frequency. . . . . -204-

Figure 6.3. Force developed by the diaphragm in response to nerve and direct muscle stimulation. . . . . -206-

Figure 6.4. Force records from E18 diaphragm muscle preparations in response to varying frequencies of long duration (10 sec) nerve stimulation . . . . -208-

Figure 6.5. End-plate potentials (epps) measured from E18 and P0 muscle fibers . -212-

List of Tables

Table 3.1. Electrophysiological properties of PMNs. . . . . -58-

Table 3.2. Changes in the firing properties of PMNs . . . . -84-

Table 4.1. Change in PMN action potential duration following block of K^+ conductances with TEA and 4-AP. . . . . -108-

Table 4.2. Modulation of PMN action potential and firing properties following blockade of Ca^{++}-activated K^+ conductances. . . . . -131-

Table 4.3. Electrophysiological properties of I_{KV} and I_A conductances in perinatal PMNs. . . . . -141-

Table 5.1. Changes in the Ca^{++}-current densities of PMNs . . . . -171-

Table 6.1. Contractile properties of rat diaphragm at embryonic age 18 (E18) and postnatal days 0-1 (P0-1) . . . . -200-

List of Abbreviations

ADP	Afterdepolarizing potential
ATP	Adenosine 5'-triphosphate
BAPTA	1,2-bis(2-aminophenoxy)ethane-N,N,N',N'-tetraacetic acid
DRG	Dorsal respiratory group
fAHP	Fast afterhyperpolarizing potential
FBM	Fetal breathing movements
HEPES	N-2-hydroxyethyl)piperazine-N'-2-ethanesulfonic acid
I_A	Transient, A-type K^+ current
I_{KV}	Outward rectifier K^+ current
ISI	Interspike interval
mAHP	Medium duration afterhyperpolarizing potential
MHC	Myosin heavy chain
PMNs	Phrenic motoneurons
REM	Rapid eye movements
SFA	Spike frequency adaptation
VRG	Ventral respiratory group
TEA	Tetraethylammonium
TTX	Tetrodotoxin

CHAPTER 1

INTRODUCTION

General Overview

The objective of this thesis was to characterize the development of rat phrenic motoneuron (PMN) electrical properties and concomitant changes in the diaphragm contractile characteristics during the major period of perinatal morphological and functional maturation. As a first step, I will briefly review our current knowledge regarding the anatomical and functional organization of the respiratory system. I will then review the morphological maturation of the major neuromuscular component of the respiratory system, the phrenic nerve and diaphragm. Since a significant portion of this work is concerned with the functional differentiation of PMN electrophysiological properties, I shall briefly discuss what is known about the maturation of electrical properties in other differentiating neurons, as well as the factors involved in regulating these changes.

I. Anatomical and functional organization of the respiratory system

Ventilation of the lungs required for gas exchange between the external environment and the internal milieu of mammalian organisms is generated by periodic movements of respiratory muscles. Rhythmic respiratory drive is generated within brainstem ponto-medullary circuits and conveyed to the spinal PMNs via bulbospinal premotor neurons. PMNs innervate the diaphragm muscle which is the primary muscle responsible for generating inspiratory movements. The diaphragmatic pump acts axially in order to increase the volume of the thoracic cavity during an inspiration. Intercostal muscles in the rib cage and muscles of the upper airways also contribute to respiratory function. The former are responsible for upward movements of the rib cage during inspiration, whereas muscles of the upper airway regulate airflow resistance. In newborns, however, due to the lower compliance of the chest wall, the role of intercostal muscle in supporting respiratory movements is minimal, and indeed paradoxical movements may occur where the chest wall may collapse during inspiratory movements.

There is still considerable debate regarding the precise location and cellular organization of the rhythm generating network in the brainstem. Currently, two medullary regions have been postulated to be important for the generation and control of respiration in mammals; the ventral and dorsal respiratory groups in the brain stem (VRG and DRG, respectively) (reviewed by Feldman, 1986; Ballanyi et al., 1995; Bianchi et al., 1995). The VRG is located ventromedial to the nucleus ambiguus (NA) whereas the DRG is located ventrolateral to the nucleus tractus solitarius (NTS). Despite some functional and anatomical differences between rodents and cats in which the majority of the experiments have been performed, there is considerable evidence that the VRG is the primary site for respiratory rhythm generation in mammals (Feldman, 1986). The DRG appears to be primarily involved in modulating, but not in generating, the respiratory rhythm as it receives considerable afferent inputs from central and peripheral receptors (including medullary and pontine regulatory centers, baroreceptor and pulmonary stretch receptors) which control body functions such as blood pressure and pH, temperature and vocalization. It appears that the DRG integrates such homeostatic inputs and modulates respiratory drive accordingly.

Major advance in our understanding of the network properties of the respiratory rhythm generator followed the introduction of the isolated rat brain stem-spinal cord preparation which allows the recording of respiratory motor drive *in vitro* (Suzue, 1984).

Further development of an isolated brain stem slice preparation has been essential for revealing the synaptic and cellular organization of the respiratory rhythm generating neurons. Use of such models have led to recent advances regarding the cellular network and functional characteristics of the rhythm generator in the brain stem (Smith et al., 1991; Koshiya and Smith, 1999). However, there has been great controversy as to whether respiratory rhythm is generated by a set of pacemaker cells or by a network model, where interacting excitatory and inhibitory neurons generate the rhythm similar to the network generating locomotor activity. Accumulating data supports a model where breathing is generated by a hybrid model, involving pacemaker cells embedded in a network (Smith et al., 1991; Koshiya and Smith, 1999). One important step in determining the cellular organization of the rhythm generator was identifying the respiratory network location within the VRG. Work in the Feldman laboratory has demonstrated that respiratory rhythm is generated within a specific area of the ventrolateral medulla called the pre-Bőtzinger complex (Smith et al., 1991). The pre-Bőtzinger complex, which contains primarily propiobulbar neurons, is localized caudal to the retrofacial nucleus and ventral to the nucleus ambiguus (Smith et al., 1991). In the isolated brain stem slice preparation, neurons in the pre-Bőtzinger complex generate periodic membrane depolarizations that are synchronized with respect to the respiratory motor output recorded at the hypoglossal nerve roots (Smith et al., 1991; Koshiya and Smith, 1999). Pharmacological experiments in the brain stem-spinal cord preparation indicate that respiratory rhythm is mediated by non-NMDA-mediated glutamatergic synaptic transmission, as both AMPA and kainate receptor blockers perturb rhythm generation (Greer et al., 1991; Funk et al., 1993). Synaptic inhibition does not appear essential for rhythm generation in the neonatal rat since inhibition of GABA or glycine receptors does not eliminate respiratory rhythm (Smith and Feldman, 1987; Onimaru et al., 1990).

Projections from several ponto-medullary structures including the locus coeruleus, raphe nucleus and pontine nuclei (including medial parabrachial and Kölliker-Fuse nuclei) converge and potentially regulate the respiratory rhythm generated in the VRG (Ellenberger et al., 1990; Dobbins and Feldman, 1994). Synaptic input from these areas outside the primary respiratory network plays a significant role in regulating the respiratory output in order to satisfy the different physiological demands of the organism. Besides the classic fast-acting excitatory and inhibitory amino acid neurotransmitters involved in rhythm and pattern generation, numerous neuromodulators have been shown to modulate respiratory synaptic activity. Serotonin, substance P and thyrotropin-releasing hormone, all play a facilitatory role in respiratory rhythm generation whereas opioids, noradrenaline and adenosine have been associated with depression of the central respiratory drive (Bennett et al., 1988; Lindsay and Feldman, 1993; Di Pasquale et al., 1994; Errchidi et al.,, 1991; Greer et al., 1995; Dong and Feldman, 1995; Reckling et al., 1996, Al-Zubaidy et al., 1996; Johnson et al., 1996).

Bulbospinal neurons in the rostral part of the VRG convey inspiratory rhythm to spinal PMNs (Ellenberger and Feldman, 1988; Dobbins and Feldman, 1994). In the rat spinal cord, PMNs are localized in the ventro-medial aspect of the ventral horn where they form a tight rostrocaudal column between the third and the sixth cervical segments (Lindsay et al., 1991; Allan and Greer, 1997b). During the inspiratory phase, PMNs receive glutamatergic excitatory drive which is primarily mediated via non-NMDA receptors (AMPA and kainate) with NMDA receptors contributing between 10-30% to the regulation of the inspiratory discharge amplitude (Greer et al., 1991; Liu et al., 1990). During the expiratory phase of respiration, PMN excitability is inhibited as a result of GABA- and glycine-mediated synaptic depression originating primarily from the the Bőtzinger complex (Merril and Fedorko, 1984; Ellenberger et al., 1990; Liu and Feldman, 1993). In adult PMNs, GABA-mediated opening of a Cl^- -mediated conductance causes a hyperpolarization of the membrane potential by promoting Cl^- influx. However, in neonatal PMNs, there is still considerable debate regarding whether the expiratory GABAergic drive evokes a depolarization of PMN membrane potential (Liu and Feldman, 1993; Su and Chai, 1998; Parkis et al., 1999). The GABA-mediated Cl^- efflux during early development is thought to result from the high concentration of intracellular Cl^- generated by an active inward transport (Zhang et al., 1991). Despite generating a depolarizing inward current, application of GABA or its agonist muscimol to the spinal cord reduced neuronal excitability (Su and Chai, 1998). This contradictory finding may be explained if inhibition of synaptic activity resulted from a large increase in the GABA-mediated Cl^- conductance which could shunt excitatory synaptic currents (Gao and Ziskind-Conhaim, 1995).

I-A. Embryonic development of the respiratory function

Fetal breathing movements (FBM) have been found in all mammals studied, including humans (starting at the 10th week of gestation), where phrenic and diaphragm activity has been associated with small tidal movements of tracheal fluid (reviewed by Boddy and Dawes, 1975). FBM are required for proper lung maturation during the fetal period (Harding et al., 1993; Kitterman, 1996). In the rat, inspiratory synaptic drive onto the PMN pool begins around embryonic (E) day 17 (gestational period in the rat is 21 days, see Fig. 1.1) (Greer at al., 1992). Anatomical tracing of brain stem axon trajectories shows that bulbospinal projections reach the phrenic pool around E17, coincident with the onset of PMN recruitment by the brain stem synaptic drive (Lakke, 1997). Recordings of the inspiratory motor drive from the fourth cervical segment, containing most of the PMN axonal output, indicate that the synaptic drive is initially very slow and irregular (Greer et al., 1992; Di Pasquale et al., 1996). During the following 4-5 days up to birth, there is a significant increase in the discharge frequency and amplitude of respiratory drive (Di Pasquale et al., 1996). Recent ultrasound recordings have confirmed that FBM commence at E17 and that the incidence and regularity of the movements increases prior to birth (Kobayashi & Greer, unpublished observations).

Breathing movements *in utero* are episodic and occur mainly during rapid eye movements (REM, Clewlow et al., 1983). Inhibition of FBM during non-REM periods may originate from midbrain or pontine structures as evidenced by lesions in those structures resulting in continuous breathing movements *in utero* (Gluckman and Johnston, 1987). The influence of midbrain and pontine structures on FBM are likely mediated by the action of neuromodulators since continuous FBM can be induced following treatment with 5-HT precursors, inhibitors of prostaglandin synthesis and thyrotropin-releasing hormone, whereas exposure to opiates reduces FBM (Wardlaw et al., 1979; Quilligan et al., 1981; Kitterman et al., 1979; Bennet et al., 1988).

An important aspect in the perinatal maturation of respiratory control is the response to hypoxia. *In utero*, hypoxia can induce depression of FBM and that effect can be reversed by lesion of the pons (Gluckman and Johnston, 1987) or red nucleus (Waites et al., 1996). In both newborns and adults, hypoxia causes a biphasic response consisting of an initial augmentation of respiratory activity followed by a secondary depression. However, the main difference in the response to hypoxia in newborns and adults lies in the magnitude of the secondary depression which is significantly greater in neonates (Bureau et al., 1984; Lawson and Long, 1983). The hypoxia-induced depression of respiratory movements in embryos and neonates would promote energy conservation in the presence of ATP depletion. The adult-type response to hypoxia is achieved within 2-3 weeks after birth and occurs as a result of poorly understood changes in the central respiratory network (Lawson and Long, 1983; Ramirez et al., 1997).

I-B. Morphological and functional maturation of PMNs

Tritiated thymidine analysis of cervical motoneuron birth date indicates that PMNs are born at approximately E11 (Altman and Bayer, 1984). By E11.5, their axons exit the spinal cord toward the primordial diaphragm (Fig. 1.1; Allan and Greer, 1997b). PMN axons reach the primordial diaphragm by E13. After a 24 hour waiting period, phrenic axons initiate intramuscular branching (Fig. 1.1). Intramuscular branching of the phrenic nerve generates three primary branches: crural, sternal and dorsolateral. This intramuscular branching is not random, rather phrenic axons establish a topographic map on the diaphragm. Phrenic motoneurons in the rostral extent of the phrenic pool within the spinal cord project to the sternal part of the diaphragm whereas more caudal motoneurons project to the dorsolateral and crural diaphragm (Laskowski and High, 1989; Laskowski and Owens, 1994).

Innervation of the target musculature and inception of respiratory drive at E17 (in the rat) coincides with, and may regulate, significant changes in the morphological organization of the phrenic pool. Following target innervation (between E15-E16), there is a significant loss of PMNs as a result of programmed neuronal cell death (Fig. 1.1; Harris and McCaig, 1984; Allan and Greer, 1997b). Programmed cell death results in the matching of the number of motoneurons to the available muscle fibers in a process that appears to be determined by presynaptic uptake of muscle-derived trophic factors (Oppenheim et al., 1978; reviewed by Oppenheim, 1991). Inception of inspiratory drive at E17 also correlates with a significant transformation of the PMN dendritic arbor and the arrival of afferent projections in the phrenic nucleus (Fig. 1.1; Allan and Greer, 1997b, Song et al., 1999). Between E18 and birth, dendrites projecting within the transverse plane begin to retract and the tightly bundled rostro-caudally projecting dendrites, which are believed to promote the synchronization of PMN discharge, begin to form.

By birth, PMNs have begun to approximate the morphological and electrophysiological features seen in adult motoneurons. However, significant maturational changes occur postnatally. Neonatal PMNs still have long ventro-medial and ventro-lateral dendritic projections into the white matter and there is still some midline crossing of ventromedial dendrites, which is not observed in adult PMNs (Lindsay et al., 1991, Allan and Greer, 1997b). As studies in cat and rat PMNs indicate, over the first few weeks after birth PMN electrical properties still undergo considerable changes (Cameron et al., 1991). The increase in cell size with age is accompanied by a reduction in input resistance and an increase in rheobase (Cameron et al., 1991). Concomitant with changes in the passive and repetitive firing properties, including a reduction in the spike half-width duration, there is a significant reduction in the number of PMNs recruited during an inspiratory burst during postnatal maturation. The high input resistance at birth guarantee that the majority of neonatal PMNs will be recruited during an inspiratory burst in order to generate adequate ventilation in newborns whereas with further development there is a refinement in the recruitment order to accommodate the various physiological demands on the respiratory system. Orderly recruitment of the approximately 240α PMNs innervating the diaphragm is required in order to achieve a smooth development of diaphragmatic force during inspiration and non-respiratory diaphragmatic movements (Allan and Greer, 1997b). Electrophysiological recordings from PMNs and electromyography (EMG) single motor unit recording from rat and cat diaphragms indicate the presence of subpopulations of motoneurons based upon their recruitment order (Berger, 1979; Jodkowski et al., 1987; Hayashi and Fukuda, 1995). Recruitment of PMNs, based on Henneman's size principle, is due to intrinsic properties of PMNs correlated to cell size (Henneman, 1957). However, differences of synaptic inputs may also influence the recruitment order of PMNs (Hilaire et al., 1983). Based upon their recruitment order, PMNs can be classified as early-recruited, late recruited and quiescent (not recruited under normal conditions, see below) (Torikai et al., 1996; Cameron et al., 1991). Recruitment order is determined by PMN input resistance (i.e., neuronal cell size) as motoneurons with the highest input resistance are recruited first, whereas low input resistance motoneurons (i.e., quiescent PMNs) will only be recruited for specific tasks requiring brief contractions such as sneezing or coughing.

I-C. Maturation of the diaphragm and the neuromuscular junction

Phrenic nerve innervation and inception of respiratory drive are two key events in the development of the diaphragm. From E14-E17, phrenic nerve innervation of the primordial diaphragm coincides with the migration and fusion of myoblasts during primary myogenesis (Allan and Greer, 1997a, 1998). By the time of the inception of the respiratory drive transmission at E17, the basic neuromuscular structure of the diaphragm has been established and the diaphragm is operational for the generation of FBM. Inception of respiratory drive coincides with the onset of secondary myogenesis and rapid muscular growth (Allan and Greer, 1997a, 1998). Major changes in the composition of the contractile apparatus of the diaphragm take place from E17 well into the postnatal period, particularly in the composition of the myosin heavy chain (MHC) expressed by diaphragmatic fibers. As biochemical studies indicate, there are at least six isoforms of MHCs (embryonic, neonatal, slow (or type 1), fast 2A, 2B and 2X) which are expressed at various stages of diaphragm muscle maturation (LaFramboise et al., 1990; Schiaffino and Reggiani, 1994 Watchko et al., 1992). The adult rat diaphragm has a mixed composition consisting of approximately 40% slow oxidative and 60% oxidative-glycolytic and fast glycolytic fibres (Padykula and Gauthier, 1967). The relatively proportional mix between slow and fast fibers could reflect both the need for resistance to fatigue and the need to increase contractility during periods of increased ventilation (i.e., during physical exercise) or forceful inspiratory movements (i.e., for sneezing, coughing, etc). During embryonic development, the diaphragm is largely composed of the embryonic/neonatal MHC isoforms, which are characterized by slow kinetics and high resistance to fatigue (LaFramboise et al., 1990; Johnson et al., 1994; Kelly et al., 1991; Lloyd et al., 1996; Sieck et al., 1991; Watchko et al., 1992). By birth, 30% of the embryonic/neonatal isoform has been replaced by the adult slow and fast isoforms which would, in part, explain the overall increase in speed of contraction during maturation of the diaphragm contractile properties (LaFramboise et al., 1990; Lloyd et al., 1996;Vasquez et al., 1993; Watchko et al., 1993). The adult MHC composition is not reached until approximately the first month of postnatal development in the rat (Watchko et al., 1992).

Concomitant with the postnatal changes in MHC expression, there are significant changes in the organization of the neuromuscular junction. In neonatal muscle, the frequency of miniature end plate potential (EPP) is lower compared to the adult. Further, acetylcholine sensitivity is present along the length of the muscle fibers, due to the presence of extrajunctional acetylcholine receptors (Diamond and Miledi, 1962). Recordings of the EPP responses indicate the existence of polyneuronal innervation in developing muscle fibers (Bennett and Pettigrew, 1974; Dennis et al., 1981; Rosenthal and Taraskevich, 1977). Polyneuronal innervation of diaphragmatic fibers is eliminated by the third week after birth (Redfern, 1970).

II. Development of electrical excitability in differentiating neurons

As discussed in the previous section, PMNs undergo considerable changes in their morphological and functional properties during the perinatal period. In this section, I will review some key aspects of neuronal differentiation that are relevant to the development of neuronal electrical excitability. Maturation of electrical excitability in developing neurons is characterized by three key features: changes in ion channel expression, generation of

Figure 1.1. Time-line indicating some of the key events involved in phrenic motoneuron-diaphragm development. The shaded area (E16 through P0-1) represents the period in which electrophysiological properties were studied. (Refs: 1. Allan and Greer, 1997a; 2. Allan and Greer, 1997b; 3. Greer et al., 1992).

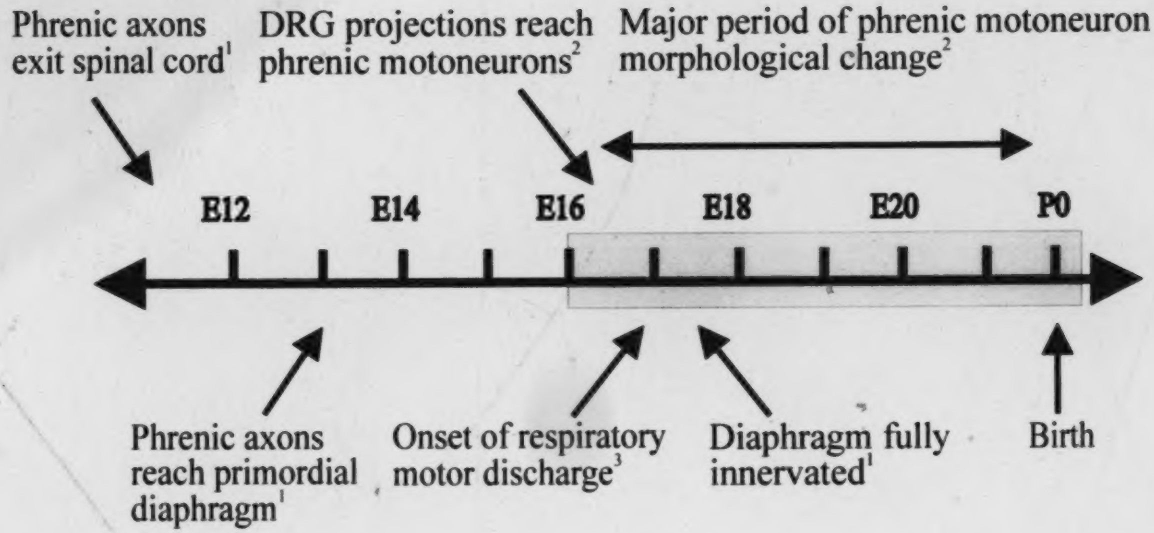
Phrenic axons exit spinal cord[1]
DRG projections reach phrenic motoneurons[2]
Major period of phrenic motoneuron morphological change[2]
E12
E14
E16
E18
E20
P0
Phrenic axons reach primordial diaphragm[1]
Onset of respiratory motor discharge[3]
Diaphragm fully innervated[1]
Birth

spontaneous electrical activity and expression of electrotonic coupling via gap junctions. The functional significance of these key features in neurodevelopment are the main topic of this and following sections. During development, electrical excitability is characterized by age-dependent, stereotyped changes in the expression of voltage-gated channels, most notably K^+ and Ca^{++} channels. Maturation of ion channel expression is not simply a progressive attainment of adult levels but is related to specific processes during neuronal differentiation (McCobb et al, 1989, 1990; Spigelman et al., 1992). In particular, the regulation of Ca^{++} influx by the interplay between K^+ and Ca^{++} conductances is critical for the maturation of the action potential and repetitive firing properties and morphological characteristics of developing neurons (see below) (Gu and Spitzer, 1995; Moody, 1998).

Voltage-gated Ca^{++} channels undergo considerable changes in their expression during development. In general terms, voltage-gated Ca^{++} channels supply the link between membrane potential and intracellular functions that either require Ca^{++} elevations as a trigger mechanism (i.e., exocytosis, muscle contractions), or are modulated by Ca^{++}-dependent signaling pathways (i.e., gene expression, cell division and migration). Depending upon their electrophysiological and pharmacological properties, Ca^{++} channels can be divided into low-voltage-activated (LVA) and high voltage-activated (HVA) Ca^{++} conductances (reviewed by Hille, 1992). LVA Ca^{++} channels are activated at low threshold potentials. They are also known as T-type Ca^{++} channels due to their transient activation and fast inactivation. HVA Ca^{++} channels require stronger depolarizations for activation and are divided into several subtypes, including L-, N-, P/Q- and R-type Ca^{++} channels. L-type Ca^{++} channels mediate large Ca^{++} currents with slow rates of voltage-dependent inactivation and are specifically inhibited by several compounds including dihydropyridines (nimodipine, nifedipine) and phenylalkylamines (verapamil). N–type Ca^{++} channels are inactivated at a wide range of voltages and are irreversibly inhibited by ω-conotoxin, from the cone snail *Conus geographus*. P/Q-type Ca^{++} channels also have slow inactivation and are preferentially blocked by low concentrations of the spider toxin ω-agatoxin.

The general pattern emerging from several studies in *Xenopus*, chick and mammalian spinal neurons is that the decrease in T-type Ca^{++} currents, present at very early ages of development, is compensated by a significant increase in the expression of HVA Ca^{++} currents (McCobb et al., 1989; Gu and Spitzer, 1993). These changes in the expression of specific Ca^{++} channels likely reflect their multiple roles in neuronal physiology. Early-expressed T-type Ca^{++} channels may be involved in the generation of transient Ca^{++} transients during early spinal neuron development (Gu and Spitzer, 1993). Due to their low threshold for activation, T-type Ca^{++} channels are more likely to depolarize the membrane potential and promote transient elevations of intracellular Ca^{++}. A change to primarily HVA Ca^{++} channels has several roles during maturation. First, Ca^{++} entry via HVA may limit axonal outgrowth by stabilizing growth cones. This may be required for the transformation of the axon terminal from a growing structure into a structure required for synaptic release (Mattson and Kater, 1987; McCobb and Kater, 1988). Second, appearance of HVA is postulated to be related to the phenomena of neuronal cell death, as expression of HVA Ca^{++} channels preceded motoneuron cell death in chick lumbar spinal cord (McCobb et al., 1989). Third, Ca^{++} influx via HVA Ca^{++} channels may regulate the firing pattern of developing neurons by regulating the expression of various spike afterpotentials including medium-duration afterhyperpolarizing and afterdepolarizing potentials (mAHP and ADP, respectively) (Walton and Fulton, 1986; Viana et al., 1993a,b; Gao and Ziskind-Conhaim, 1998).

Maturational changes in K^+ channel expression is also developmentally regulated and plays a critical role in regulating Ca^{++} influx during development. There are several families of voltage-gated K^+ channels including: i) the Kv (1-9, which included the typical outward rectifier and A-type K^+ channels); ii) inward rectifier (KIR); iii) maxi-type Ca^{++}-activated (slo), and iv) small conductance Ca^{++}-activated (SK1-3) K^+ channels (reviewed by Coetzee et al., 1999). This diversity is generated by the large number of genes that encode for the main K^+ channel subunit (the α-subunit). The general pattern emerging from several studies in *Xenopus*, chick and mammalian spinal neurons indicates that progressive upregulation of K^+ channel expression throughout development shortens action potential duration, resulting in an increase in repetitive firing (O'Dowd et al., 1988; Desarmenien et al., 1993; McCobb et al., 1991; Gao and Ziskind-Conhaim, 1998). The best characterized example of the developmental changes in action potential and repetitive firing properties, generated by changes in K^+ channel expression, is in *Xenopus* spinal neurons. At the time of neural tube closure, these neurons exhibit long duration, Ca^{++}-dependent action potentials (Baccaglini and Spitzer, 1977). At this initial stage, action potential duration is established by the balance of Ca^{++} and K^+ conductances as outward K^+ currents are very small and have a very slow activation rate, allowing an extended activation of inward Ca^{++} currents (Baccaglini and Spitzer, 1977; O'Dowd et al., 1988; Desarmenien et al., 1993; Gu and Spitzer, 1995). However, by the tailbud stage (24 hours after neural tube closure), the action potential is transformed into a brief, Na^+-dependent spike. This change is mediated by a significant increase in the expression of Na^+ and outward K^+ currents. Changes in the α-subunit expression and kinetics, in particular the Kv2.2 α-subunit, are responsible for changes in the properties of outward K^+ channels during this critical period of *Xenopus* electrical differentiation (Gu and Spitzer, 1995; Burger and Ribera, 1996; Gurantz et al., 1996). The increased density and faster activation of outward K^+ current results in a faster repolarization of the action potential and the limiting of Ca^{++} channel activation (O'Dowd et al., 1988; Desarmenien et al., 1993; Lockery and Spitzer, 1991). Similarly, during embryonic development of mammalian and chick motoneurons, upregulation of K^+ current density also provides the main drive for shortening of the action potential, thereby increasing repetitive firing (Ziskind-Conhaim, 1988; McCobb et al., 1990; Gao and Ziskind-Conhaim, 1998). By the time that chick (E4) and rat (E15) lumbar motoneurons are first identifiable by antidromic activation, the action potential is already Na^+-driven but a significant Ca^{++} component still persists (Ziskind-Conhaim, 1988; McCobb et al., 1990, Gao and Ziskind-Conhaim, 1998). Similar to changes observed in Xenopus, this Ca^{++}-dependent component is eliminated following upregulation of outward K^+ currents. However, species-specific differences in K^+ channel expression seem to be involved in the maturation of the action potential. A two-fold increase in the density of the outward rectifier as well as the onset of a Ca^{++}-activated K^+ conductances mediates the shortening of the action potential in rat lumbar motoneurons after E15 (Gao and Ziskind-Conhaim, 1998). In the chick, a similar result is obtained by a six-fold increase in the density of the transient, A-type K^+ conductance (McCobb et al., 1991).

In conclusion, expression of both K^+ and Ca^{++} channels is developmentally regulated. It is believed that, at early stages of development, the action potential may be completely dependent on Ca^{++} influx (Baccaglini and Spitzer, 1977) or may have a significant Ca^{++}-dependent component (Ziskind-Conhaim, 1988; McCobb et al., 1990). Upregulation of K^+ channel expression reduces Ca^{++} influx, transforming the action potential into a fast Na^+-dependent signal more suitable for inter-neuronal communication.

II-A. Role of electrical activity and Ca^{++} transients in regulating neuronal excitability during development

Regulation of ion channel expression (through changes in channel density and/or kinetics) has a significant effect on neuronal excitability and, thereby spontaneous electrical activity throughout development. It appears that both ion channel expression and electrical excitability are reciprocally related as the expression of specific conductances regulates spontaneous activity, and conversely, spontaneous activity regulates ion channel expression. Spontaneous electrical activity exhibits two phases during early neuronal differentiation. First, before synaptic networks have formed, individual or small clusters of electrotonically-coupled neurons express spontaneous bursts of activity (Yuste et al., 1995; Gu and Spitzer, 1995; Catsicas et al., 1998). In the best studied systems (i.e., retina, spinal cord, cortex), spontaneous electrical activity is accompanied by Ca^{++} transients (Wong et al., 1995; Holliday and Spitzer, 1990; Gu and Spitzer, 1995; Yuste et al., 1995). As studies in *Xenopus* spinal neurons indicate, during early neuronal differentiation (i.e., before synaptic contacts are established) spontaneous Ca^{++} transients can encode several aspects of neuronal differentiation (Holliday and Spitzer, 1990; Gu and Spitzer, 1995). In particular, Ca^{++} transients promote normal neurotransmitter expression (i.e., GABA), dendritic outgrowth and maturation of K^{+} channels, in a frequency-dependent manner (Gu and Spitzer, 1995). Ca^{++} influx, associated with spontaneous activity, appears to regulate transcriptional events as inhibition of protein synthesis may alter specific aspects of neuronal differentiation (Ribera and Spitzer; 1989; Gu and Spitzer, 1995; Finkbeiner and Greenberg, 1998).

After the establishment of synaptic contacts, spontaneous activity arises as the result of synaptic interactions between neurons within a specific network and by virtue of the intrinsic electrical properties of those neurons. In the majority of systems studied to date (i.e., retina, spinal cord, cortical structures), spontaneous electrical activity and the resultant Ca^{++} transients seem to arise from a state of general neuronal hyperexcitability. This originates from several factors, including: i) the depolarizing nature of inhibitory neurotransmitters during early development (i.e., GABA and glycine); ii) transient expression of electronic coupling between neurons; iii) enhanced expression of glutamate and T-type Ca^{++} channels, and iv) excess innervation (Obata et al., 1978; McCobb et al., 1989; Wu et al., 1992; Peinado et al., 1993; Kalb et al., 1992; Penn et al., 1994; Jakowec et al., 1995; Wong et al., 1998; Catsicas et al., 1998). After the establishment of inter-neuronal connections in the retina and spinal cord, synaptic release appears to be an important component in the generation of spontaneous activity (Landmesser and O'Donovan, 1984; Milner and Landmesser, 1999; Wong et al., 2000). However, the synaptic mechanisms responsible for generating spontaneous activity and Ca^{++} transients seems to undergo critical changes during maturation. For example, the excitatory neurotransmission driving retinal ganglion cell bursting activity undergoes a shift from cholinergic to glutamatergic transmission in the retina (Wong et al., 2000). Similarly, in the chick spinal cord, spontaneous activity is initially driven by acetylcholine during the onset of motoneuron interaction with target musculature (Milner and Landmesser, 1999). However, after hindlimb innervation (E7-10), spontaneous motoneuron activity becomes episodic and coordinated, with a rudimentary locomotive pattern of alternating flexor and extensor bursts driven by glutamate and shaped by GABA, glycine and acetylcholine (Landmesser and O'Donovan, 1984; Chub and O'Donovan, 1998).

Functionally, intracellular Ca^{++} oscillations associated with synchronized electrical activity are critical for the functional wiring of neuronal circuits in the retina, spinal cord and cortical structures at this stage (reviewed by Wong, 1999; O'Donovan et al., 1998; Yuste et al., 1992). In the retina, activity-dependent processes mediates the segregation of retinal ganglion fibers into eye-specific layers in the lateral geniculate nucleus and the development of ocular dominance columns in the primary visual cortex even before eye opening (reviewed by Katz and Shatz, 1996; Wong et al., 1998; Sernagor and Grzywacz, 1994; Mooney et al., 1996; Galli and Maffei, 1988). In the spinal cord, early spontaneous activity is required at the onset of axon and muscle interactions for critical aspects of neuromuscular development. These include the establishment of the neuromuscular junction and axon branching, regulation of motoneuron cell death, modification of muscle fiber contractile properties and elimination of polyneuronal innervation at the neuromuscular junction (Navarrete and Vrbova, 1993).

II-B. Role of gap junctions and electrotonic coupling during development

Gap junctions are an important factor in the regulation of electrical excitability during neuronal development. Electrotonic coupling via gap junctions is generated by a channel-like structure composed of aggregated connexin molecules. These intercellular channels allow the passage of electrical current and small molecules (<2000 Da) between coupled cells. Accumulating evidence indicates that electrotonic coupling via gap junctions is a common feature throughout the development of the nervous system (Walton and Navarrete, 1991; Mazza et al., 1992; Christie and Jelinek, 1993; Perrins and Roberts, 1995, reviewed by Kandler and Katz, 1995). Furthermore, blockade of gap junctions leads to impaired development of the nervous system in amphibian embryos (Warner et al., 1984). Gap junction expression plays numerous roles during development. First, gap junctions serve as a form of intercellular communication allowing the exchange of signaling molecules (such as cAMP and inositol 1,4,5-triphosphate) and/or essential nutrients. Second, electrical coupling via gap junctions coordinates the propagation of electrical excitability between coupled neurons either by allowing the passage of electrical currents or biochemical signals (Perrins and Roberts, 1995; Kandler and Katz, 1998). Gap junction-mediate boosting of electrical excitability of coupled neurons is particularly important for the propagation of spontaneous activity and Ca^{++} transients during early development of the retina, spinal cord and neocortex (see below, Peinado et al., 1993; Penn et al., 1994; Wong et al., 1998; Catsicas et al., 1998). Regulation of electrical and/or chemical signals through gap junctions may have a significant effect on matching functionally related neuronal populations. Thus, transient expression of gap junctions in embryonic/neonatal mammalian motoneurons may be required for the synchronization of motor activity between synergistic motoneurons during maturation of locomotor function (Walton and Navarrete, 1991). Adult motoneurons such as genioglossals, lumbar and phrenics are devoid of electrotonic coupling (Lipski, 1984; Mazza et al., 1992; Walton and Navarrete, 1991). The lack of electrotonic coupling in adult motoneurons is likely dictated by the need for graded and independent recruitment of motor units required during fine motor tasks (Walton and Navarrete, 1991).

II-C. Role of target-derived trophic factors in regulating electrical excitability during development

Besides spontaneous electrical activity and Ca^{++} oscillations, neuronal differentiation and ion channel expression can be regulated by growth factors. As studies in cerebellum and chick ciliary ganglion neurons indicate, afferent and target innervation by growing axons is pivotal to the expression of specific channel subunits. It appears that putative substances (e.g., trophic factors) released by the target act as a retrograde signal in defining the electrical specificity of the innervating neurons. In cerebellar neurons, expression of Kv3.1 α-subunit isoforms is developmentally-regulated. Functionally, Kv3.1 α-subunit regulates the excitability of rapidly firing neurons, such as fast-spiking GABAergic interneurons in the neocortex and cerebellum (Messengill et al., 1997; Liu and Kaczmarec, 1998a; Wang et al., 1998). In cerebellar neurons, the Kv3.1a isoform of the α-subunit is expressed immediately after birth (Perney et al., 1992). In contrast, Kv3.1b expression increases during the postnatal period (P8-P14) when major functional changes of the cerebellum occur. There is evidence that the increased expression of Kv3.1b is activity-dependent and involves regulation by endogenously expressed trophic factors in an activity-dependent manner (Liu and Kaczmarec, 1998b). Thus, treatment of cerebellar slices with basic fibroblast growth factor (bFGF) and high K^+- membrane induced depolarization selectively increases the expression of Kv3.1b mRNA. In contrast, similar treatment inhibits the expression of Kv3.1a isoform (Liu and Kaczmarec, 1998a).

In the chick ciliary ganglion, functional expression of Ca^{++}-activated K^+ conductance requires interaction with the target tissue and afferent preganglionic innervation (reviewed by Dryer, 1998). The role of target innervation in upregulating Ca^{++}-activated K^+ conductance expression can be mimicked *in vitro* by exposure to target tissue extracts. This appears to be mediated by expression of basic fibroblast growth factor (bFGF) in the target tissues (Subramony and Dryer, 1996; Cameron et al., 1998). On the contrary, upregulation of Ca^{++}-activated K^+ conductance expression by afferent preganglionic innervation involves β1-neuroregulin (Subramony and Dryer, 1997). Upregulation of Ca^{++}-activated K^+ conductance via bTGF and β-neuregulin seems to occur at the postranslational level as inhibition of protein synthesis does not prevent its expression.

III. Rationale for studying the functional maturation of the respiratory neuromuscular system

PMN and diaphragm functional properties must attain a relatively high degree of maturation by birth as generation of inspiratory movements is essential for the survival of the organism by birth. In fact, the PMN-diaphragm axis generates breathing movements *in utero* (Jansen and Chernick, 1991). There is an increasing interest in understanding the developmental processes associated with the maturation of the respiratory neuromuscular system which occur in conjunction with fetal respiratory drive and the potential link between the suppression of this drive (e.g., as a result of fetal exposure to hypoxia, alcohol, opiates, cigarette smoke) and subsequent neonatal respiratory disorders. For instance, it is known that lung distension associated with FBM *in utero* is essential for proper lung maturation (Miller et al., 1993; Harding et al., 1993; Kitterman, 1996).

The primary objective of the work presented here is to understand the maturation of the electrical properties of PMNs and the contractile properties of the diaphragm during the major morphological and functional transformation of the respiratory system *in utero*. The period chosen for this investigation spans from embryonic day 16 (E16) to postnatal day 1 (P1), which coincide with a period of major morphological and functional maturation of the PMN-diaphragm neuromuscular system (see shadow area in Fig. 1.1). At E17, PMNs commence receiving inspiratory drive from the brain stem (Greer et al., 1992). Concomitant with the inception of functional recruitment there are some major morphological changes including completion of target innervation and dendritic reorganization (Allan and Greer, 1997a,b). Therefore, the specific hypotheses tested herein were as follows:

1) During the critical period of functional and morphological maturation of the respiratory system, there will be concomitant maturational changes in the electrical properties of PMNs, including changes in the passive membrane properties and repetitive firing pattern of PMNs **(Chapter III)**.

2) Maturation of PMN electrical properties, in particular, elaboration of action potential afterpotentials and the resulting changes in the repetitive firing properties are due to developmental changes in the expression K^+ and Ca^{++} conductances **(Chapters IV and V)**. **3)** Changes in the electrical properties of the PMNs will occur concomitantly with changes in the diaphragm muscle properties and neuromuscular junction end plate potentials in order to accommodate for differences in firing pattern of PMNs during the perinatal period **(Chapter VI)**.

Development of electrical and functional properties of spinal neurons have been previously described in a number of systems, including cultured preparations of dissociated chick motoneurons (McCobb et al., 1989,1990; Xie and Ziskind-Conhaim, 1995), rat spinal explants (Xie and Ziskind-Conhaim, 1995), and acutely isolated spinal cord segments (Fulton and Walton, 1986; Ziskind-Conhaim, 1988; Di Pasquale et al., 1996). These system have their specific advantages and limitations. Dissociated neurons allow for manipulations of the external environment for studying the role of external factors on motoneuron development. However, the electrical properties of motoneurons may be perturbed by the isolation procedure (as the result of removal of the dendritic arbor) and it is unlikely that motoneurons will undergo similar developmental transformation in isolation as they would in their natural external milieu. The use of cultured spinal cord slices offer the advantage of being able to alter the growing conditions without removing the three-dimensional organization of the developing system. However, the chronic removal of the descending inputs and target tissue are known to perturb the normal course of development. Beside overcoming these limitations, the present study of PMN development in an acutely isolated spinal cord slice compliments the past work by offering two important advantages. First, our recordings are restricted to one class of functionally identified mammalian motoneurons rather than pooling data from mixed populations within a given spinal cord region. The PMN population consists of ~240 functionally homogeneous motoneurons which innervate a single muscle (Allan and Greer,1997b). In contrast, when examining the development of mixed populations within cervical or lumbar ventral horns, one has to contend with a myriad of functionally heterogeneous motoneurons which innervate multiple muscles that develop at differing rates (Landmesser, 1992). Second, the functional relevance of changes in PMN electrophysiological properties is placed in the overall context of our past findings regarding phrenic nerve-diaphragm development such as axon outgrowth, target innervation, functional recruitment and morphological changes (Greer et al., 1992; Allan and Greer, 1997a,b). Information regarding these aspects were not available in past studies of motoneuron development. Collectively, the data from the various studies of PMN-diaphragm ontogeny will lay the foundation for providing an understanding of how multiple aspects of a single mammalian neuromuscular system develop in concert during the perinatal period. A clear understanding of the changes in PMN electrophysiological properties and diaphragm contractile properties will be an essential aspect of this overall goal.

REFERENCES

ALLAN, D.W., GREER, J.J. (1997a) Embryogenesis of the phrenic nerve and diaphragm in the fetal rat. J. Comp. Neurol. 382: 459-468.

ALLAN, D.W., GREER, J.J. (1997b) Development of phrenic motoneuron morphology in the fetal rat. J. Comp. Neurol. 381: 469-479.

ALLAN, D.W., GREER, J.J. (1998) polysialylated NCAM expression during motor axon outgrowth and myogeneisis in the fetal rat. J. Comp. Neurol. 391: 275-292.

ALTMAN, J., BAYER, S.A. (1984) The development of the rat spinal cord. Adv. Anat. Embryol. Cell Biol. 85: 1-164.

AL-ZUBAIDY, Z.A., ERICKSON, R.L., GREER, J.J. (1996) Serotonergic and noradrenergic effects on respiratory neural discharge in the medullary slice. Pflugers Archiv (European Journal of Physiology) 431: 942-949.

BACCAGLINI, P.I., SPITZER, N.C. (1977) Developmental changes in the inward current of the action potential of Rohon-Beard neurones. J. Physiol. 271: 93-117.

BALLANYI, K., ONIMARU, H., HOMMA, I. (1995) Respiratory network function in the isolated brainstem-spinal cord of newborn rats. Progress in Neurobiol. 59: 583-634.

BENNETT, M.R., PETTIGREW, A.G. (1974) The formation of synapses in striated muscle during development. J. Physiol. 241: 515-545.

BENNET, L., GLUCKMAN, P.D., JOHNSTON, B.M. (1988) The central effects of thyrotropin-releasing hormone on the breathing movements and electrocortical activity of the fetal sheep. Pediatr. Res. 23: 72-75.

BERGER, A.J. (1979) Phrenic motoneurons in the cat: subpopulations and nature of respiratory drive potential. J. Neurophysiol. 42: 76-80.

BIANCHI, A.L., DENAVIT-SAUBIE, M., CHAMPAGNAT, J. (1995) Central control of breathing in mammals: neuronal circuitry, membrane properties and neurotransmitters. Physiol. Rev. 75: 1-45.

BODDY, K., DAWES, G.S. (1975) Fetal breathing. Br. Med. Bull. 31: 3-7.

BURGER, C., RIBERA, A.B. (1996) *Xenopus* spinal neurons express Kv2 potassium channel transcripts during embryonic development. J. Neurosci. 16 (4): 1412-1421.

BUREAU, M.A., ZINMAN, R., FOULON, P., BEGIN, P. (1984) Diphasic ventilatory response to hypoxia in the newborn lamb. J. Appl. Physiol. 56: 84-90.

CAMERON, J.S., LHUILLIER, L, SUBRAMONY, P., DRYER, S.E. (1998) Developmental regulation of neuronal K^+ channels by target-derived TGFbeta in vivo and in vitro. Neuron 21: 1045-1053.

CAMERON, W.E., JODKOWSKI, J.S., FANG, H., GUTHRIE, R.D. (1991) Electrophysiological properties of developing phrenic motoneurons in the cat. J. Neurophysiol. 65: 671-679.

CATSICAS, M., BONNESS, V., BECKER, D., MOBBS, P. (1998) Spontaneous Ca2+ transients and their transmission in the developing chick retina. Curr. Biol. 8(5): 28328-28336.

CHRISTIE, M.J., JELINEK, H.F. (1993) Dye-coupling among neurons of the rat locus coeruleus during postnatal development. Neurosci. 56(1): 129-137.

CHUB, N., O'DONOVAN, M.J. (1998) Blockade and recovery of spontaneous rhythmic activity after application of neurotransmitter antagonists to spinal networks of the chick embryo. J. Neurosci. 18(1): 294-306.

CLEWLOW, F., DAWES, G.S., JOHNSTON, B.M., WALKER, D.W. (1983) Changes in the breathing, electrocortical and muscle activity in unanesthetized fetal lambs with age. J. Physiol. 341: 463-476.

COETZEE W.A., AMARILLO, Y., CHIU, J., CHOW, A., LAU, D., MCCORMACK, T., MORENO, H., NADAL, M.S., OZAITA, A., POUNTNEY, D., SAGANICH, M., VEGA-SAENZ DE MIERA, E., RUDY, B. (1999) Molecular diversity of K+ channels. Ann. New York Acad. Sci. 868: 233-285.

DENNIS, M.J., ZISKIND-CONHAIM, D., L., HARRIS, A.J. (1981) Development of neuromuscular junctions in rat embryos. Dev. Biol. 81: 266-279.

DI PASQUALE, E., TELL, F., MONTEAU, R., HILAIRE, G. (1996) Perinatal developmental changes in respiratory activity of medullary and spinal neurons: an in vitro study on fetal and newborn rats. Devel. Br. Res. 91: 121-130.

DI PASQUALE, E., TELL, F., MONTEAU, R., HILAIRE, G. (1994) Endogenous serotonin modulates the fetal respiratory rhythm: an in vitro study in the rat. Devel. Br. Res. 80: 222-232.

DRYER, S.E. (1998) Role of cell-cell interactions in the developmental regulation of Ca^{2+}-activated K^+ currents in vertebrate neurons. J. Neurobiol. 37(1): 23-36.

DESARMENIEN, M.G., CLENDENING, B., SPITZER, N.C. (1993) In vivo development of voltage-dependent ionic currents in embryonic *Xenopus* spinal neurons. J. Neurosci. 13(6): 2575-2581.

DIAMOND, I., MILEDI, R. (1962) A study of foetal and new-born rat muscle fibres. J. Physiol. 152: 393-408.

DOBBINS, E.G., FELDMAN, J.L. (1994) Brainstem network controlling descending drive to phrenic motoneurons in rat. J. Comp. Neurol. 347: 64-86.

DONG, X-W., FELDMAN, J.L. (1995) Modulation of inspiratory drive to phrenic motoneurons by presynaptic adenosine A1 receptors. J. Neurosci. 15(5): 3458-3467.

ELLENBERGER, H.H., VERA, P.L., HASELTON, J.R., HASELTON, C.L., SCHNEIDERMAN, N. (1990) Brainstem projections to the phrenic nucleus: an anterograde and retrograde HRP study in the rabbit. Br. Res. Bull. 24: 163-174.

ELLENBERGER, H.H., FELDMAN, J.L. (1988) Monosynaptic transmission of respiratory drive to phrenic motoneurons from brainstem bulbospinal neurons in rat. J. Comp. Neurol. 269: 47-57.

ERRCHIDI, S., MONTEAU, R., HILAIRE, G. (1991) Noradrenergic modulation of the medullary respiratory rhythm generator in the newborn rat: an in vitro study. J. Physiol. (Lond.) 443: 477-498.

FELDMAN, J.L. (1986) Neurophysiology of breathing in mammals. In: Handbook of Physiology, Section 1: The nervous system; Vol. IV: Intrinsic regulatory Systems of the brain. Edd. F.E. Bloom, pp. 463-524. American Physiological Society, Bethesda, MD.

FINKBEINER, S., GREENBERG, M.E. (1998) Ca^{2+} channel-regulated neuronal expression. J. Neurobiol. 37(1): 171-187.

FULTON, B.P., WALTON, K. (1986) Electrophysiological properties of neonatal rat motoneurons studied in vitro. J. Physiol. (London) 370: 651-678.

FUNK, G.D., SMITH, J.C., FELDMAN, J.L. (1993) Generation and transmission of respiratory oscillations in medullary slices: role of excitatory amino acids. J. Neurophysiol. 70: 1497-1515.

GALLI, L., MAFFEI, L. (1988) Spontaneous impulse activity of rat retinal ganglion cells in prenatal life. Science 242: 90-1.

GAO, B.X., ZISKIND-CONHAIM, L. (1998) Development of ionic currents underlying changes in action potential waveforms in rat spinal motoneurons. J. Neurophysiol. 80(6): 3047-3061.

GAO, B.X., ZISKIND-CONHAIM, L. (1995) Development of glycine- and GABA-gated currents in rat spinal motoneurons. J. Neurophysiol. 74(1): 113-121.

GLUCKMAN, P.D., JOHNSTON, B.M. (1987) Lesion in the upper lateral pons abolish the hypoxic depression of breathing in unanesthetized fetal lambs *in utero*. J. Physiol. 382: 373-383.

GREER, J.J, SMITH, J.C., FELDMAN, J.L. (1991) Role of excitatory amino acids in the generation and transmission of respiratory drive in neonatal rat. J. Physiol. 437: 727-749.

GREER, J.J, CARTER, J.E., AL-ZUBAIDY, Z. (1995) Opioid depression of respiration in neonatal rats. J. Physiol. 485.3: 845-855.

GREER, J.J, SMITH, J.C., FELDMAN, J.L. (1992) Respiratory and locomotor patterns generated in the fetal rat brain stem-spinal cord in vitro. J. Neurophysiol. 67(4): 996-999.

GU, X., SPITZER, N.C. (1995) Distinct aspects of neuronal differentiation encoded by frequency of spontaneous Ca^{2+} transients. Nature 375: 784787.

GU, X., SPITZER, N.C. (1993) Low-threshold Ca^{2+} currents and its role in spontaneous elevations of intracellular Ca^{2+} in developing *Xenopus* neurons. J. Neurosci. 13 (11): 4936-4948.

GURANTZ, D., RIBERA, A.B., SPITZER, N.C. (1996) Temporal regulation of Shaker- and Shab-like potassium channel gene expression in single embryonic spinal neurons during K+ current development. J. Neurosci. 16 (10): 3287-3295.

HARDING, R., HOOPER, S.B., VAN, V.K. (1993) Abolition of fetal breathing movements by spinal cord transection leads to reductions in fetal lung volume, lung growth and IGF-II gene expression. Pediatr. Res. 34: 148-153.

HARRIS, A.J., MCCAIG, D.C. (1984) Motoneuron death and motor unit size during embryonic development of the rat. J. Neurosci. 4(1): 13-24.

HAYASHI, F., FUKUDA, Y. (1995) Electrophysiological properties of phrenic motoneurons in adult rats. Japn. J. Physiol. 45: 69-83.

HENNEMAN, E. (1957) Relation between size of neurons and their susceptibility to discharge. Science 126: 1345-1347.

HILAIRE, G., GAUTHIER, R.P., MONTEAU, R. (1983) Central inspiratory drive and recruitment order of phrenic and inspiratory laryngeal motoneurons. Resp. Physiol. 51: 341-359.

HILLE, B. (1992) Calcium channels. In: Ionic channels of excitable membranes (II Edit.). Sinauer Associates Inc. Massachusetts, USA, pp 83-114.

HOLLIDAY, J., SPITZER, N.C. (1990) Spontaneous calcium influx and its role in differentiation of spinal neurons in culture. Dev. Biol. 141: 13-23.

IWASAKI, S., TAKAHASHI, T. (1998) Developmental changes in calcium channel types mediating synaptic transmission in rat auditory brainstem. J. Physiol. 509.2: 419-423.

JAKOWEC, M.W., KALB, R.G., MARTIN, L.J., FOX, A.J. (1995) Quantitative and qualitative changes in AMPA receptor expression during spinal cord development. Neurosci. 67: 893-907.

JANSEN, A.H., CHERNICK, V. (1991) Fetal breathing and development of control of breathing. J. Appl. Physiol. 70: 1431-1446.

JODKOWSKI, J.S., GUTHRIE, R.D., CAMERON, W.E. (1987) The activity pattern of phrenic motoneurons during the aspiration reflex: an intracellular study. Brain Res. 505: 105-124.

JOHNSON, S.M., SMITH, J.C., FELDMAN, J.L. (1996) Modulation of respiratory rhythm in vitro: role of $G_{i/o}$ protein-mediated mechanisms. J. Appl. Physiol. 80: 2120-2133.

JOHNSON, B.D., WILSON, L.E., ZHAN, W.Z., WATCHKO, J.F., DAOOD, M.J., SIECK, G.C. (1994) Contractile properties of the developing diaphragm correlate with myosin heavy chain phenotype. J. Appl. Physiol. 77: 481-487.

KALB, R.G., LIDOW, M.S., HALSTED, M., HOCKFIELD, S. (1992) N-methyl-D-aspartate receptors are transiently expressed in the developing spinal cord. Proc. Natl. Acad. Sci. USA 89: 8502-8506.

KANDLER, K., KATZ, L.C. (1998) Coordination of neuronal activity in developing visual cortex by gap junction-mediated biochemical communication. J. Neurosci. 18(4): 1419-1427.

KANDLER, K., KATZ, L.C. (1995) Neuronal coupling and uncoupling in the developing nervous system. Current Opin. Neurobiol. 5: 98-105.

KATZ, L.C., SHATZ, C.J. (1996) Synaptic activity and the construction of cortical circuits. Science 274: 1133-1138.

KELLY, A.M., ROSSER, W.C., HOFFMAN, R., PANETTIERI, R.A., SCHIAFFINO, S., RUBINSTEIN, N.A., NEMETH, P.N. (1991) Metabolic and contractile protein expression in diaphragm muscle. J. Neurosci. 11(5): 1231-1242.

KITTERMAN, J.A. (1996) The effects of mechanical forces on fetal lung growth. Clinics in Perinatology 23: 727-740.

KITTERMAN, J.A., LIGGINS, G.C., CLEMENTS, J.A., TOOLEY, W.H. (1979) Stimulation of breathing movements in fetal lambs by inhibitors of prostaglandin synthesis. J. Dev. Biol. 1: 453-466.

KOSHIYA, N., SMITH, J.C. (1999) Neuronal pacemaker for breathing visualized in vitro. Nature 400: 360-363.

LAKKE, A.E. (1997) The projections to the spinal cord of the rat during development: a timetable of descent. In: Advances in anatomy, embryology and cell biology, vol. 135, pp. 1-143. New York, Springer-Verlag.

LAFRAMBOISE, W.A., DAOOD, M.J., GUTHRIE, R.D., BUTLER-BROWNE, G.S., WHALEN, R.G., ONTELL, M. (1990) Myosin isoforms in neonatal rat extensor digitorum longus, diaphragm and soleus muscles. Am. J. Physiol. 259(2 part 1): L116-L122.

LANDMESSER, L.T. (1992) Growth cone guidance in the avian limb: a search for cellular and molecular mechanisms. In: The nerve growth cone. Eds. P.C. Letourneau, S.B. Kater and E.R. Macagno, Raven Press, N.Y. pp. 373-386.

LANDMESSER, L.T., O'DONOVAN, M.J. (1984) Activation patterns of embryonic chick hindlimb muscles recorder *in ovo* and in an isolated spinal cord preparation. J. Physiol. 347: 189-204.

LASKOWSKI, M.B., HIGH, J.A. (1989) Expression of nerve-muscle topography during development. J. Neurosci. 9(1): 175-182.

LASKOWSKI, M.B., OWENS, J.L. (1994) Embryonic expression of motoneurons topography in the rat diaphragm. Dev. Biol. 166: 502-508.

LAWSON, E.E., LONG, W.W. (1983) Central origin of diphasic breathing pattern during hypoxia in newborns. J. Appl. Physiol. 55: 483-488.

LINDSAY, A.D., FELDMAN, J.L. (1993) Modulation of respiratory activity of neonatal rat phrenic motoneurons by serotonin. J. Physiol. 461: 213-233.

LINDSAY, A.D., GREER, J.J., FELDMAN, J.L. (1991) Phrenic motoneuron morphology in the neonatal rat. J. Comp. Neurol. 308: 169-179.

LIPSKI, J. (1984) Is there electrical coupling between phrenic motoneurons in cats? Neurosci. Lett. 46: 229-234.

LIU, G., FELDMAN, J.L., SMITH, J.C.D. (1990) Excitatory amino acid-mediated transmission of inspiratory drive to phrenic motoneurons. J. Neurophysiol. 64: 423-436.

LIU, G., FELDMAN, J.L. (1993) Bulbospinal transmission of respiratory drive to phrenic motoneurons. In: Respiratory control: central and peripheral mechanisms. Edd. Speck, DF., Dekin, M.S., Revelette, W.R., Frazier, D.T. The University of Kentucky Press. pp 47-51.

LIU, S.J., KACZMAREK, L.K. (1998a) The expression of two splice variants of the Kv3.1 potassium channel gene is regulated by different signaling pathways. J. Neurosci. 18(7): 2881-2890.

LIU, S.J., KACZMAREK, L.K. (1998b) Depolarization selectively increases the expression of the Kv3.1 potassium channel in developing inferior colliculus neurons. J. Neurosci. 18(21): 8758-8769.

LLOYD, J.S., BROZANSKI, B.S., DAOOD, M.J., WATCHKO, J.F. (1996) Developmental transitions in the myosin heavy chain phenotype of human respiratory muscle. Biology of the Neonate 69(2): 67-75.

LOCKERY R.S., SPITZER, N.C. (1991) Reconstruction of the action potential development from the whole-cell currents of differentiating spinal neurons. J. Neurosci. 12(6): 2268-2287.

MATTSON, M.P., KATER, S.B. (1987) Calcium regulation of neurite elongation and growth cone motility. J. Neurosci. 7: 4034-4043.

MAZZA, E., NÙÑEZ-ABADES, P.A., SPIELMANN, J.M., CAMERON, W.E. (1992) Anatomical and electrotonic coupling in developing genioglossal motoneurons of the rat. Brain Res. 598: 127-137.

MCCOBB, D.P., KATER, S.B. (1988) Membrane voltage and neurotransmitter regulation of neuronal growth cone motility. Dev. Biol. 130: 599-609.

MCCOBB, D.P., BEST, P.M., BEAM, K.G. (1989) Development alters the expression of calcium currents in chick limb motoneurons. Neuron 2: 1633-1643.

MCCOBB, D.P., BEST, P.M., BEAM, K.G. (1990) The differentiation of excitability on embryonic chick limb motoneurons. J. Neurosci. 10: 2974-2984.

MERRIL, E.G., FEDORKO, L. (1984) Monosynaptic inhibition of phrenic motoneurons: a long descending projection from Botzinger neurons. J. Neurosci. 4: 2350-2353.

MESSENGILL, J.L., SMITH, M.A., SON, D.I., O'DOWD, D.K. (1997) Differential expression of K4-AP currents and Kv3.1 potassium channel transcripts in cortical neurons that develop distinct firing phenotypes. gene is regulated by different signaling pathways. J. Neurosci. 17(9): 3136-3147.

MILLER, A.A., HOOPER, S.B., HARDING, R. (1993) Role of fetal breathing in control of fetal lung distension. J. Appl. Physiol. 75(6): 2711-2717.

MILNER, L.D., LANDMESSER, L.T. (1999) Cholinergic and GABAergic inputs drive patterned spontaneous motoneurons activity before target innervation. J. Neurosci. 19(8): 3007-3022.

MOODY, W.J. (1998) The development of voltage-gated ion channels and its relation to activity-dependent developmental events. Current Topics in Dev. Biol. 39: 159-185.

MOONEY, R., PENN, A.A., GALLEGO, R., SHATZ, C.J. (1996) Thalamic relay of spontaneous retinal activity prior to vision. Neuron 17(5): 863-74.

NAVARRETE, R., VRBOVA, G. (1993) Activity-dependent interactions between motoneurons and muscles: their role in the development of the motor unit. Progress in Neurobiol. 41: 93-124.

OBATA, K., OIDE, M., TANAKA, H. (1978) Excitatory and inhibitory actions of glycine on embryonic chick spinal neurons in culture. Brain Res. 144: 179-184.

O'DONOVAN, M.J., CHUB, N., WENNER, P. (1998) Mechanisms of spontaneous activity in developing spinal networks. J. Neurobiol.37(1): 131-45.

O'DOWD, D.K., RIBERA, A.B., SPITZER, N.C. (1988) Development of voltage-dependent calcium, sodium and potassium currents in *Xenopus* spinal neurons. J. Neurosci. 8(3): 792-805.

ONIMARU, H., ARATA, A., HOMMA, I. (1990) Inhibitory synaptic inputs to the respiratory rhythm generator in the medulla isolated from newborn rats. Pflügers Arch. 417: 425-432.

OPPENHEIM, R.W. (1991) Cell death during development of the nervous system. Annu. Rev. Neurosci. 14: 453-501.

OPPENHEIM, R.W., CHU-WANG, I.W., MADERDRUT, JL (1978) Cell death of motoneurons in the chick embryo spinal cord. III. The differentiation of motoneurons prior to their induced degeneration following limb-bud removal. J. Comp. Neurol. 177: 87-112.

PADYKULA, H.A., GAUTHIER, G.F. (1967) Ultrastructural features of the three fiber types in the rat diaphragm. Anat. Rec. 157: 296-297.

PARKIS, M.A., DONG, X-W., FELDMAN, J.L., FUNK, G.D. (1999) Concurrent inhibition and excitation of phrenic motoneurons during inspiration: phase-specific control of excitability. J. Neurosci. 19(6): 2368-2380.

PEINADO, A., YUSTE, R., KATZ, L.C. (1993) Extensive dye coupling between rat neocortical neurons during the period of circuit formation. Neuron 10(1): 103-1014.

PENN, A.A., WONG, R.O., SHATZ, C.J. (1994) Neuronal coupling in the developing mammalian retina. J. Neurosci. 14(6): 3805-3815.

PERNEY, T.M., MARSHALL, J., MARTIN, K.A., HOCKFIELS, S., KACZMAREK, L.K. (1992) Expression of mRNA for the Kv3.1 potassium channel gene in the adult and developing rat brain. J. Neurophysiol. 3: 756-766.

PERRINS, R., ROBERTS, A. (1995) Cholinergic and electrical synapses between synergistic spinal motoneurons in the *Xenopus* leavis embryo. J. Physiol. 485.1: 135-144.

QUILLIGAN, E., CLEWLOW, F., JOHNSTON, B.M., WALKER, D.W. (1981) Effects of 5-hydroxytryptophan on electrocortical activity and breathing movements of fetal sheep. J. Obstet. Gynecol. 141: 271-275.

RAMIREZ, J.M., QUELLMALZ, U.J.A., WILKEN, B. (1997) Developmental changes in the hypoxic response of the hypoglossus respiratory motor output in vitro. J. Neurophysiol. 78: 383-392.

REDFERN, P.A. (1970) Neuromuscular transmission in new-born rats. J. Physiol. 209: 701-709.

RECKLING, J.C.D., CHAMPAGNAT, J., DENAVIT-SAUBIE, M. (1996) Thyrotropin-releasing hormone (TRH) depolarizes a subset of inspiratory neurons in the newborn mouse brain stem in vitro. J. Neurophysiol. 75: 811-819.

RIBERA, A.B., SPITZER, N.C. (1989) A critical period of transcription required for differentiation of the action potential of spinal cord. Neuron 2: 1055-1062.

ROSENTHAL, J.L., TARASKEVICH, P.S. (1977). Reduction of multiaxonal innervation at the neuromuscular junction of the rat during development. J. Physiol. 270: 299-310.

SCHIAFFINO, S., REGGIANI, C. (1994) Myosin isoforms in mammalian skeletal muscle. J. Appl. Physiol. 77(2): 493-501.

SERNAGOR, E., GRZYWACZ, N.M. (1995) Emergence of complex receptive field properties of ganglion cells in the developing turtle retina. J. Neurophysiol. 73(4): 1355-1364.

SIECK, G.C., FOURNIER, M., BLANCO, C.E. (1991) Diaphragm muscle fatigue resistance during postnatal development. J. Appl. Physiol. 71(2): 458-464.

SMITH, J.C.D., ELLEMBERGER, H., BALLANYI, K., FELDMAN, J.L., RITCHTER, D.W. (1991) Pre-Bötzinger complex: a brainstem region that may generate respiratory rhythm in mammals. Sci. 254: 726-729.

SMITH, J.C.D., FELDMAN, J.L. (1987) Central respiratory pattern generation studied in an in vitro mammalian brainstem-spinal cord preparation. In: Respiratory muscles and their neuromotor control. Ed. Sieck, G.C., Gandevia, S.G., Cameron, W.E. Liss, New York, pp. 27-36.

SONG, A., TRACEY, D.J., ASHWELL, K.W.S. (1999) Development of the rat phrenic nerve and the terminal distribution of phrenic afferents in the cervical cord. Anat. Embryol. 200: 625-643.

SPIGELMAN, I., ZHANG, L., CARLEN, P.L. (1992) Patch-clamp study of postnatal development of CA1 neurons in rat hippocampal slices: membrane excitability and K^+ currents. J. Neurophysiol. 68: 55-69.

SU, C-K., CHAI, C-Y (1998) GABAergic inhibition of rat phrenic motoneurons. Neurosci. Lett. 248: 191-194.

SUBRAMONY, P., DRYER, S.E. (1996) The effect of inneration on the developmental expression of Ca^{2+}-activated K^+ currents in embryonic chicken parasympathetic neurons. Dev. Brain Res. 91: 149-152.

SUBRAMONY, P., DRYER, S.E. (1997) Neuregulins stimulate the functional expression of Ca^{2+}-activated K^+ channels in developing chicken parasympathetic neurons. Proc. Natl. Acad. Sci. USA 94: 5934-5938.

SUZUE, T. (1984) Respiratory rhythm generation in the in vitro brainstem-spinal cord preparation of the neonatal rat. J. Physiol. 353: 173-183.

TORIKAI, H., HAYASHI, F., TANAKA, K., CHIBA, T., FUKUDA, Y., MORIYA, H. (1996) Recruitment order and dendritic morphology of rat phrenic motoneurons. J. Comp. Neurol. 366: 231-243.

VASQUEZ, R.L., DAOOD, M.J., WATCHKO, J.F. (1993) Regional distribution of myosin heavy chain isoforms in rib cage muscles as a function of postnatal development. Pediatric Pulmonology 16: 289-296.

VIANA, F., BAYLISS, D.A., BERGER, A.J. (1993a) Calcium conductances and their role in the firing behaviour of neonatal rat hypoglossal motoneurons. J. Neurophysiol. 69(6): 2137-2149.

VIANA, F., BAYLISS, D.A., BERGER, A.J. (1993b) Multiple potassium conductances and their role in action potential repolarization and repetitive firing behavior of neonatal rat hypoglossal motoneurons. J. Neurophysiol. 69(6): 2150-2163.

WAITAS, B.A., ACKLAND, G.L., NOBLE, R., HANSON, M.A. (1996) Red nucleus lesions abolish the biphasic respiratory response to isocapnic hypoxia in decerebrate young rabbits. J. Physiol. 495: 217-225.

WALTON, K.D., NAVARRETE, R. (1991) Postnatal changes in motoneurone electrotonic coupling studied in the in vitro rat lumbar spinal cord. J. Physiol. 433: 283-305.

WALTON, K., FULTON, B.P (1986) Ionic mechanisms underlying the firing properties of rat neonatal motoneurons studied in vitro. Neurosci. 19: 669-683.

WANG, L.Y., GAN, L., FORSYTHE, I., KACZMAREK, L.K. (1998) Contribution of the Kv3.1 potassium channel to high-frequency firing in mouse auditory neurons. J. Physiol. 509.1: 183-194.

WATCHKO, J.F., SIECK, G.C. (1993) Respiratory muscle fatigue resistance relates to myosin phenotype and SDH activity during development. J. Appl. Physiol. 75(3): 1341-1347.

WATCHKO, J.F., DAOOD, M.J., VAZQUEZ, R.L., BROZANSKI, B.S., LAFRAMBOISE, W.A., GUTHRIE, R.D., SIECK, G.C. (1992) Postnatal expression of myosin isoforms in an expiratory muscle--external abdominal oblique. J. Appl. Physiol. 73(5): 1860-1866.

WARDLAW, W.S., STARK, L.R., BARC, L., FRANTZ, A. (1979) Plasma beta-endorphin and beta-lipoprotein in human fetus at delivery: correlation with arterial pH and pO_2. J. Clin. Endocrinol. Metab. 79: 888-891.

WARNER, A.E., GUTHRIE, S.C., GILULA, N.B. (1984) Antibodies to gap-junction proteins selectively disrupt junctional communication in the early amphibian embryo. Nature 311: 127-131.

WONG, W.T., MYHR, K.L. MILLER, E.D., WONG, R.O.L. (2000) Developmental changes in the neurotransmitter regulation of correlated spontaneous retinal activity. J. Neuronsci. 20(1): 351-360.

WONG, R.O.L., (1999) Retinal waves and visual system development. Annu. Rev. Neurosci. 22: 29-47.

WONG, W.T., SANES, J.R., WONG, R.O.L. (1998) Developmentally regulated spontaneous activity in the embryonic chick retina. J. Neuronsci. 18(21): 8839-8852.

WONG, R.O.L., CHARNJAVSKY, A., SMITH, S.J., SHATZ C.J. (1995) Early functional neural networks in the developing retina. Nature 374: 716-718.

WU, W., ZISKIND-CONHAIM, L., SWEET, M.A. (1992) Early development of glycine- and GABA-mediated synapses in rat spinal cord. J. Neurosci. 12: 3935-3945.

XIE, H., ZISKIND-CONHAIM, L., (1995) Blocking Ca^{2+}-dependent synaptic release delays motoneuron differentiation in the rat spinal cord. J. Neurosci. 15: 5900-5911.

YUSTE, R., NELSON, D.A., RUBIN, W.W., KATZ, L.C. (1995) Neuronal domains in developing neocortex: mechanisms of coactivation. Neuron 14(1): 7-17.

YUSTE, R., PEINADO, A., KATZ, L.C. (1992) Neuronal domains in developing neocortex. Science. 257(5070): 665-669.

ZHANG, L., SPIGELMAN, I., CARLEN, P.L. (1991) Development of GABA-mediated, chloride-dependent inhibition in CA1 pyramidal neurones of immature rat hippocampal slices. J. Physiol. (Lond.) 444: 25-49.

ZISKIND-CONHAIM L. (1988) Electrical properties of motoneurons in the spinal cord of rat embryos. Devel. Biol. 128(1): 21-29.

CHAPTER 2

METHODS AND MATERIALS

Perinatal rat models

Embryos (E16, E18) were delivered from timed-pregnant Sprague-Dawley rats anaesthetized with halothane (1.2-1.5% delivered in 95% O_2 and 5% CO_2) and maintained at 37°C by radiant heat, following procedures approved by the Animal Welfare Committee at the University of Alberta. The timing of pregnancy was determined from the appearance of sperm plugs in the breeding cages, designated E0. Fetal age was confirmed by comparing the crown-rump length of the embryos with previously published values by Angulo y Gonzalez (Angulo y Gonzalez, 1932). Newborn rats (P0-1) were anaesthetized by inhalation of metofane (2-3%) prior to surgical procedures..

Cervical slice-phrenic nerve preparation

Embryos and newborns were decerebrated and the brain stem-spinal cord with the phrenic nerve attached was dissected in artificial cerebrospinal fluid (CSF) at 27±1°C. To monitor the viability of the preparation, phrenic inspiratory motor discharges were recorded with suction electrodes (40-70 μm diameter) and displayed on a computer monitor using the data-acquisition software Axotape (Axon Instruments, USA). However, rhythmic phrenic inspiratory motor discharges are produced only in animals aged E17 and beyond (Greer et al., 1992). The spinal segment was cut with a vibratome (Pelco, Redding, CA or Leica VT1000S, Leica, Germany) into a single slice containing the C4 segment (E18, P0-1) or C3-C4 segment (E16) with the phrenic nerve and the dorsal root ganglia attached (~750 μm thick). The dorsal roots were then cut to prevent reflex-mediated synaptic stimulation of PMNs in response to antidromic stimulation of the phrenic nerve used for identification of PMNs. The spinal cord slice was transferred to a Sylgard-coated recording chamber and pinned down (at the dorsal border of the white matter) and continuously perfused with artificial CSF solution at 27±1°C (perfusion rate 2 ml/min, volume of the chamber 1.5 ml). The slice was left to equilibrate for at least 1 hour before recording and data was typically acquired for up to 5 hours after slice preparation.

Whole-cell recordings

Recording electrodes were fabricated from thin wall borosilicate glass (A-M Systems, Inc., Everett, WA). The pipette resistances were between 3-5 MΩ. To decrease capacitance transients, pipette tips were coated with Sigmacote® (Sigma Chemical Co., St. Louis, MO) and the level of fluid submerging the slice was minimized during recordings. The electrode was advanced with a stepping motor (PMC 100, Newport, Irvine, CA) into the PMN pool located in the medial zone of the ventral horn close to the border between the white and gray matter. To avoid clogging of the recording electrode, positive pressure (≈30 mm Hg) was applied while entering the tissue to a depth of at least 100 mm from the slice surface. Pressure was then removed while advancing within the PMN pool. Once the pipette made contact with a cell, negative pressure was used to form a gigaohm (>1 GΩ) cell-pipette seal and gentle suction then applied to rupture the patch membrane. Seal formation and membrane breakthrough were monitored on by observing the response to a hyperpolarizing current step (0.3 nA). Whole-cell recordings were initially established in the artificial CSF solution and performed with an AxoClamp 2B amplifier (Axon Instruments, Foster City, CA). Liquid junction potentials were corrected before seal formation with the compensation circuitry of the patch clamp amplifier. Sampling rate was between 800 Hz and 10 kHz. Current-clamp data was filtered at 30 kHz (-3dB frequency), whereas voltage-clamp data was filtered at 1 kHz. Data was digitized via an analog-to-digital interface, and analysed with the used of pCLAMP (Axon Instruments) and Origin software.

Seal formation and whole-cell recordings were carried out in current-clamp mode Once the whole-cell configuration was established, motoneurons were identified as belonging to the PMN pool by antidromic stimulation of the phrenic nerve via a suction electrode. Neurons not responding to antidromic stimulation were not analyzed. Presumptive glial cells, characterized by having resting membrane potentials hyperpolarized beyond -70 mV and incapable of firing action potentials in response to antidromic or orthodromic stimulation, were also encountered but not analyzed. Rectangular pulses of 0.5 ms duration and 0.5 Hz frequency were delivered with a pulse generator (Master 8, AMPI, Jerusalem, Israel) while pulse amplitude was manually controlled with a stimulus isolation unit (Iso-Flex, AMPI, Jerusalem, Israel). Stimulation amplitudes were ≤0.2 mA. To minimize current spread, the ground wire for antidromic stimulation was wrapped around the tip of the suction electrode. Antidromic action potentials were recorded on tape with a video cassette recorder (Sony, Japan) or captured with pCLAMP software for subsequent analysis. A schematic illustration of the slice preparation and electrode positioning is shown in Fig. 2.1 A.

Action potential and firing pattern were recorded at varying holding membrane potentials in the current-clamp configuration. Independent action potentials were evoked by antidromic stimulation of the phrenic nerve or by orthodromic injection of depolarizing step of current (0.5 ms duration). Antidromic or orthodromic action potential duration was measured at half maximal amplitude. The duration of the afterhyperpolarization (AHP) was measured from the falling phase of the action potential (at the point at which it reached the initial membrane potential) to the point in the AHP membrane potential trajectory which returned to the holding membrane potential. The fAHP amplitude was measured from resting membrane potential to the negative deflexion between the repolarizing phase of the action potential and the following afterdepolarizing potential. Repetitive firing properties were investigated following injection of 1s-long depolarizing pulses of increasing amplitude. The amount of current (in nA) required to elicit repetitive firing is indicated beside each trace. Firing frequency was determined as the number of action potentials per 1s-stimulus at the lowest intensity of current necessary for evoking repetitive firing. The effects of various drugs on firing frequency were studied at the lowest stimulation current (threshold current) necessary to elicit repetitive firing.

Intracellular and extracellular solutions: Artificial CSF contained (in mM): NaCl (128), KCl (3), NaH_2PO_4 (0.5), $CaCl_2$ (1.5), $MgCl_2$ (1), $NaHCO_3$ (23.5), glucose (30); pH 7.4 when bubbling with 95%O_2, 5% CO_2. In the calcium-free solution, calcium ions were replaced by an equimolar concentration of cobalt chloride, and $NaHPO_4$ was removed to avoid precipitation. The sodium-free solution (HEPES-based buffer) contained (in mM): Choline chloride (139), N-(2-hydroxyethyl)piperazine-N'-(2-ethanesulfonic acid) (HEPES; 10), KCl (3), $NaHPO_4$ (0.5), $CaCl_2$ (1.5), $MgCl_2$ (1), glucose (30); pH 7.4 with TrisOH and bubbled with 100%O_2. Unless otherwise specified in each chapter, the composition of the pipette solutions use to dissect individual conductances is as follows. The standard pipette solution contained (in mM): Potassium gluconate (130), NaCl (10), CaCl (1), 1,2-bis(2-aminophenoxy)ethane-N,N,N',N'-tetraacetic acid (BAPTA, 10), HEPES (10), Mg ATP (5), NaGTP (0.3); pH 7.3 with KOH. The free calcium concentration for the standard solution was 24 nM as determined with a software (Sol I.D.) kindly supplied by E.A. Erter (University of Washington, Seattle, WA). The composition of the pipette solution with a lower calcium buffer capacity was similar to that of the standard solution except for the following changes:

BAPTA was decreased to 0.1 mM, calcium was not added and potassium gluconate was increased to 155 mM (free-calcium concentration= 8 nM). The pipette solution utilized for blocking potassium conductances contained (in mM): Cesium methanesulphonate (100), tetraethylammonium chloride (TEACl, 40), BAPTA (10), HEPES (10), Mg ATP (5), NaGTP (0.3); pH 7.3 with tetraethylammonium hydroxide (TEAOH).

The osmolarity of all the external and internal solutions were between 320-325 and 315 mOsm, respectively, as measured with a freezing point osmometer (Advanced Instruments, Needham, MA).

Drugs: Stock solutions of drugs were prepared as 100-1000 times concentrates. All drugs were added into the perfusate by switching to reservoirs containing the appropriate test solution (perfusion bath volume ~ 20 ml). A waiting period of ≥ 5 min was used to allow for equilibrium before data was collected.

Figure 2.1. Schematic of experimental setup for recording PMN electrical properties **(A)**, diaphragm contractile properties **(B)** and end-plate potentials **(C)**. Whole-cell recordings in A were obtained from PMNs located in the ventromedial cervical spinal cord (shaded circle) in acutely isolated slice preparations. The phrenic nerve extending distal to the ventral root was left attached for identification of PMNs via antidromic stimulation.

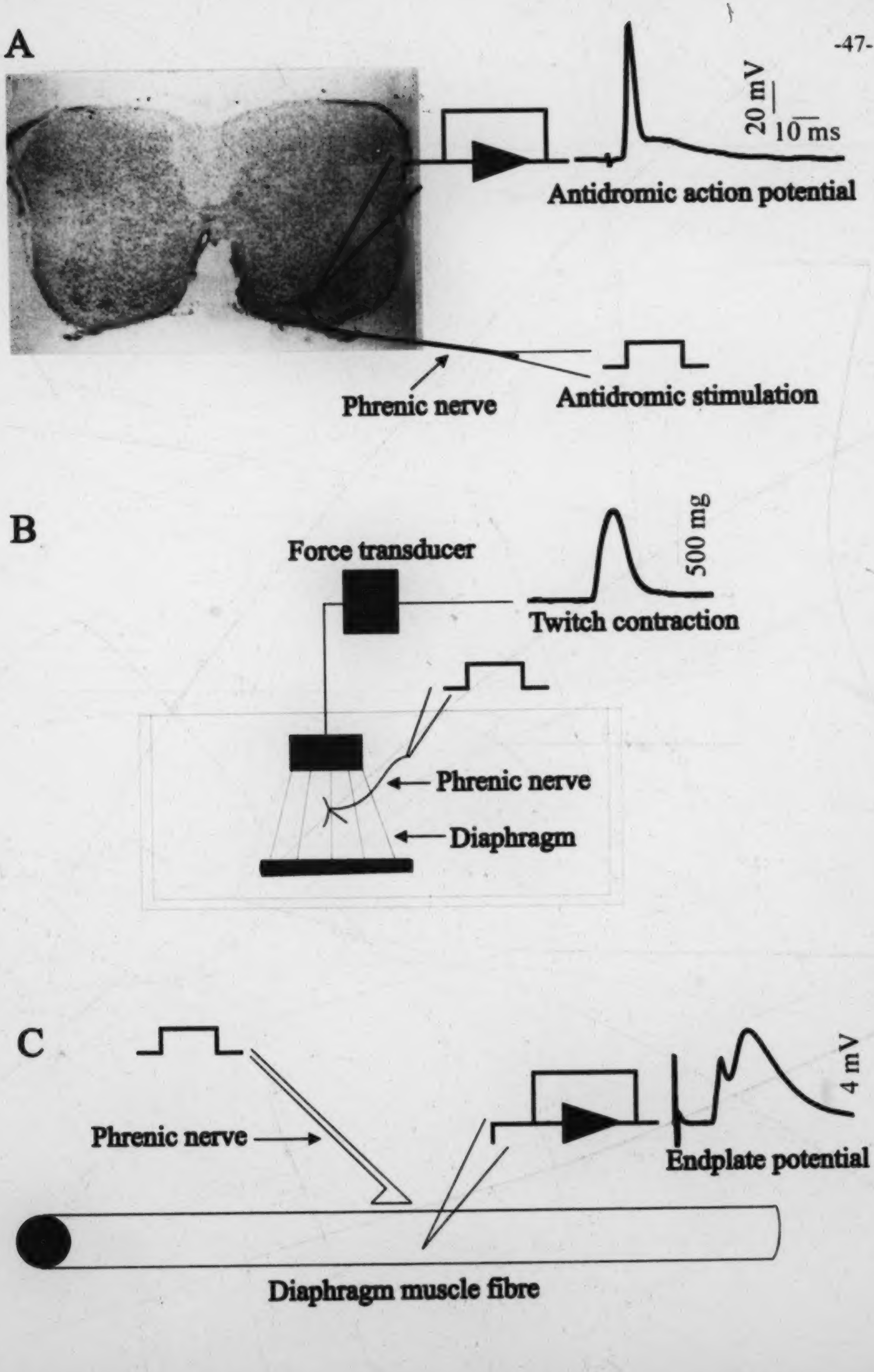
A
20 mV
10 ms
Antidromic action potential
Phrenic nerve
Antidromic stimulation
B
Force transducer
500 mg
Twitch contraction
Phrenic nerve
Diaphragm
C
Phrenic nerve
4 mV
Endplate potential
Diaphragm muscle fibre

Phrenic nerve-diaphragm preparation

Embryos and newborns were decapitated and the thoracic sections, with the ribcage and diaphragm intact, were isolated and transferred to a Sylgard-coated chamber (volume = ~ 35 ml). The tissue was bathed in a modified Krebs-Ringer solution at 27±1°C during both the dissections and recordings. The solution contained (in mM): NaCl (117), KCl (6), Na_2HPO_4 (1.3), $CaCl_2$ (2.6), $MgSO_4$ (1.3), $NaHCO_3$ (24), glucose (10); pH 7.4 following bubbling with 95%O_2 and 5% CO_2. The diaphragm with the phrenic nerve, ribs and central tendon attached was dissected free and hemisected along the midline of the central tendon. The connective tissue and excess muscle were trimmed away leaving a section of the hemidiaphragm ~ 5 mm wide, centered approximately on the point where the phrenic nerve enters the muscle. We did not find it technically feasible to obtain reliable force recordings from diaphragm strips isolated from animals younger than E18 due to the frailty of the muscle tissue.

Measurements of diaphragm contractile properties

A small piece of aluminum foil with a short length of silk suture (~5 cm) attached was glued to the central tendon. The ribs, attached to the lateral edge of the muscle strip, were fixed to the Sylgard-coated chamber base with insect pins and the suture attached to a force transducer (UF1 Dynamometer, Harvard Instruments, South Natick, MA; 0-25 g working range with ±1% accuracy) suspended above the chamber (E18, n=6; P0-1, n=5). The phrenic nerve was stimulated with a suction electrode (40-70 μm diameter) filled with bathing solution. A schematic illustration of the phrenic nerve-diaphragm preparation is shown in Fig. 2.1 B. To minimize current spread, the ground wire for antidromic stimulation was wrapped around the tip of the suction electrode. The muscle was stimulated directly using two needle electrodes, each placed on either side of the muscle strip approximately 4 mm apart. The timing and duration of all stimulation pulses were controlled by a Master-8 (AMPI, Jerusalem, Israel). These timing pulses were then converted to voltage signals by an Isoflex stimulation unit (AMPI) or a Grass SD9 stimulator (Grass Instruments, Quincy, MA) for nerve and muscle stimulations, respectively. The electrical signal from the force transducer was sent to a Grass model 7D polygraph for pre-amplification and low-pass filtering (3 kHz). Signals were then transferred (2kHz sampling rate) to a PC computer running Axotape software (Axon Instruments) via an analogue to digital interface (TL1; Axon Instruments, Foster City, CA).

Optimal preload length (L_o) was established by determining the resting tension at which maximal force was developed in response to a single square wave voltage stimulus delivered via the phrenic nerve. Muscle length was changed via a micromanipulator (0.01 mm resolution, Mitutoyo, Tokyo, Japan). L_o values were 7.1±0.4 (E18, n=6) and 10.4±1.1 mm (P0-1, n=5). The twitch response to single square wave stimuli was monitored periodically throughout the experiment to ensure that L_o was maintained and to assess tissue viability. Tissue viability was considered acceptable if single twitch responses did not change by more that 10% during the recording session. The minimum stimulus amplitude and the optimum stimulus duration (tested from 0.2-5 ms) required to achieve maximum single twitch force in response to both phrenic nerve and direct muscle stimulation were also determined. In order to ensure supramaximal stimulation, an amplitude of 1.5 times the minimum stimulus amplitude was used throughout the experiment. Single twitches were elicited via phrenic nerve and/or direct muscle stimulation and the peak force, time to peak force and half-relaxation time determined. The muscle was then stimulated directly and/or via the phrenic nerve with one second-long trains at 3, 5, 10, 20, 40, 60, 80 and 100 Hz in order to determine peak force, and fused tetanus frequency. Two minutes relaxation was allowed between pulse trains. Since direct muscle stimulation could result in an inadvertent activation of intramuscular phrenic nerve branches, the direct muscle stimulation protocol was repeated after nicotinic acetylcholine receptors were blocked with the addition of 10 μM D-tubocurarine to the bathing solution.

Maximal single twitch or tetanic force was expressed relative to wet and dry weight and protein content. Maximal tetanic force (expressed in Newtons) was normalized to muscle cross-sectional area (CSA). The CSA was estimated by the following equation: CSA=muscle weight (g)/[L_o (cm) x density (g/cm^3)] where density was considered 1.056 g/cm^3 (Watchko and Sieck, 1993). Peak force was converted to a percentage of the maximum force achieved by a given preparation in response to either muscle or nerve stimulation. For measurements of the muscle's ability to maintain force in response to prolonged nerve stimulation (1 or 10 seconds), the lowest level of force obtained during the declining phase of the contraction was calculated as a percentage of the peak force obtained at the beginning of the test pulse. To differentiate failure of neuromuscular transmission from that due to intrinsic contractile mechanisms within the muscle, direct stimulation of the muscle was superimposed during the final 250 ms of the 1 second pulse or the final 2 seconds of the 10 second pulse nerve stimulations.

Determination of muscle weight and protein content

Upon completion of force measurements, the muscle was dissected from the tendon, bone and nerve before being weighed (wet and dry after dessication). Desiccation of muscle preparations was carried out at 37°C in an incubator (Precision, CGA Corporation, USA). Desiccated preparations were frozen in liquid nitrogen, and stored at -70°C for later measurement of protein content using the method of Lowry (Lowry et al., 1951).

Measurements of endplate potentials (epp)

The phrenic nerve-diaphragm muscle preparation was dissected and prepared as described above for tension measurements (E18, n=7; P0-1, n=9). The muscle strip was pinned horizontally to the Sylgard lining the bottom of the in vitro chamber. Epp waveforms were elicited via orthodromic stimulation of the phrenic nerve and recorded from muscle fibers using sharp electrodes (10-30 MΩ) filled with 2M K^+ acetate. Signals were recorded using an Axoclamp 2B amplifier and transferred via an analogue to digital interface (TL1; Axon Instruments; 10 kHz sampling rate) to a PC computer running pClamp software (Axon Instruments). A schematic illustration of the phrenic nerve-diaphragm preparation used for recording endplate potentials is shown in Fig. 2.1 C.

In order to obtain stable intracellular recordings from muscle fibers, incremental doses of d-tubocurarine were added to the bathing medium until the minimal concentration necessary for suppressing visible muscle twitches was reached (4-6 μM). The amplitude, rise time and slope of the epp responses were calculated for the first epp in each case (due to polyneuronal innervation, >1 epp response was elicited in the majority of recordings). Epp amplitude was measured from baseline to the maximal value reached. Rise time was calculated from the onset of the epp until the time when the maximal amplitude was reached. The epp slope was calculated by a linear fitting of the rising phase of the epp between 10-90% of its maximal amplitude. Epp decay rate was determined by a single exponential fitting of the decay phase measured between maximal amplitude and baseline of the last epp response.

Statistics: All data values are presented as mean ± SE. The n value represents the number of PMNs or phrenic nerve-diaphragm preparations from which a particular measurement was made. Significant differences between values before and after a drug treatment within a given age were calculated by using paired Student's t-test, whereas differences between various age groups were tested using ANOVA followed by Newman-Keuls post hoc test.

REFERENCES

ANGULO Y GONZÁLEZ, A.W. (1932) The prenatal growth of the albino rat. Anatomical Record 52: 117-138.

LOWRY, O.H., ROSENBROUGH, N.J., FARR, A.L., RANDALL, R.J. (1951) Protein measurement with folin-phenol reagent. J. Biol. Chem. 193: 265-275.

WATCHKO, J.F., SIECK, G.C. (1993) Respiratory muscle fatigue resistance relates to myosin phenotype and SDH activity during development. J. Appl. Physiol. 75(3): 1341-1347.

CHAPTER 3

ELECTROPHYSIOLOGICAL PROPERTIES OF RAT PHRENIC MOTONEURONS DURING PERINATAL DEVELOPMENT

Adapted from the original publication:
M. Martin-Caraballo and J.J. Greer
J. Neurophysiol. 81: 1365-1378 (1999)

INTRODUCTION

PMN axons emerge from the spinal cord at embryonic day (E) 11, migrate to contact the primordial diaphragm musculature by E13, begin to form intramuscular branches concomitantly with the initial formation of diaphragm myotubes at E14, and branch within the full extent of the developing diaphragm by E17-E18 (Allan and Greer, 1997a). PMNs first receive descending inspiratory drive transmission and synaptic contacts from spinal afferents at E17 (Greer et al., 1992; Allan and Greer, 1997b). Interestingly, the time of target innervation and the inception of functional recruitment coincides with the onset of a rapid and profound morphological development of PMNs (Allan and Greer, 1997b). **Thus, for the purpose of the present study, we chose to examine the electrophysiological properties of PMNs during the critical period prior and subsequent to the major morphological reorganization, the completion of target musculature innervation, the onset of afferent and descending respiratory synaptic drive *in utero*, and continuous rhythmic activation at birth (E16 to P0-1, see shadow box in Fig. 1.1). I hypothesized that there would be a significant maturation of passive membrane properties, action potential characteristics and repetitive firing properties of PMNs during this period. To test this hypothesis, whole-cell patch recordings of identified PMNs were performed utilizing a cervical slice-phrenic nerve preparation isolated from perinatal rats ages E16, E18 and P0-1.**

METHODS

Whole-cell recording

Electrophysiological properties of PMNs were typically recorded at ~-60 mV holding membrane potential. However, the effects of holding potentials on spike and firing properties were investigated by continuous injection of hyperpolarizing or depolarizing current as required.

Resting membrane potential was determined immediately after breaking the seal between the membrane and the pipette. Action potential duration was measured at half maximal amplitude. Input resistance (R_{in}) was determined from the voltage deflection upon injection of a 400 ms-long hyperpolarizing current pulse ($\leq$0.05 nA). The membrane time constant (τ) was calculated by fitting the membrane voltage response to injection of negative current. The membrane response could be closely fit by a single exponential with the Clampfit fitting function (Axon Instruments). Threshold potential (V_{th}) was determined as the absolute membrane potential at the onset of an action potential. The mean rheobase (I_{rh}) was calculated as the depolarizing voltage required to elicit an action potential (V_{th}) divided by its input resistance, assuming an ohmic membrane (Cameron et al., 1991).

Drugs: The following drugs were used (suppliers in brackets): TTX, TEACl (Sigma, St. Louis, MO); lidocaine–ethyl bromide (QX 314; RBI, Natick, MA).

RESULTS

Electrical properties of PMNs were determined from neurons meeting the criteria of having a stable resting membrane potential more negative than -45 mV and action potential amplitudes of $\geq$50 mV. There are two points that should be taken into consideration when interpreting the results obtained utilizing the cervical slice preparation. First, PMNs were recorded at a depth of 100-200 µm from the surface of the slice which meant that while large portions of their dendritic trees were intact, the distal rostrocaudally projecting dendrites were typically severed. Second, the normal endogenous synaptic drive received in vivo which could influence PMN properties and behaviour will obviously be absent in our experimental conditions.

Membrane properties

Passive properties of developing motoneurons, in particular the resting membrane potential, threshold potential and input resistance, are important factors in determining electrical excitability in response to synaptic inputs. Thus, the first component of our study was to characterize age-related changes in PMN passive properties. Results from the population data are summarized in Table 3.1. Between ages E16 and E18, around the time of the inception of inspiratory drive transmission, the resting membrane potentials became hyperpolarized by ~8 mV. Between E18 and birth there was a slight further hyperpolarization of ~2 mV in the resting membrane potential. Despite the above changes in the resting membrane potential, the voltage threshold required for generating an action potential did not change substantially at any age studied (Table 3.1). An ~32% reduction in the input resistance occurred between E16 and E18. A further ~48% decrement in input resistance occurred by birth. With no significant variation in potential, the three-fold increase in the mean rheobase from E16 to P0-P1 was most likely due to the reduction in the input resistance of PMNs. An analysis of the voltage responses to hyperpolarizing currents (Fig. 3.1) also revealed that the membrane time constants of PMNs were significantly reduced (by ~ 29%) during the transition from E16 to P0-1 (Table 3.1).

Table 3.1. Electrophysiological properties of PMNs.

	E16 (n=21)	**E18** (n=16)	**P0-1** (n=26)
Action potential amplitude	66.5±2.0	68.1±1.6	78.3±2.5*
Action potential duration$^{(1)}$	6.2±0.5	4.1±0.3$^{\cdot}$	3.2±0.2$^{\cdot\,\circ}$
Resting membrane	-49.3±5.9	-57.4±2.0	-59.3±1.2*
Threshold potential (mV)	-33.4±2.1	-38.0±1.1	-36.2±1.8
Input resistance$^{(2)}$ (MΩ)	806±81	551±61*	266±33$^{\cdot\,\circ}$
Mean rheobase$^{(3)}$ (pA)	35±4	42±6	89±14$^{\cdot\,\circ}$
Time constant$^{(4)}$ (ms)	53.0±4.6	46.0±5.0	38.0±3$^{\cdot}$

Electrophysiological properties of PMNs were determined at -60 mV holding potential following injection of 0.5 ms depolarizing or 400 ms hyperpolarizing current of increasing amplitude in order to generate action potentials and hyperpolarizing voltage responses, respectively. Data related to neonatal age does not include motoneurons with gap junctions (as revealed by the presence of short latency depolarizations (SLD)).

$^{(1)}$Action potential duration at half maximal amplitude.

$^{(2)}$Input resistance was calculated from the voltage responses to injections of small hyperpolarizing current pulses (400 ms, 10-30 nA).

$^{(3)}$Mean rheobase was determined by dividing the threshold potential by input resistance.

$^{(4)}$Time constant was obtained by fitting the voltage transient induced by the injection of hyperpolarizing current to an exponential function.

(*) $p \leq 0.05$, ($^{\cdot}$) $p \leq 0.01$ vs E16 or ($^{\circ}$) $p \leq 0.05$ vs. E18.

Subthreshold membrane responses to hyperpolarizing current injections were studied in order to assess whether there were age-related changes in inward rectification and rebound depolarization (Dekin and Getting, 1987; Bayliss et al., 1994). The voltage deflection of membrane potentials following injections of prolonged hyperpolarizing current pulses (400 ms) are shown in Fig. 3.1 A. Plots of the voltage responses at the onset ($V_{initial}$) and end ($V_{steady\ state}$) of the current pulses resulted in superimposed linear graphs (Fig. 3.1 B), indicating the lack of sag depolarization and inward rectification at all ages examined. The level of inward rectification was also determined as the percentage ratio of $V_{steady\ state}/V_{initial}$ at -100 ± 10 mV membrane potential. The values obtained were similar at all ages [E16, 99 ± 0.4% (n=18); E18, 99 ± 0.3% (n=16); P0-1, 100 ± 0.1% (n=10)].

Rebound depolarizations following the completion of hyperpolarizing current pulses were observed in a subpopulation of PMNs, with the presence decreasing with age. Approximately 65% of E16 PMNs exhibited rebound depolarizations (11 of 17); this value decreased to 45% in E18 (5 of 11) and to 12% in P0-1 (3 of 26) PMNs. As the strength of the hyperpolarizing pulse was increased, the depolarizing rebound potential eventually reached threshold potential, triggering an action potential (Fig 3.1 A). Rebound depolarizations were not inhibited in the presence of the intracellular Na^+ channel blocker QX 314 (1.5 mM, Connors and Prince, 1982) or following blockade of K^+ channels with intracellular TEA and cesium ions (Fig. 3.2 B and C). Whereas, incubation of the spinal slice in a Ca^{++}-free solution eliminated the rebound depolarizations, thus indicating that a Ca^{++}-mediated conductance generates the rebound depolarizations (Fig. 3.2 A). As also shown in Fig. 3.2, activation of the rebound depolarization was dependent on the amplitude (B) and duration (C) of the hyperpolarizing prepulse potential. Hyperpolarizations greater than -75 mV and duration of ≥200 ms were required for the expression of rebound depolarization. Further increases in the strength and duration of the hyperpolarizing stimulation were followed by larger depolarizing responses.

Figure 3.1. Membrane responses to the injection of hyperpolarizing current pulse revealed the presence of a rebound excitation (arrow) in E16 PMNs and the lack of sag depolarization at all ages examined. **A)** Membrane voltage responses of E16 and P0 PMNs following injection of 400 ms-long hyperpolarizing current pulses of increasing amplitude. At E16, rebound excitation followed the end of the hyperpolarizing pulse (arrow). Note that an action potential was evoked by further increasing the strength of the current stimulation. The symbols shown in A (●, ○, ■, ☐) indicate the points in which the membrane voltage response was measured for the I/V plots (below). **B)** Plots of the injected current vs. membrane voltage responses for the PMNs shown in A. Voltages were measured when the membrane response reached its maximum (discontinuous line; non-filled points) and near the end (continuous line; filled points) of the pulse as indicated in A. Note that the I/V plots resulted in superimposable linear graphs indicating the lack of sag depolarization.

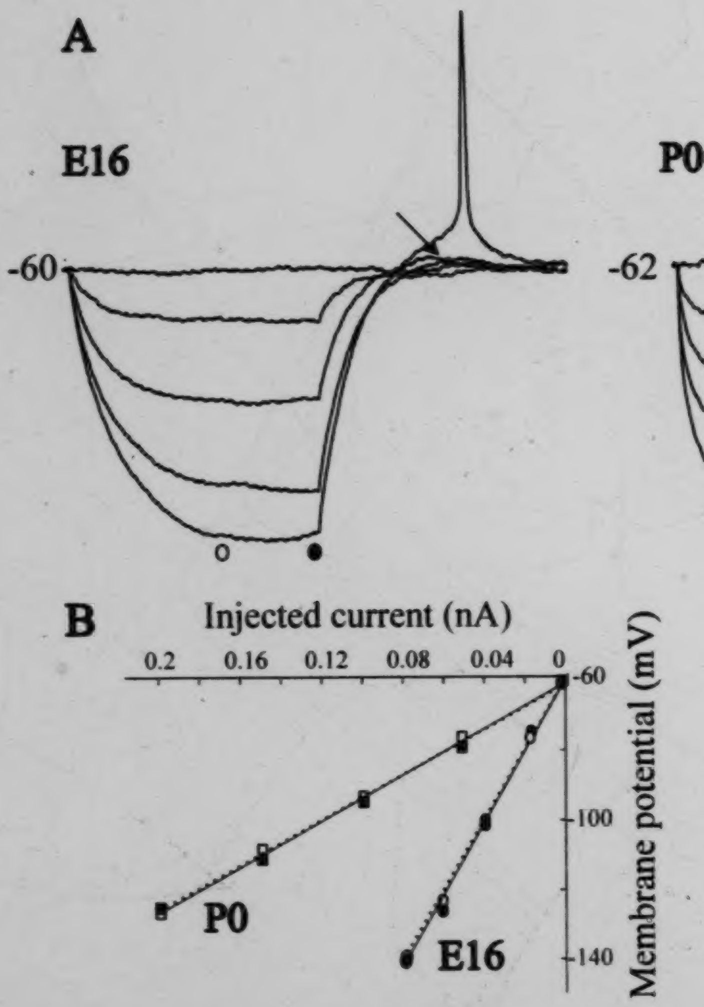
A
E16
P0
-60
-62
20 mV
200 ms
B
Injected current (nA)
0.2
0.16
0.12
0.08
0.04
0
-60
100
140
Membrane potential (mV)
P0
E16

Figure 3.2. Characterization of the rebound depolarizations observed in E16 PMNs. **A)** Rebound depolarizations were Ca^{++}-dependent. Left panel shows control recording, right panel shows the recording after Ca^{++} currents were blocked following incubation in Ca^{++}-free medium. In contrast, when Ca^{++} conductances are unperturbed and Na^+ and K^+ conductances were blocked, the rebound depolarizations persisted (see traces B and C). **B)** Rebound depolarization amplitude increased with increasing hyperpolarization. *Left*, rebound depolarization at different levels of hyperpolarization. *Right,* membrane potential-rebound depolarization amplitude plot for the cell response on the left. **C)** Rebound depolarization amplitude increased with increasing duration of the hyperpolarizing pulse. *Left*, rebound depolarization at increasing duration of hyperpolarization. *Right,* magnitude of the rebound depolarization at increasing duration of hyperpolarization for the cell response on the left. Recordings shown in B and C were carried with a pipette solution containing QX 341 (1.5 mM) to block Na^+-mediated conductance and TEA and cesium ions to block K^+-mediated conductances.

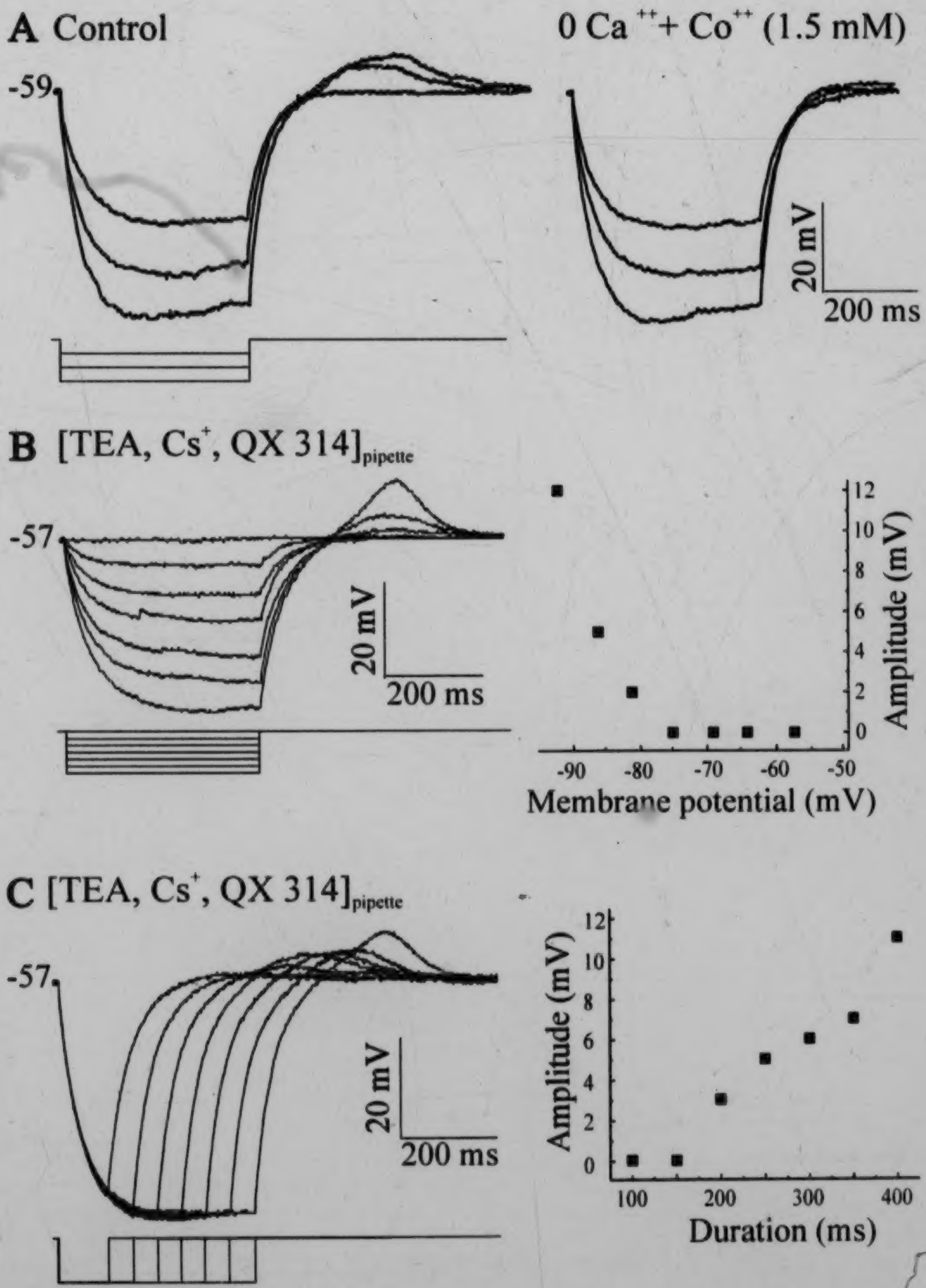
A Control
0 Ca ++ + Co ++ (1.5 mM)
-59
20 mV
200 ms
B [TEA, Cs+, QX 314]pipette
-57
20 mV
200 ms
Amplitude (mV)
0
2
4
6
8
10
12
-90
-80
-70
-60
-50
Membrane potential (mV)
C [TEA, Cs+, QX 314]pipette
-57
20 mV
200 ms
Amplitude (mV)
0
2
4
6
8
10
12
100
200
300
400
Duration (ms)

Action potential characteristics

Previous studies have demonstrated that age-related changes in action potential parameters are often influenced by the holding membrane potential (McCobb et al., 1990; Spigelman et al., 1992). Thus, age-dependent comparisons between PMNs were standardized by holding the membrane potential at approximately -60 mV at all ages, prior to investigations of the influence of depolarizing and hyperpolarizing holding potentials. From E16 to P0-1, action potential amplitude increased by ~12 mV (Table 3.1). There was a particularly striking decrease of ~34% in the action potential duration pre- and post-inception of the inspiratory drive transmission between E16 and E18 (Table 3.1). From E18 through to P0-1, the action potential duration underwent a further ~27% decrease (Table 3.1).

The action potential spike was followed by afterpotentials of various shapes depending upon age (Fig. 3.3). At E16 the action potential spike was followed by a slowly-decrementing afterdepolarization (ADP), with no clear indication of an afterhyperpolarization. Through ages E18 to P0-1, a hump-like ADP and a medium-duration afterhyperpolarizing potential (mAHP) developed. Further, a fast AHP (fAHP) separated the repolarizing component of the spike from the following ADP in a subpopulation of P0-P1 PMNs (Fig. 3.3). Note that the fAHP was expressed as an early-peaking, brief duration potential, whereas the mAHP peaked later and had a more prolonged time course (≥50 ms; Fig. 3.3, P0).

A further analysis of the age-dependent changes in the expression of the mAHP was performed as a result of potential concerns with the standard pipette solutions used during our recordings. Previous results from a variety of neuronal recordings have demonstrated that the mAHP is often due to the activation of a Ca^{++}-activated K^{+} conductance (Walton and

Fulton, 1986; Viana et al., 1993b). Our data showing that incubation of the neonatal spinal slice in Ca^{++}-free buffer (as discussed below, Fig. 3.5 C) resulted in the inhibition of the mAHP amongst neonatal PMNs supported this idea. However, we thought it possible that a significant component of the mAHP may have been blunted with our standard pipette solution which contained 10 mM of the Ca^{++} chelator BAPTA (e.g. a small mAHP may have been present but obscured in E16 PMNs). Thus, we repeated our recordings with a pipette solution with a lower Ca^{++} buffer capacity (reduced from 10 to 0.1 mM BAPTA; Fig. 3.4). The exact intracellular Ca^{++} concentrations reached during an action potential in the presence of the two levels of Ca^{++} chelation cannot be determined without direct measurements of the spatiotemporal distribution of Ca^{++} levels within the neuron during the course of an action potential. However, utilizing a software package designed to calculate the relative buffering capacities of whole-cell patch solutions (Sol I.D.; E.A. Erter, U. Washington), and taking into consideration what has been estimated regarding Ca^{++} influx during an action potential (Lockery and Spitzer, 1992; Jassar et al., 1994) we approximated the intracellular Ca^{++} concentrations which would be reached with the two solutions during an action potential. We estimated that in the presence of 1 to 50 μM range of Ca^{++} influx, the Ca^{++} concentrations would range from 8.4 to 221.1 nM with the low BAPTA solutions as compared to 24.3 to 25.3 nM with the standard solution. Thus, we were confident that any Ca^{++}-mediated conductances would be amplified with the low BAPTA solution. However, even with the low-BAPTA conditions, a mAHP was still not evident in any of the E16 PMNs recorded from (n=5; Fig. 3.4). A mAHP was observed in 2 of 5 E18 PMNs (40%) in the modified low Ca^{++}-buffering solution compared to 5 of 19 PMNs (26%) in the standard solution. In P0-1 PMNs, a clear mAHP was observed in all 5 PMNs tested with the modified low Ca^{++}-

buffering solution compared to 8 of 30 PMNs in the standard recording solution.

As shown in Fig. 3.4, the amplitudes of the afterpotentials observed in PMNs at each age were dependent on the holding potential. In E16 PMNs, the slowly decrementing ADP was enhanced with hyperpolarizing holding potentials. In P0-1 PMNs, the hump-like ADP was also enhanced with hyperpolarizing holding potentials and diminished by depolarizing potentials. In contrast, the mAHP observed in E18 and P0-1 PMNs were enhanced by depolarizing holding potentials. Thus, the repetitive firing frequencies and patterns, which are modulated by the afterpotential characteristics of the individual action potentials, will be influenced by the resting membrane potential.

Figure 3.3. Typical action potentials recorded from E16, E18 and P0 PMNs. Action potentials were evoked by antidromic stimulation of the phrenic nerve from a holding potential of ~-60 mV and using a 10 mM BAPTA pipette solution. From E16 to P0, the action potential became shorter in duration and larger in amplitude. A slowly-decrementing afterdepolarization (ADP, empty arrowhead) is present at E16, but is replaced by a hump-ADP (filled arrowhead) prominent in P0-1 PMNs. A medium-duration afterhyperpolarization (mAHP, double filled arrowheads) and a fast AHP (long arrow) are present in neonatal PMNs.

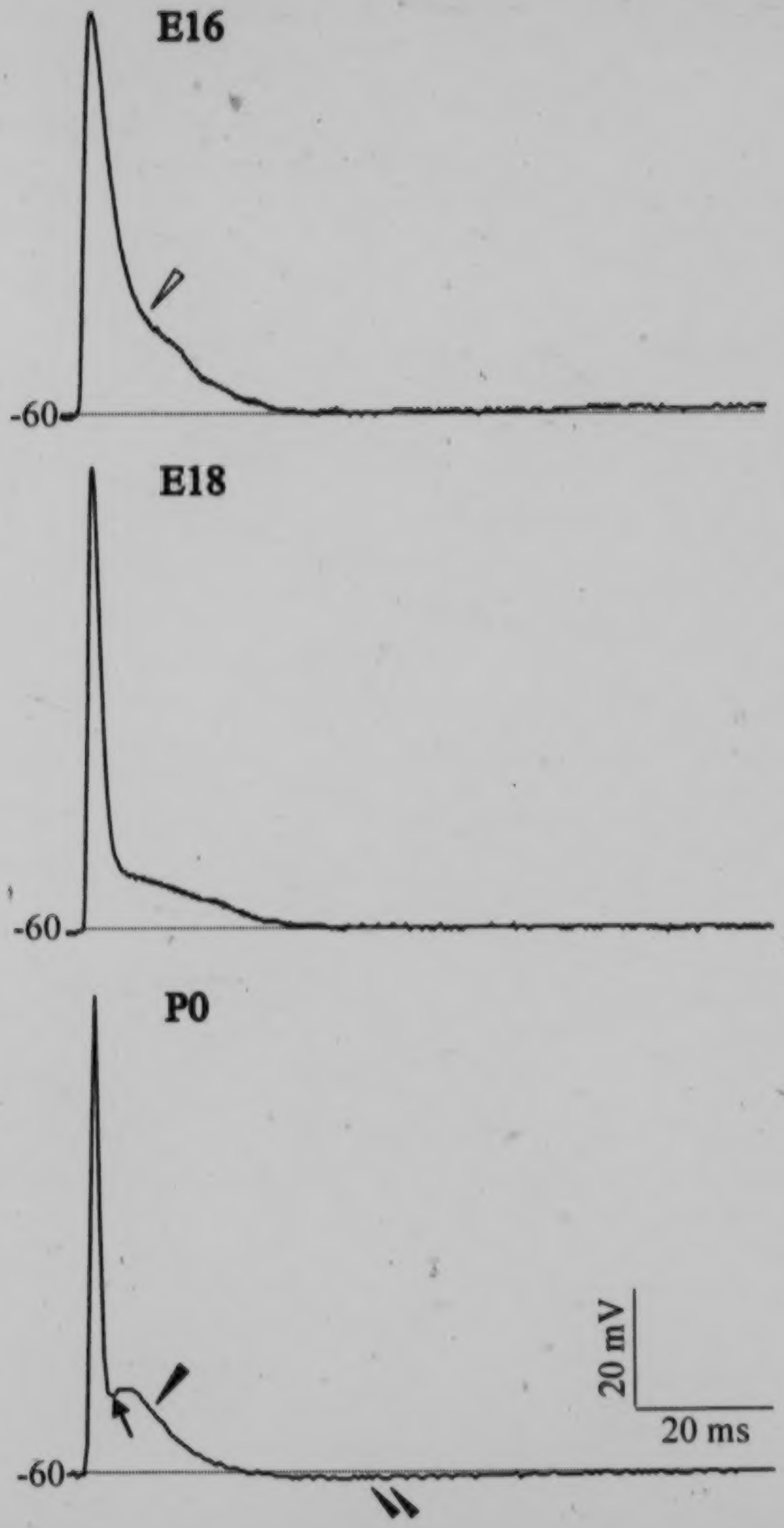
E16
-60
E18
-60
P0
-60
20 mV
20 ms

Figure 3.4. The amplitudes of ADPs and AHPs were dependent on the membrane holding potential (held at -50, -60 and -75 mV). The slowly-decrementing (empty arrowhead) and hump-ADP (filled arrowhead) were enhanced by negative holding membrane potentials (~-75 mV), whereas the mAHP potential (double filled arrowheads) was enhanced by more positive holding potentials (~-50 mV). The stimulation artifact associated with antidromic stimulation is represented by an asterisk in this and following figures. These current-clamp recordings were carried out with the low BAPTA (0.1 mM) pipette solution to accentuate afterpolarizations influenced by intracellular Ca^{++} ions.

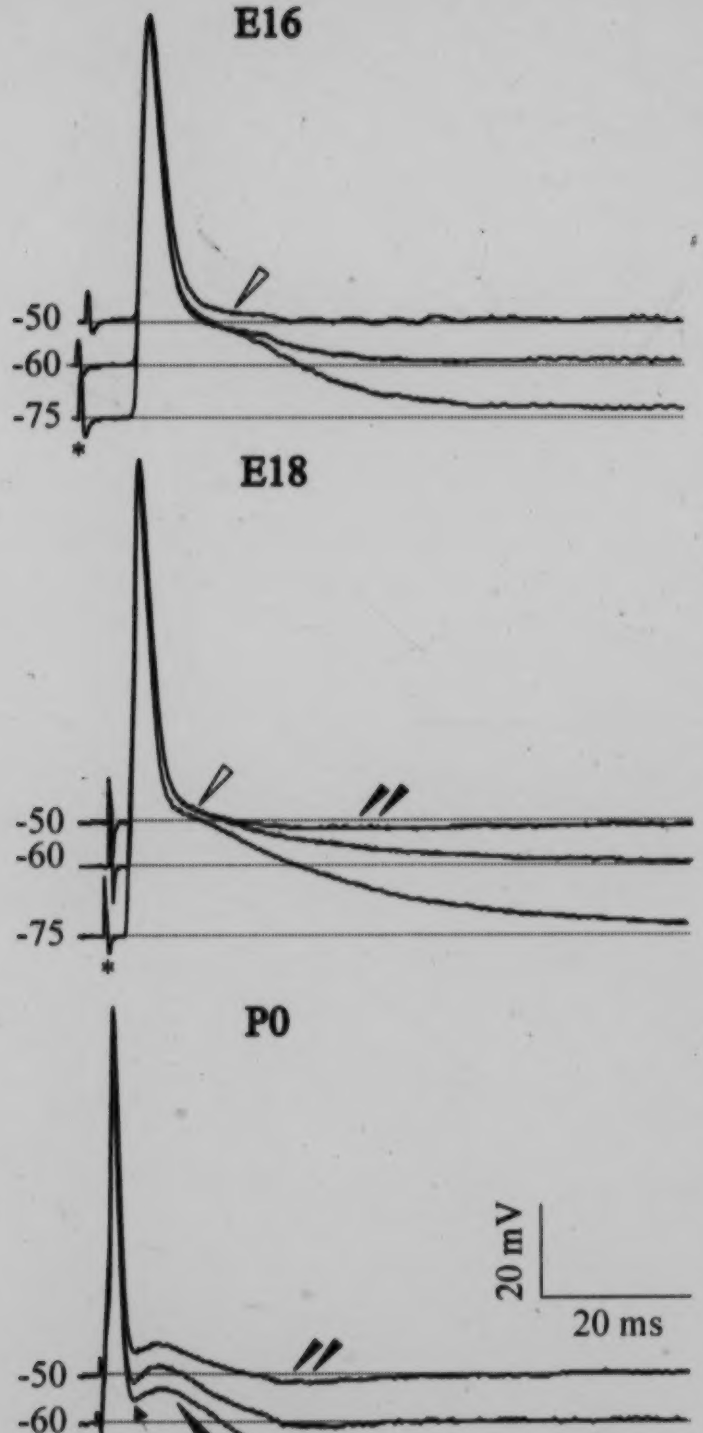
E16
-50
-60
-75
*
E18
-50
-60
-75
*
P0
20 mV
20 ms
-50
-60
-70
*

Ionic conductances underlying the components of the action potential

Ionic dependence of action potential characteristics: As early as E16, the action potentials of PMNs were Na$^+$-dependent as demonstrated by blocking Na$^+$ channels externally with TTX (0.5-1 µM; n= 5; Fig. 3.5 A). Incubation of the spinal slice in Na$^+$-free buffer (n=4) or addition of the intracellular blocker of Na$^+$ channels, QX314 (1.5 mM, n=10) to the pipette solution were also effective in preventing action potential generation in E16 PMNs (data not shown). A Ca^{++}-component contributed to prolonging the duration of the action potential of E16 PMNs, as indicated by the reduction of the spike duration following incubation in a Ca^{++}-free buffer (Fig. 3.5 B). The action potential duration of E16 PMNs decreased by 30 ± 8 % (n=5) in Ca^{++}-free buffer. However, in E18 PMNs, elimination of external Ca^{++} ions did not interfere significantly with spike duration. In 4 out of 7 P0-1 PMNs, there was a slight increase of 15 ± 6% in spike duration following incubation in Ca^{++}-free buffer (Fig. 3.5 C), suggesting that, a Ca^{++}-dependent K$^+$ current is involved in spike repolarization in neonatal PMNs. This idea was further supported by the fact that, in P0-1 PMNs, the duration of the action potential was significantly lower when recorded with a the modified low BAPTA-pipette solution [2.0 ± 0.2 (n=6) vs control high-BAPTA solution 3.2 ± 0.2 ms (n=26), $p \leq 0.05$).

***Ionic dependence of afterdepolarizing potentials**:* Previous work has indicated that ADPs observed in other motoneuronal populations are Ca^{++}-dependent (Walton and Fulton, 1986; Viana et al., 1993a). Thus, we tested whether this applies to both the slowly-decrementing and the hump-like ADPs observed in PMNs. As expected, both the slowly-decrementing and hump ADPs were reduced by bathing the slice in a Ca^{++}-free solution (Fig. 3.5 B, C, respectively). We also considered whether the ADPs could be, in part, due to passive spreading of current through gap junctions (see below). However, if this were the case, then the amplitude of the ADPs would not have been voltage-dependent (Walton and Navarrete, 1991). As illustrated in Fig. 3.4, ADP amplitudes were enhanced at hyperpolarizing potentials and reduced at depolarizing potentials.

Figure 3.5. Role of Na^+ and Ca^{++} conductance in the generation of action potentials. By age E16 the action potential is Na^+-dependent and a Ca^{++} component contributes to prolonging the spike duration. In neonatal PMNs (P0), Ca^{++} is involved in the generation of afterpotentials and affects the repolarizing phase of the action potential. **A)** The action potential is dependent on activation of Na^+ channels by E16 as indicated by the abolition of spikes resulting from TTX (0.5 μM). The diamond in this and following pictures represents the stimulation artifact following 0.5 ms intracellular current injection. **B)** Incubation in Ca^{++}-free medium shortened the action potential duration and reduced the slowly-decrementing ADP (E16). **C)** In neonatal PMNs, removal of external Ca^{++} prolonged the action potential duration and inhibited the mAHP and hump-ADP.

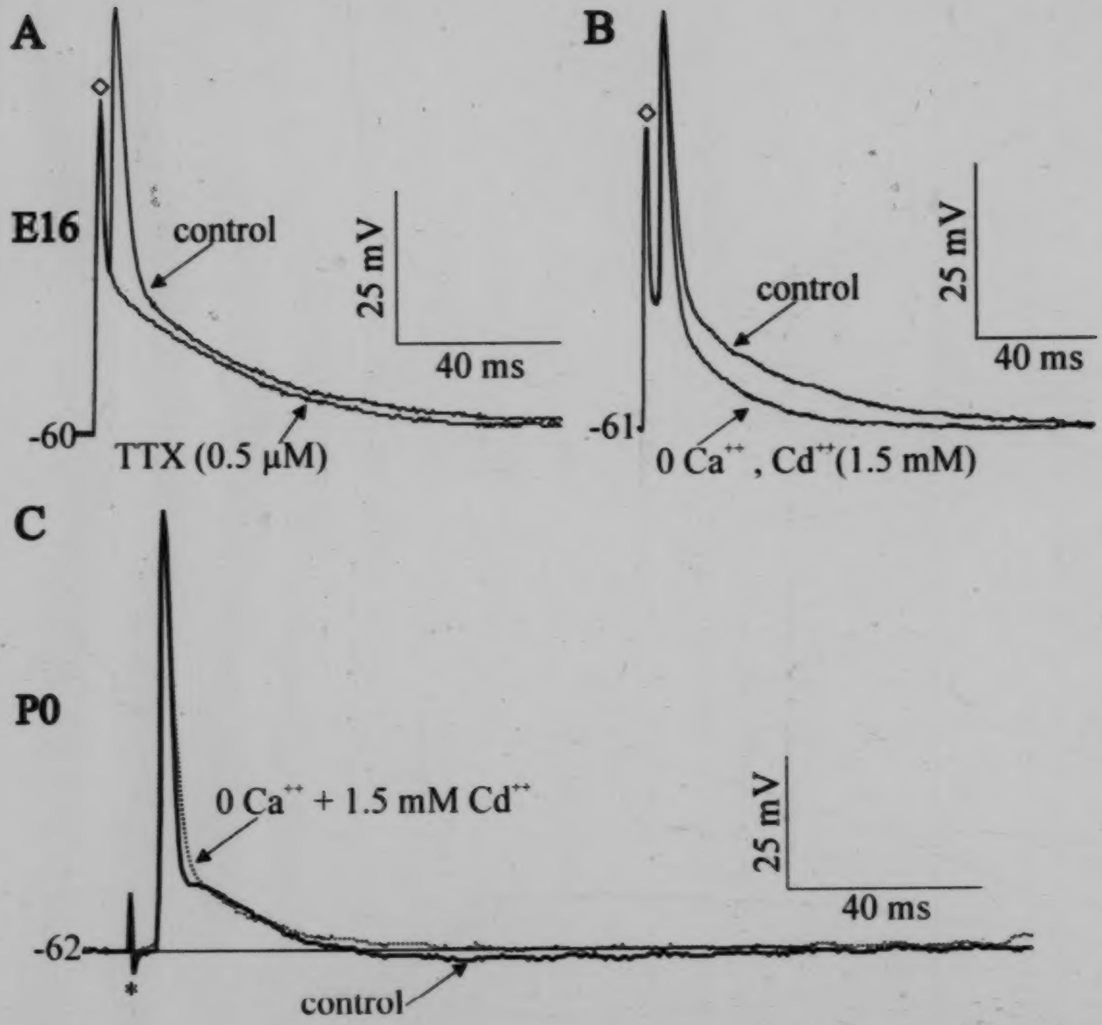
A
E16
control
25 mV
40 ms
-60
TTX (0.5 µM)
B
control
25 mV
40 ms
-61
0 Ca++ , Cd++(1.5 mM)
C
P0
0 Ca++ + 1.5 mM Cd++
25 mV
40 ms
-62
*
control

Electrotonic coupling between PMNs

Our initial intent was to use antidromic stimulation of the phrenic nerve to verify the identity of PMNs. However, rather unexpectantly, we noted that in a subpopulation of PMNs, subthreshold antidromic stimulation of the phrenic nerve resulted in the generation of a low amplitude depolarizing potentials (Fig. 3.6 A; observed in 3/22 E16, 5/19 E18 and 8/30 P0-1 PMNs). This depolarizing potential had a very short latency with respect to the onset of the antidromic action potential; referred to as a short latency depolarization (SLD; Walton and Navarrete, 1991). In accordance with previous work (Walton and Navarrete, 1991), the SLDs are indicative of electrotonic coupling between PMNs due to the presence of gap junctions. As proposed by Walton and Navarrete, (1991), we classified SLDs as electrotonic if at least three of the following criteria were met; i) depolarizing potentials had a short latency with respect to the antidromic action potential, ii) an increase in stimulation strength evoked a graded response of the SLD, iii) SLDs were resistant to high frequency stimulation (20 Hz), iv) SLDs were not affected by collision of an orthodromic action potential (generated by somatic current injection) with the antidromic spike, v) SLDs were insensitive to holding potential, and vi) SLDs were unaffected by removal of external Ca^{++} or blockage of Ca^{++} conductances. It should be noted that reflex-mediated synaptic activity in the form of excitatory or inhibitory potentials (i.e., EPSP, IPSP) were not observed during recording of electrical activity of PMNs as the dorsal roots had been cut. Further, no clear evidence for the presence of Renshaw neurons, in the form of high frequency firing neurons, following antidromic stimulation were found (Hilaire et al., 1986).

As shown in Fig. 3.6 A, subthreshold stimulation of a P0 PMN evoked low amplitude depolarizations which closely followed the onset of the antidromic action potential. In the particular PMN presented in Fig. 3.6 A, subthreshold stimulation evoked two SLDs of increasing amplitude, indicating the presence of coupling between three PMNs. Removal of external Ca^{++}, to prevent synaptic release, did not diminish the graded SLD (Fig. 3.6 B). Collision experiments were carried out in order to clearly visualize the SLDs after eliminating the contribution of the antidromic action potential during the invasion of the soma. When a soma-generated action potential was elicited prior to antidromic stimulation, a SLD (Fig. 3.6 C, continuous line) was evoked where the antidromic action potential would be expected (Fig. 3.6 C, discontinuous line). Further, high frequency stimulation of the phrenic nerve did not reduce the expression of the SLD, indicating further that this depolarization is independent of synaptic activity (Fig. 3.6 D). When the pipette solution contained the intracellular inhibitor of Na^+ channels, QX 314, the antidromic action potential was eliminated as expected within a few minutes of membrane rupture. However, the SLD which was insensitive to the holding membrane potential still persisted (Fig. 3.6 E), suggesting that this potential does not involve synaptically-mediated post-synaptic events or the activation of voltage-sensitive ionic conductances within the neuron being recorded from (i.e. SLD resulted from passive spread of current from coupled neuron).

The coupling between PMNs was also reflected in the relatively lower input resistance and higher mean rheobase measured in neurons where coupling was detected compared to those where it was not. For E18 PMNs the input resistance in PMNs with and without SLDs were 387±108 (n=5) vs 555±61 MΩ (n=16) and the mean rheobases were 76±32 (n=5) vs. 42±6 nA (n=16). For P0-1 PMNs the input resistance in PMNs with and without SLDs were 106±14 (n=7) vs 266±33 MΩ (n=26) and the mean rheobases were 259±86 (n=7) vs. 89±14 nA (n=26). Only one of the three E16 PMNs showing SLDs were recorded with an intracellular solution which did not contain QX-314 and thus insufficient numbers were available for a statistically meaningful comparison of passive properties between neurons with and without SLDs at that age.

Figure 3.6. Multiple criteria were used as evidence for electrical coupling between PMNs. **A)** Low amplitude, short latency depolarizations evoked by subthreshold antidromic stimulation of the phrenic nerve in a P0 slice. In this particular case, subthreshold stimulations generated a graded response consisting of at least two short latency depolarizations (arrow). Increments in the stimulation intensity eventually induced an antidromic action potential. **B)** Neither the antidromic spike, nor the short latency depolarizations, were eliminated by bathing in a Ca^{++}-free buffer. **C)** Collision of a somatic action potential (generated by intracellular current injection, diamond) and an antidromic action potential (*) allowed for the observation of a low amplitude depolarization (arrow) in place of the antidromic action potential (discontinuous line). The holding membrane potentials in A, B and C were -61 mV. **D)** High-frequency stimulation (20 Hz) of the phrenic nerve did not affect the low amplitude, short latency depolarizations. Two sweeps are represented in this figure, for clarity, only the firsts two antidromic artifacts are represented by an asterisk. The measurement in A,B,C and D are from the same P0 motoneuron. **E)** In a different P0 motoneuron, low amplitude short latency depolarizations were evoked with a pipette solution containing the intracellular blocker of Na^+ channels, QX 314 (1.5 mM). Holding of membrane potential at various levels did not affect the amplitude of the electrotonic potentials.

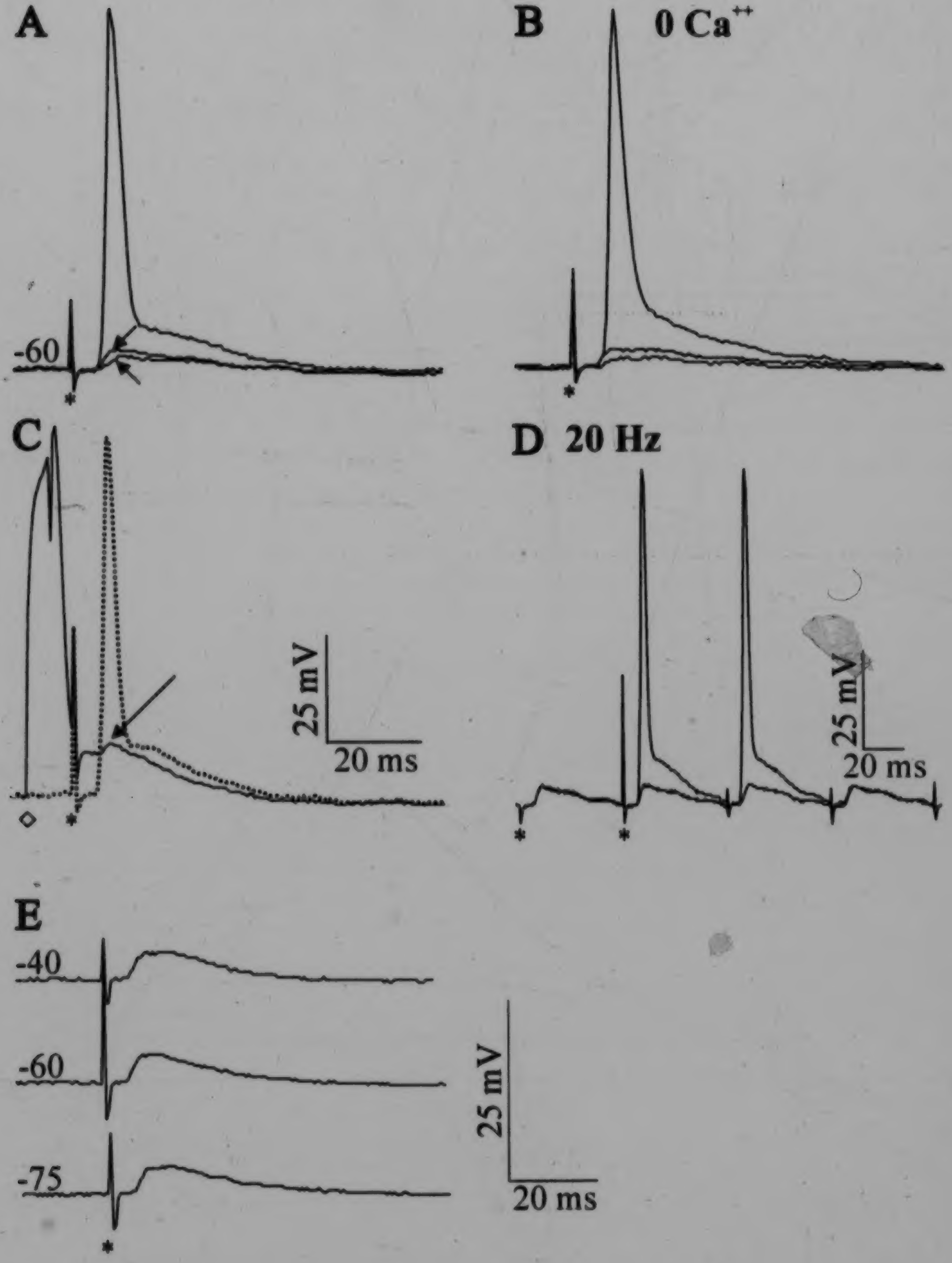
A
-60
*
B
0 Ca⁺⁺
*
C
◇
*
25 mV
20 ms
D 20 Hz
*
*
25 mV
20 ms
E
-40
-60
-75
*
25 mV
20 ms

Repetitive firing properties

Changes in the passive and action potential properties have a critical effect on the firing pattern of differentiating neurons. Thus, we investigated age-dependent changes in the firing properties of PMNs by injection of 1s-long depolarizing pulses of increasing strength. The population data illustrating age-dependent changes in firing properties are listed in Table 3.2. Representative data for PMNs of differing ages and firing characteristics are shown in Fig. 3.7. The majority of PMNs at all ages were able to generate sustained trains of action potentials with spike frequency adaptation (SFA) (~72% of E16, 73% of E18 and 63% of P0-1 PMNs; Fig. 3.7 A,B,C). At ages E16 and E18, however, ~28% of PMNs fired only one or a few action potentials during the 1s-long depolarizing pulse (not shown). It is possible that these PMNs were damaged following electrode attachment or are amongst that population of PMNs which undergo apoptosis during this period (Harris and McCaig, 1984). However, these ideas are contradicted by the fact that the motoneurons had healthy membrane potentials, high input impedances and overshooting action potentials. Thus, these embryonic PMNs with minimal firing capabilities may simply reflect a population with a relatively underdeveloped complement of ionic conductances. In P0-1 PMNs, although the majority of neurons were able to generate continuous discharges with frequency adaptation, two further populations of PMNs with different firing patterns were observed. A second group of neonatal PMNs generated a burst of action potentials at the beginning of the depolarizing pulse (20%; Fig. 3.7 D). Bursting was characterized as a group of action potentials (2-3) occurring at a high frequency and separated from other spikes by a longer interspike interval (see also Fig. 4.9 A and 5.9 C). Bursting seemed to arise from an afterdepolarizing potential that followed the first spike (Fig. 3.7 D). Bursting firing was enhanced by hyperpolarizing holding potentials (not shown). A third group of P0-1 PMNs (17%) with a very low input resistance (113±6 MΩ) required strong depolarizations (≥0.9 nA) to evoke firing (Fig. 3.7 E). Of the 7 PMNs within this group, SLDs indicative of electrical coupling were detected in 5 neurons. Thus, the high rheobase and low input resistance may be a direct result of coupling (Getting, 1974; Lo Turco and Kriegstein, 1991). Although coupling was also observed between embryonic PMNs, the lack of a clear indication of a high rheobase population may have been due to the fact that the differences between PMN passive properties amongst those neurons with and without SLDs were not as exaggerated as was the case at P0-1.

In E16, but not in older PMNs, repetitive firing significantly altered the duration of the following spikes when compared with the first spike of the train (Fig. 3.7 A vs. C,E). Thus, during repetitive firing in E16 PMNs, action potentials became longer in duration and their amplitude decreased over the first few intervals. Values for the duration of the first versus the last action potential in a 1 sec long train of spikes were as follows: E16 (6.4 ± 0.5 vs 9.7 ± 1.3, n=15, $p<0.05$); E18 (4.0 ± 0.2 vs 4.3 ± 0.3, n=14); P0-1 (3.7 ± 0.3 vs 3.7 ± 0.4, n=21).

As revealed by the threshold current required for generating repetitive firing (Table 3.2) and frequency-current plots (Fig. 3.7 F), embryonic PMNs required lower levels of depolarizing current than neonatal PMNs in order to generate repetitive firing. The significant decrease in the input resistance of PMNs from E16 to P0-1 meant that there was an age-dependent increase in the strength of the depolarizing current required to generated repetitive firing. For example, P0-1 PMNs required an approximate two-fold increase in the threshold current to evoke repetitive firing as compared with E16 and E18 PMNs (Table 3.2). Among neonatal PMNs, the low input resistance motoneurons (likely electrotonically coupled neurons) required the highest levels of current stimulation to elicit repetitive firing (Fig. 3.7 F).

Embryonic PMNs also tended to have a more limited firing range compared with neonatal PMNs (Fig 3.7 F, Table 3.2). The firing frequency during the 1s-long stimulation pulse increased steadily between E16 and P0-1 at the minimal level of depolarizing current required for repetitive firing and at twice that level (Table 3.2). The initial firing rate (i.e., the inverse of first interspike interval (ISI) duration) also increased steadily from E16 to P0-1 as a function of the injected current (Table 3.2). The slope of the f-I plot for the first ISI did not change significantly between the age groups studied although the slope of the last ISI decreased because of the decline in the firing rate with time (Table 3.2). A marked increase in the amount of SFA as a function of firing frequency (Figs. 3.7 and 3.8 A and B) were observed at all ages studied. Most of the rapid decline in the firing frequency characteristic of SFA, occurred at the beginning of the pulse (Fig. 3.8 B). As represented in Fig. 3.8 A, SFA was a function of the firing rate (i.e, injected current): at high initial firing rates (i.e., that's is stronger amounts of injected current) the adaptation was more pronounced than at lower firing rates.

Table 3.2. Changes in the firing properties[1] of PMNs.

		E16 (n=18)	**E18** (n=16)	**P0-1** (n=21)
Threshold current [2] (I_{thr}, pA)		41±5	48±13	$98\pm18^{+\,\diamond}$
Firing frequency[3] (Spikes/sec)	at I_{thr}	7.1±0.5	9.8±0.9	$13.2\pm0.7^{+\,\diamond}$
	at $2\mathrm{x}I_{thr}$	14.4±1.0	$18.4\pm1.3^{*}$	$28.0\pm2.3^{+\,\diamond}$
First ISI frequency (Hz)	at I_{thr}	12.6±0.9	13.9±1.8	$29.6\pm3.7^{+\,\diamond}$
	at 2 x I_{thr}	24.1±2.2	27.9±2.6	$52.5\pm5.3^{+\,\diamond}$
Frequency-current slope[4] (Hz/nA)	first ISI	444±51	600±75	501±60
	last ISI	340±43	327±41	271±44

[1] Results were compiled from the firing discharges of PMNs which illustrate repetitive firing patterns similar to those in Fig. 3.7 A,B,C (i.e., bursting and low-input resistance PMNs not included in data), after a series of 1s-long depolarizing current pulses of increasing amplitude from a holding potential ~-60 mV. Measurements of the ISI were carried out at the beginning and end of the depolarizing pulse.

[2] Threshold current for repetitive firing was determined as the lowest stimulation current necessary to evoke repetitive firing.

[3] Firing frequency was determined as the number of action potentials per 1s-stimulation.

[4] Frequency-current slope was the ratio of first ISI or last ISI frequency vs. injected current.

($^{+}$) $p \leq 0.01$, (*) $p \leq 0.05$ vs. E16 or ($^{\diamond}$) $p \leq 0.05$ vs. E18.

Figure 3.7. Examples of repetitive firing patterns generated in E16, E18 and P0 PMNs following injection of 1s-depolarizing square pulse from a membrane holding potential of -60 mV. The amount of applied currents (in nA), in this and following figures, is stated beside each trace. The majority of E16 (A) and E18 (B) motoneurons exhibited a continuous firing discharge with adaptation. By P0, three distinct firing patterns had developed amongst PMNs (C,D,E). The largest percentage of cells generated continuous firing with adaptation (C, 63%). In a smaller percentage of PMNs, firing was initiated by a rapid discharge of action potentials (D, 20%) or following injection of strong depolarizing currents (E, 17%), indicative of very low input resistance (i.e. high threshold). F) Frequency-current plots for each of the neurons shown in traces A-E are shown in the frequency-current plot. Embryonic PMNs required significantly less current to reach firing threshold. Amongst neonatal PMNs, high threshold neurons required significantly higher levels of current to obtain threshold in comparison to lower threshold PMN populations.

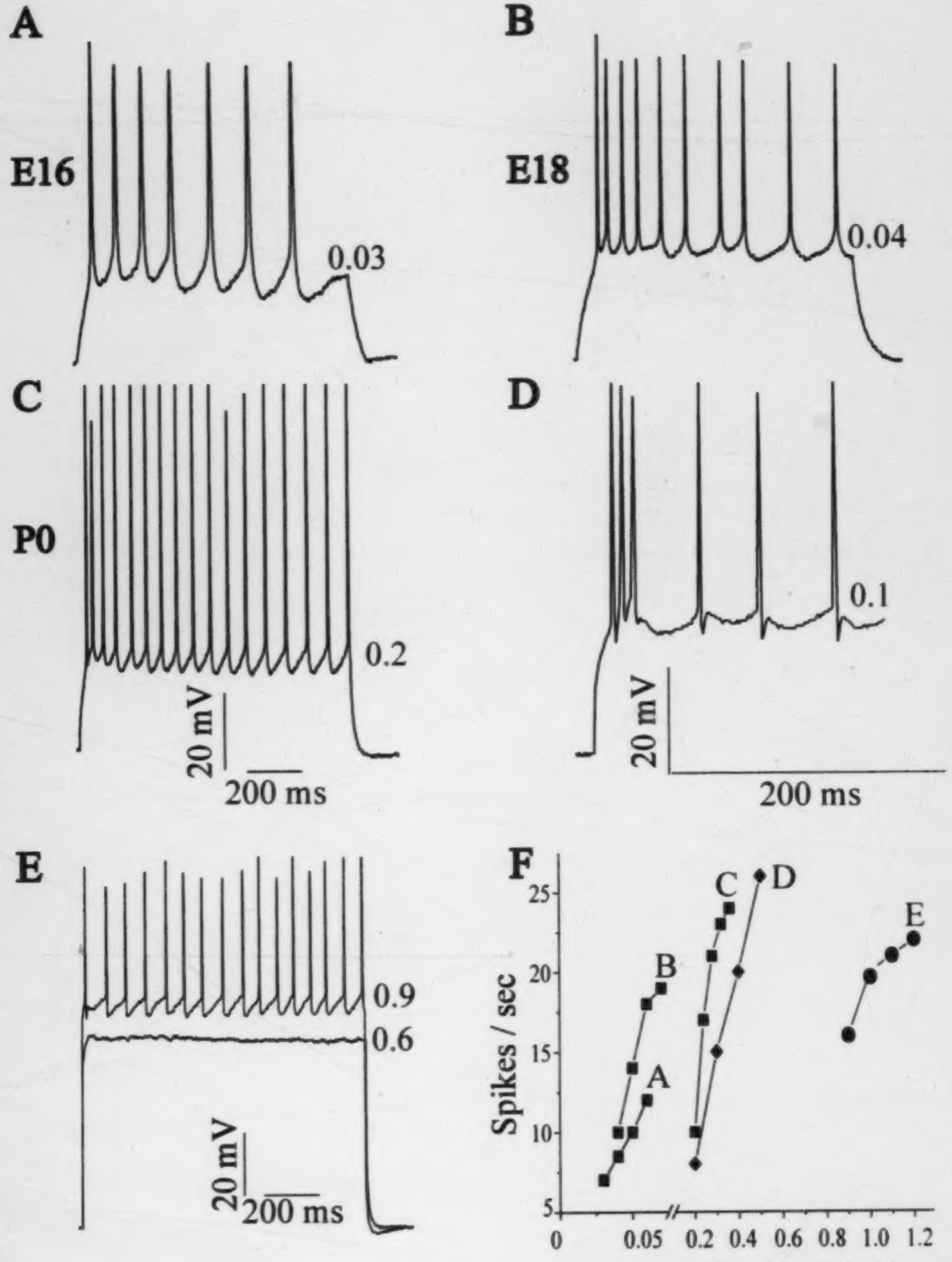
A
E16
0.03
B
E18
0.04
C
P0
0.2
20 mV
200 ms
D
0.1
20 mV
200 ms
E
0.9
0.6
20 mV
200 ms
F
Spikes / sec
25
20
15
10
5
0
0.05
0.2
0.4
0.6
0.8
1.0
1.2
Injected current (nA)
A
B
C
D
E

Figure 3.8. Plots of the instantaneous firing rates as a function of injected current or interspike interval (ISI). Data are from neurons displaying continuous firing discharge patterns at ages E16, E18 and P0 (as shown in **Fig. 3.7 A, B** and **C**, respectively), and tested with 1-s constant current pulses of increasing intensities. **A)** Instantaneous firing frequency (1/ ISI duration) versus injected current (f-I plot) for the 1st, 2nd, 3rd and last ISI. **B)** Plots of instantaneous frequency versus the ISI number for two current amplitudes. At all ages studied, there was adaptation (i.e. the instantaneous firing frequency decreased during the course of the 1 sec pulse) which was more pronounced at higher current strengths. The amount of applied currents (in nA) is stated beside each plot.

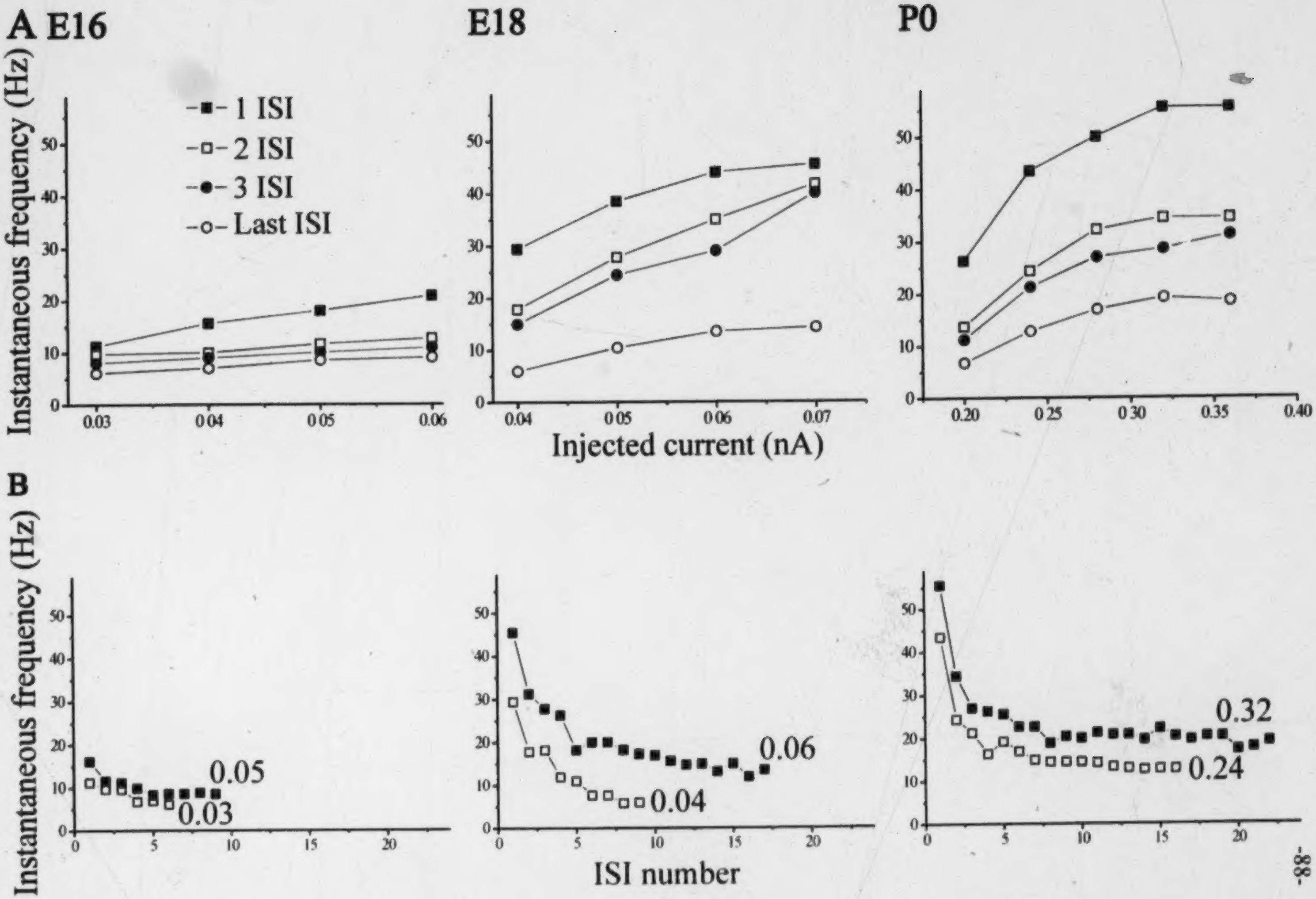
A E16
E18
P0
1 ISI
2 ISI
3 ISI
Last ISI
Instantaneous frequency (Hz)
0
10
20
30
40
50
0.03
0.04
0.05
0.06
0.07
0.20
0.25
0.30
0.35
0.40
Injected current (nA)
B
Instantaneous frequency (Hz)
0
5
10
15
20
0.05
0.03
0.06
0.04
0.32
0.24
ISI number

DISCUSSION

There are number of critical events associated with PMN development which occur at E17 including the inception of functional recruitment via synaptic drive from medullary respiratory centres, arrival of spinal afferent terminals within the PMN pool, and the completion of intramuscular innervation of the diaphragm (Greer et al., 1992; Allan and Greer, 1997a,b). During the ensuing 3-4 day period there is also a major transformation of PMN morphology (Allan and Greer, 1997b) and the continuous rhythmic activation at birth. The present results demonstrate that PMNs undergo pronounced changes in their passive and active electrical properties in association with these developmental events.

Development of membrane properties

During the period of PMN development spanning from E16 to P0-1, the resting membrane potential becomes more hyperpolarized without a significant change in voltage threshold required for generating an action potential, whereas the input resistance and time constant decreased. Thus, PMNs are electrically more excitable at the inception of inspiratory drive (E17) compared with more mature states. Functionally, the increased propensity for firing will compensate for a relatively weak descending inspiratory drive from the medullary respiratory centre, and thus facilitate the production of fetal breathing movements (Greer et al., 1992; Di Pasquale et al., 1996). It was interesting to note that there was an ~8 mV change in the resting membrane potential of PMN spanning the two day period immediately prior to and post the inception of inspiratory drive transmission (E16-E18). Future studies reexamining PMN electrophysiological properties at these ages when the descending drive transmission has been experimentally eliminated will be useful for evaluating the relative importance of activity-dependent transformations of PMN resting properties.

This trend for changes in PMN passive properties is similar to that described during embryonic and postnatal development of spinal and brainstem motoneurons (Fulton and Walton, 1986; Ziskind-Conhaim, 1988; Cameron et al., 1991b; Nunez-Abades et al., 1993; Viana et al., 1994; Xie and Ziskind-Conhaim, 1995) and hippocampal neurons (Spigelman et al., 1992). Further, a similar trend continues postnatally in PMNs (Cameron et al., 1990; 1991a,b). Several mechanisms could mediate the age-related changes in passive properties of motoneurons. A maturation in the relative permeability to Na^+ and K^+ ions would account for some of the hyperpolarizing of the resting membrane potential during PMN differentiation (Spigelman et al., 1992). Further, the regulation of the Na^+-dependent chloride co-transporter is different in embryonic motoneurons, resulting in an increase in the intracellular concentration of chloride ions and a subsequent raising of the chloride equilibrium potential compared to more mature states (Wu et al., 1992; Rohrbough and Spitzer, 1996).

The reduction in the time constant and input resistance with age seems to reflect an increased density of ionic channels and cell size. An increase in the density of ionic conductances, as previously observed in developing chick motoneurons (McCobb et al., 1990), was suggested by the reduction of the membrane time constant, and thus specific membrane resistance, ($R_{sp}=\tau_m / C_{sp}$; assuming no age-dependent changes in the specific membrane capacitance of ~1 $\mu F/cm^2$). Previous morphological studies have demonstrated that PMNs undergo a significant increase in cell size and elaboration of the dendritic branching from E16 up to birth (Allan and Greer, 1997b).

Presence of electrical coupling amongst perinatal PMNs

We have detected the presence of electrical coupling amongst subpopulations of PMNs between ages E16 and P0-1 (ranging from 14-26% of PMNs). The evidence to date suggests that at most 2-3 cells are coupled via gap junctions. Previous findings from recordings of neonatal (P0-3) rat thoracic motoneurons indicated coupling in as many 77% of lumbar motor neurons with the mean number of cells per coupling being ~4.5 (Walton and Navarrete, 1991). It may be that a similar degree of coupling is present in PMNs but at an earlier stage of development than we studied (i.e. pre-E16), as there is a clear rostrocaudal gradient of development within spinal neurons (Nornes and Das, 1974). There are at least two reasons why the presence of gap junctions may have been underestimated in our study. First, we only looked for SLDs which appeared subthreshold to the antidromic currents necessary to generate an antidromic action potential in the PMN being recorded from. Thus, in the event that the PMN being recorded from was coupled to a neuron with a higher threshold for antidromic activation (e.g. smaller diameter axon), the coupling would remain undetected. Second, one cannot be assured that all axons within the nerve are stimulated by the suction electrode and/or conduct the antidromic action potentials to the full extent of the PMN pool.

Despite these limitations for quantifying the degree of electrical coupling, this is the first data demonstrating that there is, in fact, coupling between PMNs. Neuronal coupling amongst rat PMNs are not present in the adult (Lipski, 1984) and there is no evidence to date for dye-coupling amongst postnatal PMNs (>P1; Cameron, personal communication). We propose that the presence of neuronal coupling early in development and their removal with maturation would be functionally appropriate. The CNS utilizes two fundamental strategies for increasing the force produced by a muscle. First, the firing frequency of a given motor unit can be increased. Second, additional motor units can be recruited. In the case of fetal PMNs, at the inception of fetal respiratory movements, our data demonstrate that there are limits on the firing capabilities of PMNs. However, the presence of neuronal coupling facilitates the second strategy of increasing the number of motor units recruited for a given descending synaptic drive. Thus, although the descending drive may be relatively weak and the maximum discharge frequency of PMNs limited, the presence of coupling among the neuronal population will ensure adequate synchronous drive to the diaphragm for the purposes of generating perinatal breathing movements. As the animal matures, the situation changes to one where less than 30% of the PMN pool is recruited during an inspiratory effort at rest (Cameron, et al., 1991; Torikai et al., 1996). Therefore, it would be inappropriate, and disadvantageous, for neuronal coupling to persist amongst the PMN pool at a time when precise, graded recruitment is desired.

Development of action potential characteristics and associated ionic conductances

By E16, PMNs are capable of generating overshooting action potentials following intracellular injection of depolarizing current or antidromic stimulation. As observed during the embryonic (Spitzer and Baccaglini, 1976; Di Pasquale et al., 1996) and postnatal (Fulton and Walton, 1986; Ziskind-Conhaim, 1988; Viana et al., 1994) maturation of other motoneurons, PMN action potentials increase in amplitude and decrease in duration between

E16 and P0-1. As demonstrated by McCobb et al. (1990), the increase in action potential amplitude during motoneuron differentiation results from an increase in the density of voltage-gated Na$^+$ channels. The maturation of K$^+$ conductances are important for spike repolarization and voltage-dependent changes in action potential duration in other neuronal systems (McCobb et al., 1990; Spigelman et al., 1992). Although voltage clamp experiments are required to characterize the K$^+$ conductances involved in shaping the action potential and firing properties of PMNs, the present findings suggest age-dependent changes in the expression of Ca^{++}-activated K$^+$ conductances. First, removal of extracellular Ca^{++} contributes to prolonging the duration of action potential in neonatal PMNs only whereas the use of a pipette solution with low Ca^{++} buffer capacity causes the oppositive effect on action potential duration. This is consistent with the presence of a Ca^{++}-activated K$^+$ conductance (likely of the maxi-type) which is involved in spike repolarization of neonatal motoneurons (Takahashi, 1990; Viana et al., 1993b). Second, at E18, a Ca^{++}-dependent conductance generating the afterhyperpolarization (AHP or small-type conductance) starts to develop and is fully expressed in the majority of neonatal PMNs. This conductance is prominent in neonatal motoneurons where it plays a role in regulating repetitive firing frequencies and modulating SFA (Viana et al., 1993b; Walton and Fulton, 1986).

We tested whether developing PMNs were capable of generating Ca^{++}-dependent action potentials as has been reported for developing amphibian spinal neurons (Spitzer and Baccaglini, 1976). However, in PMNs, Na$^+$ ion influx is essential for action potential generation at the earliest ages studied (E16) and throughout further development. It remains to be determined whether Ca^{++}-mediated action potentials occur in PMNs at earlier ages

(≤E15). Nevertheless, while Ca^{++} spikes do not occur at E16, Ca^{++} ions do contribute significantly to prolonging the action potential at this age. The Ca^{++}-induced broadening of the action potential in PMNs are diminished rapidly after the inception of inspiratory drive transmission at E17 as no Ca^{++} component was seen to prolong the action potential spike at E18. There was also an age-dependent decrease in the presence of a Ca^{++}-dependent rebound depolarization amongst PMNs. Functionally, beyond affecting firing properties, the influx of Ca^{++} ions is thought to be important for promoting neurite growth in developing neurons (McCobb et al., 1989; Holliday and Spitzer, 1990; Komuro and Rakic, 1996). This would be particularly important for PMNs during the period spanning E16-E19, when they undergo rapid growth and reorganization of axons and dendrites (Allan and Greer, 1997b). Further, Ca^{++} fluctuations are important for regulating the maturation of voltage-gated ion channels during periods of electrophysiological maturation (Gu and Spitzer, 1995).

Development of repetitive firing properties

The developmental changes of the passive properties and the ionic conductances shaping action potentials were responsible for a major change in the repetitive firing properties of PMNs. With the age-dependent reduction in the duration of individual action potentials, there was an increase in the overall repetitive firing abilities of PMNs. Further, by P0, a second group of PMNs emerged which fired bursts of action potentials at the onset of a depolarizing pulse and may be related to early-recruited PMNs (Cameron et al., 1991; Di Pasquale et al., 1996). A third group of PMNs required significantly stronger depolarizations to be activated. This likely reflected a group of PMNs which remained electrotonically coupled rather than the emergence of PMNs corresponding to high threshold neurons observed at later stages of development (Cameron et al., 1991; Di Pasquale et al., 1996).

In summary, following the inception of inspiratory drive transmission through to birth, PMN electrophysiological properties undergo significant maturational change. As the present findings suggest, changes in the expression of specific Ca^{++} and K^{+} ionic conductances may account for the developmental changes in action potential characteristics and repetitive firing properties of PMNs during this period. The specific role of Ca^{++} and K^{+} ionic conductances during PMN electrical differentiation is the topic of the following two chapters. Finally, in order to gain a better understanding of the development of the respiratory neuromuscular system it was of interest to determine how changes in the firing properties of PMNs correlated with changes in the diaphragm contractile properties. This problem will be further investigated in chapter VI.

REFERENCES

ALLAN, D.W., GREER, J.J. (1997a) Embryogenesis of the phrenic nerve and diaphragm in the fetal rat. J. Comp. Neurol. 382: 459-468.

ALLAN, D.W., GREER, J.J. (1997b) Development of phrenic motoneuron morphology in the fetal rat. J. Comp. Neurol. 381: 469-479.

BAYLISS, D.A., VIANA, F., BELLINGHAM, M.C., BERGER, A.J. (1994) Characteristics and postnatal development of a hyperpolarization-activated inward current in rat hypoglossal motoneurons in vitro. J. Neurophysiol. 71: 119-128.

BROCKHAUS, J., BALLANYI, K., SMITH, J.C., RICHTER, D.W. (1993) Microenvironment of respiratory neurons in the *in vitro* brainstem-spinal cord of neonatal rats. J. Physiol. 462: 421-445.

CAMERON, W.E., BROZANSKI, B.S., GUTHRIE, R.D. (1990) Postnatal development of phrenic motoneurons in the cat. Dev. Br. Res. 51:142-145.

CAMERON, W.E., H.E., F., KALIPATNAPU, P., JODKOWSKI, J.S., GUTHRIE, R.D. (1991a) Morphometric analysis of phrenic motoneurons in the cat during postnatal development. J. Comp. Neurol. 314:763-76.

CAMERON, W.E., JODKOWSKI, J.S., FANG, H., GUTHRIE, R.D. (1991b) Electrophysiological properties of developing phrenic motoneurons in the cat. J. Neurophysiol. 65: 671-679.

CONNORS, B.W., PRINCE, D.A. (1982) Effects of local anaesthetic QX-314 on the membrane properties of hippocampal pyramidal neurons. J. Pharmacol. Exp. Therap. 220: 476-481.

DEKIN, M.S., GETTING, P.A. (1987) In vitro characterization of neurons in the ventral part of the nucleus tractus solitarius. II. Ionic basis for repetitive firing patterns. J. Neurophysiol. 58: 215-229. .

DI PASQUALE, E., TELL, F., MONTEAU, R., HILAIRE, G. (1996) Perinatal developmental changes in respiratory activity of medullary and spinal neurons: an in vitro study on fetal and newborn rats. Develop. Brain Res. 91: 121-130.

FULTON, B.P., WALTON, K. (1986) Electrophysiological properties of neonatal rat motoneurons studied in vitro. J. Physiol. (London) 370: 651-678.

GETTING, P.A. (1974) Modification of neuron properties by electrotonic synapses I. Input resistance, time constant, and integration. J. Neurophysiol. 37: 846-857.

GREER, J.J, SMITH, J.C., FELDMAN, J.L. (1992) Respiratory and locomotor patters generated in the fetal rat brain stem-spinal cord in vitro. J. Neurophysiol. 67(4): 996-999.

GU, X., SPITZER, N.C. (1995) Distinct aspects of neuronal differentiation encoded by frequency of spontaneous Ca2+ transients. Nature 375: 784787.

HARDING, R., HOOPER, S.B., VAN, V.K. (1993) Abolition of fetal breathing movements by spinal cord transection leads to reductions in fetal lung volume, lung growth and IGF-II gene expression. Pediatric Res. 34: 148-153.

HARRIS, A.J., MCCAIG, C.D. (1984) Motoneuron death and motor unit size during embryonic development of the rat. J. Neurosci. 4: 13-24.

HILAIRE, G., KHATIB, M., MONTEAU, R. (1986) Central drive on Renshaw cells coupled with phrenic motoneurons. Brain Res. 376: 133-139.

HOLLIDAY, J., SPITZER, N.C. (1990) Spontaneous calcium influx and its role in differentiation of spinal neurons in culture. Dev. Biol. 141: 13-23.

JANSEN, A.H., CHERNICK, V. (1991) Fetal breathing and development of control of breathing. J. Appl. Physiol. 70: 1431-1446.

JIANG, C., AGULIAN, S., HADDAD, G.G. (1991) O_2 tension in adult and neonatal brain slices under several experimental conditions. Brain Res. 568: 159-164.

KITTERMAN, J.A. 1996 The effects of mechanical forces on fetal lung growth. Clinics in Perinatology 23:727-40.

KOMURO, H., RAKIC, P. (1996) Intracellular Ca^{2+} fluctuations modulate the rate of neuronal migration. Neuron 17: 275-285.

LIPSKI, J. (1984) Is there electrical coupling between phrenic motoneurons in cats? Neurosci. Lett. 46: 229-234.

LOCKERY, S.R., SPITZER, N.C. (1992) Reconstruction of action potential development from whole-cell currents of differentiating spinal neurons. J. Neurosci. 12: 2268-2287.

LOTURCO, J.L., KRIEGSTEIN, A.R. (1991) Clusters of coupled neuroblasts in embryonic neocortex. Science 252: 563-566.

MCCOBB, D.P., BEST, P.M., BEAM, K.G. (1989) Development alters the expression of calcium currents in chick limb motoneurons. Neuron 2: 1633-1643.

MCCOBB, D.P., BEST, P.M., BEAM, K.G. (1990) The differentiation of excitability on embryonic chick limb motoneurons. J. Neurosci. 10: 2974-2984.

NORNES, H.O., DAS, G.D. (1974) Temporal pattern of neurogenesis in spinal cord of rat. I. An autoradiographic study--time and sites of origin and migration and settling patterns of neuroblasts. Br. Res. 73:121-38.

NUNEZ-ABADES, P.A., SPIELMANN, J.M., BARRIONUEVO, G., CAMERON, W.E. (1993) In vitro electrophysiology of developing genioglossal motoneurons in the rat. J. Neurophysiol. 70:1401-1411.

ROHRBOUGH, J., SPITZER, N. C. (1996) Regulation of intracellular Cl^- levels by Na^+-dependent Cl^- cotransport distinguishes depolarizing from hyperpolarizing $GABA_A$ receptor-mediated responses in spinal neurons. J. Neuroscience 16:82-91.

SPIGELMAN, I., ZHANG, L., CARLEN, P.L. (1992) Patch-clamp study of postnatal development of CA1 neurons in rat hippocampal slices: membrane excitability and K^+ currents. J. Neurophysiol. 68: 55-69.

SPITZER, N.C., BACCAGLINI, P.I. (1976) Development of the action potential in embryonic amphibian neurons in vivo. Brain Res. 107: 610-616.

TAKAHASHI, T. (1990) Membrane currents in visually identified motoneurons of neonatal rat spinal cord. J. Physiol. (London) 423: 27-46.

TORIKAI, H., HAYASHI, F., TANAKA, K., CHIBA, T., FUKUDA, Y., MIRIYA, H. (1996) Recruitment order and dendritic morphology of rat phrenic motoneurons. J. Comp. Neurol. 366: 231-243.

VIANA, F., BAYLISS, D.A., BERGER, A.J. (1994) Postnatal changes in rat hypoglossal motoneuron membrane properties. Neurosci. 59(1): 131-148.

VIANA, F., BAYLISS, D.A., BERGER, A.J. (1993a) Calcium conductances and their role in the firing behaviour of neonatal rat hypoglossal motoneurons. J. Neurophysiol. 69(6): 2137-2149.

VIANA, F., BAYLISS, D.A., BERGER, A.J. (1993b) Multiple potassium conductances and their role in action potential repolarization and repetitive firing behaviour of neonatal rat hypoglossal motoneurons. J. Neurophysiol. 69(6): 2150-2163.

WALTON, K., FULTON, B.P. (1986) Ionic mechanisms underlying the firing properties of rat neonatal motoneurons studied in vitro. Neurosci. 19: 669-683.

WALTON, K.D., NAVARRETE, R. (1991) Postnatal changes in motoneuron electrotonic coupling studies in the in vitro rat lumbar spinal cord. J. Physiol. (London) 43: 283-305.

WU, W., ZISKIND-CONHAIM, L., SWEET, M.A. (1992) Early development of glycine- and

GABA-mediated synapses in rat spinal cord. J. Neurosci. 12(10): 3935-3945.

XIE, H., ZISKIND-CONHAIM, L. (1995) Blocking Ca^{2+} dependent synaptic release delays motoneuron differentiation in the rat spinal cord. J. Neurosci. 15: 5900-5911.

ZISKIND-CONHAIM, L. (1988) Electrical properties of motoneurons in the spinal cord of the rat embryo. Devel. Biol. 128: 21-29.

CHAPTER 4

DEVELOPMENT OF POTASSIUM CONDUCTANCES IN PERINATAL RAT PHRENIC MOTONEURONS

Adapted from the original publication:
M. Martin-Caraballo and J.J. Greer
J. Neurophysiol. (In press)

INTRODUCTION

Potassium conductances influence action potentials, neuronal repetitive firing patterns and the summation of synaptic inputs in neural cells (reviewed by McLarnor, 1995). Several types of K^+ channels have been identified based on their electrophysiological, pharmacological and molecular properties (reviewed by Rudy, 1988; Coetzee et al., 1999). The most widely distributed K^+ channels are the delayed outward rectifier, transient A-type and Ca^{++}-activated K^+ conductances. Other K^+ conductances which have a more limited expression in neuronal systems include the inward rectifier, muscarine-activated and ATP-sensitive K^+ channels. The delayed rectifier and A-type K^+ conductances regulate the timing of action potential formation and the repetitive firing pattern of neuronal cells (Dekin and Getting, 1987; Spigelman et al., 1992). Ca^{++}-activated K^+ conductances are important in generating afterhyperpolarizing potentials which ultimately influence neuronal firing properties. The expression pattern of these various classes of K^+ conductances are developmentally regulated (O'Dowd et al., 1988, McCobb et al., 1990; Spigelman et al., 1992; Mienville and Barker, 1997; Gao and Ziskind-Conhaim, 1998). At very early stages of neuronal development there are pronounced increases in the expression of delayed rectifier and A-type K^+ conductances (O'Dowd et al., 1988; McCobb et al., 1990; Spigelman et al., 1992; Gao and Ziskind-Conhaim, 1998).

As described in the previous chapter, PMNs undergo considerable changes in their action potential waveform during the E16-P1 period. These include obvious changes in action potential duration, amplitude and afterpotentials. In E16 PMNs, the main spike was followed by a slowly decrementing ADP which is transformed to a hump-type ADP by birth

(Fig 3.3). The fAHP and mAHP, which were absent at E16, developed by birth (Fig. 3.3). **In this study, I tested the hypothesis that the elaboration of action potential afterpotentials and the resulting changes in repetitive firing properties are due in large part to developmental changes in PMN K^+ conductances.** As described below, a combination of current- and voltage-clamp experiments in conjunction with pharmacological channel blockers were used to dissect out the role of various K^+ conductances during this period of PMN electrophysiological transformation.

METHODS

Whole-cell recordings

Electrophysiological properties of PMNs were studied in 48 E16, 50 E18 and 58 P0-1 PMNs. Upon completing the examination of PMN action potential and repetitive firing properties in current-clamp mode, we switched to the single electrode voltage-clamp configuration (discontinuous mode) in order to record K^+ currents. The switching rate was 20-40 kHz, the output bandwidth was set at 1 kHz and the clamp gain was ~0.8 nA/mV. Head stage output was monitored with a separate oscilloscope in order to monitor the voltage transients prior to sampling. Outward rectifier and A-type K^+ conductances were measured in Ca^{++}-free solution in the presence of TTX (0.5-1 μM) to eliminate Ca^{++}- and Na^+-mediated conductances, respectively. For recording outward rectifier K^+ currents, a 200 ms depolarizing prepulse (to -40 mV) was applied from a holding potential of -70 mV whereas a 200 ms hyperpolarizing prepulse (to -110 mV) was applied in order to maximally activate A-type K^+ currents. Leak and capacitative currents were subtracted from the scaled control currents by a P/4 protocol. Ionic currents at different stages of development were expressed as current densities by dividing current amplitudes by cell capacitance. Cell capacitance was determined from the integral area under the current transient following a 10 mV-voltage step at –70 mV holding potential.

The steady-state activation and inactivation of the transient component and the activation of the non-inactivating component were plotted as a function of membrane potential. For the inactivation plots, the current at a given membrane potential was normalized to maximal current. For activation, conductances (G) were calculated from currents as $G=I/(V_c-V_r)$ where V_c is the command potential and V_r is the calculated reversal potential for K^+ (-97 mV). The plots of normalized current or conductance versus membrane potential were fitted with a Boltzman function in the form I/I_{max} (or G/G_{max})$=1/[1+\exp(V_{1/2}-V)/k)]$, where V is the step potential, $V_{1/2}$ is the potential at half-maximal normalized value and k characterizes the steepness of the activation or inactivation curves.

Intracellular and extracellular solutions: The composition of the pipette solution, used to investigate the role of Ca^{++}-activated K^+ conductances on the action potential and repetitive firing of PMNs, was similar to that of the standard solution except for the following changes: BAPTA was decreased to 0.1 mM, Ca^{++} was not added, K^+ gluconate was 126 mM and phosphocreatine (10 mM) was added. Voltage-activated K^+ currents were recorder with the standard pipette solution (Chapter 2).

Drugs: The following drugs were used (suppliers in brackets): TTX, TEACl, apamin, 4-

aminopyridine (4-AP), cytochrome-c (Sigma); iberiotoxin, lidocaine–ethyl bromide (QX 314; RBI); ω-agatoxin (Peninsula Laboratories, Belmont, CA); ω-conotoxin GVIA (Alomone Laboratories, Jerusalem, Israel). The perfusion medium of the spinal slice with ω-conotoxin GVIA or ω-agatoxin also contained cytochrome-c (0.05%) in order to avoid non-specific binding to plastic tubing.

Western Analysis

Spinal cord segments from the C4-5 level were dissected free of connective tissue and the ventral region of the spinal cord containing cervical motoneurons was excised for immunoblotting. Tissue was homogenized for 30 sec followed by sonication for 20 sec. The homogenization buffer contained 100 mM Tris; 320 mM sucrose and 1% Triton (pH 7.6 with HCl). The homogenate was centrifuged at 10000g for 30 min at 4°C and the pellet discarded. Protein concentration was determined with a BCA protein assay kit (Pierce, Rockford, IL). The protein samples (40 µg/lane) were subjected to electrophoresis on a 9% polyacrylamide-SDS gel and electrophoretically transferred to nitrocellulose membranes (0.45 µm, Bio-Rad, Hercules, CA). To block non-specific binding, the blotted membranes were saturated with 3% skimmed milk in a TTBS-buffer containing 20 mM Tris-HCl, 45 mM NaCl and 0.1% Tween 20 (pH 7.6) for 1h at room temperature. Membranes were incubated with the primary antibodies overnight at room temperature. The primary antibodies used were supplied by Alomone Labs (Jerusalem, Israel) and included the polyclonal ANTI-SK3 and ANTI-BK_a antibodies against the small-conductance and maxi-type, Ca^{++}-activated K^+ channels, respectively (Butler et al., 1993; Kohler at al., 1996). The SK3 antibody recognizes the amino acid residues 2-21 in the N-terminal of rat SK3 (Mol. Weight ~61kD) whereas the BK_a antibody recognizes the amino acid residues 1098-1196 in the C-terminal of the mouse Slo α subunit (Mol. Weight ~125 kD). Minimum titer was determined by serial antibody dilution (1:200 and 1:300 dilutions for ANTI-SK3 and ANTI-BK_a, respectively). Blots were washed three times in TTBS buffer for 20 min followed by incubation with the secondary antibody horseradish peroxidase (HRP)-goat anti-rabbit (1:4000). After three 20 min-washes in TTBS buffer, the blots were incubated for 1 min with enhanced chemiluminescent (ECL; Santa Cruz, CA, cat #SC-2048) substrate and exposed to Hiper chemiluminescent film (Amersham, England). The appropriate molecular weight of the SK3 and BK_a protein was determined by the mobilities of pre-stained protein standards (Bio-Rad, Hercules, CA). Control experiments testing the specificity of the primary antibody were performed by pre-incubating the antibody with the appropriate antigen or fusion protein for 1h at room temperature. The protein content and its molecular weight per band was quantified with SigmaGel (Jansen Inc; San Rafael, CA).

RESULTS

Effects of blocking multiple K^+ conductances

The role of K^+ conductances in regulating action potential duration was initially studied using TEA and cesium-filled recording electrodes to block multiple K^+ conductances. Upon general blockade of K^+ conductances, a long-duration spike was evident at all ages studied (Fig. 4.1 A). The conductances underlying the long-duration component were examined by selectively blocking Na^+ and Ca^{++} conductances with intracellular QX 314 (1 mM) or following incubation in Ca^{++}-free medium, respectively. As shown in Fig. 4.1 B (left panel), stimulation with ten consecutive depolarizing pulses resulted in the disappearance of the fast, Na^+-dependent spike due to the use-dependent blockade of Na^+ channels with QX 314 (Connors and Prince, 1982). The long-duration component, which remained after Na^+ current blockade, was attenuated following incubation in Ca^{++}-free medium (Fig. 4.1 B, right panel). The duration of the Ca^{++}-dependent long-duration component decreased dramatically with age. The times for the plateau to attenuate to half-maximal amplitude were as follows: E16 = 320 ± 45 ms (n=8); E18 =126 ± 23 ms (n=6); P0 = 41 ± 10 ms (n=7).

Effects of blocking K^+ currents with TEA

The maturation of outward K^+ conductances plays an important role in shaping the action potential waveform and repetitive firing patterns in several differentiating neuronal systems (McCobb et al., 1990; Spigelman et al., 1992). Externally applied TEA (10 mM) was used to block outward K^+ conductances in order to evaluate their role in the spike repolarization of PMNs. At all ages tested, TEA significantly increased the action potential duration (Table 4.1). The effect of TEA on the regulation of the repetitive firing of PMNs was more difficult to quantify since motoneurons became very excitable. In E16 and E18 PMNs, TEA treatment evoked complex spikes, such as plateau potentials, whereas in neonatal PMNs, TEA application increased the firing frequency by ~28% (11±1 vs 15±1 Hz, n=4; Fig. 4.2).

Effects of blocking A-type K^+ conductances with 4-AP

The effects of TEA on the action potential duration were less pronounced at hyperpolarised holding potentials. Thus, we tested whether this was due to the presence of an A-type K^+ current which has a transient character and is inactivated at depolarised potentials (McCobb et al., 1990; Spigelman et al., 1992). Bath application of the A-type current inhibitor 4-AP (1-3 mM) prolonged the duration of the spike with no changes to action potential amplitude at all ages tested (Fig. 4.3 A, Table 4.1). Further, the prolongation of action potential duration by 4-AP was enhanced when action potentials were elicited from hyperpolarized holding potentials (Fig. 4.3 A).

In addition to its contribution to action potential repolarization, the 4 AP-sensitive K^+ conductance was involved in regulating the firing behaviour of PMN at all ages studied. When PMNs fired from hyperpolarized holding potentials a delayed excitation was observed (Fig. 4.3 B). The delay excitation was defined as a lag between the onset of depolarization and the onset of firing. Delayed excitations were observed in 47% of E16 (8 of 17), 54% of E18 (13 of 24) and 21% (4 of 19) of neonatal PMNs. The ramp-like depolarization characteristic of delayed excitation was blocked by 4-AP ($\geq$ 1 mM; Fig. 4.3 B) and insensitive to TTX (0.5-1 μM, n=6) or incubation in Ca^{++}-free medium (n=6; not shown). Despite the removal of the delayed excitation by 4-AP, the firing frequency of PMNs did not increase. This is likely explained by the concomitant increase in action potential duration caused by 4-AP (Fig. 4.3 B).

Table 4.1. Change in PMN action potential (AP) duration(1) following block of K^+ conductances with TEA and 4-AP.

	V_h(2) (mV)	Normalised AP duration (1) (%)		
		E16	E18	P0
TEA (10 mM)	-50	375±75*(3)	ND	ND
	-60	217±29*(3)	190±20*(5)	132±8*# (4)
	-75	190±10*(3)	ND	ND
4-AP (3 mM)	-60	349±84*(5)	471±170*(3)	633±159*(3)

(1) AP duration at half-maximal amplitude was expressed as a percentage of the control response without any treatment.

(2) Membrane holding potential.

(*) $p \leq 0.05$ vs control (no treatment, 100 %); (#) $p \leq 0.05$ vs E16; ND, no data.

Figure 4. 1. A) Block of multiple of K$^+$ conductances revealed plateau potentials in PMNs which varied in duration depending on age. Plateau potentials were generated following intracellular current injection though the recording pipette filled with a TEA$^+$ (110 mM) and Cs$^+$ (30 mM) solution in order to block K$^+$-mediated conductances. QX 314 (1 mM) was also included in the intracellular pipette solution to block Na$^+$ channels. The duration of the Ca^{++}-dependent spike decreased with age. **B)** Recordings illustrating that plateau potentials are Ca^{++}-dependent and insensitive to Na$^+$ channel blockade. Recordings were from P0 (left) and E16 (right) PMNs with a pipette solution containing TEA$^+$ (110 mM), Cs$^+$ (30 mM) and QX 314 (1 mM). Left panel shows 10 consecutive spikes (arrow 1-10) and the QX 314 use-dependent inhibition of the fast Na$^+$ transient (arrow) with no effect on the long-duration component. Right panel shows that the plateau was eliminated following incubation in Ca^{++}-free medium.

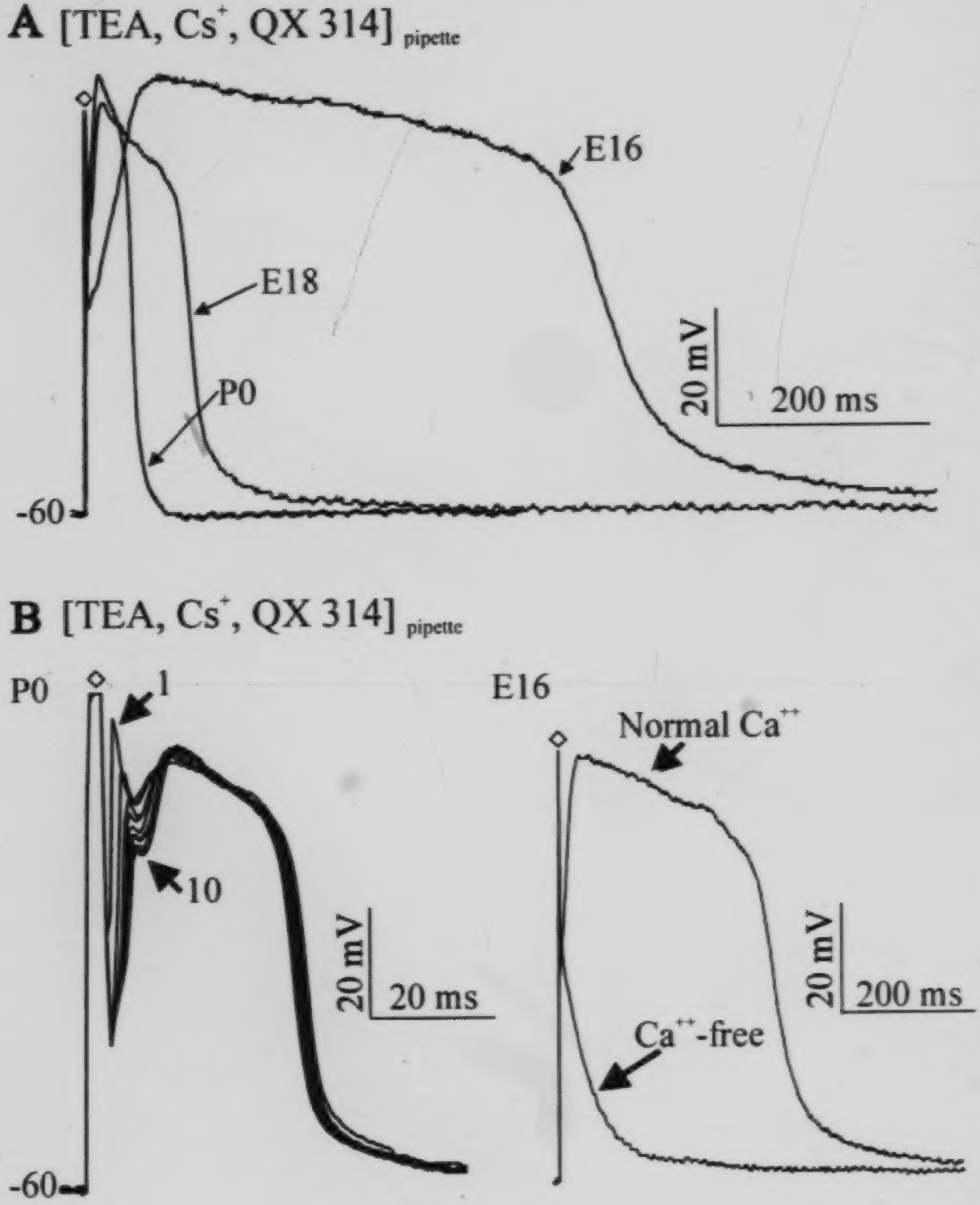

A [TEA, Cs^+, QX 314]$_{\text{pipette}}$

B [TEA, Cs^+, QX 314]$_{\text{pipette}}$

Figure 4.2. Effect of externally applied TEA (10 mM) on the firing pattern of PMNs. Repetitive firing was evoked following intracellular current injection for 1s. Holding potential is -60 mV. Since inhibition of K^+ channels by TEA is use-dependent, the TEA effect take some time to develop.

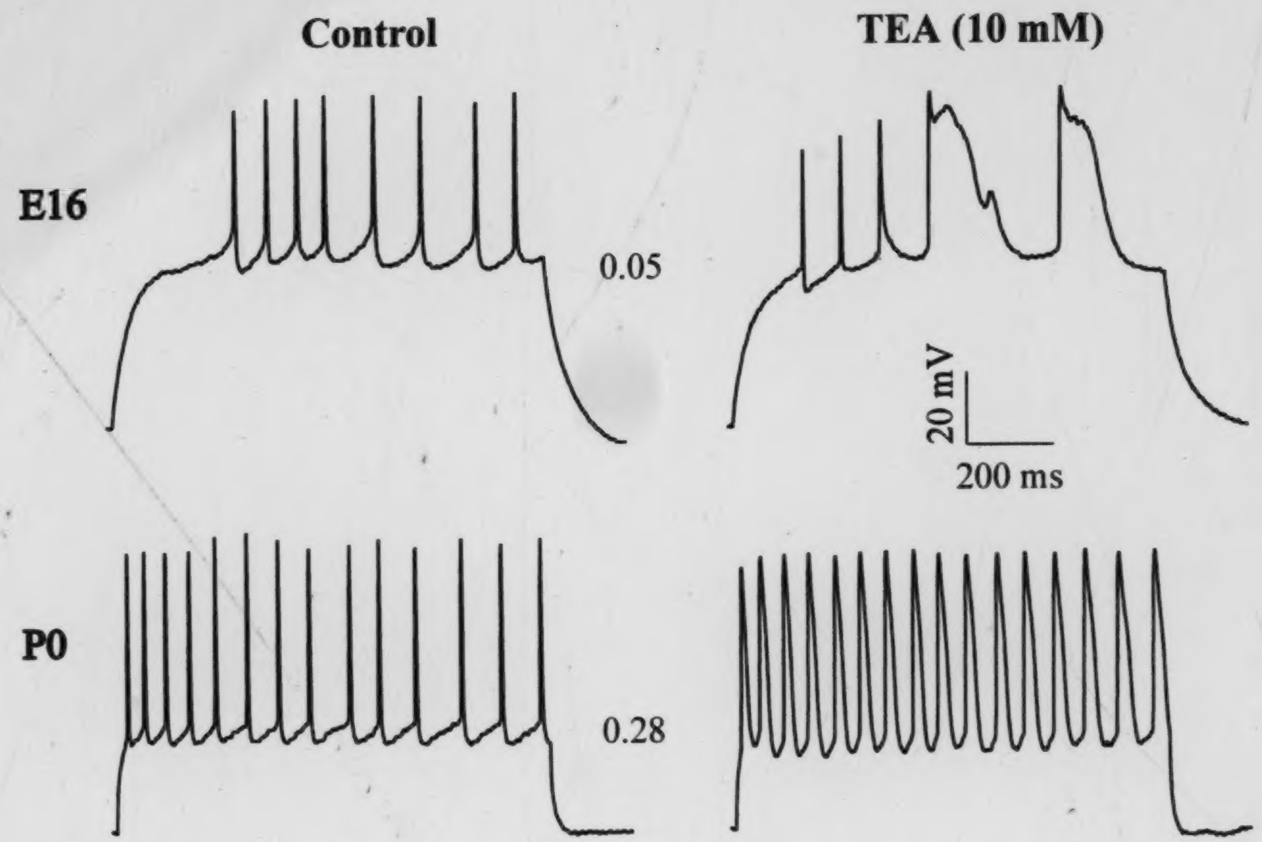
Control
TEA (10 mM)
E16
0.05
20 mV
200 ms
P0
0.28

Figure 4.3. Effect of 4-aminopyridine (4-AP, 1 mM) on the action potential duration and firing pattern of one representative E18 PMN. **A)** 4-AP prolongs the duration of the action potential and this effect was enhanced at hyperpolarized holding potentials (-75 mV). The discontinuous line represents the 0 mV mark. **B)** Hyperpolarizing holding potentials generated a delayed excitation (short arrow in middle panel). Treatment with 4-AP (1 mM) prevented the expression of the delayed excitation (right panel). Firing of PMNs was determined in the current-clamp configuration following injection of 1s-long depolarizing pulses at various holding potentials. Delayed excitation was present at all ages tested.

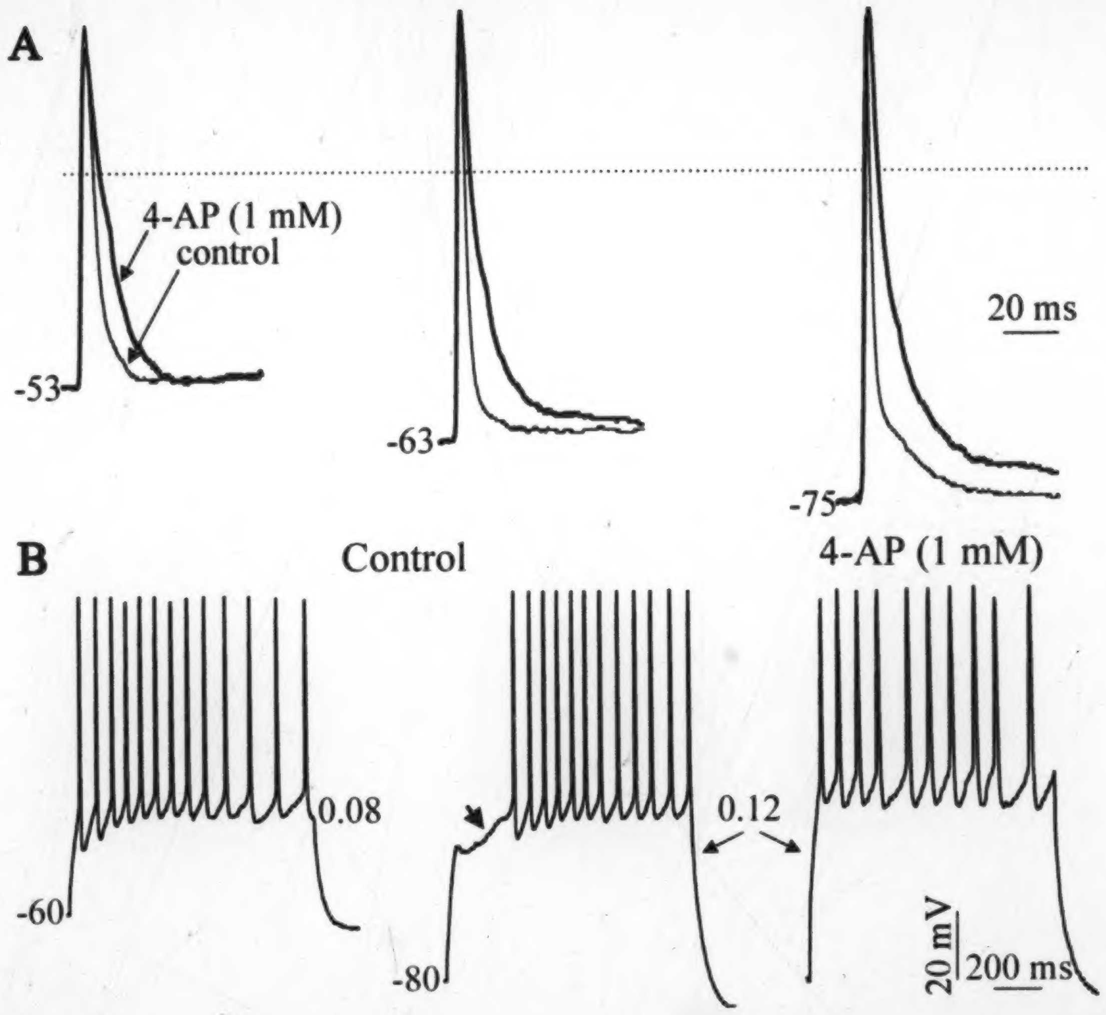
A
4-AP (1 mM)
control
-53
-63
-75
20 ms
B
Control
4-AP (1 mM)
0.08
0.12
-60
-80
20 mV
200 ms

Role of Ca^{++}-activated K^+ conductances in controlling firing properties and afterpotential formation

Previous results indicate that Ca^{++} ions contribute to shape the action potential in developing PMNs (Chapter 3). In particular, incubation in Ca^{++}-free medium eliminates the mAHP in E18 and neonatal motoneurons and results in the widening of action potentials postnatally. Thus, we investigated whether these Ca^{++}-dependent effects were mediated by Ca^{++}-activated K^+ conductances.

To investigate the role of Ca^{++}-activated K^+ conductances in the regulation of repetitive firing properties we tested the effect of Ca^{++}-free medium (Fig. 4.4 and 4.5). The diminution of Ca^{++} conductances had little effect on the repetitive firing properties of PMNs at E16. However, the removal of Ca^{++} from the medium had pronounced effects on the steady-state firing frequency of PMNs at E18 and PO. When measured at the threshold current required to elicit repetitive firing, the steady-state frequency in control versus Ca^{++}-free medium were as follows: E16, 10±1 vs 11±2 (n=4); E18, 8±1 vs 19±1* (n=7); P0-1, 15±1 vs. 21±1* Hz (n=6) (* $p \leq 0.05$ vs. control). Further, the spike-frequency adaptation (SFA), which starts to develop by E18 and becomes quite pronounced by P0, is reduced when Ca^{++}-activated K^+ conductances are diminished (Fig. 4.5, lower panel).

Figure 4.4. Effect of Ca^{++}-free medium on the repetitive firing properties of PMNs. Repetitive firing of PMNs was determined in the current-clamp configuration following injection of 1s-long depolarizing pulses and recorded with a low-BAPTA pipette solution. Incubation in Ca^{++}-free medium increased the firing frequency of PMNs at E18 and P0, but not at E16 (E16, n=4; E18, n=7; P0-1, n=6).

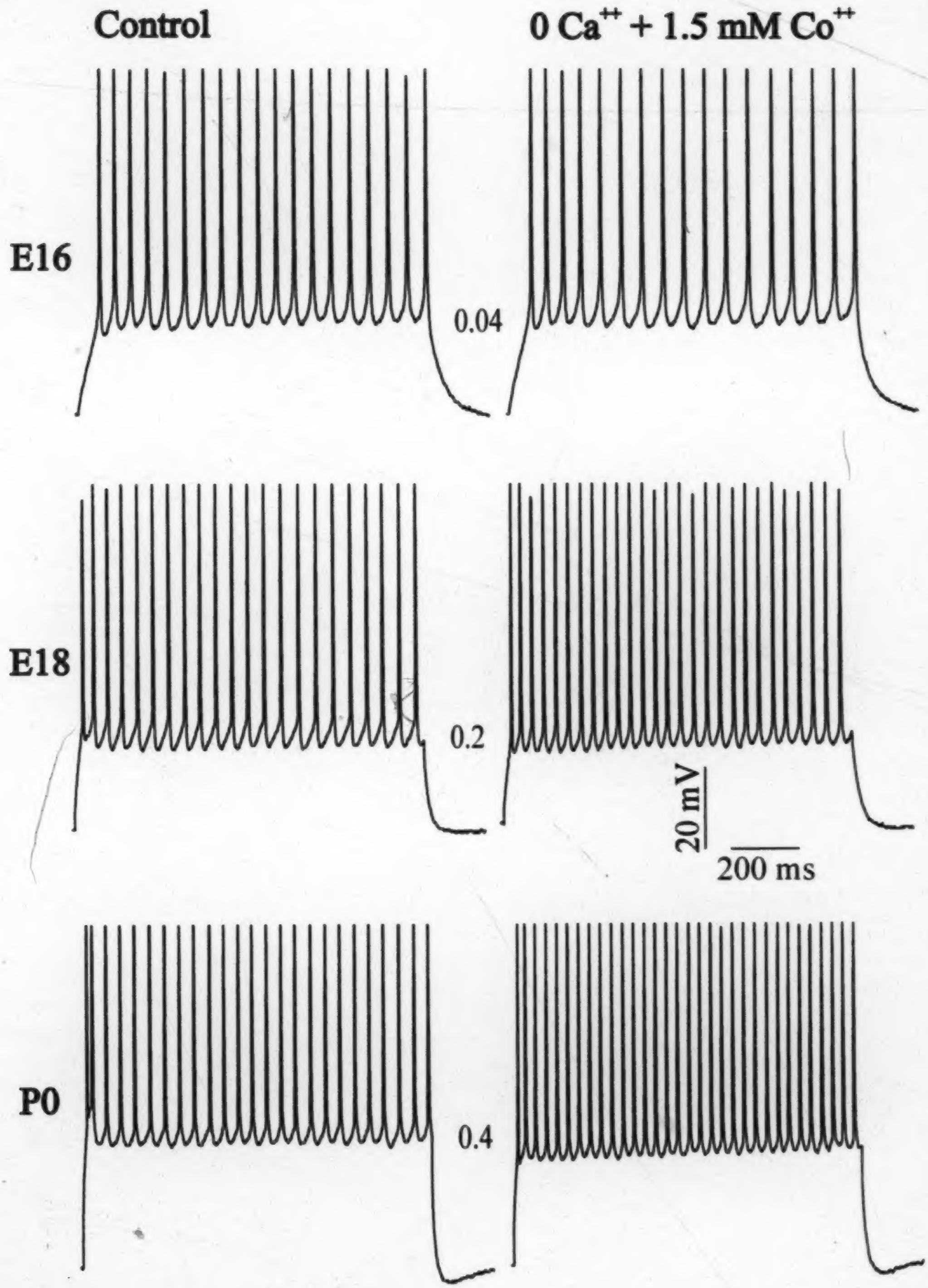
Control
0 Ca^{++} + 1.5 mM Co^{++}
E16
0.04
E18
0.2
20 mV
200 ms
P0
0.4

Figure 4.5. Plots of the firing frequency of PMNs as a function of injected current or interspike interval. **A)** Current-frequency plots of PMNs in control and following incubation in Ca^{++}-free medium. Firing frequency represents the number of action potentials generated following injection of a constant amount of current for 1s. **B)** Plots of instantaneous frequency versus the ISI number. Spike frequency adaptation was more pronounced in E18 and P0 motoneurons and was diminished in Ca^{++}-free medium. Data used to generate plots in **A** and **B** are from the same PMNs represented in **Fig. 4.4**.

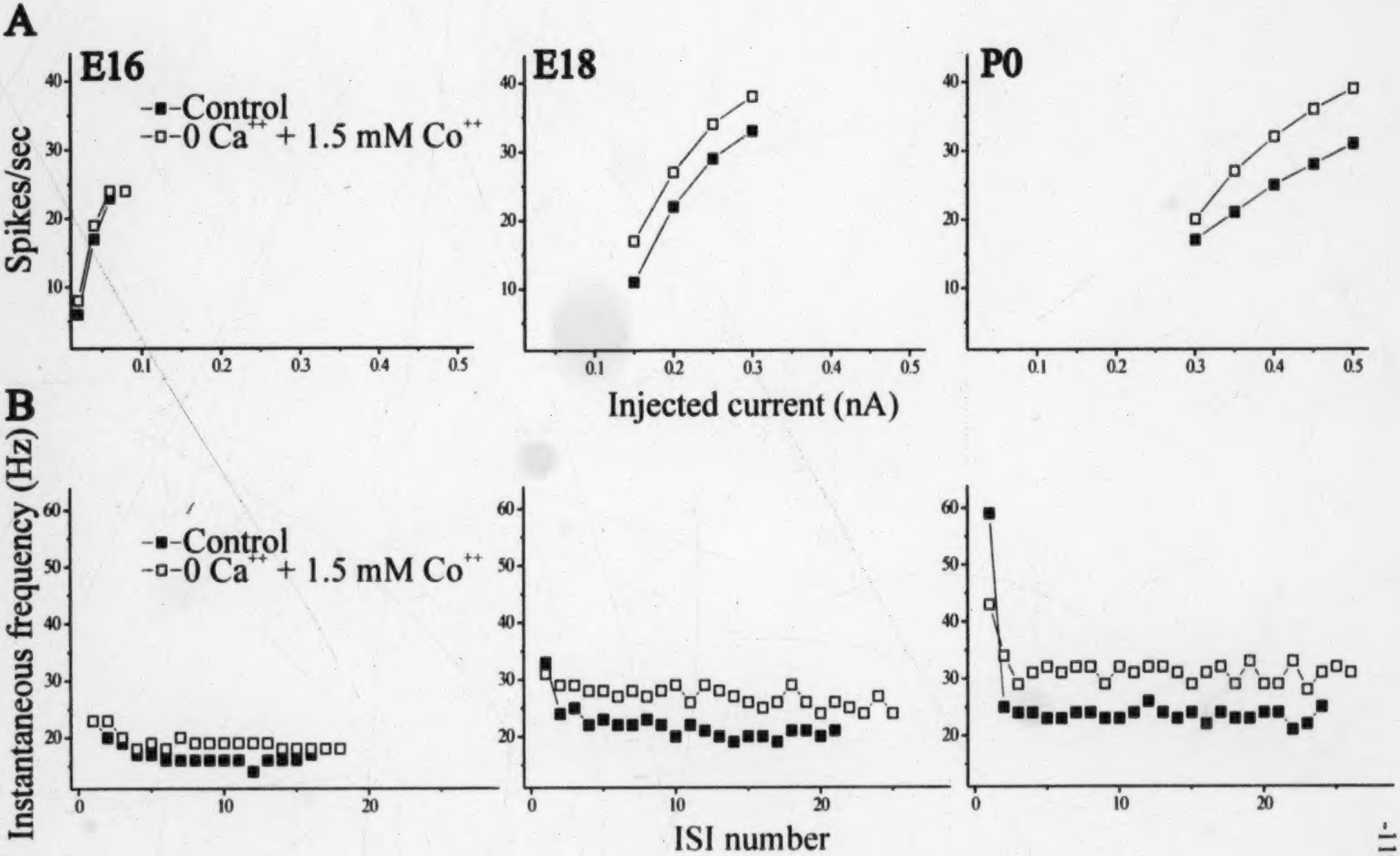
A
E16
E18
P0
Spikes/sec
-■-Control
-□-0 Ca^{++} + 1.5 mM Co^{++}
10
20
30
40
0.1
0.2
0.3
0.4
0.5
Injected current (nA)
B
Instantaneous frequency (Hz)
-■-Control
-□-0 Ca^{++} + 1.5 mM Co^{++}
20
30
40
50
60
0
10
20
ISI number

Electrophysiological and pharmacological properties of the mAHP

The expression of a mAHP in PMNs is first observed in a minority of E18 motoneurons (Chapter 3). By birth, 80% (16 of 20) of PMNs express a clear mAHP. (Fig. 4.6 A). Despite the greater contribution of Ca^{++} ions to prolong action potential in E16 motoneurons, no mAHP was ever found at this age (Fig. 3.2). Either K^+ channels mediating the mAHP are not expressed at this early stage or the inward Ca^{++} current mediating the afterdepolarizing potentials obscure the expression of the mAHP (Chapter 3). Thus, we restricted our analyses of the pharmacological and electrophysiological properties of mAHPs to neonatal PMNs.

The amplitude of the mAHP was voltage-dependent, increasing and decreasing at depolarizing and hyperpolarizing holding potentials, respectively (Fig. 4.6 A). The estimated reversal potential of the mAHP was -88 ± 5 mV (n=8), close to the calculated reversal potential for K^+ ions (-97 mV). The duration of the mAHP was not significantly different at holding potentials of -50 (52 ± 7 ms), -60 (50 ± 10 ms) and -75 mV (46 ± 8 ms; n=8).

As shown in the previous chapter, the mAHP is sensitive to incubation in Ca^{++}-free medium suggesting that Ca^{++} influx is responsible for triggering the mAHP. As shown in Fig. 4.6 B, the mAHP was blocked by the N-type Ca^{++} channel blocker ω-conotoxin GVIA (also see Table 4.2). Inhibition of the mAHP by ω-conotoxin GVIA induced a 35% increase in the firing frequency of neonatal motoneurons (Table 4.2). Inhibition of L-, P-, and T-type Ca^{++} conductances with nimodipine (10 μM, n=3), ω-agatoxin (500 nM, n=3) and nickel (200 μM, n=3), respectively, had no effect on PMN mAHPs (not shown). Further experiments demonstrated that the mAHP was blocked by the bee venom peptide toxin apamin (1 μM), an inhibitor of the small-conductance Ca^{++}-activated K^{+} channels (Fig. 4.6 C, Table 4.2). Collectively, these data demonstrate that the mAHP is generated as a result of the entry of Ca^{++} via N-type Ca^{++} channels followed by the activation of small-conductance Ca^{++}-dependent K^{+} channels. Functionally, the blockade of mAHPs with apamin had a marked facilitatory action on PMN firing rates as it increased firing rate by 68% (Fig 4.8 A and 4.9A, Table 4.2). Beside increasing firing rate, apamin-treatment of neonatal PMN induce bursting firing in P0-1 PMNs (Fig. 4.9 A, arrow).

Electrophysiological and pharmacological properties of the fAHP

A fast AHP was not observed in E16 or E18 PMNs. However, by P0-1, 29% (8 of 29) of PMNs had a clear fast AHP (Fig. 4.7 A). The amplitude of the fAHP was enhanced by hyperpolarizing holding potentials. Further, the membrane potential reached by the peak fAHP varied with the holding potential PMNs (Fig. 4.7 A). The amplitude of the fAHP, as a function of voltage, was fitted by a linear regression and the reversal potential of the fAHP was estimated by extrapolation to be -40 ± 2 mV (n=8; Fig. 4.7 B).

K^{+} channel blockers were applied to determine the ionic conductances underlying the generation of the fAHP in neonatal PMNs. As shown by the data regarding mAHP characteristics, blockade of the small conductance Ca^{++}-activated K^{+} conductance with apamin did not block the fAHP (Fig. 4.6 C). The potential roles of other major Ca^{++} activated K^{+} current, the maxi-type, were assessed by two methods. First, TEA at doses (1mM) sufficient for blocking the maxi-type Ca^{++}-activated K^{+} channel yet low enough not to cause significant block of the delayed rectifier, was applied (Viana et al., 1993). The addition of

1 mM TEA resulted in the disappearance of the fAHP (n=3, Fig. 4.7 C) and an increase in the duration of the action potential by ~50% (1.9 ± 0.2 vs. 3.7 ± 0.4 ms, n=3) without any significant change in action potential amplitude (79.7 ± 1.4 vs 79.7 ± 1.2 mV). Second, the selective blocker of maxi-type Ca^{++}-activated K^+ channels, iberiotoxin from the venom of the *Buthus tamulus* scorpion (0.3 μM) was added to the bath (Galvez et al., 1990). The effects of iberiotoxin were similar to that of low concentrations of TEA, both prolonged the duration of action potentials and eliminated the fAHP (Fig. 4.7 D, Table 4.2). Thus, these data suggest that maxi-type Ca^{++}-activated K^+ channels are involved in the generation of the fAHP in neonatal PMNs. Functionally, despite increasing action potential duration, the blockade of the maxi-type Ca^{++}-activated K^+ conductance by iberiotoxin resulted in only a slight increase in the firing frequency of neonatal PMNs (Fig. 4.8 B and 4.9 B, Table 4.2). It should be noted that we were not successful in elucidating the Ca^{++} current subtype responsible for activating the maxi-type Ca^{++}-activated K^+ conductance. There was no significant effect on fAHP amplitude or duration with the addition of ω -conotoxin GVIA (Fig. 4.6 B, Table 4.2), nimodipine (10 μM, n=3), ω-agatoxin (500 nM, n=3) or nickel (200 μM, n=3; data not shown).

Figure 4.6. Electrophysiological and pharmacological properties of the medium-duration AHP in a P0 PMN. **A)** Voltage-dependence of the mAHP amplitude. Note that the mAHP was enhanced by depolarizing holding potentials (arrowhead). **Insert:** plot of the mAHP amplitude vs. holding potential. Extrapolation of the linear regression to the y-axis revealed the reversal potential of the mAHP. In this particular neuron the reversal potential was -91 mV. **B)** The blocker of N-type Ca^{++} channels, ω-conotoxin GVIA (0.3 μM) inhibited the expression of the mAHP and increased the afterdepolarizing potential. **C)** The blocker of Ca^{++}-activated K^{+} channels (small conductance), apamin (1 μM) eliminated the mAHP and enhanced the afterdepolarizing potential. Antidromic action potentials were recorded with a low BAPTA (0.1 mM)- intracellular pipette solution.

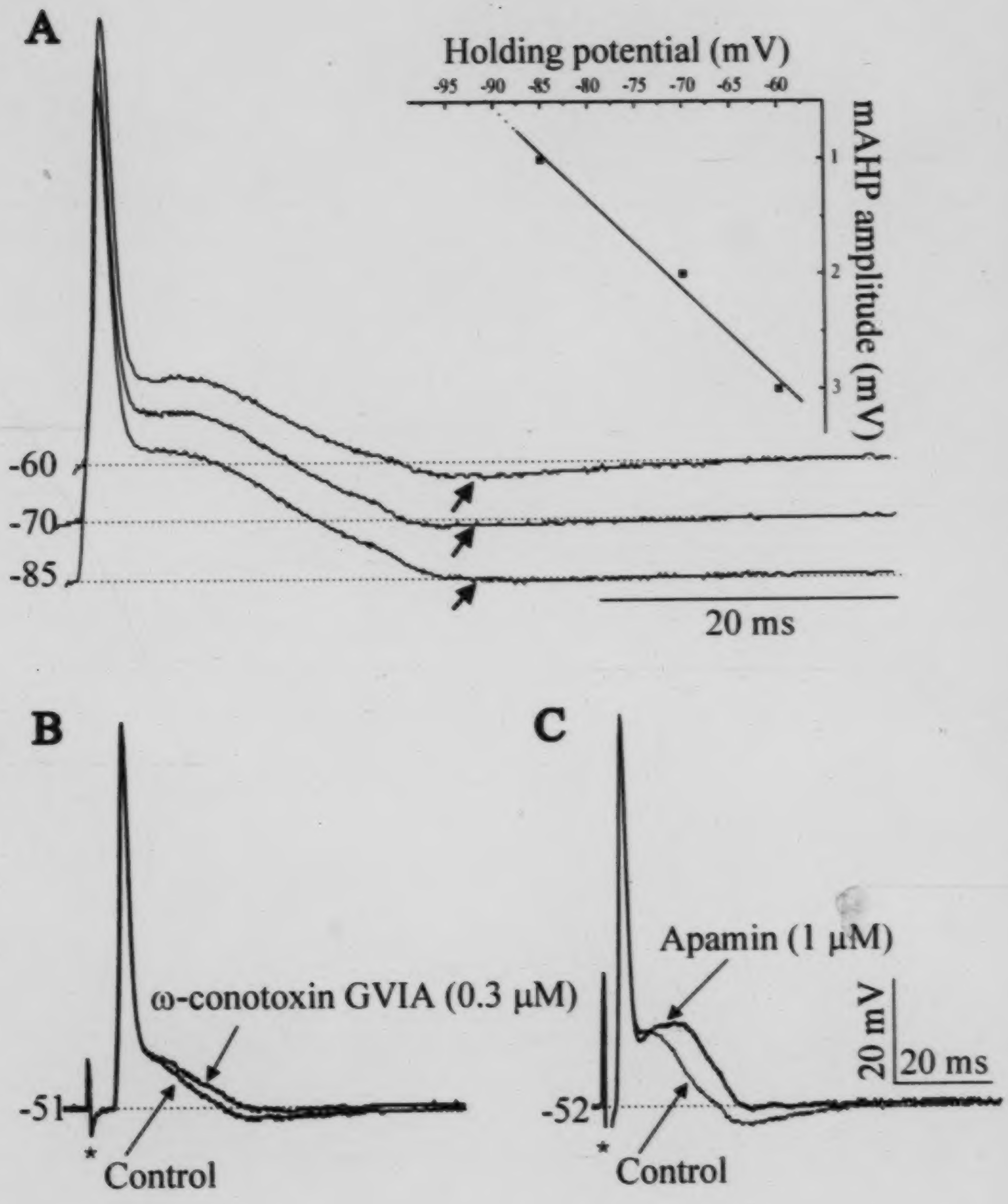
A
Holding potential (mV)
-95
-90
-85
-80
-75
-70
-65
-60
mAHP amplitude (mV)
1
2
3
-60
-70
-85
20 ms
B
ω-conotoxin GVIA (0.3 μM)
-51
*
Control
C
Apamin (1 μM)
20 mV
20 ms
-52
*
Control

Figure 4.7. Electrophysiological and pharmacological properties of the fast AHP in a P0 PMN. **A)** The amplitude of the fAHP was voltage dependent as hyperpolarizing potentials tended to enhance the fAHP. **B)** Plot of the fAHP amplitude vs. holding potential. Extrapolation of the linear regression to the y-axis revealed the reversal potential of the fAHP which in this particular neuron was -48 mV. **C)** TEA (1 mM) prolonged the action potential duration and prevented the expression of the fAHP. **D)** The blocker of Ca^{++}-activated K^{+} channels (maxi-type), iberiotoxin (0.3 μM), eliminated the expression of the fAHP while increasing action potential duration. Notice that holding potential is more depolarized in D to show that iberiotoxin did not have any effect on the mAHP.

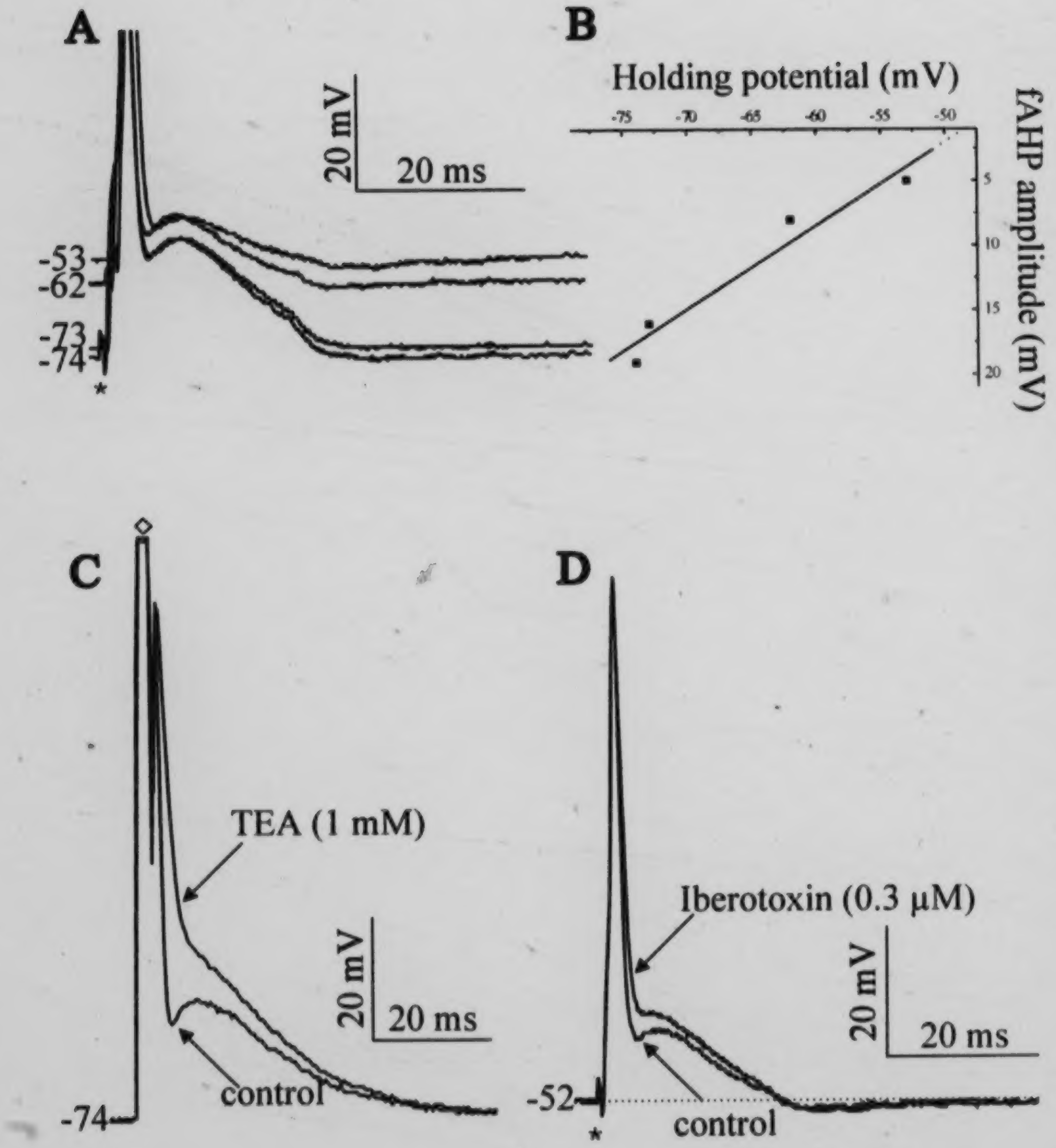
A
20 mV
20 ms
-53
-62
-73
-74
*
B
Holding potential (mV)
-75
-70
-65
-60
-55
-50
fAHP amplitude (mV)
5
10
15
20
C
◇
TEA (1 mM)
20 mV
20 ms
control
-74
D
Iberotoxin (0.3 μM)
20 mV
20 ms
-52
*
control

Figure 4.8. Effect of Ca^{++}-activated K^+ conductances in regulating the firing pattern of two representative P0 PMNs. **A)** Apamin-treatment greatly increased the firing frequency of a P0 motoneuron without any significant change in the input resistance of the PMN. **B)** Iberiotoxin (0.3 μM) slightly increased the firing frequency of PMNs. Change in input resistance was determined from the voltage response to a depolarizing current injection (0.15 or 0.3 nA), sub-threshold for repetitive firing. Note that following apamin-treatment, firing was characterized by an initial burst of spikes (arrow) followed by tonic firing. Bursting was characterized by 2-3 spikes originating from the afterdepolarizing potential that followed the first action potential of the train.

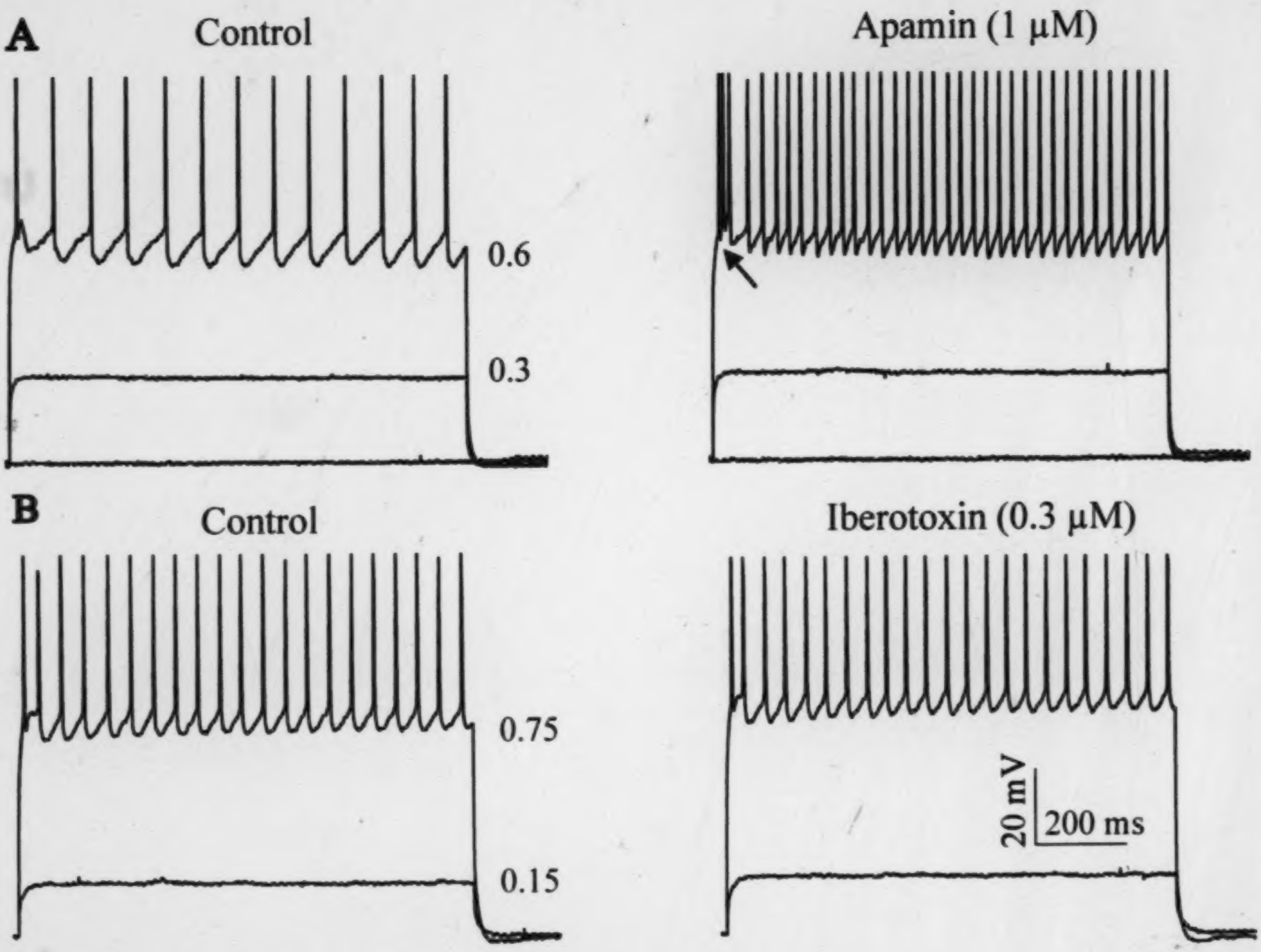
A
Control
Apamin (1 μM)
0.6
0.3
B
Control
Iberotoxin (0.3 μM)
0.75
0.15
20 mV
200 ms

Figure 4.9. Plots of the firing frequency of PMNs as a function of injected current or interspike interval following treatment with apamin and iberiotoxin. **A)** Current-frequency plots of PMNs in control and following inhibition of Ca^{++}-dependent conductances. Firing frequency represents the number of action potentials generated following injection of a constant amount of current for 1s. **B)** Plots of instantaneous frequency versus the ISI number. Note that following apamin-treatment, the initial burst of spikes was characterized by a high instantaneous firing frequency that rapidly decayed to a steady-state level. The steady-state firing rate following apamin treatment was significantly higher than in control. Data used to generate plots in **A** and **B** are from the same neonatal PMNs represented in **Fig. 4.8 A** and **B**.

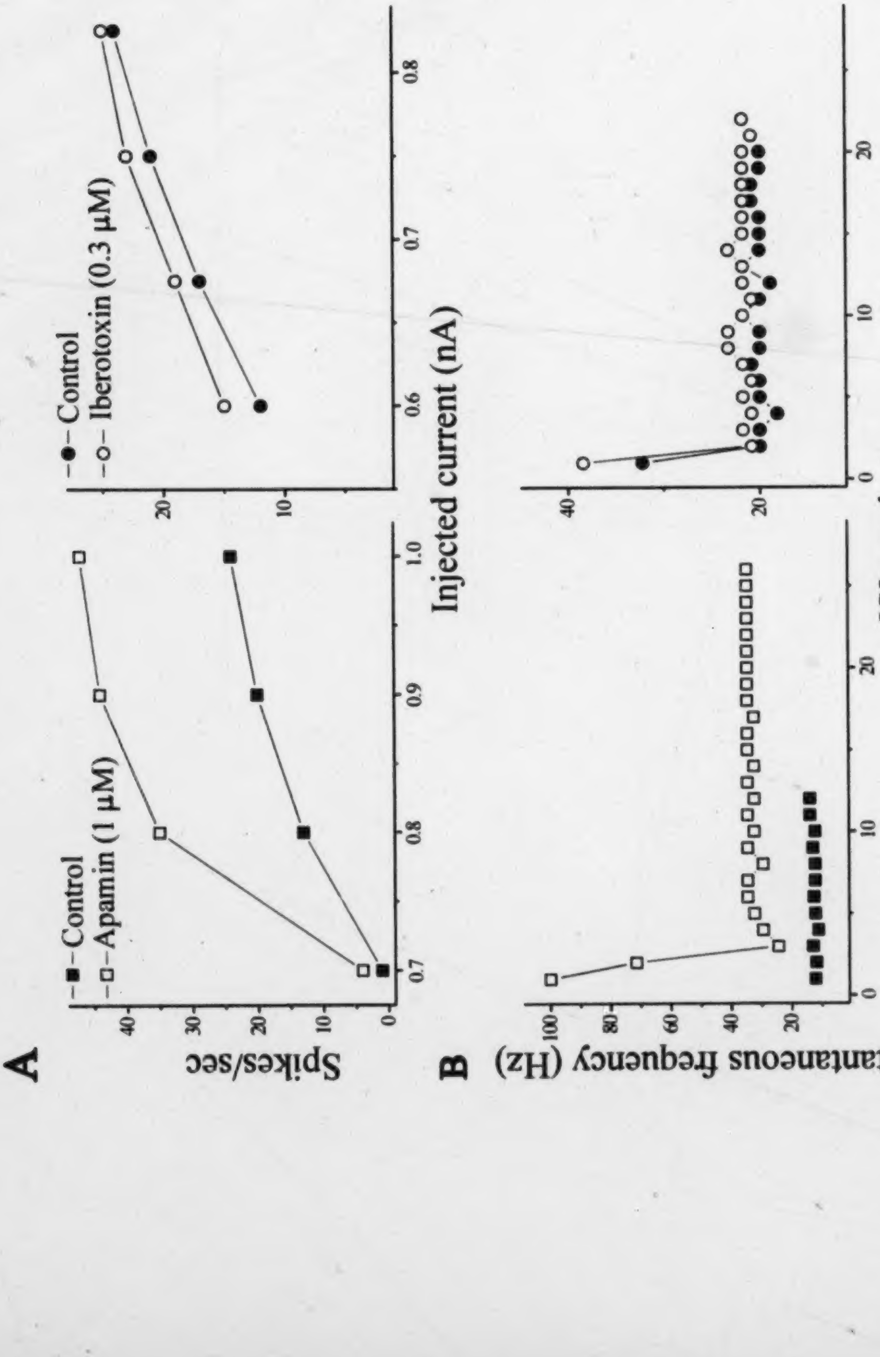
A
Spikes/sec
0
10
20
30
40
—■— Control
—□— Apamin (1 µM)
0.7
0.8
0.9
1.0
10
20
—●— Control
—○— Iberotoxin (0.3 µM)
0.6
0.7
0.8
Injected current (nA)
B
Instantaneous frequency (Hz)
20
40
60
80
100
0
10
20
20
40
0
10
20
ISI number

Table 4.2. Modulation of PMN action potential (AP) and firing properties following blockade of Ca^{++}-activated K^+ conductances.

	Control				Treatment				
	AP amplitude (mV)	AP duration (ms)$^{(1)}$	mAHP amplitude (mV)	Firing frequency (Hz)	AP amplitude (mV)	AP duration (ms)	mAHP amplitude (mV)	Firing frequency (Hz)	Change in firing frequency (%)
Apamin (1 μM) (n=7)	77±3	2.2±0.2	2.2±0.2	15.8±1.1	74±3	2.2±0.2	0.2±0.1*	26.2±3.0*	+ 68±29*
ω-conotoxin GVIA (0.3 μM) (n=4)	73±4	2.3±0.2	1.8±0.3	15.7±1.0	71±3	2.4±0.2	0.1±0.1*	20.0±1.8	+ 35±10*
Iberiotoxin (0.3 μM) (n=6)	80±4	1.8±0.1	2.6±0.6	14.7±1.1	77±3	2.2±0.1*	2.6±0.7	15.7±1.0	+ 11±4*

(*) $p \leq 0.05$ vs control (no treatment).

$^{(1)}$ AP duration was calculated at half-maximal amplitude.

Voltage-clamp analysis of voltage-dependent K^+ currents

To determine if age-dependent changes in PMN action potential duration and amplitude resulted from changes in the density and/or kinetics of K^+-mediated conductances, recordings were made in voltage-clamp mode. Voltage-clamp experiments revealed that by E16 outward K^+ currents expressed two voltage-dependent components: a transient, fast inactivating and a non-inactivating conductance (Fig.4.10 A). The transient component was revealed when K^+ currents were recorded following a hyperpolarizing prepulse (to -110 mV for 200 ms; Fig. 4.10 Aa). Holding the membrane potential at more depolarized potentials (at -40 mV for 200 ms) resulted in the inactivation of the transient component (Fig. 4.10 Ab) and the generation of a non-inactivating K^+ conductance. The absolute value of the transient component was isolated by subtraction of the non-inactivating current generated by a depolarizing prepulse from total current generated by the hyperpolarizing prepulse (Fig. 4.10 Aa-b). Based on previous results in other developing neurons (McCobb et al., 1990; Spigelman et al., 1992), the non-inactivating and transient components of K^+ currents were classified as being the delayed outward rectifier (I_{KV}) and A-type (I_A) K^+ conductances, respectively. The transient component reached its peak earlier than the non-inactivating component indicating differences in their activation. The time to peak of the transient component underwent a ~50% increment between E16 and P0-1 (Table 4.3). The time to reach maximal value of the non-inactivating component was longer in duration than that of the transient component and there was a ~55% reduction in the time to peak for the non-inactivating component. These findings demonstrate that the activation of the non-inactivating component increases with age. The transient component was also found to inactivate during a depolarizing pre-pulse potential (Fig. 4.10 B), indicating voltage-dependent inactivation of the transient component. Activation and inactivation of the transient components were plotted as a function of voltage and fitted to a Boltzman equation (Fig. 4.10 C, Table 4.3). No age-dependent changes in the fitting parameters were found at the three ages studied for I_A. However, kinetic analysis of I_Kv activation suggested age-dependent changes in its activation pattern. Between E16 and P0-1, there was an ~8mV left ward shift in the voltage for half-maximal activation of the steady component (Fig. 4.12 A, Table 4.3).

At all ages tested, the I_{KV} and I_A had similar pharmacological sensitivities. The transient A-type K^+ conductance was completely eliminated following incubation with 3 mM of 4-AP without significant changes in the outward rectifier K^+ conductance (Fig. 4.11 A and B, respectively). However, 4-AP tended to delay the rising phase of the I_{KV} K^+ conductance (Fig 4.11 B). Previous results from studies of spinal motoneurons indicate that I_{KV} is sensitive to TEA treatment (Schwindt and Crill, 1988; Takahashi, 1990). As shown in Fig. 4.12 B, treatment of the non-inactivating steady current with 10 mM TEA greatly diminished the expression of I_{KV} in this particular P0 PMN. When the effect of TEA on I_{KV} was measured at a test pulse of +30 mV, the change in the absolute value of I_K at E16 and P0-1 was similar (23 ± 7 and 25 ± 8 %, n=4, respectively). Thus, there is no indication of age-dependent change in the sensitivity of I_{KV} to TEA.

To examine changes in the expression of I_{KV} and I_A which could explain the age-dependent maturation of action potential, current densities were determined during the E16-P1 period. I_{KV} and I_A were determined using the prepulse protocols shown in Fig. 4.10 A to a test potential of +30 mV and normalized to cell capacitance (see METHODS). Whole-cell capacitance for E16, E18 and P0-1 PMN was 57 ± 3 (n=23), 63 ± 3 (n=25) and 71 ± 4 (n=26) pF (* $p \leq 0.05$ vs E16), respectively. However, as presented in Table 4.3, there were no significant changes in the current densities for the outward rectifier and A-type K^+ conductances during perinatal development of PMNs.

It was evident from the kinetics of the current recordings that there were space-clamp problems that effected the accuracy of current measurements. The space-clamp problems were particularly pronounced in neonatal PMNs which have elaborate dendritic trees and increased soma diameter relative to embryonic PMNs (Allan and Greer, 1997b). While the space-clamp problems did not preclude the obtainment of useful measurements of I_{KV} and I_A currents at P0, we were unable to reliably record Ca^{++}-activated K^+ currents in P0-1 PMNs. Thus, we do not present voltage-clamp records to complement our findings from current-clamp recordings. However, we did perform Western analyses of protein subunits specific to maxi- and small conductance channels as an independent measure of age-dependent changes in Ca^{++}-activated K^+ channels.

Figure 4.10. Voltage-clamp recordings of K^+ currents in a E16 PMN. **Aa)** K^+ currents generated following a hyperpolarizing pre-pulse potential to -110 mV. Note the expression of a transient component (with fast activation and inactivation kinetics). **Ab)** K^+ currents generated following a depolarizing pre-pulse potential to -40 mV. Note the presence of a steady component only. **Aa-b)** Subtraction of the K^+ currents generated with the two previous protocols revealed the transient component alone. **B)** Steady-state inactivation of the transient component is voltage dependent. K^+ currents were generated by a fixed depolarizing pulse to -20 mV preceded by hyperpolarizing pre-pulses to various levels (from -90 to -50 mV). The value of the calibration bars is identical to those in A. **C)** Plots of the steady-state activation and inactivation of the transient component as a function of membrane potential. The activation and inactivation values of the transient K^+ currents were determined from data shown in Aa-b and B and fitted with a Boltzman function (activation and inactivation values are listed in **Table 4.3**).

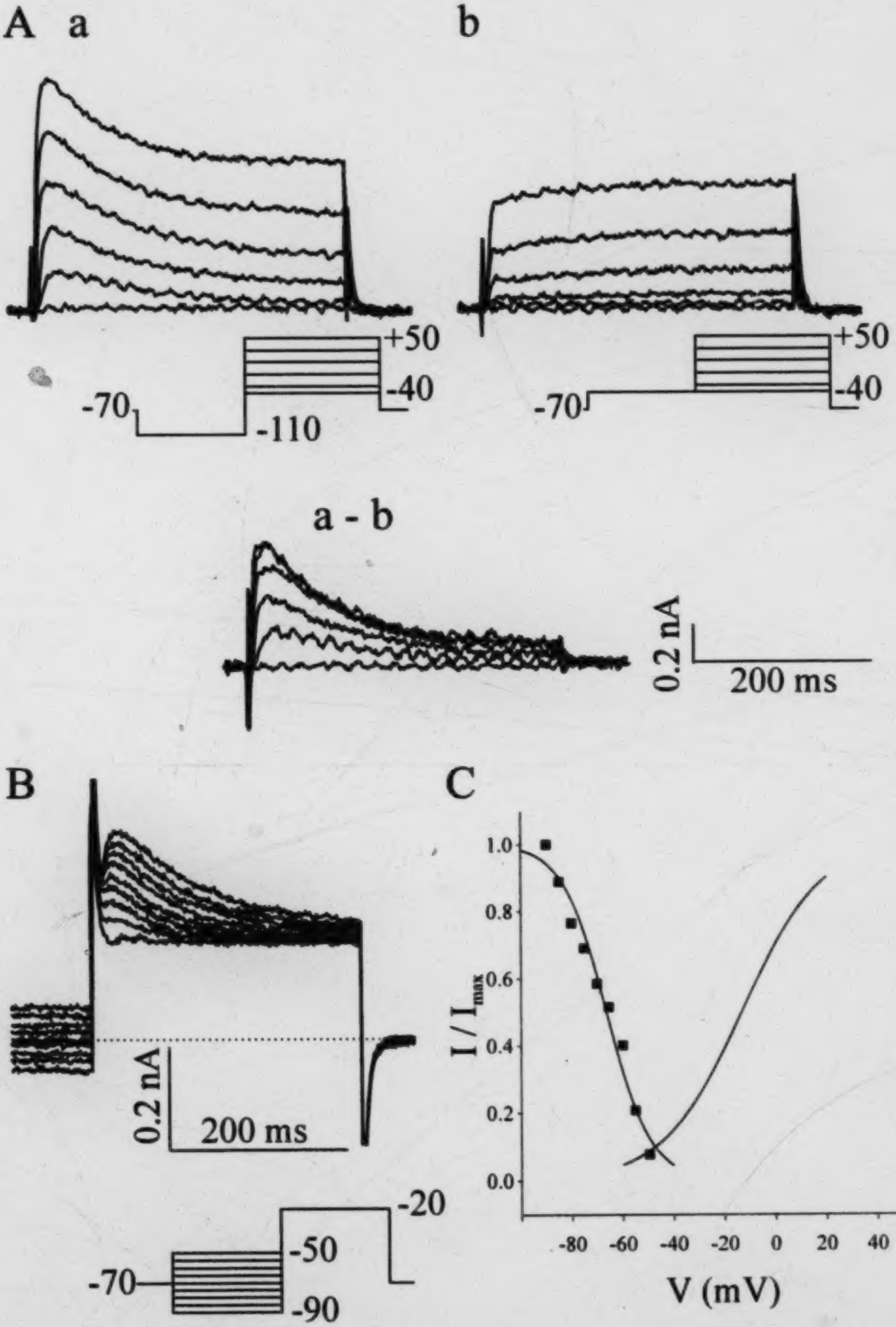
A a
b
+50
-40
-70
-110
+50
-40
-70
a - b
0.2 nA
200 ms
B
0.2 nA
200 ms
-20
-50
-70
-90
C
I / I$_{max}$
G / G$_{max}$
1.0
0.8
0.6
0.4
0.2
0.0
-80
-60
-40
-20
0
20
40
V (mV)

Figure 4.11. Effect of 4-AP (3 mM) on the A-type and outward rectifier K^+ conductances. 4AP-treatment of E18 PMN motoneuron resulted in complete blockage of the A-current **(A)** with little change in the amplitude of the outward rectifier K^+ conductance **(B)**.

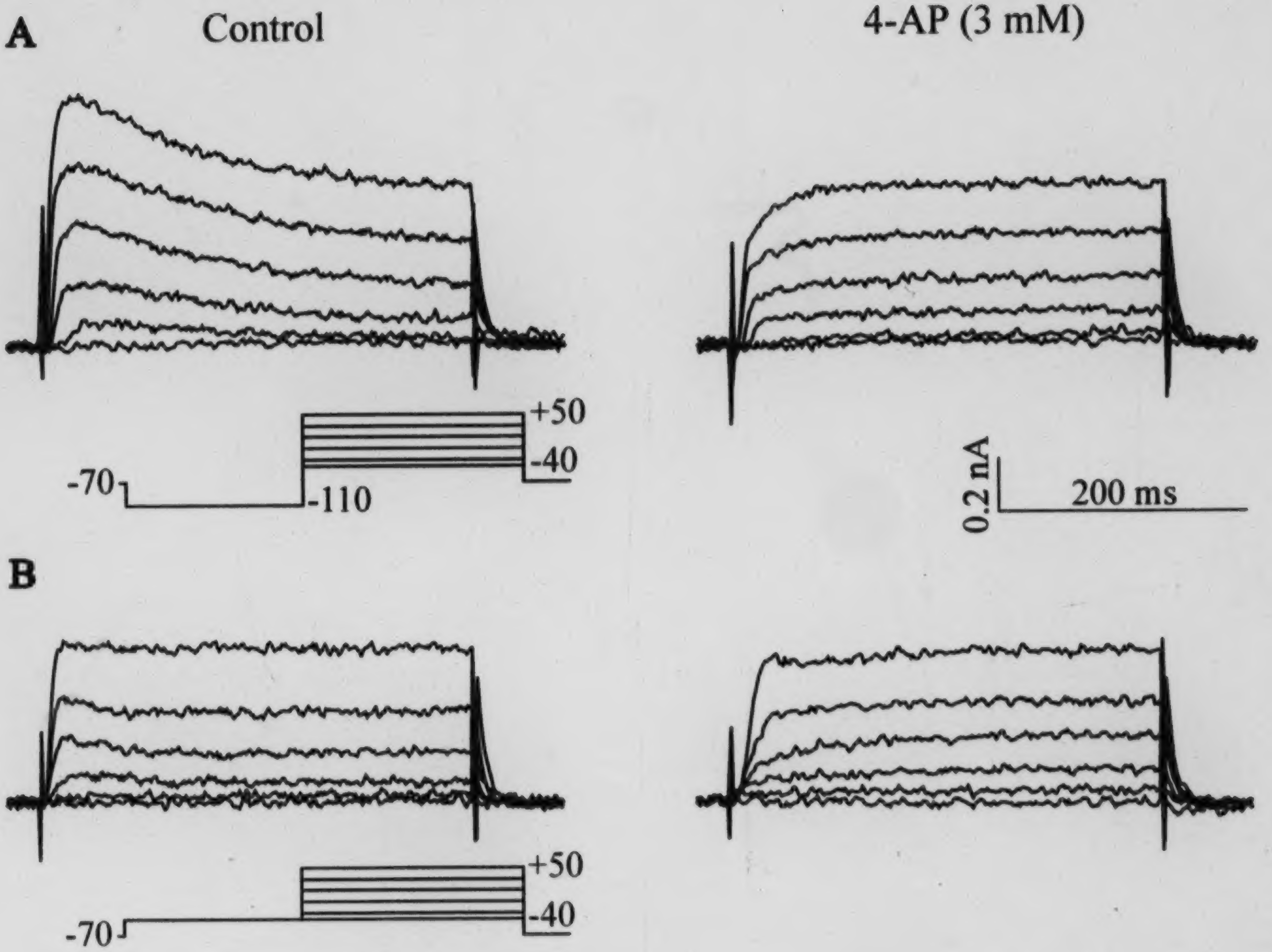
A
Control
4-AP (3 mM)
+50
-40
-70
-110
0.2 nA
200 ms
B
+50
-40
-70

Figure 4.12. Electrophysiological and pharmacological properties of the outward rectifier K^+ conductance. **A)** Developmental changes in the activation of the I_{KV} as a function of voltage. Steady-state K^+ conductances were determined following the protocol in **Fig. 4.10 Ab**, corresponding to outward rectifier K^+ conductance and fitted with a Boltzman function (activation values are listed in **Table 4.3**). **B)** Effect of tetraethylammonium ions (TEA, 10 mM) on the outward rectifier K^+ conductance in a P0 motoneuron. Considerable inhibition of the outward rectifier K^+ conductance with TEA was observed.

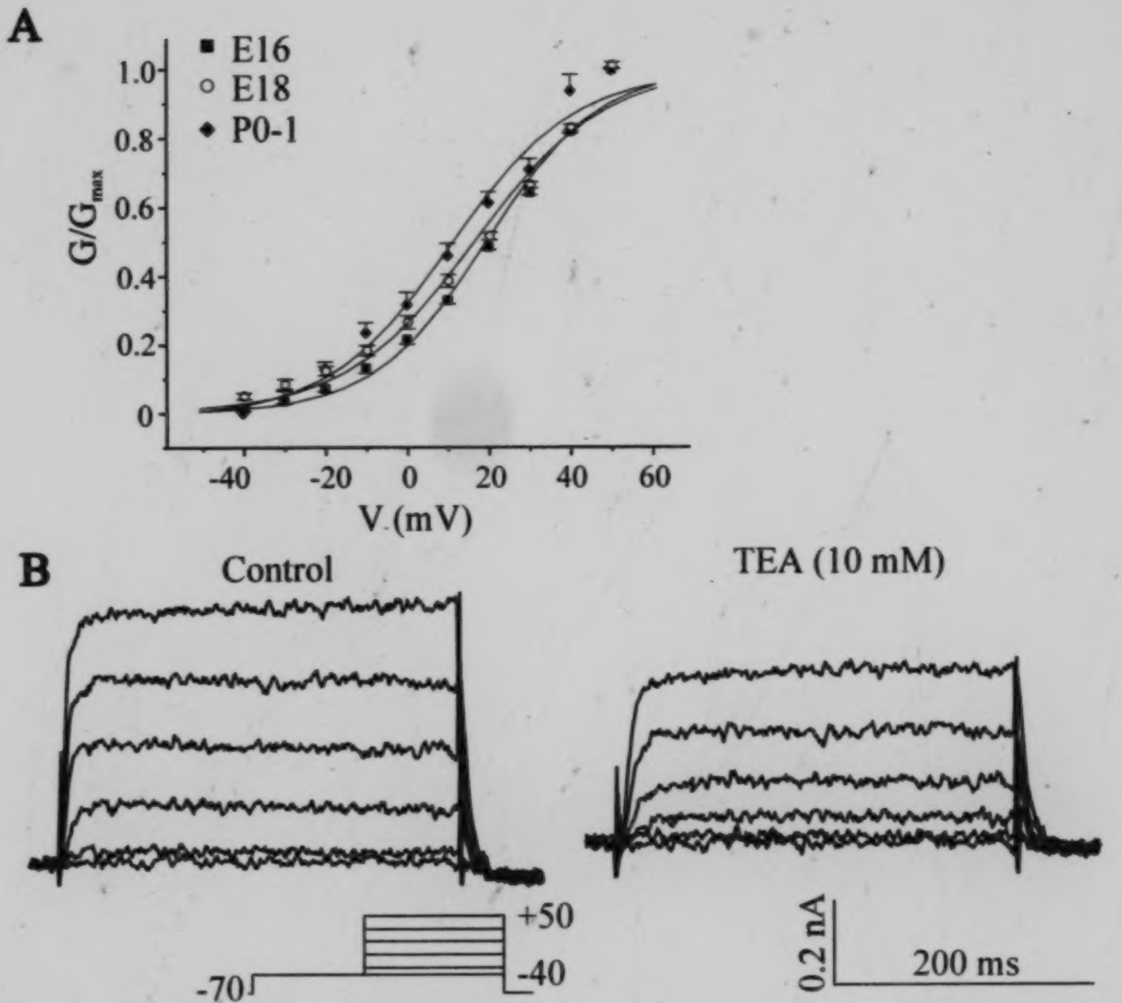
A
B
E16
E18
P0-1
G/G$_{max}$
1.0
0.8
0.6
0.4
0.2
0
-40
-20
0
20
40
60
V (mV)
Control
TEA (10 mM)
+50
-40
-70
0.2 nA
200 ms

Table 4.3. Electrophysiological properties of I_{KV} and I_A conductances in perinatal PMNs.

			E16	**E18**	**P0-1**
I_{KV}	Current density (pA/pF)		8.9 ± 0.6 (23)	8.8 ± 0.6 (25)	7.6 ± 0.8 (26)
	Time to peak (ms)		133 ± 26	56 ± 9*	57 ± 21*
	Activation	$V_{1/2}$ (mV)	19 ± 1 (10)	17 ± 1* (11)	11 ± 2* (12)
		k (/mV)	14 ± 1	16 ± 1	15 ± 1
I_A	Current density (pA/pF)		11 ± 1 (20)	9.1 ± 0.9 (17)	9 ± 2 (16)
	Time to peak (ms)		10 ± 1.3	16.6 ± 1.8*	19.0 ± 2.6*
	Activation	$V_{1/2}$ (mV)	-6 ± 4 (15)	-8 ± 3 (14)	-5 ± 3 (13)
		k (/mV)	15 ± 1	17 ± 1	15 ± 1
	Inactivation	$V_{1/2}$ (mV)	-72 ± 4	-70 ± 5	-77 ± 3
		k (/mV)	-7 ± 2	-8 ± 1	-7 ± 1

(*) $p \leq 0.05$ vs E16.

Western analysis of Ca^{++}-activated K^{+} channels

Western blot analysis was performed to corroborate the electrophysiological data indicating an age-dependent change in the expression of the maxi- and small conductance Ca^{++}-activated K^{+} channel proteins. The antibodies ANTI-BK$_{a}$ and ANTI-SK3 against the maxi- and small conductance channels, respectively, were tested on equal amounts of protein from the ventral regions of rat spinal cords at four different ages: E16, E18, P0 and P5. Immunoblots with the ANTI-BK$_{a}$ antibody generate a prominent band ~130 kD (Fig. 4.13 A). There was no change in the molecular weight of the band with age. Additional faint bands (1-2) also appear at lower molecular weights. It is possible that these bands represent distinct molecular isoforms or are the result of protein degradation. Immunoblots with the ANTI-SK3 antibody show a prominent band ~70 kD without age-dependent changes in its molecular weight (Fig. 4.13 B). Two other bands were seen at a lower molecular weight. Analysis of protein content at those ages indicates a marked increment in channel expression between E16 and P0 (Fig. 4.13 A,B right plots). The maximal level of expression for both proteins was reached in P0 motoneurons with a small reduction in protein expression by P5. No bands were detected in control experiments (not shown).

Figure 4.13. Age-specific expression of maxi-type and small-conductance, Ca^{++}-activated K^+ channel proteins as detected by immunoblot analysis. **A)** Western blot of the maxi-type, Ca^{++}-activated K^+ channel at E16, E18, P0 and P5 using the ANTI-BK_a antibody. The plot on the right indicates changes in the area of the BK_a band (130 kD) with age (n=3). **B)** Western blot of the small-conductance, Ca^{++}-activated K^+ channel at E16, E18, P0 and P5 using the ANTI-SK3 antibody. The plot on the right shows changes in the area of the SK3 band (70 kD) with age (n=4). The numbers on the left of the immunoblots indicate the molecular weight of the pre-stained standard proteins. Note the increase in the expression of the analysed proteins between E16 and P0 without any change in their molecular weight. $^+$ $p \leq 0.05$ vs E18, * $p \leq 0.05$ vs P0.

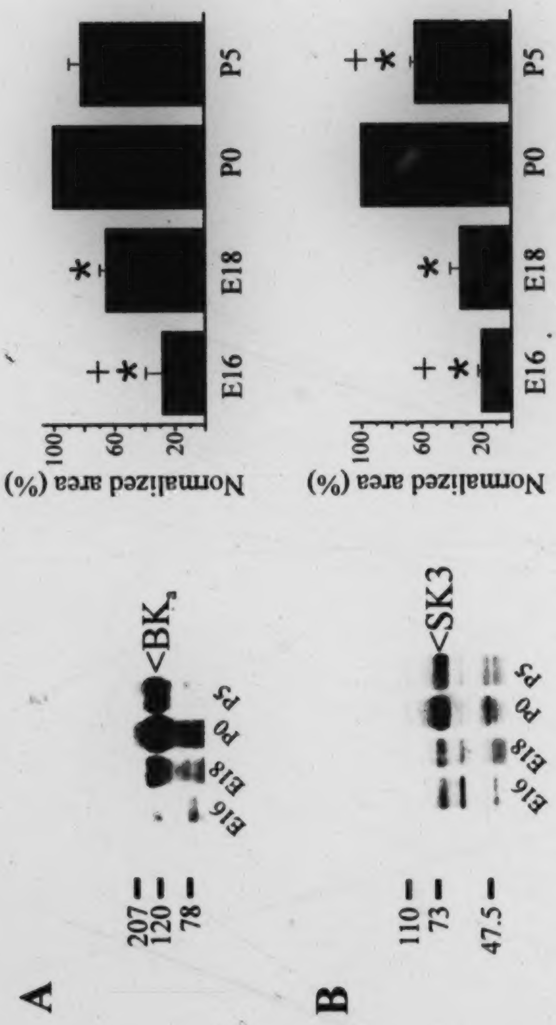
A
207
120
78
E16
E18
P0
P5
<BK$_a$
Normalized area (%)
100
60
20
E16
E18
P0
P5
B
110
73
47.5
E16
E18
P0
P5
<SK3
Normalized area (%)
100
60
20
E16
E18
P0
P5

DISCUSSION

The present findings demonstrate that the outward rectifier and A-type K^+ currents are involved in regulating PMN action potential and repetitive firing properties throughout the perinatal period spanning from E16 through to P0-1. The most profound change in K^+ conductances during this period resulted from the onset of Ca^{++} activated K^+ channel expression following the inception of inspiratory drive transmission. The emergence of these conductances appear to be in large part responsible for the marked transformation in action potential shape and firing properties of PMNs prior to birth.

Ca^{++}-dependent K^+ conductances

PMNs began to express two Ca^{++}-dependent K^+ conductances after the inception of inspiratory drive transmission.

Maxi-type Ca^{++}-dependent K^+ current: Block of the maxi-type Ca^{++}-dependent K^+ conductance with iberiotoxin caused a significant increase in action potential duration in neonatal PMNs, implicating a Ca^{++}-dependent K^+ conductance in spike repolarization. A similar conductance has been implicated in spike repolarization in neonatal lumbar and hypoglossal motoneurons (Takahashi, 1990, Viana et al., 1993) and the shaping of the locomotion pattern in *Xenopus* tadpoles (Sun and Dale, 1998). Functionally, besides decreasing action potential duration, the presence of Ca^{++}-activated K^+ conductances will prevent the large accumulation of Ca^{++} ions during alternating bursts of activity such as respiration and locomotion.

The maxi-type Ca^{++}-dependent K^+ conductance also regulates the expression of the fAHP observed in a subpopulation of neonatal PMNs. The fAHP was found in the transition between the repolarizing phase of the action potential and the afterdepolarizing potential of PMNs. The nature of fAHP generated in PMNs differed somewhat from that reported for some other neurons. First, the reversal potential of the fAHP found in PMNs appears to be more depolarized than that in hypoglossal and sensory neurons (Viana et al., 1993; Schwindt et al., 1988). Second, the membrane potential reached by the peak of the fAHP in PMNs changed with the amount of current injected into the cell to hold the membrane at various holding potentials. This was not the case in cat sensory neurons (Schwindt et al., 1988). Thus, there may be a mixed cationic conductance responsible for the fAHP in PMNs which differed from previously examined neurons.

The Ca^{++} conductance responsible for the activation of the maxi-type Ca^{++} activated K^{+} channels could not be identified in the present work as blockers of the LVA (or T-type) and HVA (N-, P/Q-, L–type) Ca^{++} channels did not cause any effect on the repolarization of the action potential. Instead, activation of maxi-type Ca^{++} activated K^{+} channels may involved Ca^{++} release from intracellular stores or Ca^{++} entry via other channels subtypes (i.e., R-type).

Small conductance Ca^{++}-dependent K^{+} current: Block of the small conductance Ca^{++}-dependent K^{+} channels in PMNs with apamin did not have any effect on spike repolarization. However, there was a marked suppression of the mAHP and an increase in the repetitive firing frequency of PMNs. The activation of small-conductance K^{+} conductances has also been implicated in SFA in other mammalian motoneurons (Viana et al., 1993; Gao and Ziskind-Conhaim, 1998; Walton and Fulton, 1986; Schwindt and Crill, 1988). The data from the current study demonstrates that the Ca^{++} ions responsible for generating the mAHP in PMNs entered via ω-conotoxin GVIA-sensitive Ca^{++} channels, suggesting that the small conductance Ca^{++}-activated K^+ channels are localized near the N-type Ca^{++} channels in PMNs. This is similar to the findings from studies of hypoglossal motoneurons (Viana et al., 1993). However, given that the ADP was not blocked by ω-conotoxin GVIA, it is likely that the Ca^{++} influx necessary for generating the ADP and mAHP are separate.

The expression of the two types of Ca^{++}-activated K^+ conductances were also examined with Western blot analysis of tissue excised from the ventral horn of cervical regions. The tissue contained a mixture of brachial motoneurons, spinal interneurons and phrenic motoneurons, which limits the interpretation of the data. Nevertheless, the data from the Western blots were consistent with the electrophysiological data showing that there is an age-dependent increase in the expression of the Ca^{++}-activated K^+ channel proteins during the E16-P0 period. Both the maxi-type and small-conductance, Ca^{++}-activated K^+ channel proteins reached their highest level of expression in neonatal motoneurons.

Outward rectifier and A-type K^+ conductances

Transient, 4-AP-sensitive I_A and slowly activating, non-inactivating TEA-sensitive I_{KV} conductances are functional in PMNs as early as E16 and continue to be expressed into the postnatal period. Unlike what has been reported for early embryonic development of chick and *Xenopus* spinal neurons (McCobb et al., 1990; O'Dowd et al., 1988; Harris et al., 1988), we found no age-dependent increases in the density of these two conductances in perinatal PMNs. However, we did observe age-dependent changes in the activation voltage and rise time for the I_{KV} similar to those found for *Xenopus* spinal neurons (Burger and Ribera, 1996; Gurantz et al., 1996). Specifically, there was a leftward shift in the activation voltage and a decrease in the time to peak of I_{KV} during the period from E16 through to birth. Functionally, the leftward shift in the activation voltage of I_{KV} and the increment in its time to peak will result in a faster repolarization of the action potential as delayed rectifier K^+ channels activate faster and at lower voltages.

It should be noted that the times to peak of I_A and I_{KV} conductances were slower and the activation $V_{1/2}$ value of the I_A conductance was more depolarized in our recordings from perinatal PMNs compared to data from other motoneurons (Mc Cobb et al., 1990; Safronov and Vogel, 1995). These differences may result from variations in the specific subunit composition of voltage-dependent K^+ channels amongst the motoneuron pools (Castellano et al., 1997; Robertson, 1997). Alternatively, space-clamp problems due to the extensive dendritic trees of PMNs may have interfered with the accurate quantification of current kinetics in our recordings. However, given that the space-clamp problem is accentuated as the PMNs become larger and the dendritic trees become longer and more elaborate, one might have expected the time to peak for the I_{KV} conductance to increase with age. Yet the trends reflected in the data are exactly opposite. Two possible explanations are as follows. First, the putative space-clamp problems did not significantly distort measurements of the these parameters. Second, space-clamp problems did skew the data and thus the age-dependent differences in I_{KV} kinetics are actually larger than the measurements reflect.

The actions of I_{KV} and I_A for regulating action potential duration and repetitive firing properties of PMNs were examined. Blockade of both I_{KV} and I_A resulted in a prolongation of action potential duration, the prolonged influx of Ca^{++} and the generation of plateau potentials that were particularly pronounced in embryonic PMNs. Repetitive firing properties were affected by a delayed excitation mediated by a I_A conductance. The degree to which the I_A-mediated delayed excitation influences PMN firing during the inspiratory phase of the respiratory cycle would vary depending on the magnitude of the membrane hyperpolarization during the preceding expiratory phase. Thus, although there is a similar level of I_A conductances in PMNs during the perinatal period, the I_A-mediated effects on firing will change as a function of inhibitory synaptic drive during development (Wu et al., 1992; Gao and Ziskind-Conhaim, 1995; Singer et al., 1998) and changes in resting membrane potential (becomes more hyperpolarized with age; Chapter 3; Liu and Feldman, 1992).

In conclusion, the changes in K^+ conductances result in a reduction in duration and an increase in the complexity of PMN action potentials. These changes result in increases in the rate and range of PMN repetitive firing frequencies attainable at birth. The transformations in PMN firing properties, in concert with the concomitant changes observed in diaphragm muscle properties (see Chapter 6), ensure a fully functioning neuromuscular system necessary for sustaining respiration. In neonatal motoneurons, expression of the maxi-type and small conductance Ca^{++}-dependent K^+ channels contribute to repolarize the action potential and to regulate the firing pattern. Functionally, this will increase the firing frequency of neonatal PMNs required to recruit the diaphragm. Further, a significant component of state-dependent regulation of neuronal excitation by neuromodulators is mediated by modifications of ionic channel function and the subsequent alterations in action potential and repetitive firing properties (for review see Jones and Kaczmarek, 1996, Levitan, 1999). Thus, with the development of an increased pallette of ionic conductances in PMNs prior to birth, access to potential modulatory control mechanisms is readily available to meet the varied demands of breathing after birth.

REFERENCES

ALLAN, D.W., GREER, J.J. (1997a) Embryogenesis of the phrenic nerve and diaphragm in the fetal rat. J. Comp. Neurol. 382: 459-468.

ALLAN, D.W., GREER, J.J. (1997b) Development of phrenic motoneuron morphology in the fetal rat. J. Comp. Neurol. 381: 469-479.

BUTLER, A., TSUNODA, S., MCCOBB, D.P., WEI, A., SALKOFF, L. (1993) mSlo, a complex mouse gene encoding "Maxi" calcium-activated potassium channels. Science 261: 221-224.

BURGER, C., RIBERA, A.B.(1996) *Xenopus* spinal neurons express Kv2 potassium channel transcripts during embryonic development. J. Neurosci. 16 (4): 1412-1421.

CASTELLANO, A., CHIARA, M.D., MELLSTRÖM, B., MOLINA, A., MONJE, F., NARANJO, J.R., LOPEZ-BARNEO, J. (1997) Identification and functional characterization of K^+ channel α-subunit with regulatory properties specific to brain. J. Neurosci. 17(12): 4652-4661.

CONNORS, B.W., PRINCE, D.A. (1982) Effects of local anaesthetic QX-314 on the membrane properties of hippocampal pyramidal neurons. J. Pharmacol. Exp. Therapeutics 220: 476-481.

GAO, B.X., ZISKIND-CONHAIM, L. (1998) Development of ionic currents underlying changes in action potential waveforms in rat spinal motoneurons. J. Neurophysiol. 80(6): 3047-3061.

GAO, B.X., ZISKIND-CONHAIM, L. (1995) Development of glycine- and GABA-gated currents in rat spinal motoneurons. J. Neurophysiol. 74(1): 113-121.

GALVEZ, A., GIMENEZ-GALLEGO, G., REUBEN, J.P., ROY-CONTANCIN, L., FEIGENBAUM, P., KACZOROWSKI, G.J., GARCIA, M.L. (1990) Purification and characterization of a unique, potent, peptidyl probe for the high conductance calcium-activated potassium channel from venom of the scorpion *Buthus tamulu*. J. Biol. Chem. 265: 11083-11090.

COETZEE W.A., AMARILLO, Y., CHIU, J., CHOW, A., LAU, D., MCCORMACK, T., MORENO, H., NADAL, M.S., OZAITA, A., POUNTNEY, D., SAGANICH, M., VEGA-SAENZ DE MIERA, E., RUDY, B. (1999) Molecular diversity of K+ channels. Ann. New York Acad. Sci. 868:233-285.

DEKIN, M.S., GETTING, P.A. (1987) In vitro characterization of neurons in the ventral part of the nucleus tractus solitarius. II. Ionic basis for repetitive firing patterns. J. Neurophysiol. 58: 215-229.

GURANTZ, D., RIBERA, A.B., SPITZER, N.C. (1996) Temporal regulation of Shaker- and Shab-like potassium channel gene expression in single embryonic spinal neurons during K+ current development. J. Neurosci. 16 (10): 3287-3295.

HARRIS, G.L., HENDERSON, L.P., SPITZER, N.C. (1988) Changes in densities and kinetics of delayed rectifier potassium channels during neuronal differentiation. Neuron 1: 739-750.

JONES, E.A., KACZMAREK, L.K. (1996) Regulation of potassium channels by protein kinases. Curr. Opinion Neurobiol. 6: 318-23.

KOHLER, M., HIRSCHBERG, B., BOND, C.T., KINZIE, J.M., MARRION, N.V., MAYLIE, J., ADELMAN, J.M. (1996) Small-conductance, calcium-activated potassium channels from mammalian brain. Science 273: 1709-1714.

LEVITAN, I.B. (1999) Modulation of ion channels by protein phosphorylation. How the brain works. Adv. Sec. Mess. Phos. Res. 33:3-22.

LIU, G., FELDMAN, J.L. (1992) Bulbospinal transmission of respiratory drive to phrenic motoneurons. In: *Respiratory Control, Central and Peripheral mechanisms*, edited by Speck, D.F., Dekin, M.S., Revelette, W.R. and Frazier, D.T., The University Press of Kentucky, Kentucky, USA, pp. 47-51.

MCCOBB, D.P., BEST, P.M., BEAM, K.G. (1990) The differentiation of excitability on embryonic chick limb motoneurons. J. Neurosci. 10: 2974-2984.

MCLARNOR, J.G. (1995) Potassium currents in motoneurons. Progress in Neurobiology 47: 513-531.

MIENVILLE, J.M., BARKER, J.L. (1997) Potassium current expression during prenatal corticogenesis in the rat. Neurosci. 81: 162-172.

O'DOWD, D.K., D., RIBERA, A.B., SPITZER, N.C. (1988) Development of voltage-dependent calcium, sodium and potassium currents in *Xenopus* spinal neurons. J. Neurosci. 8(3): 792-805.

ROBERTSON, B. (1997) The real life of voltage-gated K+ channles: more than model behaviour. Trends in Pharmacol. Sci. 18: 474-483.

RUDY, B. (1988) Diversity and ubiquity of K channels. Neurosci. 25(3): 729-749.

SAFRONOV, B.V., VOGEL, W. (1995) Single voltage-activated Na+ and K+ channels in the somata of rat motoneurons. J. Physiol. 487: 91-106.

SINGER, J.H., TALLEY, E.M., BAYLISS, D.A., BERGER, A.J. (1998) Development of glycinergic synaptic transmission to rat brain stem motoneurons. J. Neurophysiol. 80: 2608-2620.

SCHWINDT, P.C., SPAIN, W.J., FOEHRING, R.C., STAFSTROM, C.E., CHUBB, M.C., CRILL, W.E. (1988) Multiple potassium conductances and their functions in neurons from cat sensorimotor cortex in vitro. J. Neurophysiol. 59: 424-449.

SCHWINDT, P.C., CRILL, W.E. (1988) Differential effects of TEA and cations on outward ionic currents of cat motoneurons. J. Neurophysiol. 46: 1-17.

SPIGELMAN, I., ZHANG, L., CARLEN, P.L. (1992) Patch-clamp study of postnatal development of CA1 neurons in rat hippocampal slices: membrane excitability and K^+ currents. J. Neurophysiol. 68: 55-69.

SUN, Q.Q., DALE, N. (1998) Developmental changes in expression of ion currents accompany maturation of locomotor pattern in frog tadpole. J. Physiol. 507: 257-264.

TAKAHASHI, T. (1990) Membrane currents in visually identified motoneurons of neonatal rat spinal cord. J. Physiol (London) 423: 27-46.

VIANA, F., BAYLISS, D.A., BERGER, A.J. (1993) Multiple potassium conductances and their role in action potential repolarization and repetitive firing behaviour of neonatal rat hypoglossal motoneurons. J. Neurophysiol. 69(6): 2150-2163.

WALTON, K., FULTON, B.P. (1986) Ionic mechanisms underlying the firing properties of rat neonatal motoneurons studied in vitro. Neurosci. 19: 669-683.

WU, W., ZISKIND-CONHAIM, L., SWEET, M.A. (1992) Early development of glycine- and GABA-mediated synapses in rat spinal motoneurons. J. Neurosci. 12(10): 3935-3945.

CHAPTER 5

VOLTAGE-SENSITIVE CALCIUM CURRENTS AND THEIR ROLE IN REGULATING PHRENIC MOTONEURON ELECTRICAL EXCITABILITY DURING THE PERINATAL PERIOD

Adapted from the original publication:
M. Martin-Caraballo and J.J. Greer
J. Neurophysiol. (Submitted March 2000)

INTRODUCTION

Ca^{++} entry regulates many aspects of neuronal differentiation including outgrowth and retraction of axons and dendrites (Cohan et al., 1987; McCobb & Kater, 1988; Holliday & Spitzer, 1990), naturally-occurring neuronal cell death (Choi, 1987; Tymiansky et al., 1993), and maturational changes in both ionic conductances and neurotransmitter phenotype (Spitzer et al., 1988; Holliday & Spitzer, 1990; Desarmenien & Spitzer, 1991; Xie & Ziskind-Conhaim, 1995). One of the major routes for Ca^{++} entry in developing neurons is through voltage-activated Ca^{++} channels. Based on their voltage-dependence, pharmacology and single-channel properties, Ca^{++} channels have been classified as low- and high-voltage activated (LVA and HVA) conductances (Bean, 1989; Tsien et al., 1991; Umemiya & Berger, 1995). LVA Ca^{++} conductances contribute to the generation of afterdepolarizing potentials (Umemiya & Berger, 1995), spontaneous elevation of intracellular Ca^{++} (Gu & Spitzer, 1993) and rebound depolarizations (Viana et al., 1993). In contrast, HVA Ca^{++} channels activate at more depolarized potentials and are divided into several subtypes, including L-, N-, P/Q- and R-types. HVA Ca^{++} channels are involved in the generation of plateau potentials (Walton & Fulton, 1987; Barish, 1991), spike afterpotentials (Viana et al., 1993; Umemiya & Berger, 1994), as well as in neurotransmitter release (Katz & Miledi, 1967; Siri & Uchitel., 1999).

The aim of this study was to examine the ontogeny of voltage-sensitive Ca^{++} conductances in rat phrenic motoneurons (PMNs) and their role in regulating electrical excitability during the perinatal period. Specifically, we examined the interval spanning from embryonic day (E)16 through to postnatal day (P)1. This is the period during which

PMNs undergo fundamental transformations in neuronal morphology, passive properties, ionic channel phenotype, synaptic inputs and electrical excitability (Greer et al., 1992; Allan & Greer, 1997a,b; chapters III and IV). Thus, these data provide a further understanding of how voltage-sensitive Ca^{++} conductances change in concert with these major developmental processes within a single population of mammalian motoneurons. Further, these studies provide insights into the relationship between the ontogeny of voltage-sensitive Ca^{++} conductances and the maturation of PMN electrophysiological properties from the time when fetal inspiratory drive commences to the onset of continuous breathing at birth.

METHODS

Whole-cell recordings

HVA and LVA Ca^{++} conductances were recorded in discontinuous single electrode voltage-clamp. Switching rates were <40 kHz, the output bandwidth was set at 1 kHz, and clamp gain was ~0.8 nA/mV. Head-stage output was monitored with a separate oscilloscope in order to monitor the voltage transients prior to sampling. Inward currents were recorded with a pipette solution containing 110 mM CsCl and 30 mM TEA-Cl in order to block K^+ conductances. To block inward sodium conductances, the slice was bathed with an external solution containing 0.5-1 μM tetrodotoxin. For recording HVA currents, a 200 ms depolarizing prepulse (to -40 mV) was applied from a holding potential of -70 mV whereas a 200 ms hyperpolarizing prepulse (to -90 mV) was applied in order to activate LVA Ca^{++} currents. Leak and capacitative currents were subtracted from the control currents by a P/4 protocol.

An ATP-regenerating system containing ATP and phosphocreatine was added to the patch pipette to minimize rundown of Ca^{++} currents. The measurement of Ca^{++} currents commenced immediately after establishing the whole-cell configuration. If the Ca^{++} currents decreased by 10% or more from initial values, the recording was terminated and data were not analysed. Current density values shown in Table 5.1 were calculated from the current traces obtained within a few minutes of establishing a whole-cell recording.

Intracellular and extracellular solutions: The pipette solution used to block K^+ conductances contained (in mM): CsCl (110), TEACl (30), BAPTA (10), HEPES (10), Mg ATP (5), NaGTP (0.3); phosphocreatine (10 mM), pH 7.3 with TEA-OH.

Drugs: The following drugs were used (suppliers in brackets): TTX, TEA-Cl, cytochrome-c, verapamil (Sigma, St. Louis, MO); nimodipine (RBI, Natick, MA); ω-agatoxin IVA (Peninsula Laboratories, Belmont, CA); ω-conotoxin GVIA (Alomone Laboratories, Jerusalem, Israel). Cytochrome-c (0.05%) was included in solutions containing ω-conotoxin GVIA or ω-agatoxin IVA in order to avoid non-specific binding to plastic tubing.

RESULTS

Voltage- and current-clamp recordings were used to examine Ca^{++} currents and their role in shaping action potential and repetitive firing patterns of E16 (n=31), E18 (n=35) and P0-1 (n=45) PMNs. In order to clearly identify the neurons as being PMNs via antidromic activation, it was essential that we used a cervical slice thick enough (~750 μm) to ensure the integrity of the attached phrenic nerve. This also allowed the maintenance of a relatively intact dendritic tree, which is important given that dendrites make up the largest component of motoneuron surface area (Cameron et al., 1985; Torikai et al., 1996) and contain a significant proportion of voltage-sensitive ion channels (Llinas & Yaron, 1980; Yuste & Tank, 1996). However, by maintaining an extensive dendritic tree there are inherent space-clamp problems which can distort the quantification of ionic conductances. Thus, we did not attempt to characterize age-dependent changes in the kinetics of the various types of LVA and HVA Ca^{++} conductances.

Whole-cell voltage-clamp recordings

Voltage-clamp protocols were used to identify the presence of LVA and HVA Ca^{++} conductances. Typical current traces from embryonic (E16) and neonatal (P0) PMNs are shown in Figs. 5.1 and 5.2, respectively. LVA and HVA Ca^{++} conductances were expressed at all ages investigated. Following a hyperpolarizing prepulse potential to -90 mV, a transient current was activated with a threshold between -50 to -40 mV. This transient, LVA Ca^{++} current reached its peak at around 15 ms and completely inactivated within 50-70 ms.

Voltage steps to more depolarized potentials generated a large amplitude inward current that had both inactivating and non-inactivating components. A prepulse potential to -40 mV resulted in a reduction of the inactivating component as compared to that obtained with a prepulse potential to -90 mV (Fig 5.1 B). Differences in the voltage-dependent activation of LVA and HVA currents were evident from the I-V plots (Fig. 5.1 C). The LVA currents activated at lower voltages which is evident from the 'shoulder' in the rising phase of the I-V plot. This 'shoulder' was eliminated following a depolarizing prepulse to -40 mV. Ca^{++} was the major charge carrier in LVA and HVA inward currents as demonstrated by the complete elimination of the currents in a zero Ca^{++} solution (Fig. 5.2). Maximum HVA current amplitude was evoked by voltage steps between -10 and -20 mV. The majority of embryonic PMNs (10/11) had a maximum HVA current at -10 mV, whereas 8 of 13 neonatal PMNs reached a peak at -20mV (compare I-V plots in Figs. 5.1 C and 5.2 B).

Pharmacological characterization of Ca^{++} currents: To further characterize LVA and HVA Ca^{++} currents, pharmacological blockers were used in conjunction with voltage-clamp paradigms. While there are no known specific blockers of LVA Ca^{++} currents, the application of low concentrations of nickel are typically used to inhibit T-type Ca^{++} currents (Fox et al., 1987; Barish, 1991). As shown by the current traces (Fig. 5.3 A) and I-V plot (Fig. 5.3 B) from an E16 PMN, low concentrations of nickel (100 μM) completely eliminated the transient low threshold Ca^{++} currents. The inhibition of LVA Ca^{++} currents by nickel occurred in all PMNs studied, regardless of age.

Several channel blockers were used to identify the subtypes of HVA Ca^{++} currents present in perinatal PMNs. N- and P-type Ca^{++} channels are selectively inhibited by the peptides ω-conotoxin GVIA and ω-agatoxin IVA, respectively (Fox et al., 1987; Mintz et al., 1992). L-type Ca^{++} channels are inhibited by dihydropiridines (i.e., nimodipine) and phenylalkylamines (i.e., verapamil) (Fox et al., 1987; Barish, 1991).

As shown in Fig. 5.4 A, block of N-type Ca^{++} currents with ω-conotoxin GVIA reduced the HVA Ca^{++} current in embryonic and postnatal PMNs. The reduction in peak

HVA Ca^{++} current was 34±4% (n=3) in E16 PMNs and 25±4% (n=6) in P0-1 PMNs. Block of P-type Ca^{++} currents with ω-agatoxin IVA reduced peak HVA Ca^{++} current in E16 and P0-1 PMNs by 11±1 % (n=3) and 15±4% (n=3), respectively (example shown in Fig. 5.4 B). The effect of blocking L-type Ca^{++} currents with verapamil is shown in Fig 5.5. Verapamil inhibited the HVA Ca^{++} current by 32±13% in E16 PMNs (n=4) and 37±8% (n=8) in P0-1 PMNs. Approximately 33% of the HVA Ca^{++} current in embryonic and neonatal PMNs was insensitive to the channel blockers used in this study.

Developmental changes in LVA and HVA Ca^{++} current densities: Age-dependent changes in current density of LVA and HVA Ca^{++} conductances were determined during the E16-P1 period. Whole-cell current amplitudes were normalized to cell capacitance (see METHODS) and are summarized in Table 5.1. Between E16 and P0-1, there was an ~2 fold increase in the peak density of Ca^{++} conductances. The density of LVA Ca^{++} conductances was stable during the E16-E18 period, but underwent a 2-fold reduction by birth. The increase in the peak density was the result of an ~3 fold increase in the HVA current density. The ratio of HVA to LVA Ca^{++} current density in E16 PMNs was 1.5, whereas in neonatal PMNs it was 10.9, demonstrating that the proportion of Ca^{++} entry through LVA Ca^{++} channels was significantly higher in embryonic PMNs.

Figure 5.1. Whole-cell voltage-clamp recordings of LVA and HVA Ca^{++} conductances from an E16 PMN. **A)** Ca^{++} currents were evoked after a pre-pulse potential to -90 (left) or -40 mV (right). **B)** Left panels show the currents elicited by stepping to -40 mV (top) and -10 mV (bottom) from a holding potential of -90 mV. A transient LVA current was activated at low voltage (-40 mV), whereas HVA currents are activated by increasing the depolarizing command potential to -10 mV. Right panel shows the currents to the same conditioning steps but with an initial holding potential of -40 mV. The LVA currents were inactive with the more depolarized holding potential. **C)** Current-voltage (I/V) relationship for the peak (right) and steady-state (left) Ca^{++} currents shown in part A of the figure. Note that the peak and steady state measurements were made from the locations within the current traces demarcated by the filled and empty symbols in part **A**.

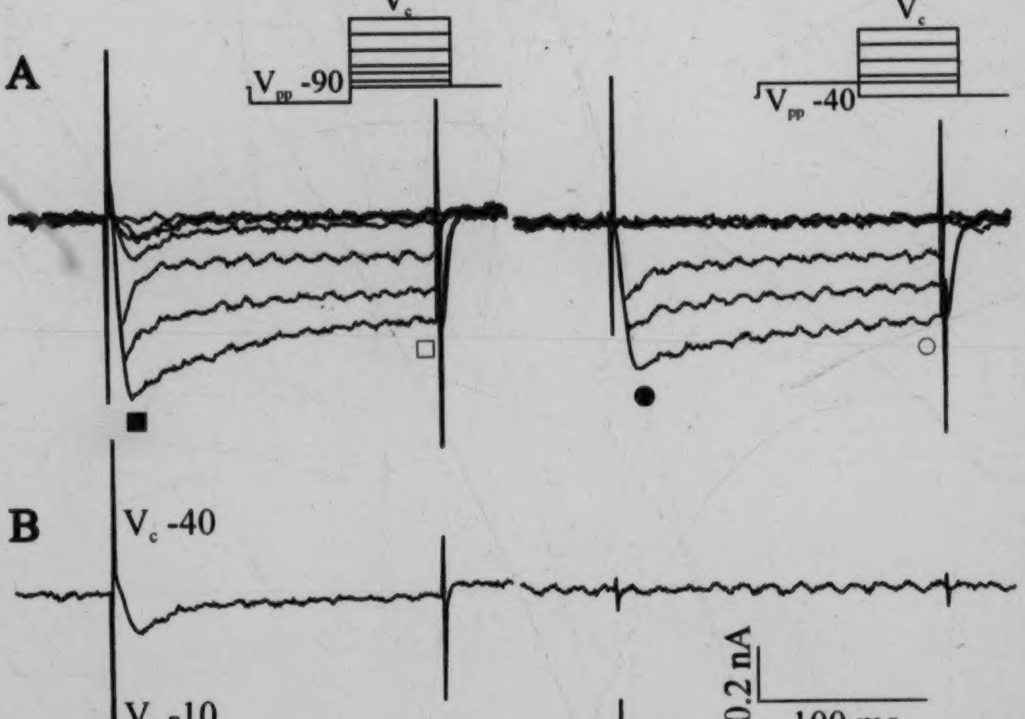
A
V_c
V_pp -90
V_c
V_pp -40
■
□
●
○
B
V_c -40
V_c -10
0.2 nA
100 ms
C
Voltage (mV)
-80
-60
-40
-20
0
20
40
60
0.0
-0.5
-1.0
Current (nA)
I peak (-90mV)
I peak (-40 mV)
Voltage (mV)
-80
-60
-40
-20
0
20
40
60
0.0
-0.5
-1.0
Current (nA)
I steady (-90 mV)
I steady (-40 mV)

Figure 5.2. Effects of Ca^{++}-free medium on the Ca^{++} currents measured in a P0 PMN. **A)** Inward Ca^{++} currents generated following a prepulse potential to -90 mV were eliminated following incubation in Ca^{++}-free medium. **B)** Current-voltage relationship for the peak value of the Ca^{++} current in control (filled square) and following incubation in Ca^{++} free medium (empty square). As discussed in the Results, LVA and HVA currents were present at all ages studied. However, a comparison of the I-V plots in **Figs. 5.2 B** and **5.1 C** demonstrate the increased amplitude of Ca^{++} currents and the slight shift of the peak total current to a more hyperpolarized value in neonatal relative to embryonic PMNs.

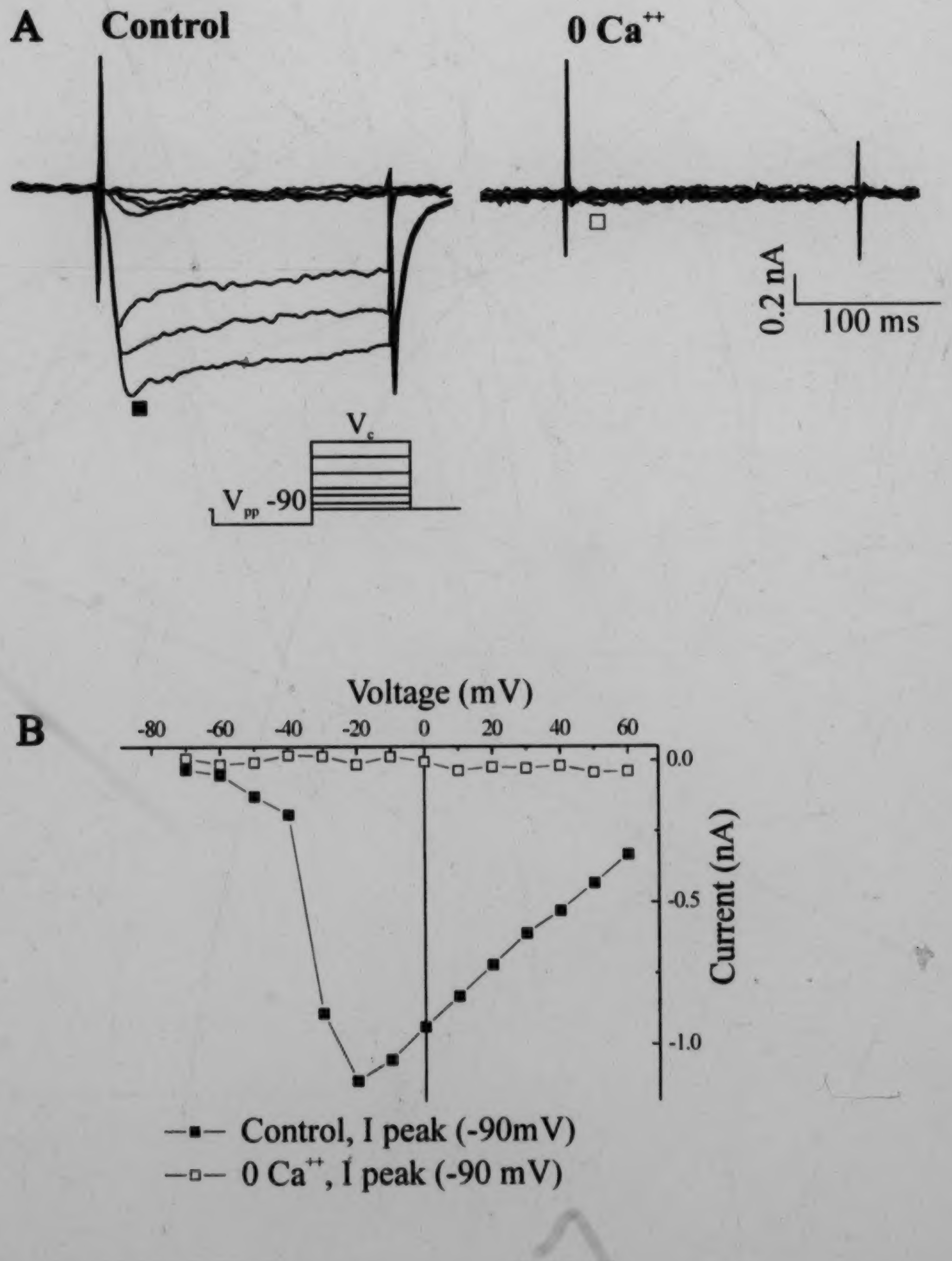
A
Control
0 Ca^{++}
0.2 nA
100 ms
V$_c$
V$_{pp}$ -90
B
Voltage (mV)
-80
-60
-40
-20
0
20
40
60
0.0
-0.5
-1.0
Current (nA)
Control, I peak (-90mV)
0 Ca^{++}, I peak (-90 mV)

Figure 5.3. Effect of blocking T-type Ca^{++} conductances in a E16 PMN. **A)** Nickel (100 μM) completely blocked the LVA Ca^{++} current. **B)** Current-voltage relationship for the peak current after incubation with 100 μM Ni^{+2}. Notice that the 'shoulder' in the I-V plot (arrow) following a pre-pulse potential to -90 mV was eliminated after treatment with Ni^{+2}.

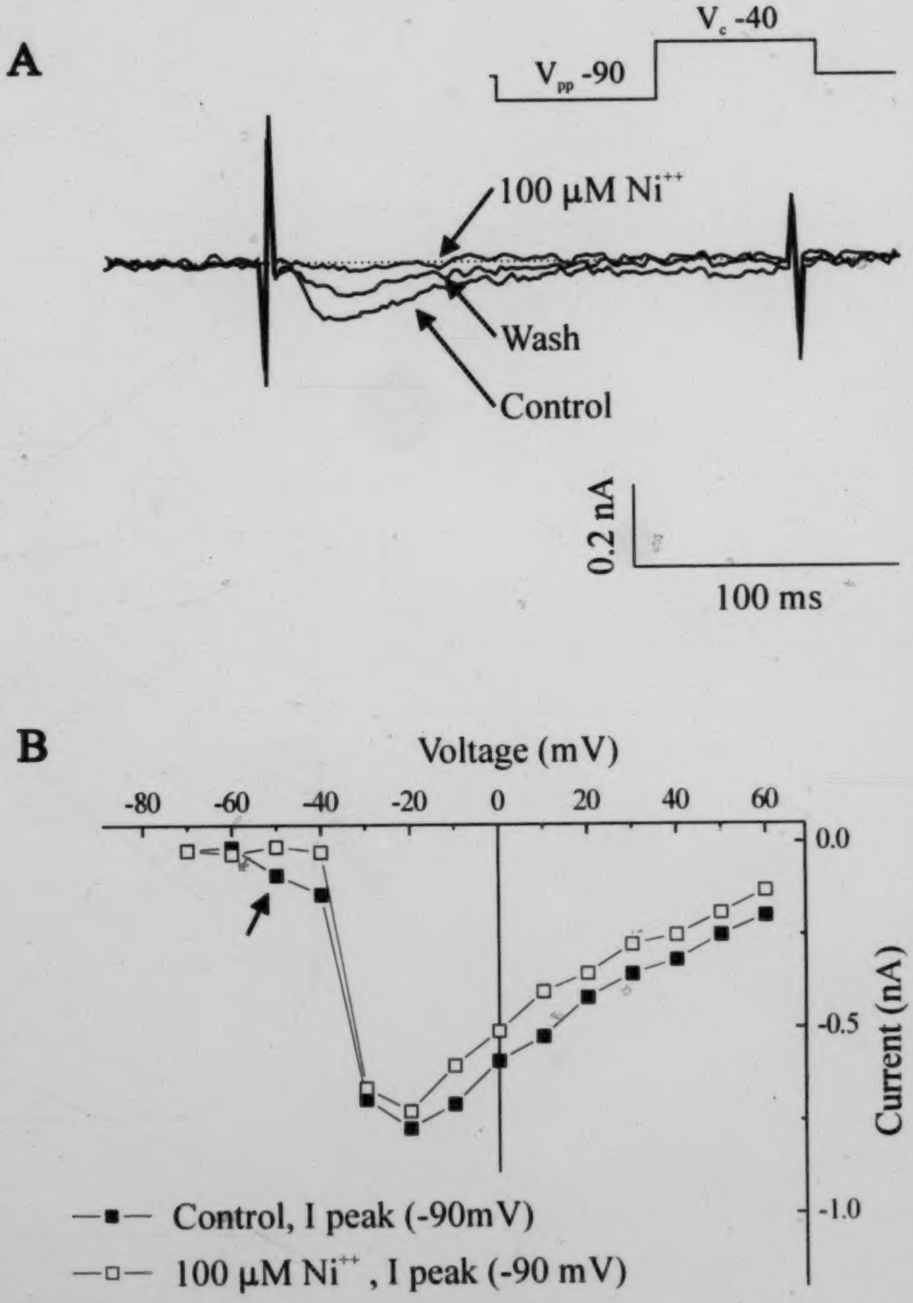
A
V_c -40
V_pp -90
100 µM Ni++
Wash
Control
0.2 nA
100 ms
B
Voltage (mV)
-80
-60
-40
-20
0
20
40
60
0.0
-0.5
-1.0
Current (nA)
Control, I peak (-90mV)
100 µM Ni++ , I peak (-90 mV)

Figure 5.4. Effects of blocking N- and P-type Ca^{++} currents in P0 PMNs. **A)** The N-type Ca^{++} channel blocker ω-conotoxin GVIA (0.5 μM) reduced the HVA component of the current by ~30%. **B)** The P-type Ca^{++} channel blocker ω-agatoxin IVA (0.5 μM) reduced HVA component of the current by ~10%.

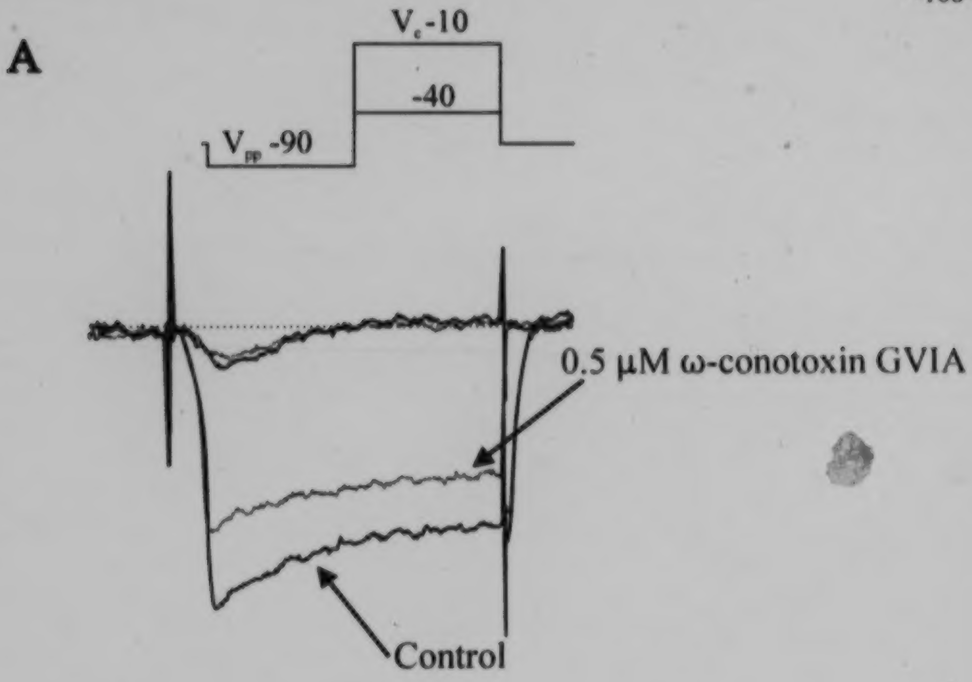
A
Vc -10
-40
Vpp -90
0.5 µM ω-conotoxin GVIA
Control

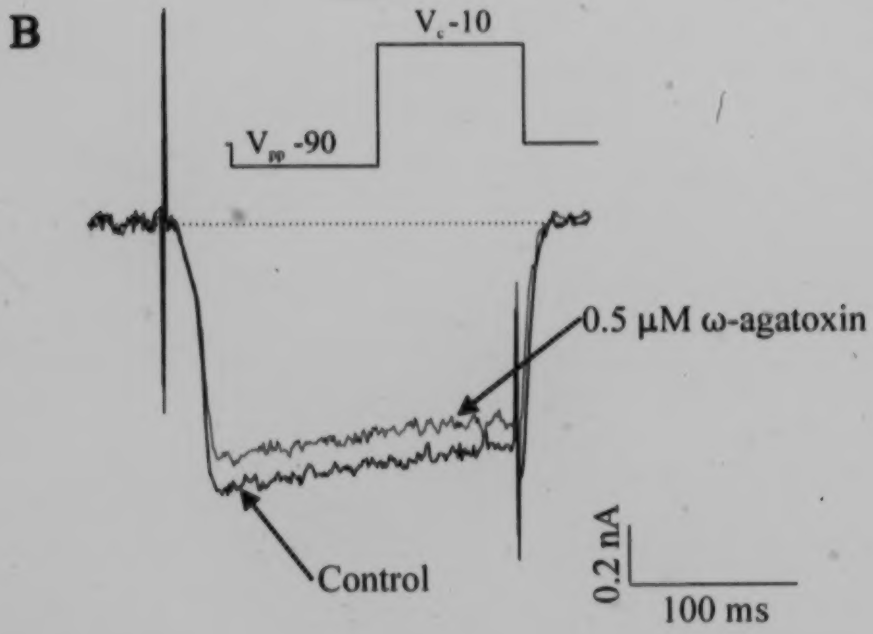
B
Vc -10
Vpp -90
0.5 µM ω-agatoxin
Control
0.2 nA
100 ms

Figure 5.5. Effects of blocking L-type Ca^{++} currents in a P0 PMN. **A)** The L-type Ca^{++} channel blocker verapamil reduced the HVA Ca^{++} current by ~35%. **B)** The I/V plot from the same neuron represented in A, further demonstrates that verapamil was more effective in reducing the calcium current amplitude at voltages ≥-40 mV, corresponding to the HVA component.

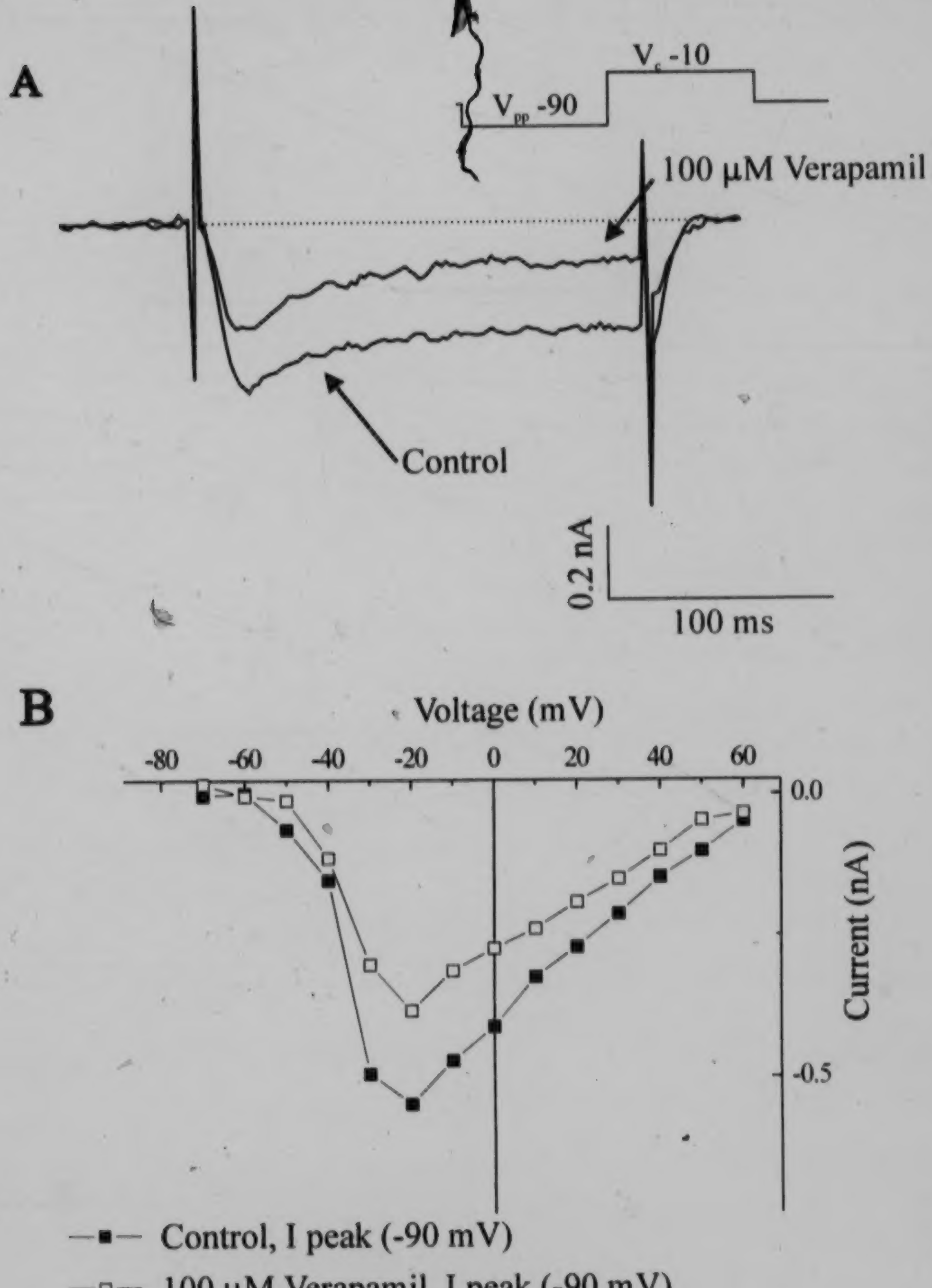
A
V_pp -90
V_c -10
100 µM Verapamil
Control
0.2 nA
100 ms
B
Voltage (mV)
-80
-60
-40
-20
0
20
40
60
0.0
-0.5
Current (nA)
Control, I peak (-90 mV)
100 µM Verapamil, I peak (-90 mV)

Table 5.1. Changes in the Ca^{++}-current densities of PMNs.

Current density (pA/pF)	**E16** (n=11)	**E18** (n=15)	**P0-1** (n=13)
Peak density(1)	6.0±0.6	9.4±0.5	14.4±1.8$^{*\,\diamond}$
LVA current density(2)	1.7±0.2	1.8±0.2	0.8±0.2$^{*\,\diamond}$
HVA current density(3)	2.6±0.5	5.7±0.4*	8.7±1.1$^{*\,\diamond}$

(1) Peak current was measured as the maximal current amplitude generated by a command potential to -10 mV following a pre-pulse potential to -90 mV. Current density was calculated by dividing current amplitude by cell capacitance. Cell capacitance was determined from the area under the current transient following a 10 mV-voltage step from a holding potential of -70 mV. Whole-cell capacitance for E16, E18 and P0-1 PMNs was 56±3 (n=11), 66±3 (n=15) and 69±2* pF (n=13) (*$p \leq 0.05$ vs E16).

(2) T-type Ca^{++} current density was determined from the current amplitude generated by a command potential to -40 mV following a pre-pulse potential to -90 mV.

(3) High voltage-activated (HVA) Ca^{++} current amplitude was measure as the peak current after a test potential to -10 mV following a pre-pulse potential to -40 mV.

(*) $p \leq 0.05$ vs. E16, ($^{\diamond}$) $p \leq 0.05$ vs. E18.

Whole-cell current-clamp recordings

Current-clamp recordings were obtained to further characterize the functional role of voltage-sensitive Ca^{++} conductances in the shaping of PMN action potentials and firing pattern. As shown in chapter III, there were age-dependent changes in PMN action potential shape and firing patterns. A Ca^{++}-sensitive, slowly-decrementing afterdepolarization is a prominent characteristic of embryonic PMN action potentials, whereas neonatal PMNs express a Ca^{++}-sensitive, 'hump-like' afterdepolarization (ADP) followed by an apamin-sensitive, medium-duration hyperpolarization (mAHP). In this study, we examined the contribution of LVA and HVA Ca^{++} conductances to the generation of the afterpotentials and the modulation of repetitive firing properties. Note, that the effects of blocking LVA and HVA Ca^{++} conductances were examined at potentials slightly hyperpolarized and depolarized from resting membrane potential to enhance the amplitudes of ADP and mAHP, respectively.

LVA Ca^{++} currents: The potential influence of LVA Ca^{++} conductances on action potential characteristics were evaluated by the addition of low concentrations of nickel. The slowly-decrementing afterdepolarization in embryonic PMNs was clearly reduced in the presence of 200 μM nickel (Fig. 5.6). The change in action potential duration resulted in a slight, but significant increase in the firing frequency of E16 PMNs (11.3 ±0.3 vs 13.7±0.7 spikes /sec, n=4, $p \leq 0.05$). In neonatal PMNs, nickel had no effect on the ADP, mAHP (Fig. 5.6), or the repetitive firing frequency (13±2 vs 15±1 spikes/sec, n=4, $p \geq 0.05$).

As demonstrated in chapter III, the release of PMNs from a hyperpolarizing potential generates a rebound depolarization in the majority of embryonic (~60%) and only a small proportion of neonatal (12%) PMNs. This rebound depolarization persisted in the presence of sodium and K^+ channel blockers, but was completely inhibited by nickel [Fig. 5.7 A; confirmed in E16 (n=5) and E18 (n=6) PMNs]. As shown in Fig. 5.7 B, the rebound depolarization increased with the duration of the hyperpolarizing prepulse. Interestingly, not all PMNs expressed a rebound depolarization despite the presence of LVA Ca^{++} currents. Fig. 5.8 A shows an example of a PMN which displayed a prominent rebound depolarization. However the PMN in Fig. 5.8 B, rather than having a rebound depolarization, displayed a pronounced delayed excitation. As indicated in chapter IV, delayed excitation in perinatal PMNs is attributed to the actions of an A-type outward K^+ current. It is only when the A-type K^+ current is inhibited with 4-AP that a rebound potential is evident (Fig. 5.8 C). Therefore, the balance of A-type K^+ and LVA Ca^{++} currents in a given PMN is a major determinant for the strength of the rebound depolarization.

HVA Ca^{++} currents: We were also interested in determining the role of HVA Ca^{++} conductances in the determination of embryonic PMN action potential shape and repetitive firing properties. The slowly-decrementing afterdepolarization present in embryonic PMNs was not altered by the addition of blockers to L- (nimodipine, 10 μM; n=3), N– (ω-conotoxin GVIA, 0.5 μM; n=3) or P- (ω-agatoxin IVA, 0.3 μM, n=3) type Ca^{++} channels. Therefore, LVA Ca^{++} currents are the major contributors to the afterdepolarization in E16 PMNs.

In striking contrast, the afterpotentials that are expressed in neonatal PMNs had clear HVA Ca^{++} current components, in particular, L- and N-type Ca^{++} currents. The 'hump-like' ADP was sensitive to interventions with L-type Ca^{++} channels modulators. The L-type Ca^{++}

agonist (±)-Bay K 8644 increased the amplitude of the ADP (Fig. 5.9 A, n=3). Conversely, the blockers of L-type Ca^{++} channels, verapamil (Fig. 5.9 B, n=4) and nimodipine (10μM, n= 4, not shown) reduced the amplitude of the ADP. The most striking effect of blocking L-type Ca^{++} conductances was the inhibition of the burst of action potentials (2-3 action potentials) which fired in association with the ADP at the start of a train of repetitive action potentials (Fig. 5.10). As reported in chapter III, this burst-firing was observed in ~ 20% of neonatal PMNs. In this study, we found that the bursting was eliminated by either verapamil or nimodipine in all bursting neonatal PMNs. The net reduction in ADP amplitude by verapamil led to an increase in PMN firing rate in response to threshold levels of injected current (control 12±1 vs. verapamil-treated 16±1 spikes/sec, n=4, $p \leq 0.05$).

The mAHP was completely inhibited by the N-type Ca^{++} channel blocker ω-conotoxin GVIA (Fig. 5.11 A, insert). As shown in chapter IV, the mAHP results from the activation of a small-conductance, Ca^{++}-activated K^{+} current. Thus, Ca^{++} entry via N-type Ca^{++} channels regulates the apamin-sensitive Ca^{++}-activated K^{+} conductance. The ADP was also affected by block of the N-type Ca^{++} current. As shown in Fig. 5.11 A (insert), the ADP was accentuated in the presence of ω-conotoxin GVIA. However, the prolongation of the ADP was secondary to the elimination of the mAHP as evident from the fact that ω-conotoxin GVIA did not affect the ADP following the prior block of the mAHP with apamin,(Fig. 5.11, n=4). Block of the P-type (ω-agatoxin IVA) Ca^{++} channels did not effect the ADP or mAHP in neonatal PMNs (Fig. 5.11 B; n = 3 in each).

Figure 5.6. Effects of blocking T-type Ca^{++} conductances on action potential characteristics of perinatal PMNs. The slowly-decrementing afterdepolarizations in embryonic PMNs were decreased by Ni^{+2}. By P0, a hump-like ADP and mAHP develops. Neither of these afterpotentials were significantly effected by Ni^{+2}.

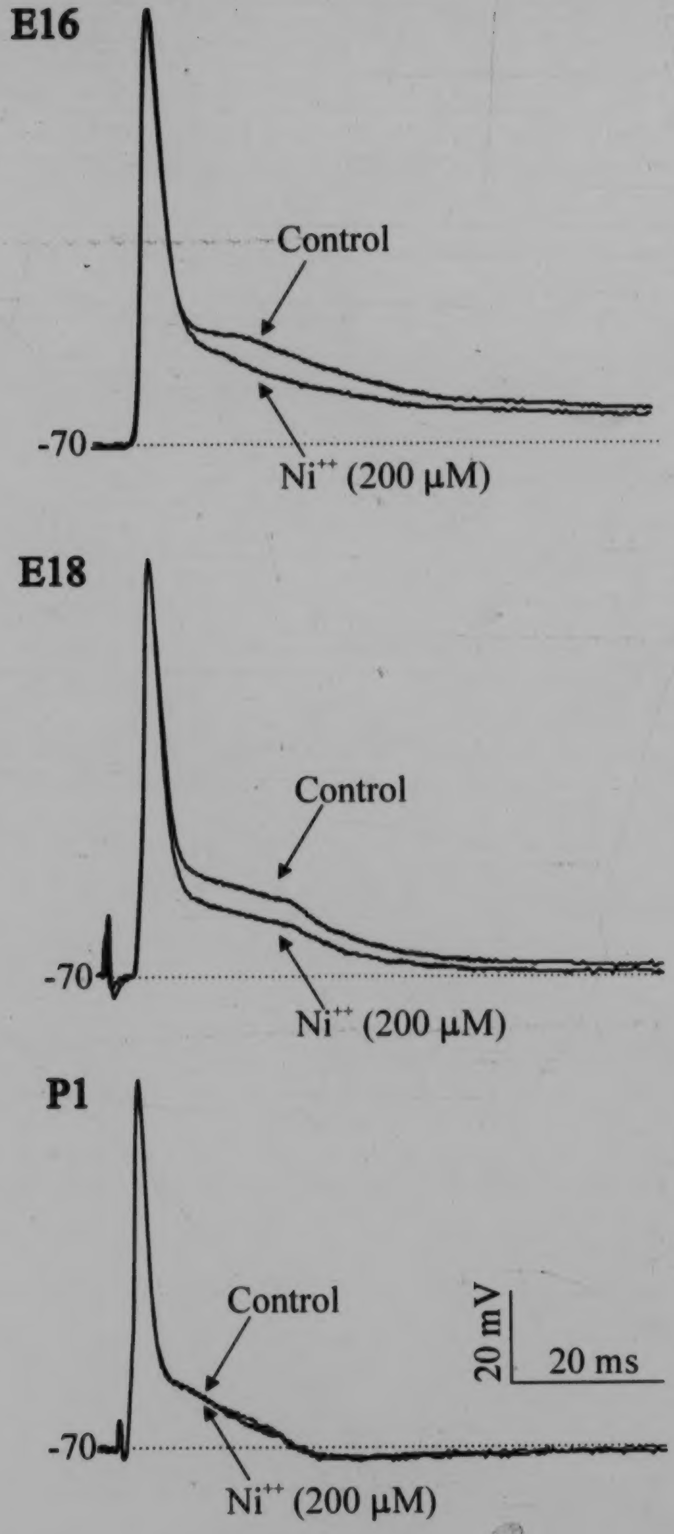
E16
Control
-70
Ni⁺⁺ (200 µM)
E18
Control
-70
Ni⁺⁺ (200 µM)
P1
Control
20 mV
20 ms
-70
Ni⁺⁺ (200 µM)

Figure 5.7. Electrophysiological and pharmacological properties of the rebound depolarization in an E16 PMN. **A)** The rebound depolarization (filled arrow) which was expressed following inhibition of K^+ and Na^+ conductances (left panel) was completely inhibited by Ni^{+2} (right panel). **B)** The magnitude of the rebound depolarization was increased with increasing durations of the hyperpolarizing pulses (left panel). The same protocol in the presence of Ni^{+2} is shown in the right panel.

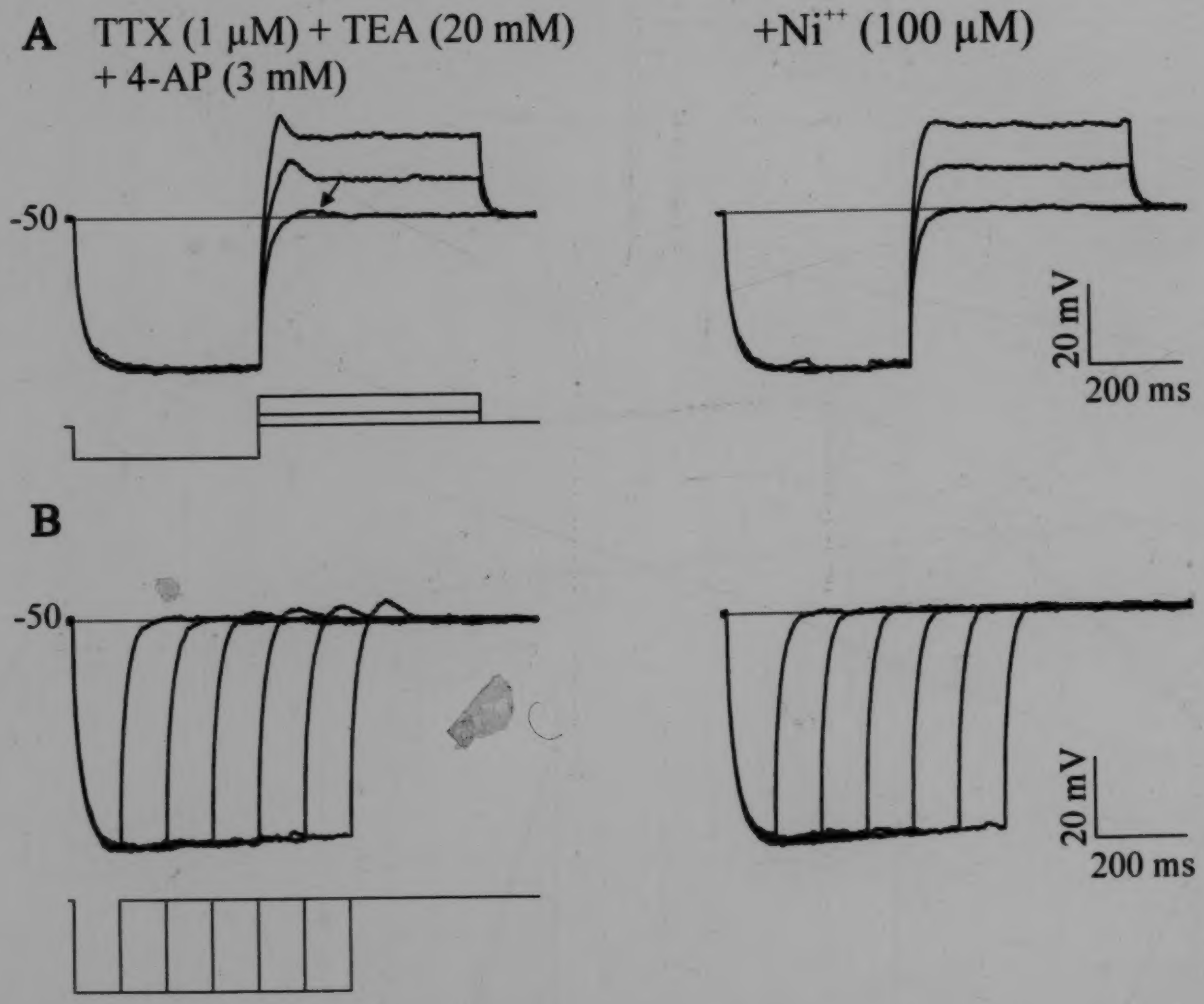
A
TTX (1 µM) + TEA (20 mM)
+ 4-AP (3 mM)
+Ni⁺⁺ (100 µM)
-50
20 mV
200 ms
B
-50
20 mV
200 ms

Figure 5.8. Interactions of T-type Ca^{++} and A-type K^+ currents in determining the response of PMNs to hyperpolarizing pulses. **A)** Example of a E18 PMN which showed a very prominent rebound excitation (filled arrow) upon release from a hyperpolarizing pulse. **B)** Example of a E18 PMN which displayed a prominent delayed excitation (empty arrow) upon release from a hyperpolarizing pulse. **C)** The response of the PMN shown in **B** after block of sodium and K^+ conductances. A rebound excitation (filled arrow) was evident when the A-current mediated delayed excitation was suppressed. The balance of T-type and A-current densities is a major determinant of PMN response to hyperpolarizing pulses (see text for further discussion).

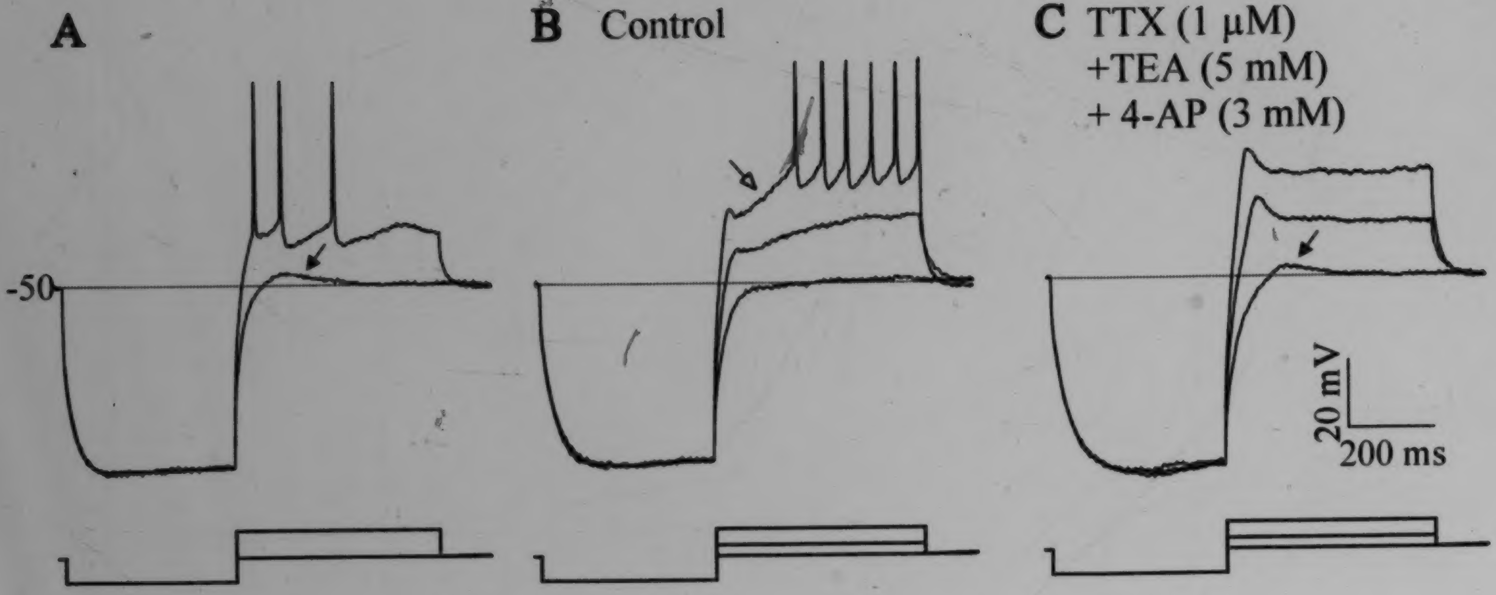
A
B Control
C TTX (1 µM)
+TEA (5 mM)
+ 4-AP (3 mM)
-50
20 mV
200 ms

Figure 5.9. The contribution of L-type Ca^{++} conductances to the afterpotentials of two representative P0 PMNs. **A)** The L-type Ca^{++} channel opener (±)-Bay K 8644 enhanced the afterdepolarizing potential in neonatal PMNs **B)** The L-type Ca^{++} channel inhibitor verapamil reduced the amplitude of the depolarizing potential. Note that the mAHP was not effected by modulating L-type Ca^{++} conductances.

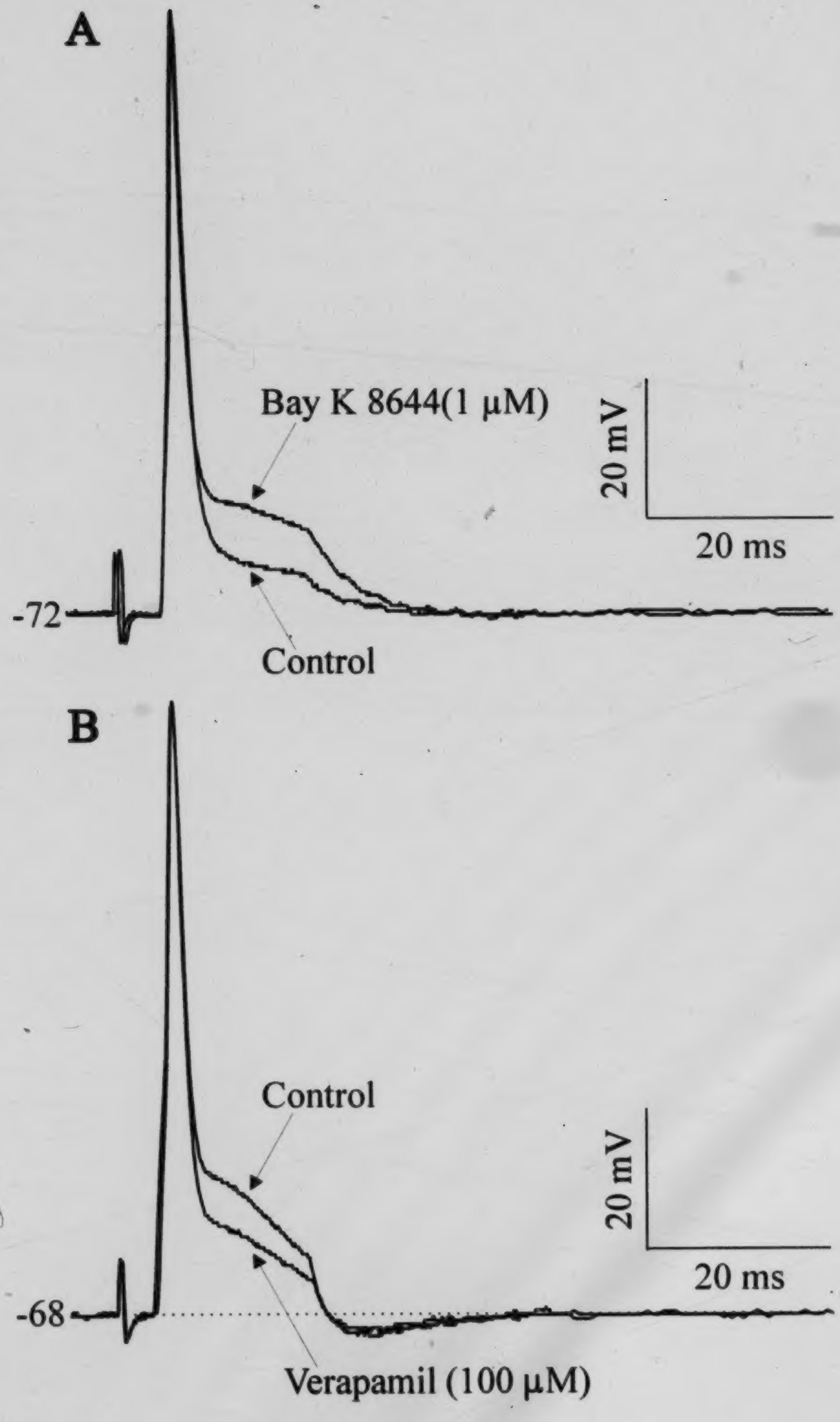
A
Bay K 8644(1 μM)
20 mV
20 ms
-72
Control
B
Control
20 mV
20 ms
-68
Verapamil (100 μM)

Figure 5.10. Effect of L-type Ca^{++} channels blocker, verapamil on the repetitive firing pattern of a P0 PMN. **A)** Control recording showing a train of action potentials with a burst firing pattern (arrow) at the initiation of the spike train (injected current=0.9 nA). **B)** The most prominent effect of verapamil-treatment was the elimination of the burst of action potentials generated at the initiation of the spike train. **C)** Plots of instantaneous firing frequency versus the ISI number for the PMN shown in traces **A** and **B**. The initial high frequency firing (arrow), associated with bursting, was eliminated following treatment with verapamil.

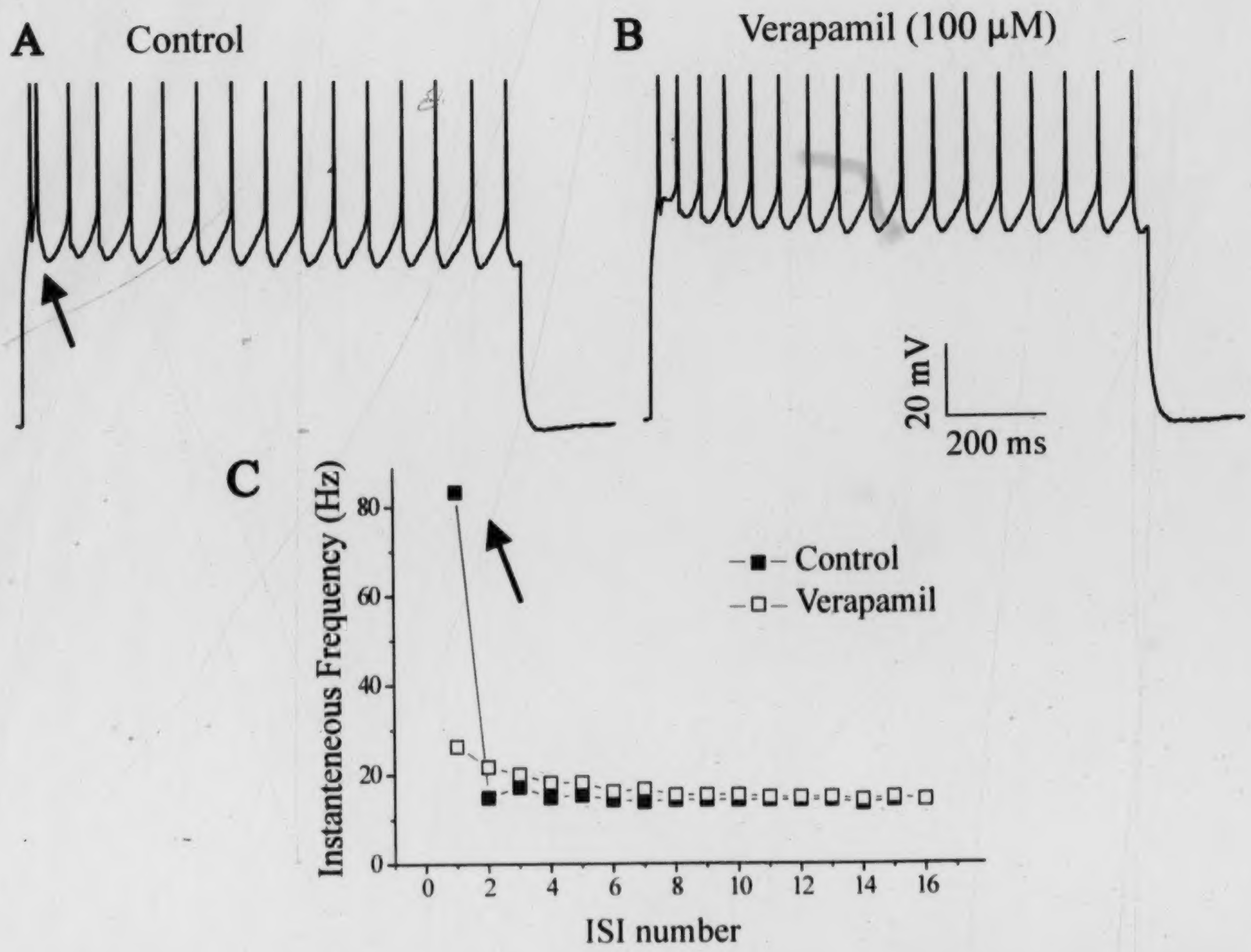
A
Control
B
Verapamil (100 μM)
20 mV
200 ms
C
Instanteneous Frequency (Hz)
0
20
40
60
80
ISI number
0
2
4
6
8
10
12
14
16
Control
Verapamil

Figure 5.11. Effect of blocking N- and P-type Ca^{++} currents on action potential characteristics of PO PMNs. The amplitude of the afterpotentials (ADP and mAHP) in neonatal PMNs are voltage-sensitive, thus we held the neurons at hyperpolarized and depolarized levels to accentuate the amplitude of the ADP and mAHP, respectively. A) Inset: Block of the N-type Ca^{++} channel with ω-conotoxin GVIA resulted in a prolongation of the ADP and elimination of the mAHP. In order to examine the effects of ω-conotoxin GVIA on the ADP independent of changes in the mAHP we blocked the mAHP with apamin. We knew from past studies that the mAHP was dependent on a Ca^{++}-dependent, apamin-sensitive K^{+} channel (see text for further discussion). In an apamin-treated neonatal PMN, ω-conotoxin GVIA did not have any significant effect on the ADP. Thus, the effect of N-type Ca^{++} channel block on ADP amplitude was secondary to the effects on the mAHP. B) The block of P-type Ca^{++} conductances with ω-agatoxin IVA did not significantly effect any of the action potential properties.

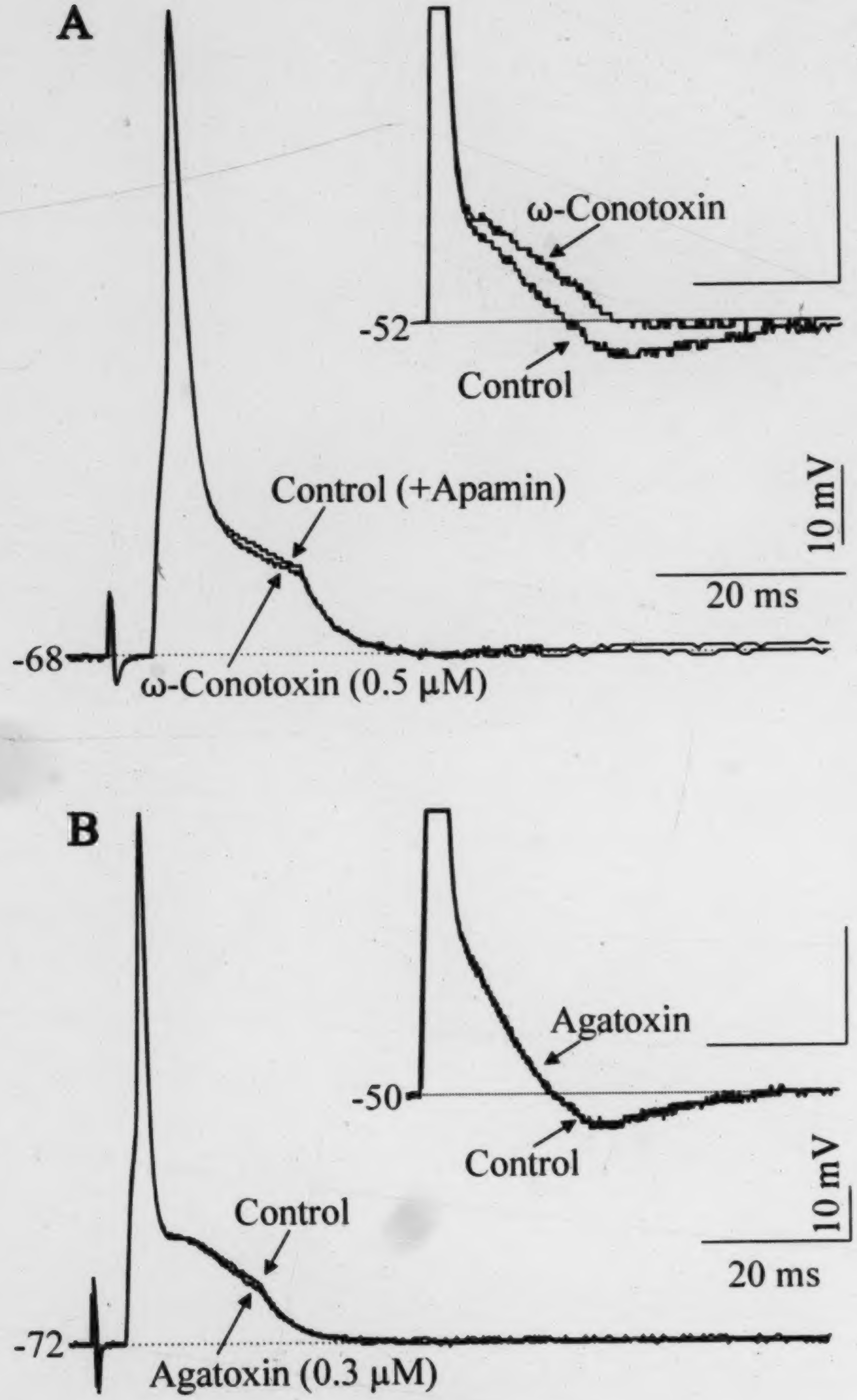
A
ω-Conotoxin
-52
Control
Control (+Apamin)
10 mV
20 ms
-68
ω-Conotoxin (0.5 µM)
B
Agatoxin
-50
Control
10 mV
Control
20 ms
-72
Agatoxin (0.3 µM)

DISCUSSION

These data characterize the developmental changes in Ca^{++} conductances in rat PMNs before and after the commencement of inspiratory drive transmission. This is the period in which PMNs undergo a number of developmental transformations typically involving Ca^{++} regulation, such as neurite remodelling, changes in ionic channel phenotype and electrical excitability. We determined that at least four conductances (T, L, N and P) are expressed in PMNs during this perinatal period. Furthermore, there were significant age-dependent changes in the density of LVA and HVA Ca^{++} currents and their roles in regulating PMN action potential shape and neuronal excitability.

LVA or T-type Ca^{++} conductance

T-type Ca^{++} channels measured in perinatal PMNs demonstrated the classical characteristics of being activated at a low threshold, inactivating quickly and being sensitive to low nickel concentrations (McCobb et al., 1989; Barish, 1991; Viana et al., 1993). The density of T-type Ca^{++} conductances in PMNs decreased markedly (~ 50%) during the perinatal period, similar to the trend observed in some other developing neuronal systems (McCobb et al., 1989; Thompson & Wong, 1991). However, the measured T-type Ca^{++} current density was twofold lower than that previously recorded in chick lumbar motoneurons during a similar period of neuromuscular development (McCobb et al., 1989). This could be explained by the short prepulse potential used for removing the inactivation of T-type Ca^{++} channels in the present experiments. As indicated by the effect of increasing the duration of the hyperpolarizing pulses on the amplitude of the rebound depolarization

(Fig.5.7 B), the hyperpolarizing prepulse in the voltage-clamp experiment could have been insufficient to remove the inactivation of the T-type Ca^{++} channels. This may also explain the higher percentage of T-type Ca^{++} channel inhibition by low nickel concentration. Our finding of a significant T-type Ca^{++} current component in embryonic PMNs is inconsistent with the results of Scamps et al. (1998) who reported very low levels of LVA Ca^{++} currents in a mixed population of cervical embryonic motoneurons. This discrepancy in results could reflect the different recording conditions. We maintained a significant component of the motoneuron dendritic tree with our slice preparation, while the former study used dissociated motoneurons which have lost most of their dendrites. While the dissociated neuron approach offers the advantage of minimizing the space-clamp problem during voltage-clamp recordings, the loss of dendrites would result in the removal of substantial portion of Ca^{++} channels.

Functionally, the T-type Ca^{++} conductances increased the duration of the slowly-decrementing afterdepolarization in embryonic PMNs, but did not contribute significantly to the production of afterpotentials in neonatal PMNs. In particular, we did not find a significant contribution of LVA Ca^{++} currents to the hump-like ADP in neonatal PMNs as has been reported for neonatal hypoglossal motoneurons (Viana et al., 1993). T-type Ca^{++} currents also played a prominent role in influencing rebound depolarizations observed in a subpopulation of PMNs throughout the perinatal period. As shown clearly in Fig. 5.8, the balance of T-type Ca^{++} versus A-type K^{+} current is a major determinant of whether a given PMN display a rebound depolarization. Indeed, the density of A-current was similar throughout the perinatal period, although the incidence of rebound depolarization declined in an age-dependent manner. Taken together, it is clear that an age-dependent decline in the density of T-type Ca^{++} currents an important mechanism for this change.

A prominent T-type Ca^{++} current in embryonic PMNs will promote the influx of Ca^{++} ions during the period in which they are undergoing profound changes in their morphological and electrophysiological properties. As has been shown for other types of developing neurons, enhanced Ca^{++} fluxes promote axonal and dendritic outgrowth and reorganization (McCobb & Kater, 1988; Holliday & Spitzer, 1990) and electrical excitability (Gu & Spitzer, 1993). Ca^{++} influx through T-type Ca^{++} channels will also serve to amplify small synaptically-mediated membrane depolarization towards threshold. This could be particularly critical at early embryonic ages when inspiratory synaptic drive, which starts at E17, is weak and vulnerable to failure (Greer et al., 1992; Di Pasquale et al., 1996). However, this would depend on the membrane potentials reaching sufficiently hyperpolarized levels during the expiratory phase to remove the inactivation of T-type Ca^{++} channels. Currently, this cannot be determined from the limited data concerning respiratory-related synaptic drive and modulation of PMN membrane potential during the perinatal period.

HVA Ca^{++} currents

The density of HVA Ca^{++} currents increased more than three-fold during the perinatal period. The HVA Ca^{++} currents in PMNs consist of at least three pharmacologically different components (P, N and L). Block of P-type Ca^{++} conductances had only minimal effects on the total inward HVA Ca^{++} current. Furthermore, there were no obvious changes in PMN action potential shape or repetitive firing frequency at any age when P-type Ca^{++} currents were blocked. This is in contrast to what has been reported for trigeminal motoneurons where P-type Ca^{++} current contributes to the ADP (Kobayashi et al., 1997). However, it should be noted that P-type Ca^{++} channels are expressed in perinatal PMN axon terminals where they play an important role in Ca^{++}-mediated neurotransmitter release (Siri & Uchitel, 1999).

The emergence of PMN afterpotentials just prior to birth involve the increased expression of N– and L-type Ca^{++} currents. N-type Ca^{++} current is essential for the production of the mAHP. Ca^{++} entry via N-type Ca^{++} channels is coupled to the apamin-sensitive, Ca^{++}-activated K^{+} conductance which underlies the mAHP. There is also a significant N-type Ca^{++} current involved in transmitter release in the perinatal rat phrenic nerve terminals, which is later down-regulated postnatally (Siri & Uchitel, 1999).

L–type Ca^{++} current contributed to the hump-like ADP that develops in PMNs by birth, as well as the characteristic bursting in neonatal PMNs. This bursting property in PMN firing may have important functional consequences for diaphragmatic contractility. Activation of a single motor unit by two closely spaced stimuli produces the well-known 'catch-property' whereby a tension, larger and longer lasting than a twitch evoked by a single stimulus, is produced (Burke et al., 1970). Therefore the burst of action potentials in PMNs will serve to increase and extend the tension of the diaphragm musculature.

In conclusion, throughout the perinatal period, from just prior to the commencement of inspiratory drive transmission (E16) through to birth, there are marked reductions of LVA Ca^{++} current and increases in HVA Ca^{++} current densities in PMNs. The elevated expression of LVA Ca^{++} channels during the embryonic period lengthens the ADP and enhances electrical excitability. The increase in HVA Ca^{++} current density in neonatal PMNs is concomitant with the emergence of Ca^{++}-dependent afterpotentials and burst-like firing properties. We show important age-depended interactions between Ca^{++} and K^{+} currents which regulated the expression of rebound excitation and mAHP. Moreover, the net age-dependent increase in Ca^{++} influx through voltage-dependent channels likely contributes to Ca^{++}-regulated mechanisms underlying the rapid maturation of PMN phenotype during the perinatal period.

REFERENCES

ALLAN, D.W., GREER, J.J. (1997a) Embryogenesis of the phrenic nerve and diaphragm in the fetal rat. J. Comp. Neurol. 382: 459-468.

ALLAN, D.W., GREER, J.J. (1997b) Development of phrenic motoneuron morphology in the fetal rat. J. Comp. Neurol. 381: 469-479.

BARISH, M.E. (1991) Voltage-gated calcium currents in cultured embryonic Xenopus spinal neurons. J. Physiol. Lond. 444: 523-543.

BEAN, B.P. (1989) Classes of calcium channels in vertebrate cells. Ann. Rev. Physiol. 51: 367-384 .

BURKE, R.E., RUDOMIN, P., ZAJAC, F.E. (1970) Catch properties in single mammalian motor units. Science 168: 122-140.

CAMERON, W.E., AVERILL, D.E., BERGER, A. (1985) Quantitative analysis of the dendrites of cat phrenic motoneurones stained intracellularly with horseradish peroxidase. J. Comp. Neurol. 231:91-101.

CHOI, D.W. (1987) Ionic dependence of glutamate neurotoxicity. J. Neurosci. 7: 369-379.

COHAN, C.S., CONNOR, J.A., KATER, S.B. (1987) Electrically and chemically mediated increases in intracellular calcium in neuronal growth cone. J. Neurosci. 7: 3588-3599.

DESARMENIEN, M.G., SPITZER, N.C. (1991) Role of calcium and protein kinase C in development of the delayed rectifier potassium current in Xenopus spinal neurons. Neuron 7: 797-805.

DI PASQUALE, E., TELL, F., MONTEAU, R., HILAIRE, G. (1996) Perinatal developmental changes in respiratory activity of medullary and spinal neurons: an in vitro study on fetal and newborn rats. Dev. Brain Res. 91: 121-130.

FOX, A.P., NOWYCKY, M.C., TSIEN, R.W. (1987) Kinetic and pharmacological properties distinguishing three types of calcium currents in chick sensory neurons. J. Physiol. 394: 149-172.

GREER, J.J, SMITH, J.C., FELDMAN, J.L. (1992) Respiratory and locomotor patters generated in the fetal rat brain stem-spinal cord in vitro. J. Neurophysiology 67 (4): 996-999.

GU, X., SPITZER, N.C. (1993) Low-threshold Ca^{2+} current and its role in spontaneous elevations of intracellular Ca^{2+} in developing Xenopus neurons. J. Neurosci. 13 (11): 4936-

4948.

HOLLIDAY, J., SPITZER, N.C. (1990) Spontaneous calcium influx and its role in differentiation of spinal neurons in culture. Dev. Biol. 141: 13-23.

KATZ, B., MILEDI, R. (1967) The timing of calcium action during neuromuscular transmission. J. Physiol. (Lond.) 189: 535-544.

KOBAYASHI, M., INOUE, T., MATSUO, R., MASUDA, Y., HIDAKA, O., KANG, Y., MORIMOTO, T. (1997) Role of calcium conductances on spike afterpotentials in rat trigeminal motoneurons. J. Neurophysiol. 77: 3273-3283.

LLINAS, R., YARON, Y. (1980) Properties and distribution of ionic conductances generating electroresponsiveness of mammalian inferior olivary neurons in vitro. J. Physiol. 315: 569-584.

MCCOBB, D.P., BEST, P.M., BEAM, K.G. (1989) Development alters the expression of calcium currents in chick limb motoneurons. Neuron 2: 1633-1643.

MCCOBB, D.P., KATER, S.B. (1988) Membrane voltage and neurotransmitter regulation of neuronal growth cone motility. Dev. Biol. 130: 599-609.

MINTZ, I.M., VENEMA, V.J., SWIDEREK, K.M., LEE, T.D., BEAN, B.P., ADAMS, M.E. (1992) P-type calcium channels blocked by the spider toxin ω-Aga-IVA. Nature 355: 827-829.

SCAMPS, F., VALENTIN, S., DAYANITHI, G., VALMIER, J. (1998) Calcium channel subtypes responsible for voltage-gated intracellular calcium elevations in embryonic rat motoneurons. Neurosci. 87 (3): 719-730.

SIRI, M.D.R., UCHITEL, O.D. (1999) Calcium channels coupled to neurotransmitter release at neonatal rat neuromuscular junctions. J. Physiol. 515.2: 533-540.

SPITZER, N.C., DEBACA, C., HOLLIDAY, J. (1988) Developmental acquisition of GABA-like immunoreactivity by amphibian spinal neurons differentiating in vivo. Soc. Neuronsci. Abst. 14: 163.

THOMPSON, S.C., WONG, R.K.S. (1991) Development of calcium current subtypes in isolated rat hippocampal pyramidal cells. J. Physiol. (London) 439: 671-689.

TORIKAI, H., HAYASHI, F., TANAKA, K., CHIBA, T., FUKUDA, Y., MIRIYA, H. (1996) Recruitment order and dendritic morphology of rat phrenic motoneurons. J. Comp. Neurol. 366: 231-243.

TSIEN, R.W., ELLINOR, P.T., HORNE, W.A. (1991) Molecular diversity of voltage-dependent Ca^{2+} channels. Trends in Pharmacol. 12: 349-354.

TYMIANSKY, M., CHARLTON, M.P., CARLEN P.L., TATOR, C.H. (1993) Source specificity of early calcium neurotoxicity in cultured embryonic spinal neurons. J. Neurosci. 13(5): 2085-2104.

UMEMIYA, M., BERGER, A.J. (1994) Properties and function of low- and high-voltage-activated Ca^{2+} channels in hypoglossal motoneurons. J. Neuroscience 14(9): 5652-5660.

VIANA, F., BAYLISS, D.A., BERGER, A.J. (1993) Calcium conductances and their role in the firing behaviour of neonatal rat hypoglossal motoneurons. J. Neurophysiol. 69(6): 2137-2149.

WALTON, K., FULTON, B.P. (1986) Ionic mechanisms underlying the firing properties of rat neonatal motoneurons studied in vitro. Neurosci. 19(3): 669-683.

XIE, H., ZISKIND-CONHAIM, L. (1995) Blocking Ca^{2+}-dependent synaptic release delays motoneuron differentiation in the rat spinal cord. J. Neurosci. 15: 5900-5911.

YUSTE, R., TANK, D.W. (1996) Dendritic integration in mammalian neurons, a century after Cajal. Neuron 16:701-716.

CHAPTER 6

CONTRACTILE AND FATIGUE PROPERTIES OF THE RAT DIAPHRAGM MUSCULATURE DURING THE PERINATAL PERIOD

Adapted from the original publication:
M. Martin-Caraballo, P.A. Campagnaro, Y. Gao and J.J. Greer
J. Appl. Physiol. 88: 573-579 (2000)

INTRODUCTION

As described in previous chapters, there are pronounced changes in the passive membrane, action potential and repetitive firing properties of rat phrenic motoneurons (PMNs) during the period spanning from E16, one day prior to the commencement of fetal breathing movements (Greer et al., 1992), through to birth. **The focus of the current study was to examine the concomitant changes in diaphragm muscle properties during the perinatal period.**

There have been several studies examining the developmental changes in diaphragm contractile and fatigue properties postnatally (Sieck et al., 1991; Feldman et al., 1991; Moore et al., 1993; Bazzy, 1994; Johnson et al., 1994). Those studies found that, with age: i) the ratio of peak twitch force to maximum tetanic force decreases, ii) twitch contraction and half-relaxation times decrease, iii) the maximum unloaded shortening velocity (V_o) increases, iv) the force-frequency curve is shifted to the right, and v) neuromuscular fatigue decreases. In the present study, I complement past work by extending the examination of diaphragm properties to earlier perinatal stages, demonstrating that there is a major transformation of contractile and fatigue properties following the inception of inspiratory drive transmission *in utero*. Furthermore, the present results indicate that these properties develop during the perinatal period to functionally match changes occurring in PMN electrophysiological properties (Chapter 3).

METHODS

Drugs: The following drugs were used (suppliers in brackets): d-tubocurarine, μ-conotoxin, 2,3-butanedione,2-monoxime (BDM, Sigma).

RESULTS

Force measurements

Table 6.1 lists the values of twitch and maximal tetanic forces generated as a function of muscle weight, protein content and estimated cross sectional area at E18 and P0-1. Single twitch force per weight or mg protein content were less at E18 compared with P0-1, although, only values comparing force/wet weight were statistically significant. Maximal tetanic forces, expressed either as force per unit wet weight, dry weight, per unit protein content, or estimated cross sectional area were all significantly less at E18 compared to P0-1. The ratios of single twitch force to maximal tetanic force were also different at each age (Table 6.1). The ratios ranged from approximately 50-70% at E18 compared to 20-40 % at P0-1.

Feldman et al. (1991) previously reported the presence of post-stimulation contractions (i.e. a second smaller contraction which appeared spontaneously during the relaxation phase of the tetanic contraction) in a subpopulation of neonatal diaphragm preparations. We observed this unexplained phenomenon in a few preparations (2 of 6 E18 preparations, 1 of 5 P0-1 preparations; data not shown).

Twitch characteristics

As demonstrated by the data in Table 6.1 and Fig. 6.1A, there were clear age-dependent differences in the characteristics of single muscle twitches. By P0-1, the mean twitch contraction and half-relaxation times had decreased by 53% and 67%, respectively, compared with those at E18.

Relationship between force development and stimulation frequency

There were marked age-dependent differences in the relationship between the tetanic force generated by the diaphragm musculature and the frequency of phrenic nerve stimulation. First, the fused tetanus frequency was much lower at E18 (~15 Hz) compared to P0-1 (~40 Hz; Fig. 6.1 B). Second, there was a striking difference between the embryonic and neonatal muscle with regards to the range of forces generated by modulating the frequency of phrenic nerve stimulation (Fig. 6.2). At E18, the range was limited to approximately 65-100% of the maximum tetanic force in response to phrenic nerve stimulations from 1 to 100 Hz. In contrast, at P0-1, tetanic force ranged from approximately 25-100% of maximum in response to the same range of phrenic nerve stimulation. Third, the amount of force produced at the onset of nerve stimulation was less than that produced by direct muscle stimulation at P0-1 at frequencies greater than 60 Hz (Table 6.1, Figs. 6.2 and 6.3; $p \leq 0.05$). In contrast, there was no difference between forces achieved at the onset of nerve versus direct muscle stimulation at E18. Fourth, the decay time of tetanic force production was much slower at E18 in comparison to P0-1; the force production being maintained well beyond the termination of nerve stimulation (Fig. 6.3).

Relationship between declines in diaphragm force levels and nerve stimulation paradigms

There were age-dependent changes in the ability of the muscle to sustain force levels in response to high frequency nerve stimulation. At E18, the muscle was capable of supporting the same level of force throughout a 1 second pulse of up to 100 Hz phrenic nerve stimulation in all but 1 of 6 preparations (Table 6.1, Fig. 6.3). In contrast, the force levels declined in all neonatal muscle preparations in a frequency-dependent manner at nerve stimulation rates ≥40 Hz (Table 6.1, Figs. 6.1 B and 6.3). The data illustrated in Fig. 6.3 B demonstrates that the decline in force in response to the nerve stimulation could be reversed by stimulating the muscle directly. Moreover, there was no decline in force at either age when the muscle was stimulated directly for one second. A further analysis of the E18 muscle force production in response to a train of nerve stimulation was performed. We tested whether there would be a drop in force levels if the stimulation was maintained for greater than 1 second. As shown in Fig. 6.4, if the duration of the stimulus train was increased (10 sec), a significant decline in force levels was observed in all E18 preparations. Further, the decline in force levels could be reversed by stimulating the E18 muscle directly.

Table 6.1. Contractile properties of rat diaphragm at embryonic age 18 (E18) and postnatal days 0-1 (P0-1).

		E18 (n=6)	**P0-1** (n=5)
Twitch force (1)	mg/mg wet weight	28 ± 4	51 ± 6*
	mg/mg dry weight	900 ± 149	1185 ± 228
	mg/ng protein content	72 ± 27	169 ± 51
Maximal tetanic force	mg/mg wet weight	51 ± 11	185 ± 27*
	mg/mg dry weight	1619 ± 340	4452 ± 1093*
	mg/ng protein content	121 ± 42	657 ± 216*
	Normalized force (N/cm^2)	0.4 ± 0.1	2.1 ± 0.3*
Single twitch contraction time (ms)		182 ± 20	85 ± 3*
Single twitch half-relaxation time (ms)		156 ± 12	51 ± 3*
Single twitch / maximal force ratio		0.64 ± 0.03	0.28 ± 0.02*
Fused tetanus frequency (Hz)		15 ± 2.2	40 ± 0*
Fatigue ratio (2)	40 Hz	0.96 ± 0.02	0.92 ± 0.02
	60 Hz	0.98 ± 0.01	0.84 ± 0.04*
	80 Hz	0.97 ± 0.01	0.83 ± 0.03*
	100 Hz	0.97 ± 0.02	0.90 ± 0.04*

(1) Single twitch force was the average of three consecutive twitches.

(2) The fatigue ratio was calculated as the peak tension vs the level of tension at the end of the 1s-long stimulation.

(*) $p \leq 0.05$ compared to E18.

Figure 6.1. Age-dependent changes in twitch and tetanus characteristics. **A)** Single twitch contractions generated by E18 and P0-1 diaphragm musculature following phrenic nerve stimulation (0.5 ms pulse). **B)** Contractile responses of E18 and P0-1 diaphragm musculature in response to 1 second nerve stimulation of varying frequencies. Twitch contraction times decrease and tetanus fusion frequencies increase markedly during the perinatal period.

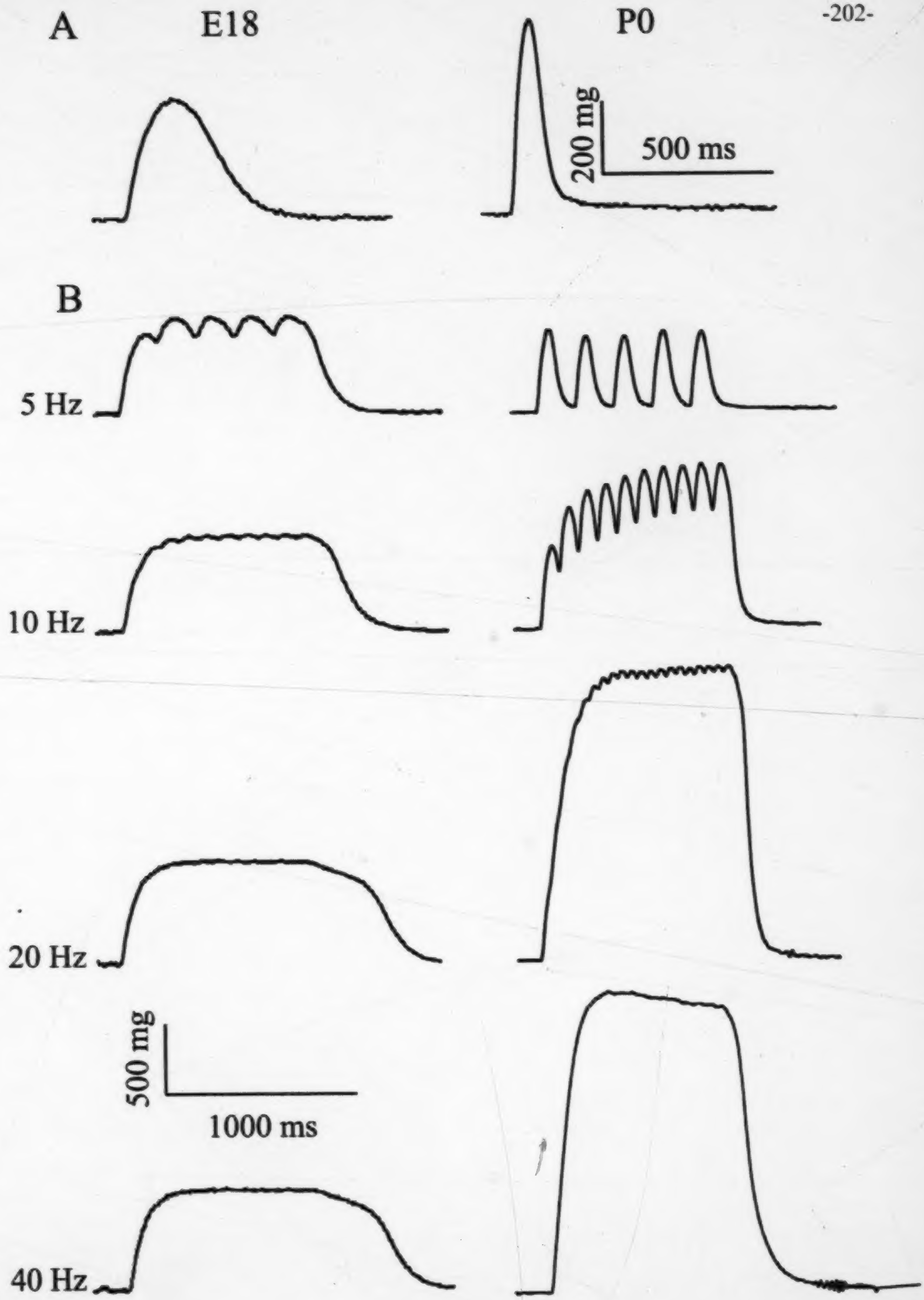
A
E18
P0
200 mg
500 ms
B
5 Hz
10 Hz
20 Hz
40 Hz
500 mg
1000 ms

Figure 6.2. Plot of the normalized peak force at the onset of muscle (open squares) and nerve stimulation (solid squares) vs. stimulus frequency. Peak force was expressed as a percentage of the maximal force generated at a given frequency. Maximal tension was attained in E18 diaphragms at a lower frequency and the range of force production was more limited compared with P0-1. Indications of neuromuscular fatigue were observed in neonatal preparations in response to nerve stimulations greater than 60 Hz.

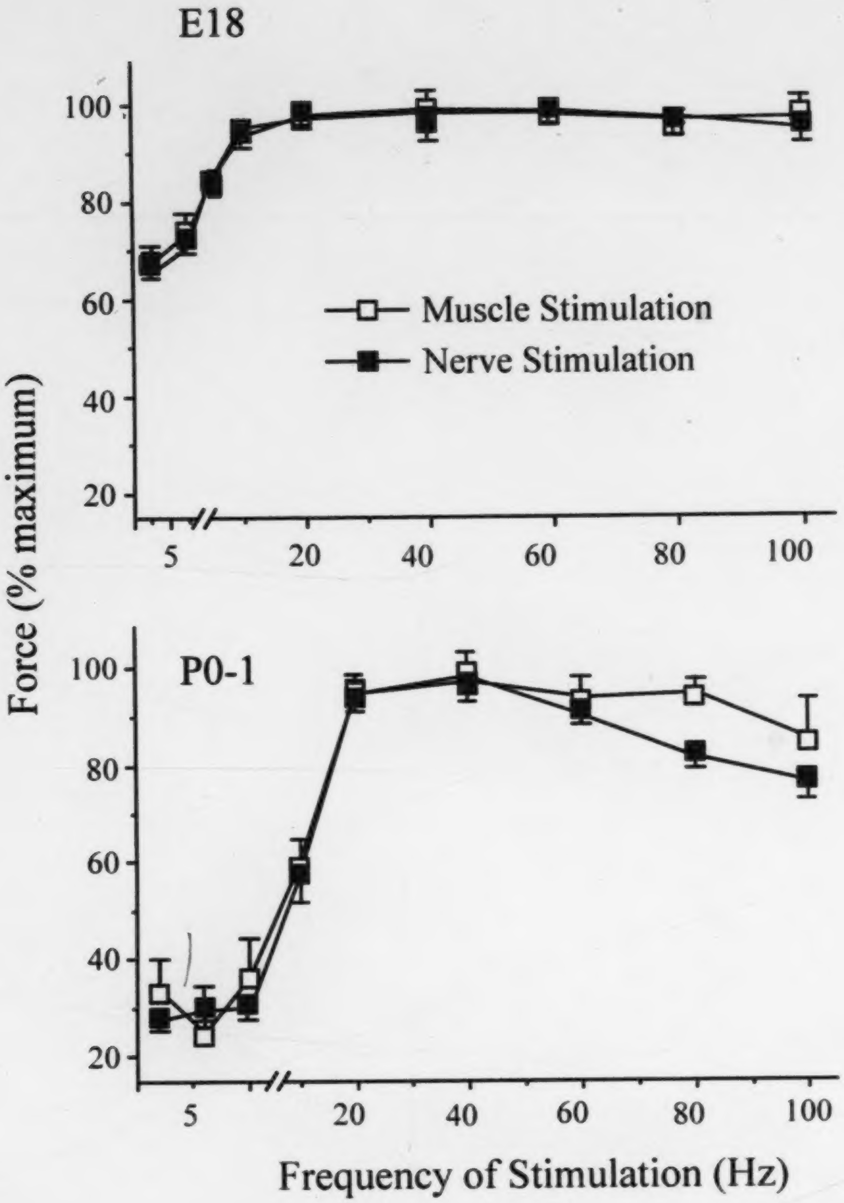
E18
100
80
60
40
20
5
20
40
60
80
100
—□— Muscle Stimulation
—■— Nerve Stimulation
Force (% maximum)
P0-1
100
80
60
40
20
5
20
40
60
80
100
Frequency of Stimulation (Hz)

Figure 6.3. Force developed by the diaphragm in response to nerve and direct muscle stimulation. **A)** Tetanic force records from E18 and P0 diaphragm musculature in response to 60 and 100 Hz nerve (N) and direct muscle (M) stimulation for one second. The dashed line indicates the time when the one second stimulation pulses were terminated. The delay in the force decline after the termination of nerve or muscle stimulation increased with higher frequencies of stimulation and is particularly pronounced at E18. **B)** Force generated by E18 and P0 diaphragm following superimposed nerve (N) and direct muscle (M) stimulation. Direct muscle stimulation was applied after 750 ms of nerve stimulation. The decline in force in response to the nerve stimulation at P0 was alleviated by the direct muscle stimulation indicating that the source of the fatigue was not intrinsic to the muscle.

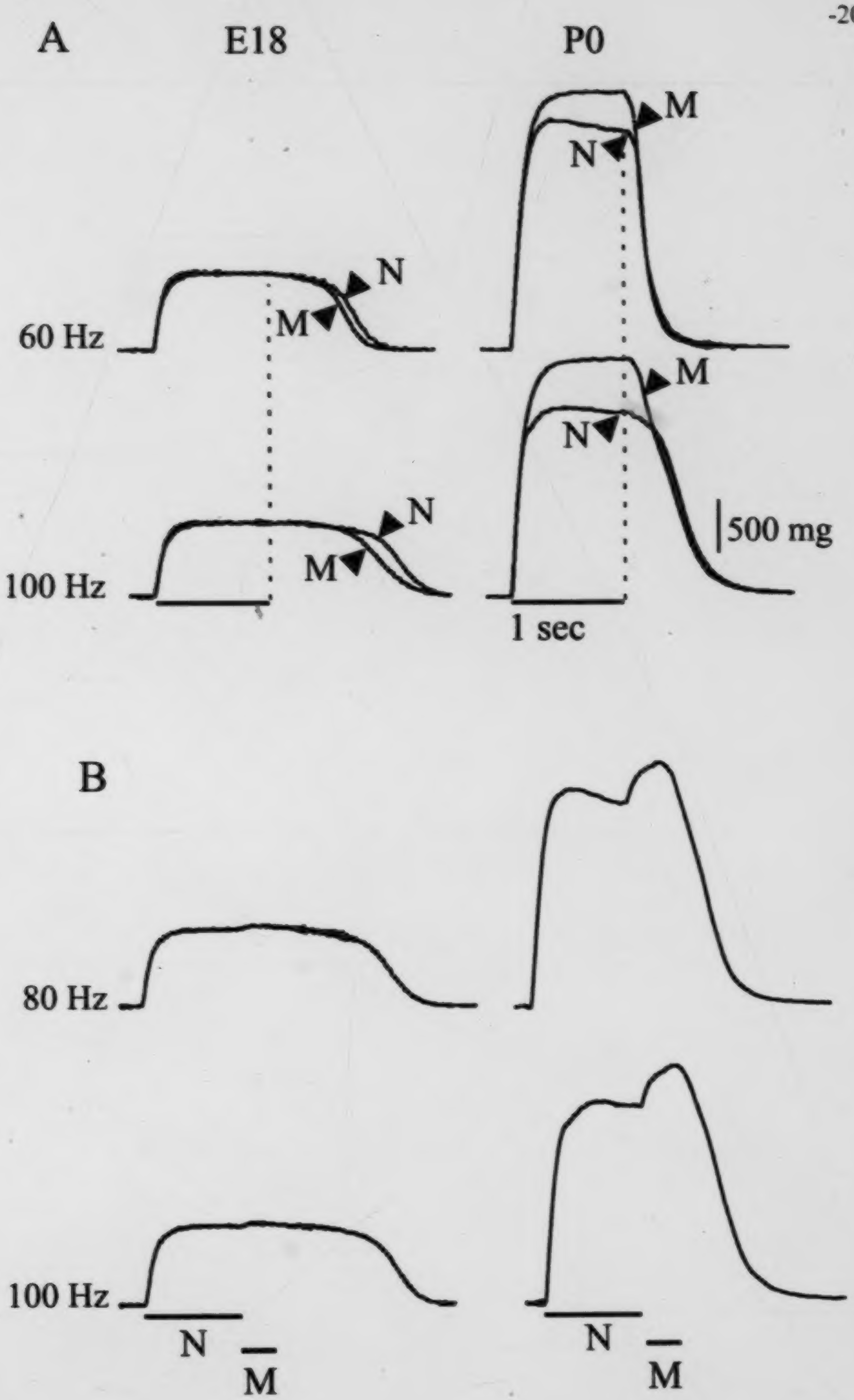
A
E18
P0
N
M
M
N
60 Hz
M
N
M
N
100 Hz
500 mg
1 sec
B
80 Hz
100 Hz
N
M
N
M

Figure 6.4. Force records from E18 diaphragm muscle preparations in response to varying frequencies of long duration (10 sec) nerve stimulation. The fatigue was evident with the longer stimulation paradigm, occurring sooner as the frequency of stimulation was increased. The decline in force was reversed in all cases by superimposing direct stimulation of the muscle (M) during final 2 seconds of the 10 second nerve stimulation.

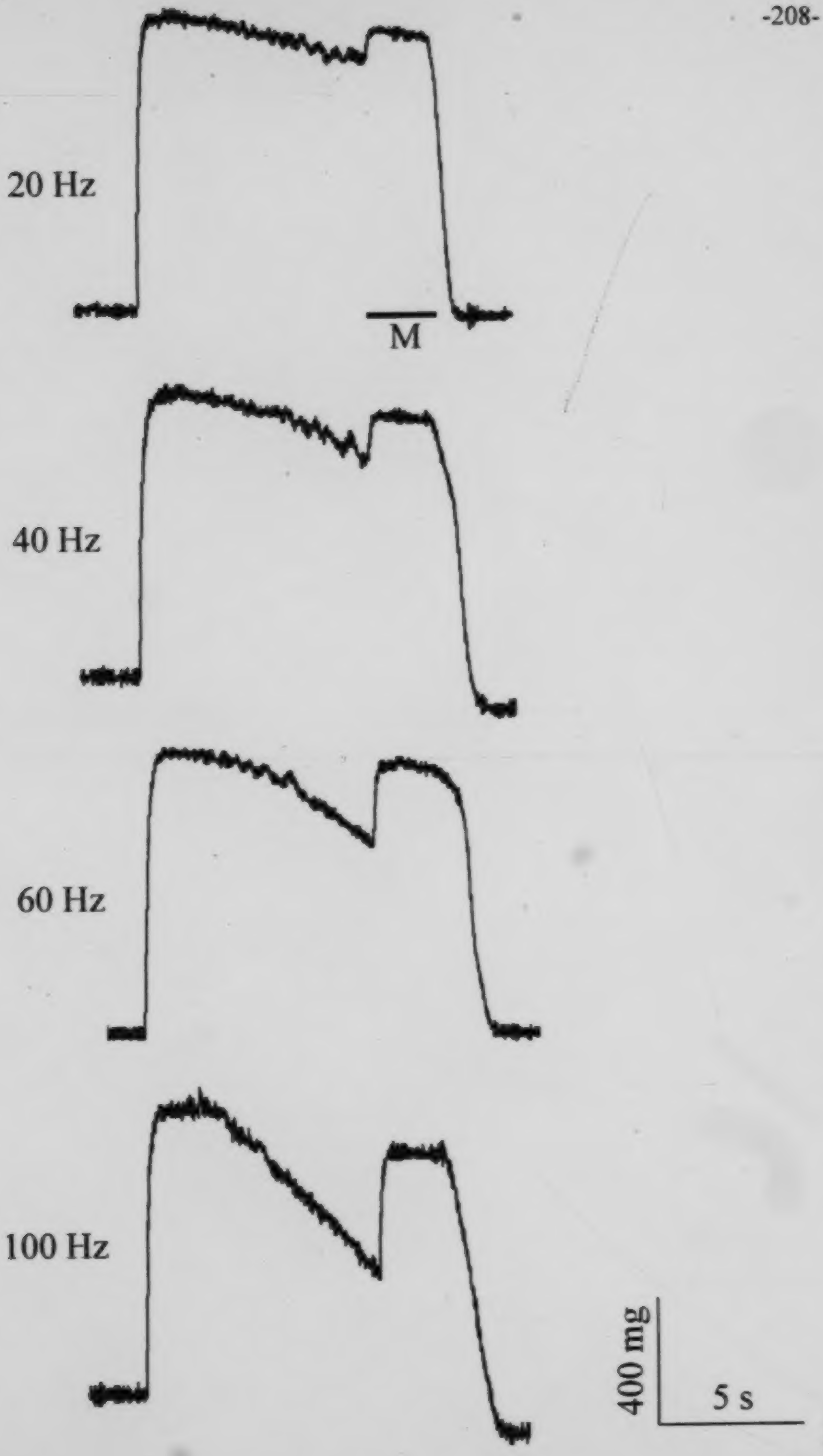
20 Hz
M
40 Hz
60 Hz
100 Hz
400 mg
5 s

Measurements of endplate potentials (epps)

To further understand the source of fatigue and to evaluate age-dependent changes in the efficacy of synaptic transmission between the phrenic nerve and diaphragm muscle fibers, epps were recorded utilizing embryonic and neonatal in vitro preparations in the presence of d-tubocurarine (4-6 µM, Sigma). Due to the concern that d-tubocurarine also suppresses presynaptic release of acetylcholine (Glavinovic, 1979), two alternative means of suppressing muscle twitches were attempted. First, we applied µ-conotoxin which has been shown to block muscle Na^+ channels (Cruz et al., 1985) and thus paralyze skeletal muscle without affecting the motor nerve or the neuromuscular junction (Hong et al., 1989). However, there was no visible inhibition of embryonic muscle contractions after adding µ-conotoxin (up to10 µM) to the bathing medium for 45 minutes and, as previously reported (Bazzy, 1994), µ-conotoxin was only partially effective in attenuating neonatal muscle contractions. Thus, presumably due to differences in Na^+ channel subunit composition in perinatal and adult muscle (Kallen et al., 1990), µ-conotoxin proved to be an ineffective means of suppressing muscle twitches. Second, we applied BDM, which has been shown to suppress muscle contractions in adult muscle by reducing Ca^{++} release from the sarcoplasmic reticulum and interfering with cross-bridge cycling (Fryer et al., 1988; McKillop et al., 1994). However, addition of up to 40 µM BDM was ineffective for blocking embryonic muscle twitches and only partially effective in neonatal muscle preparations.

Figure 6.5 illustrates typical recordings of epps elicited from E18 and P0 muscle fibers in response to phrenic nerve stimulation. The majority of epps at E18 (5 out of 6) and at P0-1 (8 out of 9) obtained in this experiment contained two components. This is thought to be the result of polyneuronal innervation of muscle fibres that occurs during development (Bennett and Pettigrew, 1974; Dennis et al., 1981; Rosenthal and Taraskevish, 1977). Figure 6.5 A shows a recording obtained from a P1 muscle fiber in which two components of the epp could not be separated by modulating the strength of nerve stimulation. This observation suggests that there are at least two axons with similar activation thresholds innervating the muscle fiber.

The characteristics of individual epps were not significantly different between embryonic and neonatal muscle. The measured values were as follows: amplitude (1.4 ±0.6 vs 1.6±0.5 mV), rise time (2.8±.4 vs 3.3±0.6 ms), slope (0.5±0.2 vs 0.8±0.3 mV/ms) and decay rate (26.8±6.3 vs 21.1±3.2 ms) for E18 (n=5) vs P0 (n=9), respectively. However, it was clear that there were age-dependent differences in the ability to maintain epp amplitudes in response to a one second train of nerve stimulation (Fig. 6.5 B and C). A significant decline in epp amplitude beyond the first epp was found in all E18 preparations tested (n=7) in response to ≥20Hz nerve stimulation (Fig. 6.5 C). In contrast, at P0, a significant decline in epp amplitude was not apparent until the nerve was stimulated at ≥30 Hz (n=8; Fig. 6.5 C).

Figure 6.5. End-plate potentials (epps) measured from E18 and P0 muscle fibers. **A)** Examples of epps in response to a one second train of nerve stimulations. Compound epps can be seen in P1 fiber suggesting that two motor axon endings which converge on the endplate region were stimulated (i.e. polyneuronal innervation). **B)** Epps in response to increasing frequencies of nerve stimulation. The amplitude of epps decreases within a stimulus train at lower frequencies at E18 compared with at P0. **C)** Normalized epp amplitude versus nerve stimulation frequency. The amplitude of the final epp in response to a train of stimulation was expressed as a percentage of the first epp amplitude. There were significant decreases in epp amplitude (* $p<0.05$) at 20 and 30 Hz for all E18 and P0-1 musculature, respectively. The changes in epp amplitude were more variable at lower frequencies. At stimulation frequencies less than 20 Hz, there was actually an increase in the final epp amplitude relative to the first epp in 4 of 7 E18 preparations. Similarly, at stimulation frequencies less than 30 Hz, the final epp amplitude was greater than first epp amplitude in 5 of 8 neonatal preparations.

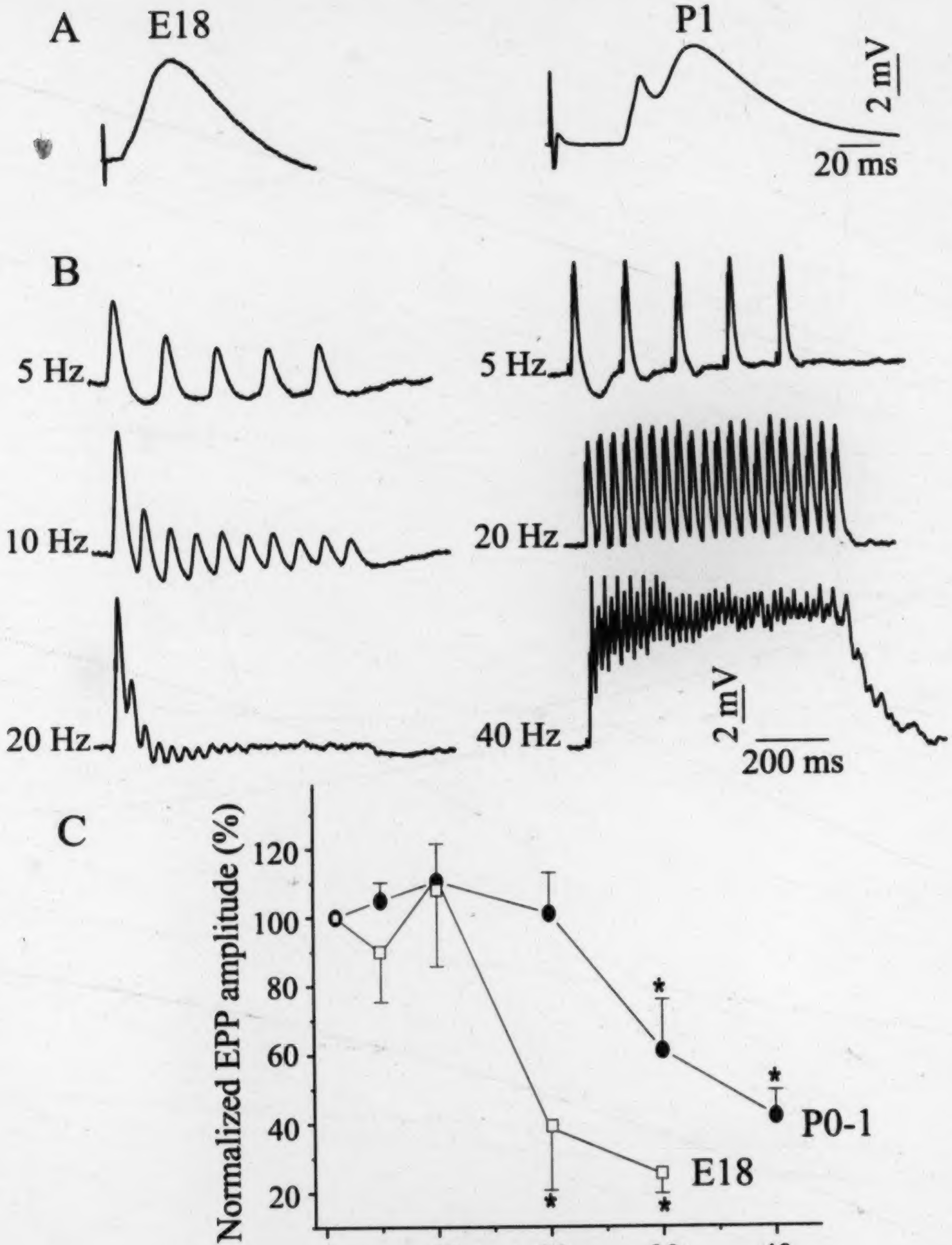
A
E18
P1
2 mV
20 ms
B
5 Hz
10 Hz
20 Hz
5 Hz
20 Hz
40 Hz
2 mV
200 ms
C
Normalized EPP amplitude (%)
120
100
80
60
40
20
0
10
20
30
40
Frequency of Stimulation (Hz)
P0-1
E18
*
*
*
*

DISCUSSION

Phrenic motoneurons in the perinatal rat undergo major changes in their morphology and electrophysiological properties during the relatively short period spanning from the inception of inspiratory drive transmission at E17 through to birth (Allan and Greer, 1997b; Greer at al., 1992). Data from the present study demonstrate that there is a concomitant development of diaphragmatic muscle properties during this period which functionally match changes in PMN properties. It is also apparent upon examining our data in conjunction with those from previous studies of postnatal diaphragm function (Feldman et al., 1991; Sieck et al., 1991; Bazzy and Donnelly, 1993; Moore et al., 1993; Johnson et al., 1994) that the overall trend for age-dependent changes in contractile, force production and fatigue characteristics can be traced back in development through to embryonic and early postnatal stages.

Consideration of in vitro conditions

The experiments in this study were performed at 27°C for two reasons. First, the reduced temperature facilitates tissue viability for the full duration of the experimental procedures (Segal and Faulkner, 1985). Second, from the perspective of understanding the functional ontogeny of the motor unit it was important to interpret findings from this study of diaphragm contractile properties with those from a parallel study of PMN electrophysiological properties (Chapter 3). The study of PMN properties was performed using perinatal cervical splice preparations maintained *in vitro* at 27°C. The absolute values of the various parameters measured in both studies will clearly be affected by the temperature-dependent properties of both neuronal (Thompson et al., 1985) and muscle (Segal and Faulkner, 1985; Mutungi and Ranatunga, 1998) properties. However, by studying the neuronal and muscle properties under similar *in vitro* conditions, reasonable conclusions regarding a functional correlation between the development of the two components of the neuromuscular system can be derived.

Twitch contraction and relaxation times

The twitch contraction and relaxation times were much slower at E18 compared to P0-1. Differences in myosin heavy chain (MHC) content are likely responsible for a significant component of the variations in contraction speed. At E18, the diaphragm is composed largely of the embryonic/neonatal MHC isoforms which are characterized by slow kinetics and high resistance to fatigue (Kelly et al., 1991; Sieck et al., 1991; Watchko et al., 1992; Johnson et al., 1994; Lloyd et al., 1996). By birth, 30% of the embryonic/ neonatal isoform is replaced by the adult slow and fast 2A isoforms which would, in part, explain the overall increase in contraction speed (Reiser et al., 1985; LaFramboise et al., 1990; Vazquez et al., 1993; Watchko and Sieck, 1993; Johnson et al., 1994). Differences in the twitch and tetanic relaxation times can be accounted for by age-dependent elaborations of the T-tubule/sarcoplasmic reticulum system and increases in Ca^{++} ATPase activity. Both of these mature perinatally resulting in an increased ability to rapidly sequester Ca^{++} from sarcomeres and terminate force production (Yamashiro et al., 1984; Duncey and Harrison, 1998).

Force development

The diaphragm musculature at E18 is visibly more fragile, and develops less single twitch or tetanic force per weight or protein content compared to the newborn. The initial wave of myotube formation (primary myogenesis) in the diaphragm is completed by approximately E17 (coinciding with the time of the inception of inspiratory drive transmission). Subsequently, there is a secondary stage of myogenesis during which the majority of the future diaphragm musculature is formed (Allan and Greer, 1997a; Allan and Greer, 1998). Thus, between E18 and P0-1 there are substantial increases in the ratio of muscle/connective tissue and the thickness and surface area of the diaphragmatic musculature. Moreover, increases in the density of myofilaments within individual muscle fibers, changes in MHC isoform expression and the elaboration of the T-tubule/sarcoplasmic reticulum apparatus all lend themselves to enhancing the force producing capabilities of developing muscle (Yamashiro et al., 1984; McCarter et al., 1987).

Force-frequency relationship

At E18, the kinetics of muscle twitches were slow and thus fused tetanic contractions were achieved at a relatively low frequency (~15 Hz). The frequency at which the diaphragm is driven by the phrenic nerve *in utero* is not known. However, we have examined the repetitive firing properties of PMN at E18 under *in vitro* conditions similar to those utilized in this study for measuring muscle properties. As is the case for diaphragm twitch contractions, the duration of PMN action potentials are considerably longer at E18 compared with those at P0-1 (as described in Chapter 3). Consequently, the slow kinetics of the PMN action potentials at E18 limits the maximum rate of repetitive firing in response to a 1 second depolarizing pulse to approximately 20 Hz. This is also within the range of cervical motoneuron firing rates observed during inspiratory bursts generated by brainstem-spinal cord in vitro preparations isolated from E18 rats (DiPasquale et al., 1996). Interestingly, the range necessary to produce the full gradation of tetanic force in the diaphragm musculature spans from approximately 1 to 20 Hz (Fig. 6.2). Thus, it would appear that there is a functional matching of PMN firing and diaphragm contractile properties at E18. It was also apparent that the actual range of forces generated by the diaphragmatic embryonic musculature is quite narrow; approximately 60% of the maximum tetanic force is generated at minimal rates of stimulation. Perhaps a fine gradation of force generation in the diaphragm musculature is not an essential component of fetal breathing movements *in utero*. Rather, given the low rheobase current necessary to activate PMNs (Chapter 3) and the utilization of the upper end of the force output range for the diaphragm musculature, it seems that the neuromuscular system is designed to assure breathing movements of adequate magnitude for ribcage expansion despite a rather weak inspiratory drive transmission present during the early stages following the inception of respiratory rhythmogenesis (DiPasquale et al., 1996).

By birth, the single twitch contractions were considerably faster and the tetanic frequency higher relative to E18. At P0-1, PMN action potentials are also of shorter duration and thus the repetitive firing frequency is higher, reaching an approximate maximum of 30 Hz in response to a one second depolarizing pulse (Chapter 3). This range is similar to that observed from recordings of PMNs during inspiratory bursts generated by neonatal rat brainstem spinal cord preparations (Lindsay and Feldman, 1993). Similar to the situation observed at E18, the range of neonatal PMN firing matches those necessary to generate the full range of potential force levels from the diaphragm musculature.

It is also apparent from Fig. 6.2, that the range of forces generated by the diaphragm at P0-1 in response to graded increments of nerve stimulation is much wider than at E18. This property would allow for the modulation of diaphragmatic force development to produce tidal volumes which meet the variety of respiratory demands encountered postnatally.

Neuromuscular fatigue

The diaphragm musculature at P0-1 was capable of maintaining a constant level of force in response to a one second train of nerve stimulations at 20 Hz. However, at higher frequencies of nerve stimulation there was an incremental decline in force during the latter phases of the 1 second stimulation. The experiments involving combined nerve and muscle stimulation showed that the force reduction was related to some aspect of transmission between the nerve and muscle. Subsequent analyses of epp amplitudes determined that there was a gradual decrement in epp amplitude during the one second period of phrenic nerve stimulation at rates greater than 20 Hz. Bazzy and Donnelly (1993) demonstrated that part of the failure to follow high frequency stimulation in neonatal phrenic nerve-diaphragm preparations was due to failure at the neuromuscular junction. Fournier et al., (1991) also determined that failure of action potential propagation to the motor axon nerve terminals at higher frequencies could contribute to neurotransmission fatigue in neonatal rats. Both of these processes are thought to mature during the first two weeks postnatally and then remain unchanged thereafter (Fournier et al., 1991). Regardless, neuromuscular fatigue may not be a significant problem for newborn rats because the range of repetitive stimulation rates necessary to produce fatigue at P0-1, at least in vitro, is beyond the typical maximum sustained frequency at which PMNs fire under similar conditions (Lindsay and Feldman, 1993; DiPasquale et al., 1996).

The absence of a decline in the force output of the E18 diaphragm musculature in response to one second-long trains of nerve stimulation was, at least initially, a surprising result. We had assumed that the above mentioned factors contributing to neurotransmission failure at P0-1 would be more pronounced at E18. Indeed, the ensuing measurements of epps clearly showed that neuromuscular transmission failure was much more severe at E18 compared to P0. The fact that the neuromuscular fatigue did not translate into a failure of force production could be explained by the prolonged maintenance of Ca^{++} ions within the sarcomeres of embryonic muscle. The T-tubule-sarcoplasmic reticulum system is underdeveloped prenatally (Yamashiro et al, 1984; Duncey and Harrison, 1996). Thus, as is evident from examining the slow decay of individual twitches or tetanic force output (Figs. 6.1 and 6.3), the force levels persist well beyond the termination of the synaptic drive from the phrenic nerve. Further, our measurements of force production in response to a prolonged phrenic nerve stimulation at E18 (10 sec; Fig. 6.4) support this hypothesis by showing that the decline in force levels were manifest if sufficient time was allowed for the sequestering of Ca^{++} ions. Functionally, these data imply that, *in utero*, diaphragm contractions persist beyond the period of inspiratory drive from phrenic motoneurons (despite any neuromuscular transmission fatigue). This would be advantageous for ensuring a prolonged expansion of the ribcage and stretching of the lungs despite a weak synaptic drive from the PMN pool to the diaphragm. In contrast, by birth, the PMN-diaphragm properties are such that there is a more controlled duration and range of diaphragm contractions by motoneuronal inspiratory drive.

In summary, from the day following the inception of inspiratory drive transmission through to birth, diaphragmatic muscle properties undergo significant development and maturation. Further, the diaphragm contractile and PMN repetitive firing properties develop in concert so that the full-range of potential diaphragm force recruitment can be utilized and problems associated with diaphragm fatigue are minimized. During embryonic development the diaphragm is able to reach maximal levels of forces at stimulation frequencies lower than in neonatal diaphragmatic muscles. Since phrenic motoneurons also have a lower firing frequency at this age, there seems to be a functional matching between firing frequencies of PMNs and contractile properties of the diaphragm which will allow the generation of fetal breathing movements required for overall maturation of the respiratory system.

REFERENCES

ALLAN, D.W., GREER, J.J. (1997a) Embryogenesis of the phrenic nerve and diaphragm in the fetal rat. J. Comp. Neurol. 382:459-468.

ALLAN, D.W., GREER, J.J. (1997b) Development of phrenic motoneuron morphology in the fetal rat. J. Comp. Neurol. 381: 469-479.

ALLAN, D.W., GREER, J.J. (1998) PSA-NCAM expression during nerve outgrowth and myogenesis in the fetal rat. J. Comp. Neurol. 391:275-292.

BAZZY, A.R. (1994) Developmental changes in rat diaphragm endplate response to repetitive stimulation. Dev. Brain Res. 81: 314-317.

BAZZY, A.R., DONNELLY, D.F. (1993) Failure to generate action potentials in newborn diaphragms following nerve stimulation. Brain Res. 600: 349-352.

BENNETT, M.R., PETTIGREW, A.G. (1974) The formation of synapses in striated muscle during development. J. Physiol. 241: 515-545.

CRUZ, L.J., GRAY, W.R., OLIVERA, B.M., ZEIKUS, B.M., KERR, L., YOSHIKAMI, D., MOCZYDLOWSKI, E. (1985) Conus geographus toxins that discriminate between neuronal and muscle sodium channels. J Biol. Chem. 260: 9280-9288.

DENNIS, M.J., ZISKIND-CONHAIM AND, L., HARRIS, A.J. (1981) Development of neuromuscular junctions in rat embryos. Dev. Biol. 81: 266-279.

DI PASQUALE, E., TELL, F., MONTEAU, R., HILAIRE, G. (1996) Perinatal developmental changes in the respiratory activity of medullary and spinal neurons: an *in vitro* study on fetal and newborn rats. Dev. Brain Res. 91: 121-130.

DUNCEY, M.J., HARRISON, A.P. (1996) Developmental regulation of cation pumps in skeletal and cardiac muscle. Acta Physiol. Scand. 156: 313-323.

FELDMAN, J.D., BAZZY, A.R., CUMMINS AND , T.R., HADDAD, G.G. (1991) Developmental changes in neuromuscular transmission in the rat diaphragm. J. Appl. Physiol. 71:280-286.

FOURNIER, M., ALULA, M., SIECK, G.C. (1991) Neuromuscular transmission failure during postnatal development. Neurosis. Let. 125: 34-36.

FRYER, M.W., NEERING, I.R., STEPHENSON, D.G. (1988) Effects of 2,3-butanedione-2-monoxime on the contractile activation of fast- and slow-twitch rat muscle fibres. J.

Physiol. 407: 53-75.

GLAVINOVIĆ, M.I. (1979) Presynaptic action of curare. J. Physiol. 290: 499-506.

GREER, J.J., SMITH, J.C., FELDMAN, J.L. (1992) Generation of respiratory and locomotor patterns by an *in vitro* brainstem-spinal cord fetal rat preparation. J. Neurophysiol. 67:996-999.

HONG, S.J., CHANG, C.C. (1989) Use of geographus II (μ conotoxin) for the study of neuromuscular transmission in mouse. Br. J. Pharmacol. 97: 934-940.

JOHNSON, B.D., WILSON, L.E., ZHAN, W.Z., WATCHKO, J.F., DAOOD, M.J., SIECK, G.C. (1994) Contractile properties of the developing diaphragm correlate with myosin heavy chain phenotype. J. Appl. Physiol. 77: 481-487.

KALLEN, R.G., SHENG, Z.H., YANG, J., CHEN, L., ROGART, R.B., BARCHI, R.L. (1990) Primary structure and expression of a sodium channel characteristic of denervated and immature rat skeletal muscle. Neuron 4: 233-242.

KELLY, A.M., ROSSER, W.C., HOFFMAN, R., PANETTIERI, R.A., SCHIAFFINO, S., RUBINSTEIN, N.A., NEMETH, P.M.. (1991) Metabolic and contractile protein expression in diaphragm muscle. J. Neurosci. 11 (5): 1231-1242.

LAFRAMBOISE, W.A., DAOOD, M.J., GUTHRIE, R.D., BUTLER-BROWNE, G.S., WHALEN, R.G., ONTELL, M.(1990) Myosin isoforms in neonatal rat extensor digitorum longus, diaphragm and soleus muscles. Am. J. Physiol. 259(2 part 1): L116-L122.

LINDSAY, A., FELDMAN, J.L. (1993) Modulation of respiratory activity of neonatal rat phrenic motoneurons by serotonin. J. Physiol. 461: 213-233.

LLOYD, JS., BROZANSKI, B.S., DAOOD, M.J., WATCHKO, J.F. (1996) Developmental transitions in the myosin heavy chain phenotype of human respiratory muscle. Biology of the Neonate 69(2): 67-75.

MCCARTER, R., MAXWELL, L.C., COMPTON, C., KUEHL, T.J. (1987) Development of contractile and metabolic properties of the diaphragm in Respiratory Muscles and Their Neuromotor Control, edited by G.C. Sieck, S.C. Gandevia and W.E. Cameron. New York:Liss, vol 26, pp. 391-401.

MCKILLOP, D.F.A., FORTUNE, N.S., RANATUNGA, K.W., GEEVES, M.A. (1994) The influence of 2,3-butanedione-2-monoxime (BDM) on the interaction between actin and myosin in solution and in skinned muscle fibres. J. Muscle Res. Cell Motility 15: 309-318.

MOORE, B.J., FELDMAN, H.A., REID, M.B. (1993) Developmental changes in diaphragm contractile properties. J. Appl. Physiol. 75: 522-526.

MUTUNGI, G., RANATUNGA, K.W. (1998) Temperature-dependent changes in the viscoelasticity of intact resting mammalian (rat) fast- and slow-twitch muscle fibres. J. Physiol. (London) 508:253-265.

REISER, P.J., MOSS, R.L., GIULIAN, G.G., GREASER, M.L. (1985) Shortening velocity and myosin heavy chain of developing rabbit muscle fibers. J. Biol. Chem. 260: 14403-14405.

ROSENTHAL, J.L., TARASKEVICH, P.S. (1977) Reduction of multiaxonal innervation at the neuromuscular junction of the rat during development. J. Physiol. 270: 299-310.

SEGAL, S.S., FAULKNER, J.A. (1985) Temperature-dependent physiological stability of rat skeletal muscle *in vitro*. Am. J. Physiol. 248: C265-C270.

SIECK, G.C., FOURNIER, M., BLANCO, C.E. (1991) Diaphragm muscle fatigue resistance during postnatal development. J. Appl. Physiol. 71(2): 458-464.

THOMPSON, S.M., MASUKAWA, L.M., PRINCE, D.A. (1985) Temperature dependance of intrinsic membrane properties and synaptic potentials in hippocampal CA1 neurons *in vitro*. J. Neurosci. 5: 817-824.

VASQUEZ, R.L., DAOOD, M.J., WATCHKO, J.F. (1993) Regional distribution of myosin heavy chain isoforms in rib cage muscles as a function of postnatal development. Pediatric Pulmonology 16: 289-296.

WATCHKO, J.F., SIECK, G.C. (1993) Respiratory muscle fatigue resistance relates to myosin phenotype and SDH activity during development. J. Appl. Physiol. 75(3): 1341-1347.

WATCHKO, J.F., DAOOD, M.J., VAZQUEZ, R.L., BROZANSKI, B.S., LAFRAMBOISE, W.A., GUTHRIE, R.D., SIECK, G.C. (1992) Postnatal expression of myosin isoforms in an expiratory muscle-external abdominal oblique. J. Appl. Physiol. 73(5): 1860-1866.

YAMASHIRO, S., HARRIS, W., STOPPS, T. (1984) Ultrastructural study of developing rabbit diaphragm. J. Anat. 139: 67-79.

CHAPTER 7

GENERAL DISCUSSION

The phrenic nerve and the diaphragm are the major neuromuscular components necessary for breathing and must be fully functional by birth (Allan and Greer, 1997a,b; Greer et al., 1992). Therefore, to study the fundamentally important events that shape the formation of the phrenic nerve and diaphragm, one must study events occurring prenatally. Some of these prenatal events include target innervation and phrenic nerve intramuscular branching between E14-E17, the inception of synaptic respiratory drive and the arrival of spinal afferent projections onto the phrenic pool at E17, and dramatic changes in PMN dendritic morphology between E17-E21 (Allan and Greer, 1997a,b; Greer et al., 1992). Therefore, I chose to study the maturation of the electrical properties of PMNs and the contractile properties of the diaphragm beginning at E16, a day prior to the onset of synaptic respiratory drive, up to birth, when most of the morphological changes are completed and continuous rhythmic recruitment of the respiratory neuromuscular system is required. In this section I will discuss the major findings arising from this thesis and their physiological significance for the functional development of the PMN-diaphragm functional properties.

Role of calcium influx during PMN development

It is widely accepted that Ca^{++}-dependent mechanisms are important factors in controlling morphological and electrical differentiation in developing neurons (Shen et al., 1993; Gu and Spitzer, 1993,1995; Finkbeiner and Greenberg, 1998). As the present results indicate, the action potential of embryonic PMNs (E16) prior to the onset of functional drive is characterized by a long duration and a significant Ca^{++} component. During this early period, the action potential duration depends upon the interplay between Ca^{++} and K^{+}

conductances. The slow activation of outward K^+ conductances allows a significant Ca^{++} influx which is further facilitated by a higher level of LVA Ca^{++} channel expression. Further work is required to determine the specific role of Ca^{++} during this phase of PMN anatomical and functional development including the formation of dendritic arbors and expression of specific ionic conductances. In other systems, it appears that firing frequency regulates Ca^{++} influx during electrical differentiation. The pattern of neuronal electrical stimulation in a cell regulates the amount of Ca^{++} available to trigger specific intracellular transduction pathways such as those controlling gene transcription. For example, in dorsal root ganglion neurons, transcription of the immediate early gene, *c-fos,* does not depend upon a sustained increase in intracellular Ca^{++}, as would be observed during a long action potential. Rather, it depends upon the frequency of stimulation and the temporal pattern of Ca^{++} entry (Shen et al., 1993). Additional support for this conclusion derives from studies of *Xenopus* spinal neurons. Experimentally-induced Ca^{++} transients (~9 s duration) at frequencies of 6-9/hour inhibit neurite outgrowth, whereas Ca^{++} transients at ≥2/hour are required for maturation of K^+ channel and enhanced neurotransmitter expression (Gu and Spitzer, 1995). It is conceivable that the frequency of PMN recruitment following the inception of inspiratory synaptic drive, via its regulation of Ca^{++} influx, contributes to specific gene expression in PMNs during perinatal development, in particular the upregulation of Ca^{++} activated K^+ conductances and the reduction in T-channel Ca^{++} channel expression.

Following the inception of respiratory drive at E17, there is a shortening of action potential duration due to the elimination of the Ca^{++} component present at E16. It is likely that transformation of PMNs from a growing structure at early stages of development (E16-

E17) into an electrical device required for transmission of motor commands requires a tight regulation of Ca^{++} influx. Two developmentally-regulated factors appear to regulate Ca^{++} influx during PMN maturation. First, the expression of Ca^{++}-activated K^{+} conductances will offer significant protection against any detrimental effects caused by Ca^{++} accumulation during repetitive firing. This problem is compounded by the age-dependent increase in firing frequency and enhanced expression of HVA Ca^{++} channels which could induce a larger influx of Ca^{++} during repetitive firing. Second, Ca^{++} influx through various Ca^{++} channels is tightly coupled to specific membrane-bound events. Thus, Ca^{++} entry via N-type Ca^{++} channels generated the mAHP following activation of Ca^{++}-activated K^{+} conductance (small type), whereas Ca^{++} entry via L-type Ca^{++} channels was responsible for the ADP.

The differential regulation of afterpotentials (mAHP, ADP) by specific Ca^{++} conductances suggest that there is a non-homogenous distribution of Ca^{++} channels on PMN membrane. This could explain why Ca^{++} influx via N-type, but not L-type, Ca^{++} channels, can activate Ca^{++}-activated K^{+} channels (small type). As modeling and imaging studies indicate, non-homogenous distribution of Ca^{++} channels within the membrane may be related to the fact that intracellular Ca^{++} concentrations drop sharply from the site of Ca^{++} influx (Barish and Thompson, 1983; Simon and Llinas, 1985). The presence of a close interaction between Ca^{++} channels and Ca^{++}-activated K^{+} channels has also been reported at the frog neuromuscular junction (Robitaille and Charlton, 1992; Robitaille et al., 1993). Functionally, clustering of specific Ca^{++} channel subtypes with a specific effector may be required to achieve a more discriminatory regulation of certain cell functions (such as Ca^{++} influx, firing pattern and force generation, see below) by neurotransmitters.

Future direction: It would be of interest to directly measure Ca^{++} levels in PMNs in cervical slice preparations isolated from perinatal rats aged E16, E18 and P0 using flourometric techniques. The hypothesis being that there will be an accentuation of intracellular Ca^{++} levels via one or more of the following three mechanisms at earlier ages: i) influx via LVA and HVA calcium channels; ii) influx resulting from the activation of glutamate receptors or GABA-mediated membrane depolarization, iii) release from intracellular stores (caffeine- and ryanodine-sensitive stores). These experiments would be a feasible project which would complement my work on age-dependent changes in calcium-channel expression.

Regulation of PMN firing properties

From E16 to P1, PMNs undergo a ~2-fold increase in firing rate. An age-dependent reduction in action potential duration appears to be responsible for the increased firing rate over this time. Three main factors likely contribute to the reduction in action potential duration. First, inception of respiratory drive is correlated with the elimination of the Ca^{++} component that prolonged action potential duration at E16. Second, there is a significant increase in the activation kinetics of the outward K^{+} current (including a reduction in the activation rate and an ~8mV leftward shift in the activation voltage). Functionally, the higher membrane voltage reached during an action potential and the increasing of outward K^{+} channel activation will result in more K^{+} channels opening during the repolarization phase, resulting in a shortening of the action potential as PMNs mature. Third, expression of a maxi-type Ca^{++}-activated K^{+} conductance in neonatal PMNs, that was not present at E16, contributes to a faster repolarization of the action potential.

Besides the role played by action potential duration in regulating age-dependent changes in firing frequency, the present results also suggest that pre-inspiratory membrane potential can significantly alter repetitive firing in some populations of PMNs, particularly in neonates. This could have a significant effect in controlling the onset of repetitive firing during an inspiratory burst. Thus, the presence of an A-type K^+ conductance-dependent delayed excitation generates a significant delay in the initial recruitment of PMNs following a hyperpolarizing prepulse. Hyperpolarizing potentials also revealed a bursting firing pattern in 20% neonatal PMNs. It appears that delayed excitation is generated after removal of A-type K^+ channel inactivation by membrane hyperpolarization, whereas bursting is the result of an increased driving force for Ca^{++} entry through L-type Ca^{++} channels. The hyperpolarizing potentials responsible for delayed excitation and bursting could be provided by the expiratory synaptic drive impinging onto PMNs (Liu and Feldman, 1993). However, there is still considerable debate as to whether the expiratory synaptic drive is excitatory or inhibitory in developing PMNs (Su and Chai, 1998; Parkis et al., 1999). Another possibility to consider is whether the hyperpolarizing potentials required for expression of delayed excitation and bursting could be provided by neuromodulators of respiratory drive, such as opioids and/or noradrenaline (Morin-Surun et al., 1992; Trapp et al., 1994; Greer et al., 1995; Al-Zubaidy et al., 1996). Functionally, it is likely that PMNs exhibiting bursting firing and delayed excitation could be recruited during different phases of the inspiratory cycle (i.e., early vs. late phase, respectively) or for specific respiratory-related tasks.

Despite the age-dependent increase in repetitive firing frequencies, neonatal PMNs required an ~2-fold larger amounts of activation current in order to generate repetitive firing compared to E16 PMNs. This observation correlates with the ~3-fold reduction in the input resistance of PMNs from E16 to P1. The change in the amount of current required for the recruitment of PMNs is consistent with two periods of functional development. During embryonic development (≥E17), PMNs will have an increased tendency to reach firing threshold despite the relatively weak descending inspiratory drive (Greer et al., 1992; Di Pasquale et al., 1996). This may facilitate the production of fetal breathing movements prenatally. Several factors contribute to increased electrical excitability of embryonic PMNs, as compared with neonates. These include a less negative resting membrane potential (~10 mV), an increase in input resistance (3 times higher) and time constant (~1.4 times longer) as well as an enhanced expression of LVA Ca^{++} channels. By birth, PMN excitability is reduced in order to grade the amount of inspiratory muscle activation required for maintaining an appropriate respiratory volume under various physiological conditions.

Future direction: A question that requires further consideration is the role of putative neuromodulators in regulating the repetitive firing pattern of PMNs during maturation. Several neuromodulators, including serotonin, noradrenaline, substance P, prostaglandins, thyrotropin-releasing hormone and opiods, regulate respiratory activity in neonates (Kitterman et al., 1979; Quilligan et al., 1981; Bennet et al., 1988; Lindsay and Feldman, 1993; Di Pasquale et al., 1994; Greer et al., 1995; Al-Zubaidy et al., 1996). Although the majority of work has been directed toward understanding the role of neurotransmitters at the level of the central rhythm generator, an effect at the level of the spinal cord cannot be ruled out. This is especially significant considering that at least seven neuromodulators, including serotonin, substance P, thyrotropin-releasing hormone, enkephalin, cholecystokinin, galanin and neuropeptide Y, have been located in terminal varicosities within the phrenic nucleus (Ellenberger et al., 1992). Of particular interest is the role of serotonin in regulating PMN excitability. Serotonergic projections from the raphe nucleus are believed to provide an important modulatory effect on PMN motor output (Lalley, 1986). In hypoglossal motoneurons, also involved in respiration, serotonin has a facilitatory effect on the firing pattern, largely due to inhibition of the mAHP (Talley at al., 1997). As in hypoglossal motoneurons, it is possible to hypothesize that serotonin may modulate repetitive firing pattern in PMNs (perhaps by regulating the mAHP). This could account for its facilitatory role on phrenic nerve respiratory activity in newborns (Lindsay and Feldman, 1993; Di Pasquale et al., 1994). This may be pertinent toward an understanding of the role of serotonin during sleep-awake states and its possible correlation with respiratory failure during sleep in newborns.

This proposed analyses of age-dependent changes in neuromodulatory-mediated effects on PMN properties is another natural extension from my thesis work and is actually being initiated during the last month of my Ph.D. program in collaboration with a postdoctoral fellow in the laboratory, Dr. Calvin Wong.

Correlation between inception of inspiratory drive and maturation of PMN-diaphragm properties

The present work indicates that concomitant with the inception of inspiratory drive at E17, there is a significant transformation in the electrical properties of PMNs. These include a reduction of action potential duration and input resistance, a decrease in T-type Ca^{++} current expression and the appearance of an apamin-sensitive, Ca^{++}-activated K^{+} conductance. These factors are crucial in regulating motoneuron excitability following the inception of respiratory drive. Maturation of the PMN firing pattern occurs concomitantly with major changes in the contractile properties of the diaphragm.

Increased interest in understanding the maturation of electrical properties of PMNs and the contractile properties of the diaphragm associated with fetal respiratory movement is driven by the fact that the maturation of the respiratory neuromuscular system could be potentially affected by fetal exposure to hypoxia, alcohol, opiates and cigarette smoke. These factors may cause respiratory disorders in newborns. Although a systematic study of the effect on these factors at the cellular level (in particular on respiratory neurons) is missing, certain evidence suggests a possible link between those factors and possible disruption of the respiratory development. For example, in chick lumbar motoneurons, acute hypoxia inhibits generation of spontaneous activity. Considering the role of spontaneous electrical activity in the maturation of electrical excitability, it is not surprising that hypoxia prevents the maturation of motoneuron electrical properties and inhibits the functional development of specific motor pools (Gonya-Magee and Stokes, 1980). Similarly, exposure to cigarette smoking during pregnancy significantly affects lung function and increases the likelihood of respiratory disorders in newborns (Ladrup et al., 1997; Wisborn et al., 1999).

Future direction: Future work is required to determine how factors that alter respiratory drive will affect the maturation of PMN electrical properties and diaphragm contractile properties and whether this will result in neonatal respiratory dysfunction. It is conceivable that perturbations of synaptic drive from the brain stem respiratory centre will prevent normal maturation of the PMN-diaphragm neuromuscular system. It will be interesting to test whether removal of inspiratory drive by cervical trans-section of the spinal cord will delay the maturation of the PMN-diaphragm functional properties. Blockade of all synaptic activity (inspiratory, sensory, muscular) by *in utero* treatment with TTX could provide some insight as to whether PMN electrical maturation depends on the overall electrical activity. Since NMDA, AMPA and GABA are the main neurotransmitters known to regulate synaptic drive onto PMNs, further work is required to determine whether selective perturbation of their receptors may have any effect on the maturation of the functional properties of the PMNs as well.

A question arises as to what event(s) could regulate PMN maturation prior to E16. The most significant event in the morphological maturation of PMN prior to E16 appears to be innervation of the diaphragm (at E14). It remains to be tested whether target innervation (i.e., target-derived trophic factors) may have a significant effect on PMN electrical properties by E16 (and perhaps, throughout development). In particular, it will be interesting to test whether action potential characteristics and K^+ channel expression may be disrupted by eliminating trophic factor expression and/or their action. This hypothesis could be further tested in commercially available null-mutant mice for specific trophic factors (i.e., CNTF and BDNF).

Correlation between PMN firing properties and diaphragm force generation

From E18 to birth, changes in the electrical properties of the PMNs are matched by concomitant changes in the contractile properties of the diaphragm, specifically in the duration and amplitude of single twitch and tetanic contractions. This is required for optimal force generation throughout perinatal development, in particular for the generation of fetal breathing movements before birth and for continuous phasic breathing after birth. Despite the immature state of the diaphragm at E18, several factors allow the muscle to generate sufficient contractile force to produce fetal breathing movements. First, maximal tetanic force can be generated at lower rates of nerve stimulation which matches the relatively slow firing rates of E18 PMNs. Second, there was only an ~40% difference in the amount of force between a single twitch and maximal tetanic contraction, suggesting that the range of forces which can be generated with minimal rates of nerve stimulation is considerable narrow. In the neonates, this range was ~80% as would be required for graded recruitment of the diaphragm. Third, at E18, tetanic force can be maintained after termination of nerve stimulation. Force maintenance could be explained based on the expression of a slow MHC and a rather immature Ca^{++} extrusion mechanism from the sarcoplasmic reticulum (Yamashiro et al., 1984; Kelly et al., 1991). The ability to maintain high levels of force may be required for generating fetal breathing movements despite a rather weak inspiratory drive (DiPasquale et al., 1996).

The present results also suggest that in neonatal PMNs, regulation of the mAHP and ADP by neuromodulators may have a significant direct effect on the firing rate and a concomitant effect on the tension level generated by the diaphragm muscle. As the present results indicate, upregulation of the ADP (or conversely, downregulation of the mAHP) will result in a considerable increase in the initial firing frequency (i.e., bursting) in neonatal

PMNs. It is known that the amount of force produced by a muscle not only depends upon the average rate of stimulation but also upon the pattern of action potentials in the stimulation train (Burke et al., 1970; Stevens, 1996). Thus, increasing the initial repetitive firing due to the insertion of a one or a few spikes at the beginning of a train of action potentials (by either upregulating the ADP or downregulating the mAHP) may cause a significant increase in the force produced by the muscle. Functionally, in neonates and adults alike, bursting may facilitate the generation of considerable amounts of force with minimal drive and with the added benefit of significantly reducing the metabolic cost of contraction (Milano et al., 1992, Stevens, 1996). Furthermore, generation of bursting activity may be required during specific respiratory motor tasks such as vomiting and coughing which required brisk contractions of the diaphragm (Milano et al., 1992).

In conclusion, the phrenic nerve and diaphragm are optimally matched for the generation of contractions at each stage of development. In embryos, the need to generate fetal breathing movements, required for proper lung maturation, is specifically directed toward maximal force generation despite the immature state of descending inspiratory drive, the diaphragm muscle contractile properties and the electrical properties of the PMNs. In neonates, the needs for dynamically adjusting diaphragm recruitment for the ever changing respiratory challenges that are encountered outside of the womb are met by a higher expression of ionic conductances available to modulate PMN repetitive firing and a more graded responsiveness of the muscle to nerve activity. The regulation of this matching could be severely affected when the fetus is subjected to such factors as narcotics, smoke or hypoxia during the perinatal period. This, in term could lead to respiratory dysfunctions in newborns.

REFERENCES

ALLAN, D.W., GREER, J.J. (1997a) Embryogenesis of the phrenic nerve and diaphragm in the fetal rat. J. Comp. Neurol. 382: 459-468.

ALLAN, D.W., GREER, J.J. (1997b) Development of phrenic motoneuron morphology in the fetal rat. J. Comp. Neurol. 381: 469-479.

AL-ZUBAIDY, Z.A., ERICKSON, R.L., GREER, J.J. (1996) Serotonergic and noradrenergic effects on respiratory neural discharge in the medullary slice. Pflugers Archiv (European Journal of Physiology) 431: 942-949.

BARISH, M.E., THOMPSON, S.H. (1983) Calcium buffering and slow recovery kinetics of calcium-dependent outward current in molluscan neurones. J. Physiol. 337: 201-219.

BENNET, L., GLUCKMAN, P.D., JOHNSTON, B.M. (1988) The central effects of thyrotropin-releasing hormone on the breathing movements and electrocortical activity of the fetal sheep. Pediatr. Res. 23: 72-75.

BURKE, R.E., RUDOMIN, P., ZAJAC, F.E. (1970) Catch properties in single mammalian motor units. Science 168: 122-140.

DI PASQUALE, E., TELL, F., MONTEAU, R., HILAIRE, G. (1996) Perinatal developmental changes in respiratory activity of medullary and spinal neurons: an in vitro study on fetal and newborn rats. Devel. Br. Res. 91: 121-130.

DI PASQUALE, E., TELL, F., MONTEAU, R., HILAIRE, G. (1994) Endogenous serotonin modulates the fetal respiratory rhythm: an in vitro study in the rat. Devel. Br. Res. 80: 222-232.

ELLENBERGER, H.H., VERA, P.L., FELDMAN, J.L., HOLETS, V.R. (1992) Multiple putative neuromessenger inputs to the phrenic nucleus in rat. J. Chem. Neuroanat. 5(5): 375-382.

FINKBEINER, S, GREENBERG, ME (1998) Ca^{2+} channel-regulated neuronal expression. J. Neurobiol. 37(1): 171-187.

GONYA-MAGEE, T., STOKES, B.T. (1980) Acute modification of embryonic spinal cord activity induced by hypoxia. Devel. Neurosci. 3(1): 11-18.

GREER, J.J, CARTER, J.E., AL-ZUBAIDY, Z. (1995) Opioid depression of respiration in neonatal rats. J. Physiol. 485.3: 845-855.

GREER, J.J, SMITH, J.C., FELDMAN, J.L. (1992) Respiratory and locomotor patters generated in the fetal rat brain stem-spinal cord in vitro. J. Neurophysiol. 67(4): 996-999.

GU, X., SPITZER, N.C. (1993) Low-threshold Ca^{2+} current and its role in spontaneous elevations of intracellular Ca^{2+} in developing *Xenopus* neurons. J. Neurosci. 13 (11): 4936-4948.

GU, X., SPITZER, N.C. (1995) Distinct aspects of neuronal differentiation encoded by frequency of spontaneous Ca^{2+} transients. Nature 375: 784787.

KELLY, A.M., ROSSER, W.C., HOFFMAN, R., PANETTIERI, R.A., SCHIAFFINO, S., RUBINSTEIN, N.A., NEMETH, P.M. (1991) Metabolic and contractile protein expression in diaphragm muscle. J. Neurosci. 11 (5): 1231-1242.

KITTERMAN, J.A., LIGGINS, G.C., CLEMENTS, J.A., TOOLEY, W.H. (1979) Stimulation of breathing movements in fetal lambs by inhibitors of prostaglanding synthesis. J. Dev. Biol. 1: 453-466.

LADRUP, C.K.C., JAAKKOLA, J.J., NAFSTAD, P., CARLSEN, K.H. (1997) *In utero* exposure to cigarette smoking influences lung function at birth. Eur. Respirat. J. 10(8): 1774-1779.

LALLEY, P.M. (1986) Responses of phrenic motoneurons of the cat to stimulation of medullary raphe nucleus. J. Physiol. 380: 349-371.

LINDSAY, A., FELDMAN, J.L. (1993) Modulation of respiratory activity of neonatal rat phrenic motoneurons by serotonin. J. Physiol. 461: 213-233.

LIU, G., FELDMAN, JL (1993) Bulbospinal transmission of respiratory drive to phrenic motoneurons. In: Respiratory control: central and peripheral mechanisms. Edd. Speck, DF., Dekin, M.S., Revelette, W.R., Frazier, D.T. The University of Kentucky Press. pp 47-51.

MILANO, S., GRELOT, L., BIANCHI, A.L., ISCOE, S. (1992) Discharge patterns of phrenic motoneurons during fictive coughing and vomiting in decerebrated cats. J. Appl. Physiol. 73: 1626-1636.

MORIN-SURUN, M.P., BOUDINOT, E., FOURNIE-ZALUSKI, M.C., CHAMPAGNAT, J., ROQUES, B.P., DENAVIT-SAUBIE, M. (1992) Control of breathing by endogenous opioid peptides: possible involvement in sudden infant death syndrome. Neurochem Int. 20(1):103-7.

PARKIS, M.A., DONG, X-W., FELDMAN, J.L., FUNK, G.D. (1999) Concurrent inhibition and excitation pf phrenic motoneurons during inspiration: phase-specific control of excitability. J. Neurosci. 19(6): 2368-2380.

QUILLIGAN, E., CLEWLOW, F., JOHNSTON, B.M., WALKER, D.W. (1981) Effects of 5-hydroxytryptophan on electrocortical activity and breathing movements of fetal sheep. J. Obstet. Gynecol. 141: 271-275.

ROBITAILLE, R., CHARLTON, M.P. (1992) Presynaptic calcium signals and transmitter release are modulated by calcium-activated potassium channels. J. Neurosci. 12: 297-305.

ROBITAILLE, R., GARCIA, M.L., KACZOROWSKI, G.J., CHARLTON, M.P. (1993) Functional localization of calcium and calcium-activated potassium channels in control of transmitter release. Neuron 11(4): 645-655.

SIMON, S.M., LLINAS, R.R. (1985) Compartmentalization of the submembrane calcium activity during calcium influx and its significance in transmitter release. Biophys. J. 48: 485-498.

SHEN, H.Z., FIELDS, R.D., NELSON, P.G. (1993) Specific regulation of immediate early genes by patterned neuronal activity. J. Neurosci. Res. 35: 459-467.

STEVENS, E.D. (1996) The pattern of stimulation influences the amount of oscillatory work done by the frog. J. Physiol. 494.1: 279-285.

SU, C-K., CHAI, C-Y (1998) GABAergic inhibition of rat phrenic motoneurons. Neurosci. Lett. 248: 191-194.

TALLEY, E.M., SADR, N.N., BAYLISS, D.A. (1997) Postnatal development of serotonergic innervation, 5-HT 1A receptor expression, and 5-HT responses in rat motoneurons. J. Neurosci. 17(11): 4473-4485.

WISBORG, K., HENRIKSEN, T.B., OBEL, C., SKAJAA, E., OSTERGAARD, J.R. (1999) Smoking during pregnancy and hospitalization of the child. Pediatrics 104(4): e46.

YAMASHIRO, S., HARRIS, W., STOPPS, T. (1984) Ultrastructural study of developing rabbit diaphragm. J. Anat. 139: 67-79.